

Aus dem Institut für Immunologie im Biomedizinischen Centrum  
der Ludwig-Maximilians-Universität München  
Leitung: Prof. Dr. rer. nat. Thomas Brocker

# **Analyzing cooperative post-transcriptional gene regulation by Roquin in the prevention of autoimmunity**



Dissertation  
zum Erwerb des Doktorgrades der Naturwissenschaften  
an der Medizinischen Fakultät der  
Ludwig-Maximilians-Universität zu München

vorgelegt von  
**Nina Isabella Kronbeck**

aus  
Landshut

2019

**Mit Genehmigung der Medizinischen Fakultät  
der Universität München**

Betreuer: Prof. Dr. rer. nat. Vigo Heissmeyer

Zweitgutachter: PD Dr. rer. nat. Philipp Korber

Dekan: Prof. Dr. med. dent. Reinhard Hickel

Tag der mündlichen Prüfung: 19.06.2020

Für meine Familie.





## Eidesstattliche Versicherung

Ich erkläre hiermit an Eides statt, dass ich die vorliegende Dissertation mit dem Titel

**Analyzing cooperative post-transcriptional gene regulation by Roquin in the  
prevention of autoimmunity**

selbständig verfasst, mich außer der angegebenen keiner weiteren Hilfsmittel bedient und alle Erkenntnisse, die aus dem Schrifttum ganz oder annähernd übernommen sind, als solche kenntlich gemacht und nach ihrer Herkunft unter Bezeichnung der Fundstelle einzeln nachgewiesen habe.

Ich erkläre des Weiteren, dass die hier vorgelegte Dissertation nicht in gleicher oder in ähnlicher Form bei einer anderen Stelle zur Erlangung eines akademischen Grades eingereicht wurde.

München, 14.07.2020

Nina Kronbeck



## Summary

This thesis investigates the RNA-binding protein Roquin-1 and its paralog Roquin-2 and their crucial role in T cell-mediated immune responses. Roquin-1 was first identified in a screen for autoimmune regulators. Here, a single point mutation in the ROQ-domain of Roquin causes a severe systemic lupus erythematosus-like phenotype in the so-called *sanroque* mice. Conditional deletion of Roquin paralogs in T cells partially resembles the phenotype, highly emphasizing the essential role for Roquin in the prevention of autoimmunity.

The first part presented in this thesis contributed to the discovery of a cooperative type of gene regulation by multiple Roquin proteins. The present state of knowledge is that Roquin binds stem loop *cis*-elements in the 3'-untranslated region (UTR) of mRNAs that encode important factors for T cell differentiation and induces mRNA decay thereof. I identified a novel way of gene regulation, which requires multiple Roquin proteins interacting with essential and non-essential stem loops in the 3'-UTRs of *Nfkbid* and *Ox40* thereby inducing mRNA degradation. Interestingly, the *Nfkbid* transcript was controlled by Roquin not only via mRNA decay, but also by inhibition of translation. These analyses were the first evidence that multiple Roquin proteins confer a robust post-transcriptional mRNA gene regulation.

The second part of this thesis investigated another layer of the cooperative function of Roquin: its physical and functional cooperation with the endonuclease Regnase-1. Regnase-1 and Roquin share overlapping target mRNAs and ablation of Regnase-1 in T cells resembles the phenotype of *sanroque* mice and mice lacking Roquin in T cells. In addition, TCR activation in T cells triggers cleavage of Roquin as well as Regnase-1 via the MALT1 paracaspase, thereby releasing target mRNAs from repression. We therefore addressed the questions: Why do Roquin and Regnase-1 have the same functions and are equally regulated in T cells? We hypothesized that Roquin and Regnase-1 cooperatively repressed their target mRNAs in T cells and thus prevented autoimmunity. By comparing the phenotypes of mice conditionally deleted for the Roquin paralogs, Regnase-1 and all three proteins in T cells, we identified a new cooperative function in directing regulatory T cell development in the thymus and preventing autoimmunity especially by controlling T<sub>H</sub>17 and T<sub>FH</sub> differentiation. Global gene expression analysis of CD4 T cells lacking Roquin and Regnase-1 uncovered different types of post-transcriptional gene regulation by Roquin and Regnase-1, whereas most genes depended on the presence of Roquin as well as Regnase-1. Identifying a direct interaction of Regnase-1 with Roquin finally proved the concept of cooperativity. In conclusion, this thesis provides evidence that cooperative gene regulation by Roquin and Regnase-1 is a safeguard mechanism to prevent overshooting immune responses that potentially cause autoimmunity.



## Zusammenfassung

Diese Dissertation untersucht das RNS-bindende Protein Roquin-1 sowie dessen Paralog Roquin-2 und deren essentielle Funktion in T-Zell-gesteuerten Immunantworten. Roquin-1 wurde zum ersten Mal in einem *Screen* für Autoimmunregulatoren beschrieben. Hierbei wurde die sogenannte *sanroque* Maus entdeckt, die durch eine einzige Punktmutation in der ROQ-Domäne von Roquin-1 eine starke Lupus-ähnliche Autoimmunerkrankung entwickelt. Mäuse mit einer T-Zell-spezifischen Deletion beider Roquin Paraloge weisen eine ähnliche Autoimmunerkrankung auf. Dies unterstreicht die zentrale Rolle von Roquin-1 und Roquin-2 in der Prävention von Autoimmunität.

Der erste Teil dieser Arbeit konnte zur Entdeckung einer kooperativen Genregulation durch mehrere Roquin-Proteine beitragen. Nach aktuellem Wissensstand erkennt Roquin Haarnadelstrukturen sogenannter *cis*-Elemente in der 3'-untranslatierten Region (UTR) von mRNS und induziert dadurch deren Abbau. Diese mRNS kodieren für wichtige Faktoren der T-Zellaktivierung. Wir konnten eine neue Art der Regulation durch Roquin identifizieren, bei welcher mehrere Roquin-Proteine benötigt werden, um essentielle und nicht-essentielle Haarnadelstrukturen in den 3'-UTRs von *Nfkbid* und *Ox40* zu erkennen und somit deren mRNS Abbau einzuleiten. Interessanterweise konnte Roquin nicht nur den mRNS Abbau von *Nfkbid* induzieren, sondern führte auch zur Inhibition der Translation der mRNS. Diese Erkenntnisse sind erste Beweise dafür, dass mehrere Roquin-Proteine zusammenwirken, um eine robuste post-transkriptionelle Genregulation zu ermöglichen.

Im zweiten Teil dieser Arbeit wird eine weitere Ebene der Funktionsweise von Roquin untersucht: seine physische und funktionelle Kooperation mit der Endonuklease Regnase-1. Roquin und Regnase-1 teilen sich ein gemeinsames Set von Ziel-RNS und die Phänotypen von Mäusen mit konditionellen Deletionen von Regnase-1 in T-Zellen ähneln dem Phänotypen der *sanroque* Mäuse sowie Mäusen mit einer T-Zell-spezifischen Deletion von Roquin. Zusätzlich werden die Proteinmengen sowohl von Roquin als auch Regnase-1 in T-Zellen in gleicher Art und Weise kontrolliert, da die Paracaspase MALT1 beide Proteine abhängig von der T-Zellrezeptorstimulation spaltet. Wir adressierten daher experimentell die folgenden Fragen: Warum haben Roquin und Regnase-1 die gleichen Funktionen in T-Zellen und warum wird ihre Expression auf gleiche Weise kontrolliert? Wir stellten die Hypothese auf, dass Roquin und Regnase-1 kooperative Funktionen in T-Zellen ausüben, indem sie zusammen ihre Ziel-mRNS reprimieren, um damit gemeinsam Autoimmunität vorzubeugen. Ein Vergleich der Phänotypen von Mäusen mit T-Zell-spezifischen Deletionen der Roquin Paraloge, Regnase-1 und allen drei Genen zeigte eine neue kooperative Funktion in der Entwicklung

von regulatorischen T-Zellen im Thymus. Zusätzlich konnten wir beweisen, dass Roquin und Regnase-1 zusammen Autoimmunität vorbeugen, insbesondere durch die Kontrolle der Aktivierung von naiven CD4 T-Zellen und ihrer Differenzierung zu follikulären T-Helferzellen sowie IL-17-produzierenden T-Helferzellen (T<sub>H</sub>17 Zellen). Globale Genexpressionsanalysen von CD4 T-Zellen, die kein Roquin und/oder Regnase-1 exprimierten, konnten dazu beitragen, verschiedene Arten von Genregulationen durch Roquin und Regnase-1 zu identifizieren. Diese Analyse zeigte eine Abhängigkeit der meisten Gene von beiden Faktoren. Die Tatsache, dass Roquin und Regnase-1 direkt miteinander interagierten, stärkte das Modell einer kooperativen Funktionsweise.

Zusammengefasst zeigt diese Arbeit, dass die kooperative Genregulation durch Roquin und Regnase-1 einen Schutzmechanismus zur Verhinderung einer übermäßigen Immunantwort darstellt, die potentiell Autoimmunität auslösen kann.

## Table of Content

<b>Eidesstattliche Versicherung .....</b>	<b>5</b>
<b>Summary.....</b>	<b>7</b>
<b>Zusammenfassung .....</b>	<b>9</b>
<b>Table of Content.....</b>	<b>11</b>
<b>List of Figures .....</b>	<b>15</b>
<b>List of Tables .....</b>	<b>17</b>
<b>Abbreviations .....</b>	<b>19</b>
<b>1 Introduction .....</b>	<b>23</b>
<b>1.1 The immune system.....</b>	<b>23</b>
1.1.1 The innate and adaptive immunity.....	23
1.1.2 Central T cell tolerance .....	24
1.1.3 The role of CD4 and CD8 T cells in the immune system .....	25
1.1.4 Co-stimulation of T cells and downstream signaling .....	30
1.1.5 Tolerance mechanisms and the development of autoimmunity .....	34
<b>1.2 Post-transcriptional gene regulation of immune cells .....</b>	<b>37</b>
1.2.1 Principles of induced mRNA decay .....	37
1.2.2 Subcellular locations of mRNA decay .....	39
1.2.3 The interplay of <i>cis</i> -regulatory elements and <i>trans</i> -acting factors .....	40
<b>1.3 The <i>trans</i>-acting factors Roquin and Regnase-1 .....</b>	<b>42</b>
1.3.1 The Roquin protein family .....	42
1.3.2 The endonuclease Regnase-1 .....	47
1.3.3 The overlapping functions of Roquin and Regnase-1 in the control of immune responses.....	51
<b>2 Aim .....</b>	<b>55</b>
<b>3 Material and Methods .....</b>	<b>57</b>
<b>3.1 Material .....</b>	<b>57</b>
3.1.1 Mice .....	57
3.1.2 Cell Culture and cell lines.....	58
3.1.3 Oligonucleotides .....	59
3.1.4 Chemicals and consumables .....	63
3.1.5 Kits, markers and enzymes.....	65
3.1.6 Buffers .....	66
3.1.7 Antibodies .....	67
3.1.8 Cytokines .....	68
3.1.9 Plasmids .....	68
3.1.10 Software and technical devices.....	70
<b>3.2 Methods .....</b>	<b>72</b>

3.2.1	Molecular biology methods.....	72
3.2.2	Cell biology methods.....	74
3.2.3	Biochemical methods.....	80
3.2.4	RNA methods.....	82
3.2.5	Secondary structure prediction of the <i>Nfkbid</i> 3'-UTR.....	83
3.2.6	Next generation sequencing and bioinformatical analysis .....	83
<b>4</b>	<b>Results .....</b>	<b>85</b>
<b>4.1</b>	<b>Roquin recognizes multiple types of <i>cis</i>-elements.....</b>	<b>85</b>
4.1.1	The ROQ domain of Roquin harbors residues required for <i>cis</i> -element recognition in the <i>Ox40</i> 3'-UTR.....	85
4.1.2	<i>Nfkbid</i> is a prototypical Roquin target.....	87
<b>4.2</b>	<b>Investigating the phenotypic consequences of conditional deletion of Roquin and Regnase-1 in T cells .....</b>	<b>99</b>
4.2.1	Published mouse models of Roquin and Regnase-1 .....	99
4.2.2	Analyzing thymic T cell development in mice lacking Roquin- and Regnase-1 in T cells.....	101
4.2.3	Investigating cell-intrinsic effects of Roquin- and Regnase-1-deficiency.....	107
4.2.4	T-cell-specific deletion of Roquin and Regnase-1 induces autoimmunity in mice .....	115
4.2.5	Roquin and Regnase-1 proteins control T cell activation and differentiation..	121
<b>4.3</b>	<b>Analyzing the functional cooperativity of Roquin and Regnase-1 proteins in T cell differentiation.....</b>	<b>125</b>
4.3.1	Roquin and Regnase-1 share a mRNA target set in immune cells .....	125
4.3.2	Roquin and Regnase-1 control overlapping immune-associated target mRNAs .....	127
4.3.3	Global mRNA-sequencing analysis in Roquin and Regnase-1-deficient CD4 T cells .....	129
4.3.4	Analyzing the functional cooperativity of Roquin and Regnase-1 .....	143
<b>5</b>	<b>Discussion .....</b>	<b>151</b>
<b>5.1</b>	<b>Binding of multiple Roquin proteins enables a cooperative post-transcriptional gene regulation of complex <i>cis</i>-regulatory elements.....</b>	<b>151</b>
5.1.1	Roquin-mediated regulation involves <i>cis</i> -elements with multiple binding sites .....	151
5.1.2	Roquin controls mRNA stability by integrating multiple decay pathways .....	154
<b>5.2</b>	<b>The cooperative molecular function of Roquin and Regnase-1 in T cells ...</b>	<b>155</b>
5.2.1	Identifying new target genes of Roquin and Regnase-1 .....	156
5.2.2	Roquin and Regnase-1 enable distinct ways of cooperativity .....	158
5.2.3	The physical interaction of Roquin and Regnase-1 supports the concept of cooperativity.....	161
<b>5.3</b>	<b>Roquin and Regnase-1 are essential regulators of T cell-mediated immune responses .....</b>	<b>162</b>
5.3.1	Deficiency of Regnase-1 in T cells affects the cellular composition in the thymus due to cell-extrinsic effects.....	162
5.3.2	Roquin and Regnase-1 control T cell development.....	163



---

5.3.3	Roquin and Regnase-1 cooperatively prevent autoimmunity.....	167
5.3.4	Roquin- and Regnase-1-deficiency causes expansion of non-functional T <sub>reg</sub> cells in the periphery .....	171
5.3.5	The fate of T <sub>H</sub> 17 cells is under control of Roquin and Regnase-1.....	172
5.3.6	Summarizing the phenotypes of different Roquin and Regnase-1 mouse models .....	175
5.3.7	Can we connect the mouse phenotypes with the global mRNA expression data?.....	176
5.3.8	How does the observed cooperativity of Roquin and Regnase-1 fit with recent concepts?.....	177
<b>5.4</b>	<b>Conclusions, model and future perspectives .....</b>	<b>178</b>
	<b>Literature .....</b>	<b>183</b>
	<b>Appendices.....</b>	<b>199</b>
	<b>Publications.....</b>	<b>206</b>
	<b>Presentations .....</b>	<b>207</b>
	<b>Acknowledgement .....</b>	<b>208</b>



## List of Figures

Figure 1   Schematic representation of CD4 T cell differentiation into T helper cell subsets. ....	27
Figure 2   The principles of mRNA decay.....	38
Figure 3   Domain organization and sequence similarity of Roquin family proteins. ....	44
Figure 4   RNA structures and sequences targeted by Roquin.....	45
Figure 5   Domain organization of Regnase family proteins. ....	49
Figure 6   Current models of Roquin- and Regnase-1-mediated gene regulation. ....	52
Figure 7   Schematic representation of genetically modified alleles of <i>Rc3h1</i> , <i>Rc3h2</i> and <i>Zc3h12a</i> .....	57
Figure 8   Schematic representation of T cell culture under T <sub>H</sub> 1 conditions.....	75
Figure 9   Schematic representation of T cell culture under T <sub>H</sub> 1 conditions with 4'OH-tamoxifen-induced gene deletion.....	76
Figure 10   Schematic representation of T cell culture under T <sub>H</sub> 1 conditions with 4'OH-tamoxifen-induced gene deletion and retroviral transduction.....	77
Figure 11   Schematic representation of <i>in vitro</i> differentiation of naïve T cells deleted by tamoxifen gavage <i>in vivo</i> .....	79
Figure 12   Common flow cytometry gating strategy for splenocytes and thymocytes using the software FlowJo. ....	80
Figure 13   Mutational analysis of Roquin-1 for the regulation of Ox40 and Icos. ....	86
Figure 14   Defining the minimal response element of the <i>Nfkbid</i> 3'-UTR for Roquin-mediated regulation.....	88
Figure 15   The <i>Nfkbid</i> 3'-UTR minimal response element harbors six conserved stem loops. ....	90
Figure 16   Mutational analysis of loop structures within the <i>Nfkbid</i> minimal response element.....	92
Figure 17   Mutational analysis of stem sequence within the <i>Nfkbid</i> minimal response element.....	93
Figure 18   Introducing Loop Exchange (LE) mutations in SL1, SL2 and SL5. ....	94
Figure 19   Analyzing the contribution of multiple stem loops in the <i>Nfkbid</i> 3'-UTR for Roquin-mediated regulation. ....	95
Figure 20   <i>Nfkbid</i> regulation requires Roquin-1 to interact with at least three SLs.....	96
Figure 21   Polysome Profiling of <i>Nfkbid</i> mRNA in WT and Roquin-deficient CD4 T cells. ...	97
Figure 22   Validation of knockouts in <i>Rc3h1</i> <sup>fl/fl</sup> ; <i>Zc3h12a</i> <sup>fl/fl</sup> ; <i>Cd4-cre</i> (TKO <sup>T</sup> ) mice. ....	101
Figure 23   Determination of thymic T cell development in Roquin- and Regnase-1-deficient mice. ....	102
Figure 24   Analyzing positive selection and maturation of SP T cells in TKO <sup>T</sup> mice. ....	104
Figure 25   Altered thymic T <sub>reg</sub> development in KO <sup>T</sup> and TKO <sup>T</sup> mice.....	105
Figure 26   Analyzing IκB <sub>NS</sub> and cRel protein expression during thymic T <sub>reg</sub> development..	106
Figure 27   Generation of mixed bone marrow chimeric mice.....	108
Figure 28   T cell development in WT <sup>45.1</sup> / TKO <sup>T</sup> CD45.2 mixed BM chimera mice.....	109
Figure 29   Investigating positive selection in thymi of mixed BM chimera mice. ....	110

Figure 30	Determination of apoptosis in thymi of mixed BM chimeric mice. ....	111
Figure 31	Altered frequencies of regulatory T cells in thymi of mixed bone marrow chimeric mice. ....	112
Figure 32	Impaired T <sub>reg</sub> development in TKO <sup>T</sup> CD45.2 cells of mixed BM chimeric mice. ....	114
Figure 33	Analysis of the T cell composition in spleens and lymph nodes of mice with a T cell-specific deletion of Roquin and Regnase-1. ....	115
Figure 34	Discrimination of naïve, central-memory and effector-memory T cells in mice with a T cell-specific ablation of Roquin and Regnase-1. ....	116
Figure 35	Analyzing the GC reaction and antibody response of mice with T cell-specific deletion of Roquin and Regnase-1. ....	117
Figure 36	Determining frequencies and absolute numbers of Foxp3-expressing CD4 T cells in mice conditionally deleted for Roquin and Regnase-1 in T cells. ....	118
Figure 37	Flow cytometry analysis of splenocytes from mixed bone marrow chimeric mice. ....	119
Figure 38	Analyzing T <sub>FH</sub> , T <sub>FR</sub> and T <sub>reg</sub> populations in splenocytes from mixed bone marrow chimeric mice. ....	120
Figure 39	<i>Ex vivo</i> cytokine expression levels of CD4 T cells from WT, DKO <sup>T</sup> , KO <sup>T</sup> and TKO <sup>T</sup> mice. ....	122
Figure 40	Flow cytometry analysis of naïve CD4 T cells from WT, iDKO, iKO and iTKO mice differentiated into T <sub>H</sub> 1, T <sub>H</sub> 17 and T <sub>reg</sub> cells. ....	123
Figure 41	Protein and RNA expression levels of known Roquin and Regnase-1 targets in WT, iDKO and iKO CD4 T cells. ....	128
Figure 42	Validation of the inducible triple knockout (iTKO) of Roquin and Regnase-1. ....	129
Figure 43	Schematic overview of T <sub>H</sub> 1 cell culture for mRNA-sequencing experiment. ....	130
Figure 44	Quantitative analysis of the overall gene expression in unstimulated and restimulated WT, iDKO, iKO and iTKO CD4 T cells. ....	131
Figure 45	Cluster analysis of genes identified by mRNA-sequencing in WT, iDKO, iKO and iTKO CD4 T cells. ....	132
Figure 46	Analyzing gene expression of <i>Hdac2</i> and potential target genes thereof in cluster 3. ....	135
Figure 47	Hierarchical clustering of genes identified in cluster 4. ....	138
Figure 48	Genes identified by mRNA-sequencing in Cluster 2 and 4 and RT-qPCR validation thereof. ....	139
Figure 49	<i>Icos</i> , <i>Ox40</i> , <i>D1ertd622e</i> and <i>Ctla4</i> expression in Roquin- and Regnase-1-deficient CD4 T cells. ....	142
Figure 50	Flow cytometry analysis of Roquin and Regnase-1 targets in splenocytes of WT, KO <sup>T</sup> , DKO <sup>T</sup> and TKO <sup>T</sup> mice. ....	144
Figure 51	Reconstitution of Roquin and Regnase-1 in WT and Roquin-deficient CD4 T cells. ....	145
Figure 52	Reconstitution of Regnase-1 in WT and Roquin-deficient CD4 T cells. ....	147
Figure 53	Proving direct interaction of Roquin and Regnase-1 by co-immunoprecipitation. ....	148
Figure 54	Schematic representation of different types of regulation by Roquin and Regnase-1. ....	159
Figure 55	Model for changes in the selection processes in mice with a T-cell-intrinsic deletion of Roquin and Regnase-1. ....	166
Figure 56	Model for Roquin- and Regnase-1-mediated gene regulation in CD4 T cells. ...	179

## List of Tables

Table 1   Mouse lines utilized in this thesis. ....	58
Table 2   Cell lines utilized in this study.....	58
Table 3   Cell Culture components and media for mouse embryonic fibroblast (MEF) and T cell culture.....	59
Table 4   DNA oligonucleotides for cloning.....	59
Table 5   DNA oligonucleotides and probes from the Universal Probe Library (UPL) system (Roche) used for RT-qPCR analyses.....	62
Table 6   Chemicals and consumables. ....	63
Table 7   Kits and markers. ....	65
Table 8   Enzymes.....	65
Table 9   Buffers. ....	66
Table 10   Antibodies used for flow cytometry, immunoblotting and T cell cultures. ....	67
Table 11   Cytokines used for T cell cultures.....	68
Table 12   Retroviral expression plasmids.....	69
Table 13   Entry vectors for Gateway cloning.....	70
Table 14   Software.....	70
Table 15   Technical devices and instruments.....	70
Table 16   Reagents and PCR-cycle conditions used in a standard PCR reaction. ....	72
Table 17   Antibody and cytokine concentrations for T helper cell differentiations.....	78
Table 18   Comparison of previously published phenotypes in <i>sanroque</i> mice and mice deficient for Roquin-1, Roquin-2 and Regnase-1 in T cells.....	100
Table 19   Previously published Roquin-1/2, <i>sanroque</i> and Regnase-1 target genes in cells of the immune system. ....	125
Table 20   Differential expressed genes identified in cluster 2.....	136
Table 21   Differential expressed genes identified in cluster 4.....	137
Table 22   Definition of different types of gene regulation by Roquin and Regnase-1 by $\log_2(\text{FC})$ expression in mRNA-sequencing analyses. ....	140
Table 23   Comparing phenotypes of <i>Cd4</i> -cre driven deletions of Roquin and Regnase-1 mouse models and mixed bone marrow chimeric mice. ....	175



## Abbreviations

Human genes and proteins are written in capital letters.

Mouse genes and proteins are written in lowercase.

-/-	knockout
$\alpha$	alpha
$\beta$	beta
$\delta$	delta
$\gamma$	gamma
$\kappa$	kappa
$\lambda$	lambda
$\mu$	micro
$\zeta$	zeta
%	percent
°C	degree celsius
3'	3 prime
4'OH-tamoxifen	4'hydroxy-tamoxifen
5'	5 prime
A	adenine
A	alanine (Ala)
aa	amino acid
ab	antibody
ADE	alternative decay element
ANA	anti-nuclear antibody
APC	antigen-presenting cell
ARE	AU-rich element
ATP	adenosine triphosphate
BCR	B cell receptor
BM	bone marrow
BM	bone marrow
bp	base pairs
BSA	bovine serum albumin
C	cytosine
C-terminus	carboxy-terminus
CAR	chimeric antigen receptor
CCR	C-C chemokine receptor type
CD	cluster of differentiation
CDE	constitutive decay element
CDS	coding sequence
CLIP	cross-linking immunoprecipitation
D	aspartic acid (Asp)
DC	dendritic cell
DKO	double knockout
DMEM	Dulbecco's Modified Eagle Medium
DMSO	dimethyl sulfoxide
DN	double negative
DNA	desoxyribonucleic acid

dNTP	desoxyribonucleosidetriphosphate
dox	doxycycline
DP	double positive
DTT	dithiothreitol
ECL	enhanced chemiluminescence
EDTA	ethylenediaminetetraacetic acid
ELISA	enzyme-linked immunosorbent assay
EMSA	electrophoretic mobility shift assay
ERT2	estrogen-receptor type 2
FACS	fluorescence-activated cell sorting
FBS	fetal bovine serum
FC	fold-change
FCS	fetal calf serum
fl	full length
Foxp3	forkhead-box-protein P3
FSC	forward scatter
g	gram
GC	germinal center
GFP	green-fluorescent protein
GO	gene ontology
Gy	gray
h	hour
H <sub>2</sub> O	water
HBS	Hank's balanced salt solution
HEK	human embryonic kidney cells
HEPES	4-(2-hydroxyethyl)-1-piperazineethanesulfonic acid
HEPN	higher eukaryotes and prokaryotes nucleotide-binding domain
HITS-CLIP	high-throughput sequencing of RNA isolated by crosslinking immunoprecipitation
HRP	horseradish peroxidase
Icos	inducible T cell co-stimulator
IFN	interferon
Ig	immunoglobulin
IL	interleukin
iono	ionomycin
IP	immunoprecipitation
IRES	internal ribosome entry site
Irf	interferon regulatory factor
K	lysine (Lys)
kb	kilo base pair
kd	knockdown
kDa	kilodalton
KO	knockout
L	Leucine (Leu)
LB	lysogeny broth
LBE	linear binding element
LE	loop exchange mutation
LM	loop mutation
LN	lymph node
m	milli
M	molar



M	methionine (Met)
MCPIP	monocyte chemotactic protein-induced protein
MEF	mouse embryonic fibroblast
MFI	median fluorescent intensity
MHC	major histocompatibility complex
min	minutes
Mio	million
mRNA	messenger RNA
n	nano
N	asparagine (Asn)
N-terminus	amino-terminus
NaCl	sodium chloride
NKT	natural killer T cell
nm	nanometer
NMD	nonsense-mediated decay
nt	nucleotide
OD	optical density
ON	over night
P	phosphate
PABP	poly(A)-binding protein
PAGE	polyacrylamide gel electrophoresis
PAR-CLIP	photoactivatable-ribonucleoside-crosslinking immunoprecipitation
PBS	phosphate buffer saline
PI	protease inhibitor
PRR	proline-rich region
PTM	post translational modification
pu	purine base
PVDF	polyvinylidene difluoride
py	pyrimidine base
R	arginine (Arg)
RA	rheumatoid arthritis
rad	radiation absorbed dose
RBP	RNA-binding protein
RIP	RNA Immunoprecipitation
RNA	ribonucleic acid
RPF	ribosome-protected fragment
rpm	rounds per minute
RSM	reversed stem mutation
RT	room temperature
S	serine (Ser)
san	sanroque mutation (M199R)
SDS	sodium dodecyl sulfate
sec	second
seq	sequencing
SL	stem loop
SLE	systemic lupus erythematosus
SM	stem mutation
SP	single positive
T	threonine (Thr)
tam	tamoxifen

---

TBS	tris-buffered saline
TCR	T cell receptor
T <sub>FH</sub>	T follicular helper cell
T <sub>H</sub>	T helper cell
TKO	triple knockout
TNF	tumor necrosis factor
T <sub>reg</sub>	regulatory T cell
TTP	tristetraprolin
U	units
U	uracil
UT	untransduced
UTR	untranslated region
UV	ultraviolet
V	volt
v/v	volume per volume
vs	versus
w/v	weight per volume
WB	Western blot
WT	wild-type
Y	tyrosine (Tyr)
ZnF	zinc finger

---

# 1 Introduction

## 1.1 The immune system

Our body is exposed to pathogens, toxins, and environmental cues throughout its lifetime. To ensure health and survival, the immune system has evolved and found ways to defend against foreign microorganisms including viruses, bacteria, fungi, and parasites. Anatomic and chemical barriers like the skin epithelium or the complement system are the most primitive ways of protection against harmful organisms. Since pathogens have evolved to evade these relatively simple barriers, vertebrates developed a more specialized host defense: the innate and the adaptive immune system.

### 1.1.1 The innate and adaptive immunity

All immune cells derive from pluripotent hematopoietic stem cells of the bone marrow that diverge into two types of stem cell lineages: Stem cells either give rise to a common lymphoid progenitor that comprises the lymphoid lineage of leukocytes formed by T and B lymphocytes, natural killer cells (NK) and innate lymphoid cells (ILC) or a common myeloid progenitor that gives rise to cells of the innate immune system such as macrophages, granulocytes, mast cells and dendritic cells. The innate immune cells exhibit protective function by recognizing infections, sensing foreign pathogens and directly mediating clearance of pathogens or recruiting cells of the adaptive immune response. These processes are based on the recognition of pathogen-associated molecular patterns (PAMPs) via pattern recognition receptors (PRRs) for example the toll-like receptors (TLRs) on the cell surface of innate immune cells. (Janeway and Medzhitov, 2002). Activation of PRRs on macrophages or neutrophils directly induces phagocytosis of bacteria but can in turn cause inflammation via secretion of cytokines and chemokines. However, the innate immune cells are only capable of recognizing invariant molecules, that are shared by multiple pathogens, but are incapable of recognizing pathogen-specific structures and defending the host from reinfections (Murphy and Weaver, 2017).

The lymphoid lineage is composed of T and B lymphocytes as well as NK cells and ILCs, whereas the latter have been described as more “innate” lymphocytes. NK cells are large lymphoid-like cells that directly eliminate infected target cells. Besides a lymphoid morphology, ILCs are described for their protective role in early immune responses especially at epithelial

barriers (Neill and Flynn, 2018). In contrast to cells of the innate immune response, T and B lymphocytes have evolved ways to fight pathogens in a more specialized and sensitive manner: Different from NK and ILCs, T and B lymphocytes carry a highly variable clonal antigen-receptor that facilitates recognition of a unique foreign antigen. Therefore, lymphocytes can detect a multiplicity of pathogens and are capable to generate memory to rapidly respond to reinfections with the same pathogen.

B cells mature in the bone marrow and express the B-cell receptor (BCR). As soon as the BCR encounters antigen, naïve B-lymphocytes differentiate towards plasma cells that are specialized to produce their antigen receptor in two forms: soluble antibodies (immunoglobulins) or membrane-bound BCRs. Besides antibodies, also BCRs directly engage with the epitope of the respective antigen in the extracellular fluids including interstitial and intravascular compartments.

In turn, T lymphocytes arise and mature in the thymus and carry the T cell receptor (TCR), which recognizes protein-antigens only if presented on MHC-molecules (major histocompatibility complex) on the surface of various cell types including antigen-presenting cells (APCs). Receptors of the adaptive immune system (BCR and TCR) are encoded by gene segments that undergo somatic rearrangement, which is termed V(D)J-recombination. Gene rearrangement of variable (V), diversity (D) and joining (J) regions during cell maturation is mediated by RAG proteins (recombination-activating gene) (Grawunder et al., 1998). This somatic recombination occurs independently in individual lymphocytes and results in a polyclonal receptor repertoire of  $10^{13}$ - $10^{18}$  (Nikolich-Zugich et al., 2004). As soon as the receptor on a naïve mature lymphocyte encounters its cognate foreign antigen, the cell is activated and starts to divide, thereby serving as a “clone” for identical progeny with the same receptor-antigen-specificity. The model of clonal selection was first proposed in the 1950s by Macfarlane Burnet, who set a milestone for the understanding of T cell immunity (Burnet, 1962).

### **1.1.2 Central T cell tolerance**

Removing thymi from young mice (thymectomy) results in a drastic immunodeficiency, emphasizing the importance of this lymphoid organ in maintaining a functional immune response (Metcalf, 1960). Common lymphoid progenitors from the bone marrow enter the thymus where they become mature T lymphocytes (T cells). T cells characteristically express either CD4 or CD8 co-receptors, which classifies them as T helper cells (CD4<sup>+</sup>) or cytotoxic T cells (CD8<sup>+</sup>). CD4 interacts with MHC II (class 2) expressed on antigen-presenting cells like macrophages, dendritic cells and B cells, whereas CD8 recognizes MHC I (class 1) that is

expressed on all cells and recruits its ligands from endogenous polypeptide degradation products thereby displaying antigens derived from endogenous or viral peptides.

The process of T cell maturation can last up to 7 days and starts with immature T cells that neither express CD4 or CD8 nor the TCR and accessory molecules (CD3). Within this double negative (DN) stage, cells are sub-divided into DN1, DN2, DN3 and DN4 stages defined by their characteristic surface expression of CD44, CD25 and CD117 (cKit). The pre-TCR development during DN3 and DN4 and successful rearrangement of TCR  $\beta$  and  $\alpha$  chains further induces the expression of both CD4 and CD8 resulting in double-positive thymocytes (DP). During subsequent maturation steps, the expression of one co-receptor is lost, resulting in CD4 and CD8 single positive (SP) T cells (Murphy and Weaver, 2017).

To prevent reactivity of the TCR to self-antigens, T cells go through several selection processes termed clonal selection. The widely-accepted affinity hypothesis proposes that positive and negative selection of thymocytes depend on the affinity of the TCR to self-peptide:MHC complexes (p:MHC) presented by thymic epithelial cells (Klein et al., 2014). Studies in TCR-transgenic mice have emphasized that positive selection in the thymic cortex is induced by low-affinity p:MHC interaction, whereas negative selection in the medulla is favored by high-affinity agonists leading to clonal deletion by apoptosis to prevent self-reactivity (Daniels et al., 2006). In contrast, no or very low affinity interactions of lymphocytes with p:MHC causes death by neglect. Interestingly, a subgroup of CD4 T helper cells termed regulatory T cells ( $T_{reg}$ ) derive from T cells that encounter stronger TCR p:MHC interaction than positively selected T cells, but still show less affinity than those dying by negative selection (Jordan et al., 2001). These specialized T cells function to dampen an overshooting immune response and prevent autoimmunity. However, the concept of selection in the thymus is highly controversial, since some studies propose that most of the clonal deletion occurs at the DP stage in the thymic cortex independent from processes in the medulla (McCaughy et al., 2008; Stritesky et al., 2013). These controversial findings may arise primarily due to the use of different model systems such as TCR transgenic mice that express their TCR early at DN stages and therefore do not represent physiological TCR expression or models with endogenous superantigens that fail to copy Ag-specific clonal deletion.

### **1.1.3 The role of CD4 and CD8 T cells in the immune system**

After maturation in the thymus, mature naïve, self-tolerant CD4 and CD8 T cells migrate to secondary lymphoid organs (spleen and lymph nodes) constantly searching for dendritic cells that carry the cognate peptide ligand to their TCR, the recognition of which by the naïve T cell is called the priming step. After establishing the contact of APC and naïve T cell by adhesion molecules, the T cell scans the APCs for its cognate p:MHC ligand. In order to fully activate

the T cell and cause differentiation and proliferation, it is obligatory for the T cell to receive three major signals: 1. Binding of the TCR and CD4 or CD8 co-receptor to p:MHC II or I (Chen and Flies, 2013). 2. Stimulation of a co-stimulatory receptor like CD28 or Icos on the T cell by B7 or IcosL molecules from the same APC (Gonzalo et al., 2001). 3. Sensing of cytokines in the environment. These three signals convey activation, survival and differentiation of T cells by translating signals from outside the cells into intracellular signaling pathways. The combined downstream activation of AP-1, NFAT (nuclear factor of activated T cells) and NF- $\kappa$ B (nuclear factor  $\kappa$ B) signaling pathways is essential for the production of the hallmark cytokine IL-2 which drives T cell proliferation and activation (Hoefig and Heissmeyer, 2018).

Antigen-specific CD8 T cells recognize virus-infected cells, clear those cells and form memory. Prior to developing this function, naïve CD8 T cells get their first contact to foreign cognate antigen loaded on MHC class I on DCs in the subcapsular sinus region or the interfollicular region of the draining lymph node (Hickman et al., 2008; John et al., 2009). Additional co-stimulation and inflammatory cytokines in the microenvironment contribute to full activation of cytotoxic CD8 T cells. Through re-entering in the lymphatic system and blood stream, activated CD8 T cells reach the site of infection and, upon antigenic stimulation, destroy infected cells via the secretion of granzymes or perforin subsequently inducing apoptosis of the target cell (Barber et al., 2003). Interestingly, viruses have evolved strategies to downregulate MHC class I molecules, which allows escape from CD8-mediated clearance (Halenius et al., 2015). Very recently, non-recirculating tissue-resident memory CD8 T cells ( $T_{RM}$ ) that lack molecules necessary for migration (such as Klf2, S1PR1, Ccr7) but express residency markers (such as CD103 or CD69) have been identified to derive from T cells that enter tissues during a primary immune response and then reside at the site of a cleared infection in skin, lung and gut. Interestingly, CD103<sup>+</sup>  $T_{RM}$  cells are highly abundant at solid tumor sites and their proportion is positively correlating with tumor clearance and good prognosis, making this cell type a promising tool for anti-tumor immunity (Amsen et al., 2018).

Besides CD8 T cells, CD4 T helper cells are an essential component of the adaptive immune system. They specifically contribute to clear bacterial or viral infections by providing help to other immune and non-immune cells and form memory to be re-activated upon a secondary infection. CD4 T cells can comprise different T helper cell ( $T_H$ ) subsets amongst them  $T_H1$ ,  $T_H2$ ,  $T_H17$ , follicular T helper cells ( $T_{FH}$ ) and induced regulatory T cells ( $iT_{reg}$ ) which can be distinguished by their characteristic expression of subset-specifying transcription factors and hallmark cytokine secretion (Sallusto, 2016) (**Figure 1**). The differentiation into these subsets results from integrating TCR and co-stimulatory receptor signaling with signal transduction from cytokine receptors. The latter causes phosphorylation of cytoplasmic signal transducer and activator of transcription (Stat) proteins, followed by nuclear translocation of homodimers that further induce expression of the subset-specific master transcription factors (O'Shea et

al., 2011). Besides a complex network of transcription factors, post-transcriptional regulators such as micro RNAs (miRNAs) and RNA-binding proteins (RBPs) function in cell fate decisions of T cells. Here, the turnover of mRNAs encoding for important factors that drive fate decisions of T cells during stimulation (through cytokine or co-stimulatory receptors) are controlled, thus providing a mechanism to rapidly respond to environmental changes. The miRNA cluster miR-17-92 and individual miRNAs thereof have been demonstrated to function in T cell differentiation (Baumjohann, 2018).

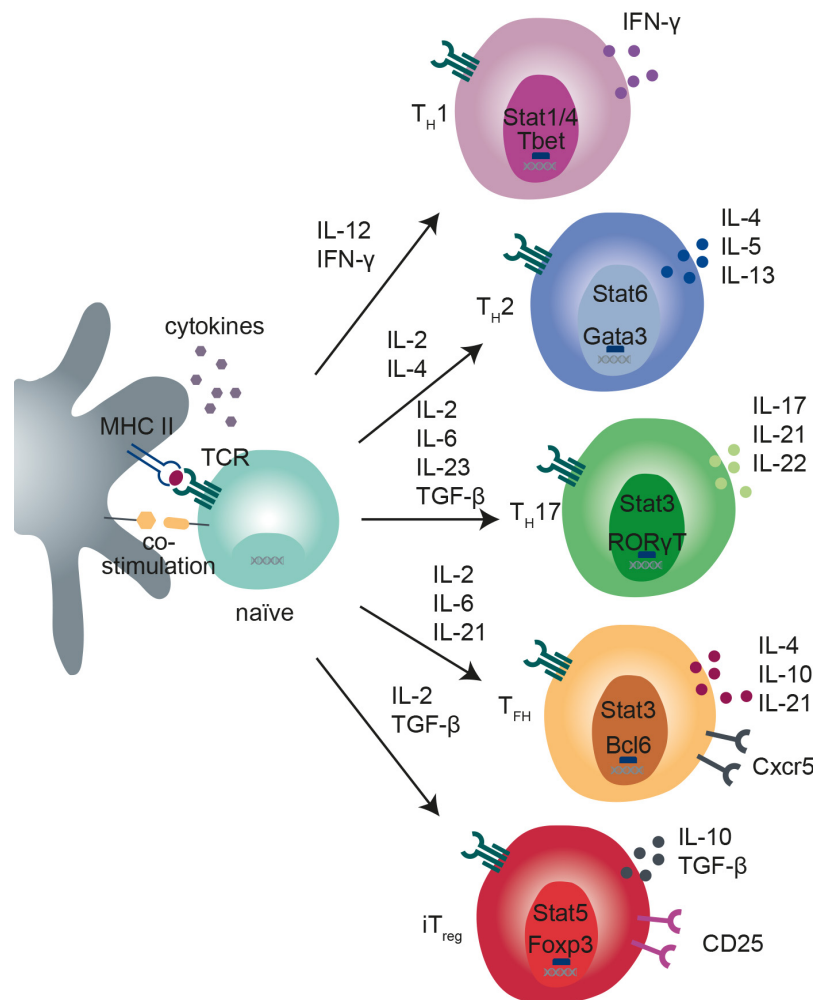


**Figure 1 | Schematic representation of CD4 T cell differentiation into T helper cell subsets.**

Differentiation of naïve CD4 T cells into TH1, TH2, TH17, TFH and iT<sub>reg</sub> results from incorporating TCR stimulation by peptide-loaded MHC II and co-stimulation by an antigen-presenting cell in the presence of a specific cytokine milieu (shown by arrows). Cytokine receptor signaling on CD4 T cells results in phosphorylation, activation and nuclear translocation of Stat proteins that then further induce the expression of the hallmark transcription factors of the different T helper cell subsets (shown in the nucleus). These specific signaling cascades result in a unique expression of receptors and secretion of pro- (TH1, TH2, TH17 and TFH) or anti-inflammatory (iT<sub>reg</sub>) cytokines.

Additionally, lineage commitment is strictly connected to epigenetic changes at lineage-specific gene loci, since transcriptional changes are fixed epigenetically by altered chromatin states,

unique enhancer landscapes and a complex network of transcriptional activators and repressors (Kanno et al., 2012).

T<sub>H</sub>1 cells provide pro-inflammatory help in case of intracellular infections with microorganisms including viruses, protozoa and bacteria. The differentiation of naïve T cells to T<sub>H</sub>1 cells is caused through an initial IL-12 and subsequent IFN- $\gamma$  receptor signaling thereby activating Stat4 and Stat1 proteins. These Stat proteins together function in the transcriptional activation of Tbet, which is the hallmark transcription factor of T<sub>H</sub>1 cells. Tbet itself induces gene expression of IFN- $\gamma$ , thus acting as a positive feedback loop for further T<sub>H</sub>1 differentiation (Amsen et al., 2009; Mosmann et al., 1986). Moreover, T<sub>H</sub>1 cells are an important source of IL-2, which augments CD4 and CD8 effector T cell functions and proliferation. Additionally, IFN- $\gamma$  production helps to clear intracellular infections by induction and activation of macrophages.

The T<sub>H</sub>2 subset is involved in clearing infections with parasites, especially helminths by secretion of the cytokines IL-4, IL-5 and IL-13 and moreover contributes to allergic immunopathology. The production of IL-5 causes recruitment of eosinophils which then produce major basic protein to directly kill parasites, whereas IL-4 and IL-13 secretion recruit macrophages that enhance tissue repair at sites of infections (Kouro and Takatsu, 2009). The development of T<sub>H</sub>2 cells is driven by the cytokine IL-4, whereas IL-4 receptor signaling further causes activation of Stat6, which in turn translocates to the nucleus and stimulates the expression of the T<sub>H</sub>2-specific transcription factor Gata3 (Zheng and Flavell, 1997). Gata3 provides a positive feedback loop by inducing its own transcription as well as IL-4 and promoting transcription of IL-13 (Ouyang et al., 2000).

Upon infection with extracellular bacteria and fungi, the secretion of IL-6 and TGF- $\beta$  by innate immune cells induces the differentiation of the T<sub>H</sub>17 subset. Engagement of IL-6 with its receptor induces downstream activation of the transcription factor Stat3, which further causes expression of the master regulator ROR $\gamma$ t that directly acts on the transcription of the signature cytokine IL-17 (Ghoreschi et al., 2010). The release of the IL-17 family members IL-17A and IL-17F leads to the recruitment of neutrophils to sites of infection and causes stimulation of fibroblasts and epithelial cells carrying IL-17 receptors to produce IL-6 which further amplifies the T<sub>H</sub>17 response. The expansion of T<sub>H</sub>17 cells additionally requires the cytokine IL-23 (Ouyang et al., 2008). Interestingly, the propagation of autoimmune diseases such as experimental autoimmune encephalomyelitis (EAE) in mice is attributed to T<sub>H</sub>17 cells, since neutralization of IL-17 secretion with a monoclonal antibody prevents the onset of disease (Hofstetter et al., 2005; Komiyama et al., 2006). Therefore, it is proposed that an imbalance of these T cell subsets may lead to tissue inflammation.



Intriguingly, an additional subset of T helper cells is induced by TGF- $\beta$ , which is termed induced regulatory T cells (iT<sub>reg</sub>). Unlike the previously described T helper cell subsets, regulatory T cells have immune-repressive activity and thereby prevent autoimmunity. The plasticity of T<sub>reg</sub> and T<sub>H</sub>17 cells is critical to keep immune homeostasis (Knochelmann et al., 2018). Disruption of regulatory T cell function or removal contributes to a vast number of autoimmune and inflammatory pathologies (Sakaguchi et al., 1995; Shevach, 2000), whereas dominance of T<sub>H</sub>17 responses have been associated to autoimmunity in humans. Different from T<sub>H</sub>17 cells, regulatory T cells are not induced by the pro-inflammatory cytokines IL-6 and IL-23. Unlike, the development of thymic T<sub>reg</sub> (tT<sub>reg</sub>) cells, which has been described previously (**chapter 1.1.2**), a smaller proportion of T<sub>reg</sub> cells is induced in the periphery (iT<sub>reg</sub>) promoted by high doses of TGF- $\beta$  and IL-2, which induces the expression of the hallmark transcription factor Foxp3 and the IL-2 receptor CD25 (Sakaguchi et al., 2008). The expression of the inhibitory co-stimulatory receptor Ctla-4 allows iT<sub>reg</sub> cells to compete with naïve CD4 T cells for their interaction with CD28 on APCs, since Ctla-4 and CD28 share the costimulatory ligands CD80 and CD86 on APCs. Thus, regulatory T cells prevent signals for activation of naïve T cells (Yamaguchi et al., 2013). Additionally, Ctla-4 controls the expression of CD28-ligands on APCs cell-extrinsically by trans-endocytosis thereof into Ctla-4-expressing cells (Qureshi et al., 2011). The suppressive capacity of regulatory T cells is further maintained by production of anti-inflammatory cytokines like TGF- $\beta$  and IL-10. TGF- $\beta$  secretion acts as a positive feedback loop for T<sub>reg</sub> induction and T<sub>H</sub>17 differentiation, whereas IL-10 has inhibitory function on T<sub>H</sub>1 cells. In contrast to the previously described T helper cell subsets, follicular T helper cell (T<sub>FH</sub>) differentiation is a two-step process. Their capability of providing help to B cells in germinal centers (GC) of secondary lymphoid organs during an infection, makes them a central component of the humoral immune response. Upon T cell activation and co-stimulation in the presence of the cytokines IL-6, IL-21 and TGF- $\beta$ , a pre-T<sub>FH</sub> stage is formed in the T-cell zone of the follicle characterized by high levels of PD-1 (programmed cell death protein 1) and Icos, which is complemented by increased expression of the hallmark transcription factor Bcl-6. By elevated abundance of Cxcr5, the cells migrate to the T-B-cell border within the B cell follicle, where T and B cells interact by offering signals required to induce GC reaction of both cell types. The B cell provides the T<sub>FH</sub> cell with antigenic stimulation and stimulatory and inhibitory signals (CD80, CD86, IcosL, Ox40L, PD-L1/2), whereas secretion of IL-21 and IL-4 as well as expression of CD40L by the T<sub>FH</sub> cell prompts B cell entry in the follicle. Here, B cells proliferate and differentiate into memory B cells or antibody-secreting plasma cells by undergoing somatic hypermutation thus shaping the humoral immune response (Webb and Linterman, 2017). In mouse models for systemic lupus erythematosus such as the Bxd2 mice, autoimmunity is

caused by aberrant frequencies of follicular T helper cells that directly correlate with the abundance of autoreactive GC B cells and production of autoantibodies (Kim et al., 2015).

Recently, thymic-derived Foxp3-expressing T cells in the GC were characterized as follicular regulatory T cells ( $T_{FR}$ ). They share  $T_{FH}$ -hallmarks like PD-1, Cxcr5 and Bcl6 expression and additionally express Foxp3, but are distinct from both T cell subtypes.  $T_{FR}$  cells have regulatory function thereby restraining the GC response and controlling  $T_{FH}$  development, but the distinct purpose of this T cell subset has not been completely solved yet (Linterman et al., 2011).

T helper cell differentiation is a highly complex process. Differentiation into one T helper cell lineage is often accompanied by inhibitory signals for reciprocally developing CD4 T cell subsets. For example,  $T_H2$ -promoting IL-2/Stat5 signaling blocks differentiation of  $T_H17$  differentiation (Yamane and Paul, 2013). Recent research has provided several examples of T cell differentiation with a high degree of plasticity, indicating that the process is far more complex than hypothesized and differentiation into the one or the other lineage is not as definite as initially thought.

#### **1.1.4 Co-stimulation of T cells and downstream signaling**

The T cell receptor (TCR) is a multiprotein complex that intracellularly comprises immunoreceptor tyrosine-based activation motifs (ITAMS). After cognate antigen binding to the TCR and stabilization by CD4 or CD8 co-receptors, Src-family kinases phosphorylate tyrosine residues on ITAMs, which initiates complex signaling cascades by recruiting scaffold proteins and activating multiple downstream signaling pathways. This signaling cascade ultimately results in the activation of three major transcription factors (AP-1, NFAT and NF- $\kappa$ B) crucial for expression of the cytokine IL-2, which is essential for T cell proliferation and survival. However, signal from the TCR requires additional signals from co-stimulatory receptors to achieve full activation. The classical “two-signal model” first proposed in 1970 that full activation of T cells requires engagement of the TCR with peptide-loaded MHC as well as co-stimulatory signals (Bretscher and Cohn, 1970). Since then, co-stimulatory receptors have been identified that can, together with TCR signaling, transduce extracellular stimulation either into positive or negative signals inside the T cells by further triggering signaling cascades that induce differentiation and peripheral T cell homeostasis (Chen and Flies, 2013). Most co-stimulatory molecules belong to either the tumor necrosis factor receptor superfamily (Tnfrsf) or the immunoglobulin superfamily (IgSF) and both inhibitory and stimulatory receptors are dynamically expressed dependent on the activation status of the T cell (Zhu et al., 2011).

#### 1.1.4.1 The CD28 receptor family

The best studied IgSF co-stimulatory receptors are the CD28 gene family proteins. CD28, cytotoxic T lymphocyte antigen 4 (Ctla-4) and inducible co-stimulator (Icos) are expressed from a gene cluster on the mouse chromosome 1, proposing that these genes derived from gene duplication (Ling et al., 2001). CD28 and Ctla-4 ligate with B7-1 (CD80) and B7-2 (CD86) on APCs and additionally interact with B7-H2 (IcosL), the ligand for Icos. Consequently, Icos, CD28 and Ctla-4 can compete for their ligand association (Yao et al., 2011). In contrast to Icos and CD28, Ctla-4 has inhibitory function on T cell activation by directly competing for positive signals via CD28 by sequestering CD80 and CD86 (Parry et al., 2005). Mice deficient for Ctla-4 exhibit fatal lymphoproliferation of CD4 T cells and injection of Ctla-4-ligand into mice deficient for Ctla-4 rescued the phenotype by blocking binding sites for CD28 on CD80/CD86, suggesting a role for Ctla-4 in controlling T cell proliferation (Chambers et al., 1997). Another inhibitory molecule of the CD28 family is PD-1 (programmed death 1), which interacts with PD-L1 or PD-L2 and is, like Icos, highly expressed on T<sub>FH</sub> cells (Crotty, 2011). CD28 is constitutively expressed in naïve T cells, whereas Icos is induced upon T cell stimulation and the inhibitory molecules Ctla-4 as well as PD-1 act as safeguards during an expiring immune response to ensure reduced T cell activity. In 2018, James P. Allison and Tasuku Honjo were awarded with the Nobel Prize in Medicine for their discovery of checkpoint inhibitors as revolutionary immune cancer therapies. They found that antibodies blocking either PD-1, PD-L1 or Ctla-4 release a break in T cells with high Ctla-4 or PD-1 expression and unleash the T cells to attack tumor cells (Ishida et al., 1992; Leach et al., 1996).

The cytoplasmic domain of CD28 harbors two motifs that can further proceed into different downstream signaling cascades. First, signaling via CD28 promotes activation of NF- $\kappa$ B, NFAT, the anti-apoptosis family BCL, mTOR and GLUT1 (glucose transporter type 1) (Boomer and Green, 2010). The transcription factors NF- $\kappa$ B, NFAT and AP-1 together directly induce IL-2 signaling by binding the IL-2 and CD25 (IL-2 receptor  $\alpha$  chain) promoters, thereby guaranteeing IL-2-mediated T cell responses and survival. Second, CD28 signaling results in complex signaling intermediates that promote JNKs, ERK1 and ERK2 activation. Interestingly, CD28<sup>-/-</sup> mice have impaired class-switching after viral infection and reduced T helper cell activity with defects in IL-2 production (Shahinian et al., 1993). Additionally, those mice lack germinal centers and T<sub>FH</sub> cells and have drastically reduced numbers of T<sub>reg</sub> cells (Ferguson et al., 1996; Salomon et al., 2000; Walker et al., 1999), emphasizing the importance of CD28 in T cell mediated immune responses.

Even though the intracellular domains of CD28 and Icos are structurally similar, they have divergent functions. Icos harbors intracellularly a unique SH2 domain that induces the Icos-PI3K-AKT cascade promoting the expression of IL4, IL-10 and IL-21 which are necessary

cytokines for  $T_H2$  and  $T_{FH}$  differentiation (Simpson et al., 2010). Furthermore, Icos involves the c-MAF pathway inducing IL-10, IL-4 and IL-21 secretion (Kroenke et al., 2012). The expression of Icos plays an important role in the germinal center reaction, as CD4 T helper cells that express Icos provide help to B cells to induce class-switch. Mice deficient for Icos secrete reduced levels of IL-4 and IL-17 but show increased IFN- $\gamma$  expression and additionally completely lack  $T_{FH}$  cells, suggesting that  $T_{FH}$  and  $T_H1$  differentiation highly depends on Icos (Akiba et al., 2005; Dong et al., 2001; McAdam et al., 2001; Tafuri et al., 2001).

Mutating the cytoplasmic domain of Ctla-4 interferes with its function in modulation of T cell activation, suggesting that downstream signaling events are necessary for Ctla-4-induced inhibition of T cell responses. Ctla-4 engages with SHP2 (SH2 domain-containing tyrosine phosphatase 2) and PP2A (serine/threonine protein phosphatase 2A) that dephosphorylate the TCR-CD3 $\zeta$  complex, LAT (linker for activation of T cells) and ZAP70 (zeta-chain associated protein) reducing cell cycle progression and cytokine production. Furthermore, Ctla-4 dampens ERK and JNK phosphorylation (Rudd et al., 2009).

The inhibitory molecule PD-1 harbors an ITIM (immunoreceptor tyrosine-based inhibition motif) and ITSM (immunoreceptor tyrosine-based switch motif), which, like Ctla-4, recruits SHP1 and SHP2. This again, results in inhibition of downstream activation of molecules like PCK $\theta$  (Sheppard et al., 2004; Yokosuka et al., 2012).

#### **1.1.4.2 The TNF receptor family**

Receptors of the TNF receptor family are expressed upon T cell activation and function in a bundle of three monomers via interacting with trimerized ligands on the APCs. Co-stimulatory function is only accomplished by some structurally diverse TNF family members amongst them the type-V family proteins including 4-1BB (CD137), Ox40 (Tnfrsf4), CD27 (Tnfrsf7), GITR (Tnfrsf18) and CD30 (Tnfrsf8) (Croft et al., 2012). Upon trimeric ligand-receptor engagement, cytoplasmic TRAF (TNF-receptor associated factor) adaptor proteins are recruited (Chattopadhyay et al., 2009) and enable several signaling pathways including canonical and non-canonical NF- $\kappa$ B, JNK, MAPK (p38 mitogen-activated protein kinase), AP1 (activator protein 1), ERK and NFAT. The mechanism of how the individual TRAF adaptor proteins integrate co-stimulatory signals with downstream signaling pathways is not solved yet (Croft, 2003). 4-1BB, Ox40 and CD27 co-stimulation induces anti-apoptotic factors like Bcl-2, Bcl-X $_L$  and Bcl2a1 thereby promoting survival of T cells. In addition, 4-1BB and Ox40 enable AKT which further activates cyclins and cell-cycle-dependent kinases (Croft, 2009).

The most prominent member of the TNF receptor superfamily is Ox40 that is like Icos not expressed on naïve T cells but gets induced during T cell activation and is highly abundant on  $T_{FH}$  cells. Ox40 expression correlates with increased expression of anti-apoptotic factors and

increased cytokine production thereby controlling survival of T cells. (Rogers et al., 2001). Additionally, it promotes proliferation of T cells during memory formation, which is in line with Ox40-deficient mice having reduced numbers of memory T cells and reduced T cell proliferation in response to viral infections (Gramaglia et al., 2000).

Integrating TCR antigen stimulation together with co-stimulatory receptor stimulation of either CD28 family or TNF receptor family with downstream signaling cascades is a complex network that is a mandatory process to determine cell fate decisions and survival of T cells.

The effect of antigen-specific T cell effector functions has been efficiently applied in cancer immune therapy. Here, chimeric antigen receptors (CARs) are utilized to engineer a patient's T cell *ex vivo* to clear tumors expressing certain antigens (Irving and Weiss, 1991). The extracellular domain of CARs consists of a scFv (single chain fragment variable) from a monoclonal antibody that recognizes a tumor-associated antigen combined with the intracellular signaling domain of TCR CD3 $\zeta$  chain and CD28 or 4-1BB. This second-generation CAR technology improves antigen-specific tumor clearance by enhancing T cell activation and proliferation due to increased secretion of IL-2 (Finney et al., 1998).

#### **1.1.4.3 Atypical NF- $\kappa$ B inhibitors and their role in immune responses**

One of the major signaling pathways in controlling lymphocyte activation, proliferation and expansion is the NF- $\kappa$ B signaling cascade. Briefly, p50/105, p52/100, p65 (RelA), cRel and RelB form the NF- $\kappa$ B transcription factor family by sharing a Rel homology domain (RHD) that comprises dimerization and DNA-binding. They associate to hetero- or homodimers and, in the presence of a transcription activation domain (TAD), modulate expression of target genes (Gerondakis et al., 2014; Hayden and Ghosh, 2012; Sen and Baltimore, 1986). In an inactive state they are prevented to enter the nucleus by classical NF- $\kappa$ B inhibitors (I $\kappa$ B $\alpha$ , I $\kappa$ B $\beta$  and I $\kappa$ B $\epsilon$ ), which bind to RHD and thereby cover the nuclear localization signal (NLS) (Kanarek and Ben-Neriah, 2012). In T cells, activation via the TCR and co-stimulation induces I $\kappa$ B kinase complex activation, which phosphorylates the NF- $\kappa$ B-bound inhibitors and induces proteasomal degradation of I $\kappa$ Bs and release of NF- $\kappa$ B transcription factor dimers to the nucleus where they bind  $\kappa$ B sites on the DNA. Atypical NF- $\kappa$ B inhibitors such as Bcl-3, I $\kappa$ B $\zeta$ , I $\kappa$ B<sub>NS</sub>, I $\kappa$ B $\eta$  and I $\kappa$ BL can fine-tune NF- $\kappa$ B activation when cytoplasmic inhibitors are degraded upon initial NF- $\kappa$ B activation. Unlike classical inhibitors, they are induced upon stimulation and localized in the nucleus, but they share an ankyrin-repeat domain (ARD) and can interact with NF- $\kappa$ B family members in the nucleus (Fiorini et al., 2002; Kitamura et al., 2000; Wulczyn et al., 1992; Yamauchi et al., 2010). I $\kappa$ B $\zeta$ , which interacts with p50 and p65, plays an important role in T<sub>H</sub>17-mediated autoimmunity, since mice deficient for I $\kappa$ B $\zeta$ , are resistant to EAE but suffer from spontaneous autoimmunity (Okamoto et al., 2010). The T<sub>H</sub>17 subset specifying

cytokines IL-6 and TGF- $\beta$  induce the expression of I $\kappa$ B $\zeta$ , which associates via TAD and ARD with the promoter of *Il17a* thereby enhancing the binding of transcriptional activators like ROR nuclear receptors to drive *Il17a* expression (Okamoto et al., 2010). Comparably, I $\kappa$ B<sub>NS</sub>, encoded by the *Nfkbid* gene, plays a role in T<sub>H</sub>1 and T<sub>H</sub>17 proliferation and polarization. It directly associates with the *Il10* gene, but how this is mediated is still unknown, since I $\kappa$ B<sub>NS</sub>, like I $\kappa$ B $\zeta$ , lacks a DNA-binding domain (Annemann et al., 2015). I $\kappa$ B<sub>NS</sub> can have transcriptional activity by directly engaging with c-Rel and p50 at the *Foxp3* gene locus. Consequently, I $\kappa$ B<sub>NS</sub>-deficient mice have reduced T<sub>reg</sub> cells in thymus and lymphoid organs, suggesting a function in the development of T<sub>reg</sub> cells. Of note, also mice deficient for the NF- $\kappa$ B factor *cRel* have comparably reduced numbers of regulatory T cells, while mice double-deficient for *cRel* and *Nfkbid* developed a much stronger loss of T<sub>reg</sub> cells. Besides controlling T cell differentiation, I $\kappa$ B<sub>NS</sub> is an essential regulator of B cell development, since I $\kappa$ B<sub>NS</sub>-deficiency results in a defective development of B1 B cells, plasma cells and marginal zone B cells (Touma et al., 2011).

Intriguingly, the expression of I $\kappa$ B<sub>NS</sub> and I $\kappa$ B $\zeta$  in T cells is tightly controlled by post-transcriptional gene regulation. The RNA-binding proteins Roquin and Regnase-1 regulate the mRNA expression of *Nfkbid* and *Nfkbiz* in naïve T cells thereby contributing to cell fate decisions of the T<sub>H</sub>17 subset (Jeltsch et al., 2014). Dissecting the requirements for Roquin-mediated regulation of the *Nfkbid* 3'-UTR will be one subject of this thesis.

### 1.1.5 Tolerance mechanisms and the development of autoimmunity

While central tolerance of T lymphocytes is achieved in the thymus to eliminate potential self-reactive T and B lymphocytes, peripheral tolerance is a second fail-safe mechanism to prevent autoimmunity by neutralizing or suppressing autoreactive cells that have escaped from the thymus (Bouneaud et al., 2000). Several mechanisms like the expression of inhibitory molecules, anergy, suppression by regulatory T cells and ignorance have evolved to ensure peripheral tolerance of autoreactive T and B cells.

Expression of inhibitory molecules (i.e. Ctla-4, PD-1, LAG-3) on T and B lymphocytes controls excessive immune responses. Mice deficient for Ctla-4 develop a strong autoimmune phenotype supporting the importance of controlling peripheral tolerance (Paterson and Sharpe, 2010).

In the absence of co-stimulation or inflammation, binding of the TCR alone causes a reversible hyporesponsiveness in mature T cells, which is termed T cell anergy. This is, amongst others like inhibition of TCR proximal signaling, a result of reduced production of IL-2, which in turn causes less activation of necessary signaling pathways or reduced cell cycle progression (Fathman and Lineberry, 2007). Interestingly, anergic T cells give rise to precursors of

peripheral T<sub>reg</sub> differentiation that further reduce immunopathology and autoimmunity (Kalekar et al., 2016).

As described previously, thymic and peripherally-induced T<sub>reg</sub> cells actively suppress autoreactivity by expression of inhibitory molecules, cytolysis, interference with metabolic processes or modulation of DC's maturation and function by direct cell-cell contact with the effector cells (Liu et al., 2015). The importance of regulatory T cells in controlling peripheral tolerance becomes evident in mutational analyses of the master transcription factor *Foxp3*. A truncated version of the *Foxp3* gene causes autoimmunity in the so-called *scurfy* mice (Brunkow et al., 2001; Godfrey et al., 1991) and in humans, mutations in the *Foxp3* gene result in multiorgan autoimmunity in IPEX ('immunodysregulation, polyendocrinopathy, enteropathy') patients (Bacchetta et al., 2018).

Due to anatomical barriers at 'immunological privileged' organs like brain, testis and eyes, autoreactive lymphocytes become ignored because of reduced access to tissue-specific antigens at these sites (Forrester et al., 2008).

However, failure of these levels of protection – first clonal selection in the thymus, then peripheral tolerance mechanisms - ends in an inappropriate activation of autoreactive T cells by autoantigens causing autoinflammatory and autoimmune diseases. Interestingly, the T cell compartment itself plays a major role in the development of autoimmunity: On the one hand, autoreactive CD4 T cells provide help to B cells to produce autoantibodies and, on the other hand, CD8 T cells infiltrate into organs and directly induce damage of tissues by secretion of pro-inflammatory cytokines. In humans, several systemic and organ-specific autoimmune diseases like type 1 diabetes mellitus (T1D), multiple sclerosis (MS), rheumatoid arthritis (RA) or systemic lupus erythematosus (SLE) have been described. The latter of these diseases are characterized by the production of antibodies against autoantigens, induce immune complex deposition and progress towards tissue damage. Patients suffering from SLE produce autoantibodies against chromatin or splice factors (Murphy and Weaver, 2017). T1D is driven by autoreactive T lymphocytes that secrete pro-inflammatory cytokines such as IFN- $\gamma$ , IL-1 and TNF- $\alpha$  thus causing apoptosis in  $\beta$  cells of the endocrine pancreas (Paschou et al., 2018). Most likely, several parameters including genetic variation and environmental variables predispose to autoimmunity by weakening tolerance mechanisms. Strong evidence on environmental cues influencing pathogenesis of T1D derives from studies of monozygotic twins where incidence of the disease is highly variable (Beyan et al., 2012). The development of SLE is influenced by genetic predispositions together with environmental factors such as UV light exposure, Epstein-Barr virus infection and hormonal changes (Tsokos et al., 2016). Interestingly, polymorphisms of genes encoded in the MHC gene locus, including genes involved in innate and adaptive immune responses, have been linked to high susceptibility to

autoimmune diseases and the majority of genes predisposing to T1D are located within the MHC region (Paschou et al., 2018). Sexual dimorphism in autoimmune diseases like SLE or MS with a higher incidence of autoimmunity in female support the huge impact of genetics. Our current knowledge about autoimmune disorders highly benefits from gene knockout studies in mice. Mutating or deleting genes encoding for important immune regulators, helps to gain novel insight in the causes of autoimmune diseases especially by dissecting autoantibody production or organ-infiltration of T cells. Hence, genes encoding for cytokines (like *Ifng*, *Tnfa*, *Il2*), co-receptors (*Cd28*), co-stimulatory molecules (*Ctla4*, *Pd1*) or genes involved in antigen-signaling cascades or apoptosis have been found to control the outcome of autoimmunity (Baccala et al., 2007; Paterson and Sharpe, 2010; Salomon et al., 2000). Besides these genes directly encoding factors of the immune system, autoimmune regulators that encode for proteins controlling the expression of those immune-associated genes post-transcriptionally or -translationally are susceptible to develop autoimmunity.

To identify novel autoimmune regulators, Christopher Goodnow and Carola Vinuesa performed a mouse genome-wide screen by treating mice with ethyl nitrosourea to introduce single-base substitutions at a rate of 1/0.5 megabases and identifying the development of autoimmunity by testing for anti-nuclear autoantibodies (ANAs). Thereby, the so-called *sanroque* mouse strain was isolated, which harbors a single point-mutation (methionine 199 to arginine, M199R) in the so far unknown gene *Rc3h1* encoding for the Roquin-1 protein, respectively. This protein comprises a highly conserved CCCH-zinc-finger domain present in many RNA-binding proteins and is localized to stress granules suggesting a functional role in mRNA stability (Vinuesa et al., 2005).

In the recent years, the role of post-transcriptional gene regulation in preventing and controlling autoimmunity and immune pathologies has become more and more important in the field. The subsequent chapters will give an overview of the basic mechanisms of post-transcriptional gene regulation and will focus in detail on the RNA-binding proteins Roquin and Regnase-1, which are key players in controlling immune regulation in the adaptive immune system. Their important role in preventing autoimmunity will be one major subject of this thesis.



## 1.2 Post-transcriptional gene regulation of immune cells

Constant exposure to pathogens and intra- and extracellular changes require fast and reliable adaptations of the immune response. Dynamic alterations can be achieved by post-transcriptional gene regulation of messenger RNAs (mRNAs) encoding for immune-related proteins such as cytokines or transcription factors that need to be stabilized or degraded in a flexible manner. Over the past decades post-transcriptional gene regulation has been of great interest owing to observations that an imbalance of mRNA decay and excessive expression of immune-related mRNAs promotes the development of autoimmune diseases. Post-transcriptional gene regulation has evolved by a compound network requiring structures in the mRNA predominantly located in the 5'- and 3'- untranslated regions (UTRs) of the mRNA, that are targeted by *trans*-acting factors such as RNA-binding proteins (RBPs) or microRNAs (miRNAs). Consequently, gene regulation by post-transcriptional mechanisms is a complex system that rapidly changes expression levels of genes in the immune system in response to environmental cues. The following section will discuss the principles of mRNA degradation particularly by the RNA-binding proteins Roquin and Regnase-1.

### 1.2.1 Principles of induced mRNA decay

The central dogma of molecular biology implies a basic two-step process by which DNA is transcribed into mRNA that is then further translated into protein. Of course, this process is not as simple as it seems and needs to be tightly and strictly controlled by a multiplicity of mechanisms to facilitate proper protein expression, which is crucial for maintaining health of an organism. Briefly, after transcribing eukaryotic mRNAs from DNA in the nucleus by a complex process requiring RNA-Polymerases, the mRNA is equipped with a 5' 7-methylguanosine cap (5'-cap) and a 3' poly(A)-tail. To initiate translation, the eukaryotic initiation factors eIF4E/G/A bind the 5'-cap and promote translation initiation through recruitment of ribosomes. Then, initiation factors interact with the poly(A)-binding protein (PABP) bound to the poly(A)-tail by circularization of the mRNA-protein complex and protecting the transcript from exoribonucleolytic degradation (**Figure 2 a**) (Garneau et al., 2007). Next to translational control of the transcript, mRNA turnover is a fundamental mechanism to control protein expression. This is facilitated by numerous protein/RNA-complexes involving factors of the mRNA decay machinery, RNA-binding proteins and miRNAs that stabilize or destabilize the mRNA.

The first step of mRNA degradation is initiated by shortening of the poly(A)-tail involving PAN2-4 proteins that remove PABP which interferes with eIF4E interaction and disrupts the circle formation (**Figure 2 b**).

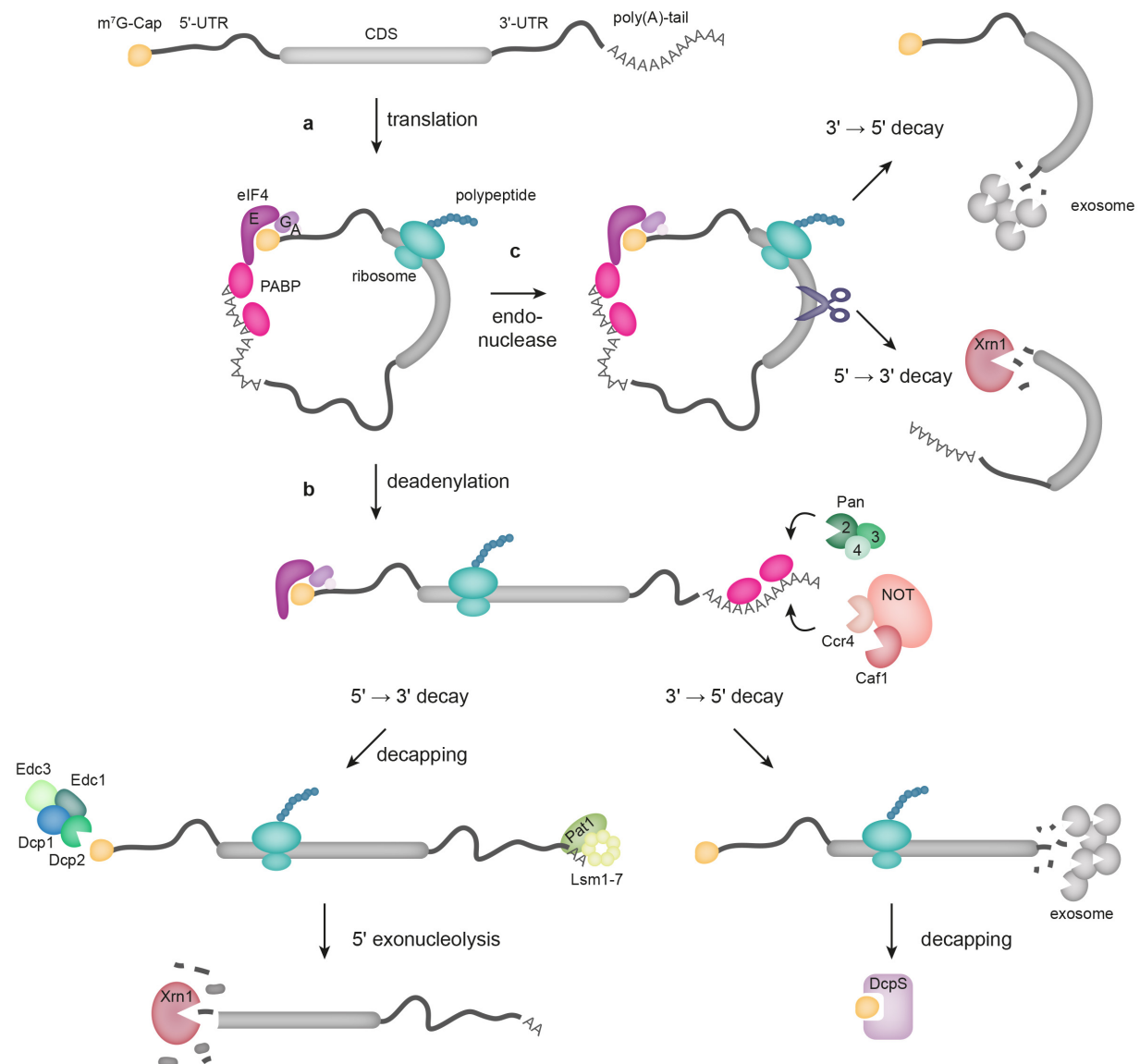


**Figure 2 | The principles of mRNA decay.**

After splicing, mature messenger RNA (mRNA) harbors a 5'-untranslated region (UTR) with an m<sup>7</sup>G-cap structure, a coding-sequence (CDS) and a 3'-UTR complemented with a poly(A)-tail. For initiation of translation, eukaryotic initiation factors 4A, G and E (eIF4A/G/E) bind the 5'-cap structure and the poly(A)-tail is bound by poly(A)-binding proteins (PABP). PABP and initiation factors interact, resulting in circularization of the protein-mRNA complex (a). Ribosomes start the translation of the CDS thereby producing polypeptide chains. (b) mRNA degradation is initiated due to Pan 2, 3 and 4 proteins removing PABP and thereby facilitating binding of the Ccr4-Caf1-NOT complex that eliminates the poly(A)-tail. 5' → 3' decay involves decapping enzymes (Dcp1, Dcp2, Edc1 and Edc3) and the Lsm1-7 ring structure. After decapping, mRNA is degraded from 5' by the Xrn1 exonuclease. In turn, the exosome complexes degrade mRNA 3' → 5', whereas the residual 5'-cap structure is digested by DcpS. (c) Direct cleavage of circulated mRNAs by endonucleases is an additional way of mRNA degradation. Here, the two resulting mRNA fragments are eliminated by Xrn1 and the exosome complex. Adapted from (Garneau et al., 2007; Mugridge et al., 2018).

Subsequently, the Ccr4-Caf1-NOT multi-protein deadenylase complex is recruited to the 3' end (Wolf and Passmore, 2014), where it facilitates removal of the poly(A)-tail via its

exonuclease activity (Collart, 2016). After successful subtraction of the poly(A)-tail, mRNA degradation can be initiated from either 5' ( $5' \rightarrow 3'$ ) and/ or 3' site ( $3' \rightarrow 5'$ ).

$5' \rightarrow 3'$  degradation is activated by decapping of the 5' cap which requires several proteins, amongst them decapping enzymes (Dcp1 and Dcp2), the heptameric Lsm1-7 complex together with Pat1 associating with the 3' end as well as the enhancer of decapping Edc1 and Edc3 followed by an initial degradation of the mRNA by the exoribonuclease XRN1 (Jonas and Izaurralde, 2015; Kshirsagar and Parker, 2004; Tharun and Parker, 2001).

$3' \rightarrow 5'$  mRNA turnover occurs via a large exosome complex. Proteins building this complex exhibit phosphorylytic exonuclease and RNA helicase function and thereby degrade the mRNA from the 3' end (Houseley et al., 2006; Zinder and Lima, 2017). The remaining oligomer carrying the 5'-cap is then finally degraded by the scavenger decapping enzyme DcpS (Houseley et al., 2006; Liu et al., 2002). Both degradation pathways have redundant function, since knocking out either component of one pathway leaves mRNA decay rates unaffected (Houalla et al., 2006).

As a third pathway, endonucleases can directly cleave mRNAs resulting in a two-fragmented transcript that is subject to  $3' \rightarrow 5'$  decay by the exosome complex or  $5' \rightarrow 3'$  degradation via the exoribonuclease XRN1 (**Figure 2 c**).

Translation of mature mRNA transcripts into proteins is a highly complex mechanism. Errors occurring during translation bear tremendous consequences, therefore several control mechanisms have evolved. Aberrant transcripts with a premature stop-codon within 20-25 nt 5' of the exon junction complex producing truncated proteins, can be eliminated by nonsense-mediated decay (NMD), which involves the helicases UPF1, 2 and 3 (Lykke-Andersen and Jensen, 2015). In contrast, non-stop-decay (NSD) senses transcripts that lack a stop codon. Here, the adaptor protein Ski7 binds and facilitates release of the ribosome and recruits the cytoplasmic SKI complex and the exosome to degrade the transcript  $3' \rightarrow 5'$  (Frischmeyer et al., 2002; van Hoof et al., 2002). A third mechanism, referred to as no-go decay (NGD) recognizes transcripts with ribosomal elongation stalls and initiates degradation by endonucleases in proximity to the stalled ribosome resulting in two transcript fragments that are targeted for degradation by XRN1 or the exosome (Doma and Parker, 2006).

### 1.2.2 Subcellular locations of mRNA decay

mRNAs are in a constant equilibrium of active translation and mRNA degradation to rapidly respond to changes in the microenvironment and subsequently adapt the gene expression. Turnover of mRNA and protein is not only controlled temporally but also spatially. Cytoplasmic, membrane-less foci termed processing- (P-) bodies contain translationally-repressed mRNAs and mRNA decay factors such as Ccr4-NOT, Dcp1/2, Pat1-LSM1-7, Edc3 and Xrn1,

suggesting that this serves as a site to accelerate mRNA decay. However, components of the mRNA decay machinery have also been found outside of P-bodies in the cytoplasm and it was suggested that these cytoplasmic foci are dynamically forming upon increased abundance of translationally silenced mRNAs that are targeted for degradation. Deletion of Dcp1, interestingly, elevated p-body abundance and inhibited mRNA decay (Parker and Sheth, 2007). Upon cellular stress, cytoplasmic foci, so-called stress granules, form. Different to P-bodies, stress granules are sites of mRNA storage to protect RNAs from reactive agents in the cytoplasm (Kedersha et al., 2005). Formation of P-bodies and stress granules arises via liquid-liquid phase separation (LLPS), which is influenced by increasing protein and RNA concentration, changes in salt concentration, temperature and crowding agents (Guo and Shorter, 2015). Proteins with low complexity sequence domains (LCDs) are prone to develop these protein-rich droplets. Recently, a dynamic process termed mRNA cycle was described whereby mRNA-protein complexes can vigorously move between polysomes, P-bodies and stress granules facilitating efficient balance of transcript turnover and translation (Decker and Parker, 2012).

### 1.2.3 The interplay of *cis*-regulatory elements and *trans*-acting factors

Besides mRNA degrading enzymes, *trans*-acting factors are located within P-bodies, emphasizing their role in controlling mRNA transcript levels. Stabilizing and de-stabilizing *trans*-acting factors such as RNA-binding proteins (RBPs), microRNAs (miRNAs) and long-non-coding RNAs impact on RNA stability by recognizing *cis*-elements either as linear sequence motifs or secondary structures. These RNA elements are predominantly encoded in the untranslated regions (UTRs). Whereas 5'-UTR binding typically controls translation initiation, elements in the 3'-UTRs bound by *trans*-acting factors often influence mRNA decay and translational efficiency (Rissland, 2017).

Approximately 30 years ago, heterogeneous AU-rich elements (ARE) were described as the first mRNA-stability elements and several studies identified genes of cytokines, proto-oncogenes and transcription factors to contain such sites in their 3'-UTRs. The zinc finger (ZnF) protein TTP (tristetraproline) acts as an mRNA decay factor by binding the ARE of *Tnfa*. It directly promotes deadenylation of the mRNAs by shortening of the poly(A)-tail due to its interaction with Ccr4 (Carballo et al., 2000; Lai et al., 1999; Lykke-Andersen and Wagner, 2005). The ARE in the TNF- $\alpha$  transcript is additionally targeted for translational inhibition by TIA-1 (T-cell-restricted intracellular antigen-1) as macrophages from TIA-1-deficient mice have elevated levels of TNF- $\alpha$  protein and the *Tnfa* mRNA shifted from fractions containing monosomes to fractions with polysomal association of mRNAs with ribosomes, while its mRNA degradation rate is not affected (Piecyk et al., 2000).

Besides linear, heterogeneous AU-rich elements, secondary RNA structures have been identified as constitutive decay elements (CDEs) in the *Tnfa* 3'-UTR (Stoecklin et al., 2003). The CDE comprises a 17 nt-long fragment that forms a secondary stem loop structure with a 7 nt base-pairing stem and a triloop bearing a pyrimidine-purine-pyrimidine (py-pu-py) sequence. Interestingly, comparison of *Tnfa* CDE sequences from 19 mammalian species reveals almost 100% sequence identity. Mutational analysis of the CDE structure uncovers that the formation of a secondary structure and the loop sequence are mandatory for efficient mRNA decay of the *Tnfa* 3'-UTR in reporter assays (Leppek et al., 2013). Pulldown with cell lysates and the *Tnfa* CDE RNA allowed for identification of enriched RNA-binding proteins by mass spectrometry. Here, the RNA-binding protein Roquin-1 (i.e. *Rc3h1*) and its homolog Roquin-2 (i.e. *Rc3h2*) showed the strongest peptide enrichment. Besides binding of the CDE, Roquin also induces CDE-mediated mRNA degradation.

Interestingly, the endonuclease Regnase-1, encoded by the *Zc3h12a* gene respectively, also destabilize mRNA transcripts that harbor CDE-like triloop structures such as *Il6*, *Il2* or its own mRNA (Mino et al., 2015; Uehata et al., 2013). The exact mechanism of Roquin- and Regnase-1-mediated mRNA regulation of immune-associated targets and their role in controlling immune homeostasis is one subject of this thesis and will be discussed in greater detail in the subsequent sections.

## 1.3 The *trans*-acting factors Roquin and Regnase-1

### 1.3.1 The Roquin protein family

In 2005, Roquin-1 was first identified in a screen for autoimmune regulators in mice with a homozygous single point mutation (M199R) causing a severe SLE-like autoimmune disease in the so-called *sanroque* mice (*Rc3h1<sup>san/san</sup>*). Later studies, identified Roquin as an RNA-binding protein involved in mRNA degradation and linked its post-transcriptional gene regulation of immune-related genes to the prevention of autoimmunity.

#### 1.3.1.1 Roquin mouse models

The *sanroque* mice develop a profound autoimmune phenotype not only by generating autoantibody-producing B cells but also by exhibiting splenomegaly and lymphadenopathy, which additionally involves spontaneous formation of germinal centers in the B cell follicles. Consequently, B cells produce polyclonal hypergammaglobulinemia of all T-dependent isotypes and activated effector-memory-like CD4 and CD8 T cells accumulate and show profound expression of the co-stimulator Icos. In line with increased Icos expression, additional markers of T<sub>FH</sub> cells like Cxcr5, Ccl5 and IL-21 are drastically elevated. To test the contribution of the aberrant Icos expression to the phenotype of the *sanroque* mice, *Icos* gene expression levels were halved in *Rc3h1<sup>san/san</sup>; Icos<sup>+/-</sup>* mice. This correlated with reduced splenomegaly, lymphadenopathy, less T<sub>FH</sub> and germinal center B cell expansion (Yu et al., 2007). However, complete ablation of Icos in *sanroque* mice did not rescue splenomegaly or hyperactivation of T cells and rather decreases regulatory T cell numbers, but maintains autoantibody production of *sanroque* mice. These findings suggest that the overexpression of Icos in *sanroque* mice does not simply explain the development of autoimmunity, suggesting that additional factors might contribute to this phenotype (Lee et al., 2012).

To test whether the single point mutation in the *sanroque* mouse results in loss-of-function of the Roquin-1 protein, different deletion systems in mice were of high interest. The systemic knockout of the Roquin-1-encoding gene (*Rc3h1<sup>-/-</sup>*) resulted in perinatal lethality (Bertossi et al., 2011). The newborn animals died within 6h after birth suffering from decreased expansion of alveoli of the lung. Surprisingly, heterozygous mice (*Rc3h1<sup>+/-</sup>*) were healthy and showed no pathology, suggesting that already a half dose expression of Roquin-1 is sufficient for survival. To investigate cell-type-specific functions of Roquin-1, mice with loxP-flanked alleles for *Rc3h1* (*Rc3h1<sup>fl/fl</sup>*) were crossed to mice with different cre-recombinase systems to induce conditional deletion in different cell subsets: *Cd4*-cre (T cell-specific deletion), *Cd19*-cre (deletion in B cells) and *vav*-cre for deletion in all hematopoietic cells. Overall, Roquin-1 deficiency in these

various hematopoietic cell types did not cause breakdown of tolerance or induction of autoimmunity. Despite a moderate increase in Icos expression, conditional deletion in T cells causes an effector-memory phenotype in CD8 T cells (CD44<sup>high</sup> CD62L<sup>low</sup>). Loss of Roquin in all hematopoietic cells results in a slight activation of CD4 and CD8 T cells with higher Icos surface expression and spontaneous formation of GC B cells but no change in T<sub>FH</sub> cells. Additionally, T<sub>reg</sub> cells, eosinophils and macrophages were altered in *vav*-cre mice. These findings were phenocopied by B-cell-specific deletion utilizing the *CD19*-cre system. The data suggest that the autoimmune syndrome in the *sanroque* mice may not be simply explained by a loss-of-function mutant of Roquin-1.

The Roquin protein family not only comprises Roquin-1 (*Rc3h1*), but also a paralog termed Roquin-2 or MNAB (membrane-associated nucleic acid-binding protein), encoded by the *Rc3h2* gene, respectively (Siess et al., 2000). Gene duplication occurred in higher vertebrates from zebrafish to humans in turn resulting in the presence of both paralogs, whereas in *drosophila melanogaster* and *caenorhabditis elegans* only one homolog exists (Heissmeyer and Vogel, 2013). Systemic deletion of *Rc3h2* induced post-natal death within the first days after birth in most animals and the reduced expansion of lung alveoli is in line with the *Rc3h1* gene ablation in mice. Surprisingly, mice with a conditional deletion of *Rc3h2* in T cells develop no detectable sign of autoimmunity or hyperactivated T cells (Vogel et al., 2013). To validate whether Roquin-1 and Roquin-2 have redundant functions, mice with a combined conditional deletion of *Rc3h1* and *Rc3h2* genes in T cells were generated. Indeed, *Rc3h1/2*<sup>fl/fl</sup>; *Cd4*-cre mice shared phenotypes with the *sanroque* mice: These mice develop splenomegaly and lymphadenopathy, spontaneous activation of CD4 and CD8 T cells with elevated Icos expression levels. Additionally, Roquin deficiency causes formation of GCs due to increased frequencies of T<sub>FH</sub> and GC B cells comparable to *Rc3h1*<sup>san/san</sup> mice (Vogel et al., 2013). Additionally, lack of Roquin-1 and -2 in T cells results in an inflammatory lung phenotype characterized by infiltration of T<sub>H</sub>17 cells and neutrophils in the lungs and secretion of autoantibodies directed against pancreatic tissue (Jeltsch et al., 2014). Natural killer T cells (NKT), which are a specialized subset of glycolipid-recognizing T cells involved in autoimmune and malignant diseases, were shown to be strictly dependent on Roquin. Deficiency of both paralogs during early thymic NKT development results in a drastic cell-intrinsic increase of the NKT<sub>17</sub> subset but a complete loss of peripheral mature NKT cells, suggesting a role in preventing excessive differentiation into NKT<sub>17</sub> cells. (Drees et al., 2017). In addition, T<sub>reg</sub>-specific deletion using *Foxp3*-cre, revealed that Roquin is required for T<sub>reg</sub> function since T<sub>reg</sub> cells lacking Roquin proteins adopt a T<sub>FR</sub> phenotype and lose suppressive function of T<sub>reg</sub> cells (Essig et al., 2017). Overall, these data suggest that deletion of the Roquin paralogs in T cells phenocopies many of the autoimmune phenotypes of the *sanroque* mice. However, the functional Roquin-2 protein in the *sanroque* mice is not capable of rescuing the phenotype and

additionally, Roquin-1 M199R does not interfere with RNA binding ability (Athanasopoulos et al., 2010). Therefore, the molecular basis for the altered function of M199 in Roquin-1 is still under debate and of high interest in the field.

### 1.3.1.2 Domain organization and molecular functions of Roquin proteins

Comparing the phenotypes in the different Roquin mouse models suggest that the Roquin RNA-binding proteins play an important role in the homeostasis of the adaptive immune response. Both protein family members are localized in the cytoplasm and especially enriched in P-bodies and, upon induction of stress, relocate to stress granules (Athanasopoulos et al., 2010; Glasmacher et al., 2010; Srivastava et al., 2015; Vinuesa et al., 2005). However, Roquin-1 protein levels are significantly higher in comparison to Roquin-2 in lymphoid tissues, but both paralogs have redundant functions in T cells where Roquin-2 can compensate for the absence of Roquin-1 (Pratama et al., 2013; Vogel et al., 2013).

The functional redundancy of both paralogs becomes clear when comparing the domain organization of their amino acid sequences (**Figure 3**). The first 500 amino acids reveal high sequence similarity harboring several domains: a RING- (really interesting new gene) domain, a ROQ-domain embedded in HEPN<sub>N</sub> (higher eukaryotes and prokaryotes nucleotide-binding, N-terminal) and HEPN<sub>C</sub> (C-terminal) stretches, a CCCH-type zinc finger followed by a varying conservation in the C-terminus. A proline-rich region (PRR) can be found in the carboxy terminus of Roquin-1, whereas Roquin-2 owns a hydrophobic stretch.

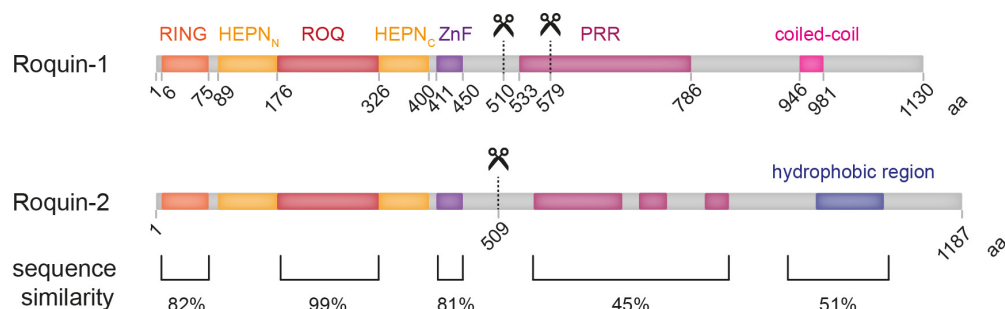


**Figure 3 | Domain organization and sequence similarity of Roquin family proteins.**

Schematic representation of the domain structures of Roquin-1 and Roquin-2. Both proteins share a RING domain (really interesting new gene), a ROQ-domain embedded in HEPN<sub>N</sub> (higher eukaryotes and prokaryotes nuclear-binding domain, N-terminal) and HEPN<sub>C</sub> (C-terminal), a CCCH-type zinc finger (ZnF) and a proline-rich region (PRR). Carboxyl-terminal Roquin-1 harbors a coiled-coil domain, whereas Roquin-2 has a hydrophobic region at its C-terminus. Amino acid (aa) positions of the domains are depicted. Scissor symbols represent MALT1 cleavage sites. Structure and sequence similarity information are adapted from Jeltsch & Heissmeyer, 2016; Pratama et al., 2013; Schlundt et al., 2016 and Srivastava et al., 2015.

The function of the RING domain is not completely solved, yet. In the *C. elegans* homolog RLE-1 it exhibits E3 ubiquitin ligase activity (Li et al., 2007), whereas the Roquin-2 RING-



domain was found to have ubiquitination function of ASK1 (apoptosis-signaling kinase 1) thus inducing proteasomal degradation thereof (Maruyama et al., 2014).

Roquin-1 mutants lacking the RING-domain are incapable of localizing to stress granules (Athanasopoulos et al., 2010). In addition, this domain has been associated to auto-ubiquitination of Roquin-1 and counteracting AMPK (adenosine monophosphate-activated protein kinase) function resulting in aberrant mTOR signaling and T<sub>FH</sub> accumulation (Ramiscal et al., 2015).

The ROQ-domain is a unique domain with high sequence conservation in Roquin family proteins. It is embedded in HEPN<sub>N</sub> and HEPN<sub>C</sub> domains that fold together and can bind double-stranded RNA independent of the ROQ-domain (Srivastava et al., 2015). High-resolution structure analyses have been solved for the ROQ-domain of both paralogs and indeed identified this domain to directly interact with RNA (Sakurai et al., 2015; Schlundt et al., 2014; Schuetz et al., 2014; Tan et al., 2014). It directly binds CDE elements in the 3'-UTR of mRNAs with characteristic secondary RNA structures consisting of 5-7 nucleotides and a py-pu-py triloop sequence (Leppek et al., 2013) (**Figure 4**). As mentioned previously, the CDE-element has first been described in the *Tnfa* 3'-UTR, however in the meantime several additional mRNA targets have been reported to harbor CDE or CDE-like stem loop structures including *Icos*, *Nfkbid*, *Nfkbiz* and *Ox40* (Braun et al., 2018; Codutti et al., 2015; Janowski et al., 2016; Jeltsch et al., 2014; Leppek et al., 2013; Schlundt et al., 2014; Vogel et al., 2013).

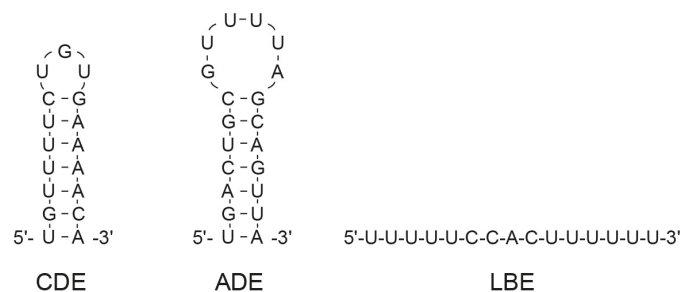


**Figure 4 | RNA structures and sequences targeted by Roquin.**

Schematic representation of sequences of the Roquin-targeted constitutive decay element (CDE of the *Tnfa* 3'-UTR), alternative decay element (ADE) identified by SELEX (Systematic Evolution of Ligands by Exponential Enrichment) and linear binding element (LBE) consensus sequence. Structures were adapted from Schlundt et al., 2015; Janowski et al., 2015 and Essig et al., 2018.

Mutational analysis revealed that the Roquin-RNA interaction depends at least on three critical amino acids (Lys220, Lys239 and Arg260) for binding of *Icos*, *Tnfa* and *Ox40* mRNA and these residues are crucial for efficient post-transcriptional gene regulation, respectively (Schlundt et al., 2014). Recently, a second type of secondary structure for Roquin-mediate gene regulation was identified as alternative decay element (ADE) (**Figure 4**). This motif comprises a U-rich hexaloop embedded in a 5-8 nt base-pairing stem with one unpaired base. Interestingly, an

ADE-like hexaloop stem loop was found in the *Ox40* 3'-UTR. Crystal structure and mutational analysis of the Roquin-*Ox40* interaction revealed that this interaction requires the amino acid Tyr250 for binding and gene regulation (Janowski et al., 2016). My contribution to this finding, the functional importance of amino acid Tyr250 for *Ox40* regulation, will be discussed in more detail in the results section of this thesis. Recently, our group also identified a novel 15 nt-long linear sequence consisting of a CAC trinucleotide flanked by U-rich sequences as a linear binding element (LBE) of Roquin-1 (Essig et al., 2018) (**Figure 4**).

Roquin proteins are not capable of directly degrading the target mRNAs. Therefore, several investigations have been made to identify the mechanism of Roquin-mediated post-transcriptional gene regulation. The C-terminus of Roquin proteins including the proline-rich region (PRR) interacts with the deadenylation machinery involving the Ccr4-NOT complex thus inducing the first steps of mRNA decay. This is in line with Roquin localization to P-bodies that requires the carboxyl-terminal glutamine and asparagine-rich sequence stretch, which is required for protein-protein-interaction in post-transcriptional gene regulation (Glasmacher et al., 2010; Leppek et al., 2013; Murakawa et al., 2015; Reijns et al., 2008). However, the localization of human Roquin to stress granules has also been demonstrated (Athanasopoulos et al., 2010). As a second mRNA decay pathway, N-terminal Roquin involving ROQ-domain and ZnF directly associates with the decapping factors Edc4 and Rck, whereas the function of Rck is crucial for Roquin-mediated *Icos* repression (Glasmacher et al., 2010). Recently, the direct interaction of N-terminal Roquin with the CCH-type ZnF protein NUFIP2, which acts as a co-factor for Roquin-mediated repression of the human ICOS and *OX40* mRNA, has been described. Here, tandem stem loops containing *cis*-elements are bound with higher affinity by Roquin in the presence of NUFIP2 thereby facilitating repression of the mRNA (Rehage et al., 2018).

Is Roquin-mediated initiation of mRNA degradation the only way of controlling expression of its targets? As part of this thesis, we identified Roquin to also play a role in controlling translation, which I studied for its target *Nfkbid* (Essig et al., 2018). Whether this translational control mechanism of Roquin is mediated by interaction with translational regulators or by direct engagement of ribosomal proteins is still unknown and is subject to further investigations.

### 1.3.1.3 Control of Roquin protein expression

As mentioned before, Roquin controls the expression of several essential immune-related genes encoding for *Icos*, *Ctla-4* or *Ox40*. During an active immune response, these proteins must fulfill their functions and need to escape Roquin-mediated repression. Therefore, a mechanism has evolved to control Roquin protein abundance and allow expression of Roquin-

targeted genes. Upon stimulation of the TCR with cognate antigen and co-stimulation of CD28 by APCs, the paracaspase MALT1 gets activated and cleaves both Roquin paralogs. Roquin-1 bears two cleavage sites, whereas for Roquin-2, one cleavage site has been described so far (**Figure 3**). T cells treated with the MALT1 inhibitor Mepazine or MALT-1 deficient T cells as well as T cells with an inactive form of MALT1 are incapable of cleaving Roquin proteins (Gewies et al., 2014; Jeltsch et al., 2014). However, whether the residing cleavage products (1-510 or 1-579 aa) that still own the essential ROQ-domain, are functional, has not been addressed so far. Additionally, in human Jurkat T cells autoregulation of Roquin through its own 3'-UTR has been proposed (Cui et al., 2017). Furthermore, Roquin-1 and Roquin-2-encoding mRNAs were enriched in pulldown experiments with Roquin-1, whereas both mRNAs were predicted to contain CDE elements (Leppek et al., 2013). Interestingly, the endonuclease Regnase-1 is targeted for degradation in a very comparable way and will therefore be discussed in more detail in the subsequent section.

### 1.3.2 The endonuclease Regnase-1

Besides Roquin proteins and TTP, the Regnase family proteins are essential regulators of immune-related mRNAs. *Zc3h12a* encodes for monocyte chemoattractant protein-1-induced protein (MCPIP1), which was later, due to its endonucleolytic function, termed Regnase-1. The initial name MCPIP1 derived from identifying a role as a transcription factor-like protein in cardiomyocytes upon monocyte chemoattractant protein-1-mediated inflammation (Zhou et al., 2006). A few years later the kinetic of Regnase-1 expression in murine macrophages was described as strongly increased upon LPS stimulation. After LPS stimulation, the expression of Regnase-1 declines again, suggesting that its expression is tightly controlled during an acute immune response (Matsushita et al., 2009). It is highly abundant in cells of the innate as well as the adaptive immune system such as macrophages, T and B cells, where it functions in the degradation of target mRNAs. In addition, several studies investigated the function of Regnase-1 in non-immune cells and cancer. Regnase-1 was reported to induce apoptosis in cancer cell lines by degrading mRNAs from anti-apoptotic genes like *Bcl2l1*, *RelB* and *Bcl3* and controlling neuroblastoma proliferation and survival (Boratyn et al., 2017; Lu et al., 2016). Moreover, genes involved in fat and iron metabolism are under control of Regnase-1 (Habacher et al., 2016; Yoshinaga et al., 2017). Additionally, its role in targeting viral mRNAs and restricting HIV-infections has been extensively studied in the past (Lin et al., 2013; Lin et al., 2014; Liu et al., 2013b). These data support the central role of Regnase-1 in protecting from infections and cancer in various cell types. However, this thesis will focus on the function of Regnase-1 in immune cells, especially the T cell subset.

### 1.3.2.1 Regnase-1 mouse models

To study the function of Regnase-1, *Zc3h12a*<sup>-/-</sup> mice were generated independently by two research groups. Loss of Regnase-1 resulted in a strong autoimmune phenotype characterized by splenomegaly and lymphadenopathy, multiorgan infiltration of plasma cells and the production of antibodies of all immunoglobulin subtypes as well as anti-double-stranded DNA antibodies. On cellular level, Regnase-1-deficient mice develop class-switched B cells and accumulate highly activated splenic T cells. Macrophages lacking Regnase-1 and stimulated with LPS revealed increased expression of the cytokines IL-6 and IL-12 $\beta$  (Liang et al., 2010; Matsushita et al., 2009). In addition, all lymphoid organs are drastically disorganized including spleen, lymph nodes and thymus (Miao et al., 2013). However, combining *Zc3h12a* deficiency with a knockout of either *Il6* or *Il12p40*, encoding for IL-12 $\beta$ , did not rescue the phenotype. Generating mice with conditionally deleted Regnase-1 in T cells, revealed that the autoimmune phenotype in the systemic knockout mice is T-cell intrinsic. Indeed, *Zc3h12a*<sup>fl/fl</sup>; *Cd4-cre* mice have profound hyperactivated T cells, accumulate plasma cells and secrete elevated levels of all immunoglobulin subtypes and anti-nuclear autoantibodies (Uehata et al., 2013).

### 1.3.2.2 Domain organization and function of Regnase family members

Next to Regnase-1, the Regnase protein family comprises three additional members: Regnase-2, Regnase-3 and Regnase-4 encoded by *Zc3h12b*, *Zc3h12c* and *Zc3h12d*, respectively. By comparing the structural domains of these family members (**Figure 5**), it becomes evident that they all share a CCCH-type zinc finger similar to Roquin-1 and Roquin-2 (**Figure 3**) (Liang et al., 2008). In addition, all Regnase proteins bear a PiT N-terminal (PIN)-like RNase domain (NYN domain) that, in Regnase-1, comprises endoribonuclease activity which is facilitated by a catalytic center composed of magnesium ion complexed by acidic residues (Asp141, Asp225, Asp226, Asp244 and Asp248) (Xu et al., 2012). This surface is probably forming an RNA-interaction platform, however the co-crystal structure of Regnase-1 in association with RNA has not been solved, yet (Anantharaman and Aravind, 2006; Matsushita et al., 2009; Mino et al., 2015).

The physiological role of Regnase-2 is hardly understood whereby cells of the immune system exhibit only low expression thereof (Liang et al., 2008).

Regnase-3 is involved in vascular inflammation by counteracting inflammatory responses due to inhibiting the NF- $\kappa$ B pathway and pro-inflammatory gene expression (Liu et al., 2013a). Very recently, the knowledge about Regnase-3 has been expanded by a study that demonstrates a role as endonuclease in regulating mRNA degradation of transcripts involved in the IFN- $\gamma$  pathway and immune homeostasis which is functional complement to Regnase-1. Here the authors showed that systemic Regnase-3 deficiency causes strong IFN signaling thereby

suppressing GC formation. Interestingly, Regnase-3 exhibits endonucleolytic function thereby degrading mRNAs, such as *Zc3h12a*, localized to endosomes (von Gamm et al., 2019).

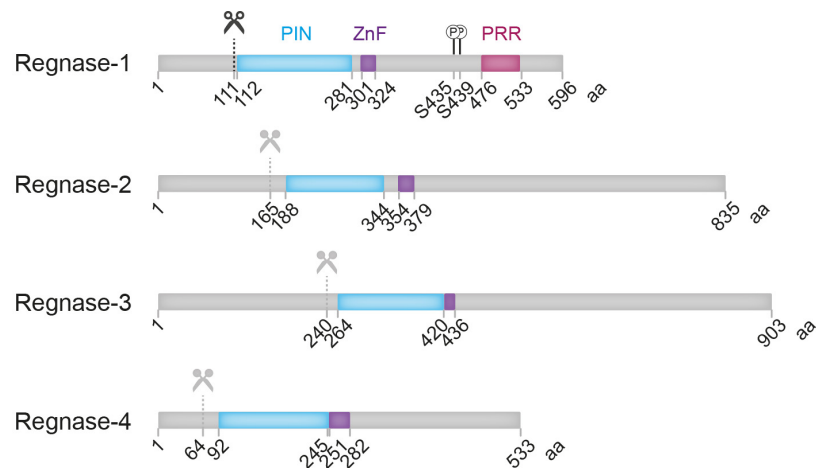


**Figure 5 | Domain organization of Regnase family proteins.**

Schematic representation of the domain organization of Regnase-1, Regnase-2, Regnase-3 and Regnase-4. All proteins share a PiT N-terminal (PIN)-like RNase domain and a CCCH-type zinc finger (ZnF), whereas Regnase-1 harbors a C-terminal proline-rich region (PRR) and S435 as well as S439 are sites for phosphorylation (P). Amino acid (aa) positions of the domains are indicated. Black Scissor symbol represents proven and grey scissor symbols indicate predicted MALT1 cleavage sites. Structures are adapted from Jeltsch & Heissmeyer, 2016 and Takeuchi, 2017.

Regnase-4 like Regnase-1 exhibits endonucleolytic function thereby regulating gene expression of *Il6*, *Il1b* and *Tnf* via their 3'-UTRs. In addition, interactions between Regnase-1 and -4 have been suggested (Huang et al., 2012; Wawro et al., 2017; Zhang et al., 2015). However, Regnase-4-deficient mice appear healthy, but stimulation of T cells *ex vivo* induces hyperactivation, suggesting a role for Regnase-4 in controlling T cell effector functions (Minagawa et al., 2014).

It is still unknown whether Regnase family members are functionally redundant, but differentially expressed, or if they have evolved to fulfill entirely different functions. Sites for MALT1-targeted cleavage have been predicted for Regnase-2, 3 and 4, but have not been proven, yet. Therefore, more investigations are required to understand the function of the Regnase family members 2, 3 and 4 in the immune response.

### 1.3.2.3 Molecular functions of Regnase-1

In the last years, Regnase-1 has been intensively studied and a variety of molecular functions have been identified. The PIN-like domain of Regnase-1 allows deubiquitylation by association with USP10, which in turn negatively regulates NF- $\kappa$ B by removing polyubiquitylation chains of the I $\kappa$ B kinase subunit IKK $\gamma$  or NEMO. Moreover, Regnase-1 removes ubiquitin moieties

from TRAF proteins by involving the CCCH ZnF thereby negatively regulating JNK and NF- $\kappa$ B activity. Yet, it is unsolved how this contributes to the function of Regnase-1 (Liang et al., 2010; Niu et al., 2013). It was additionally suggested that the PIN domain of Regnase-1 has the capacity to form head-to-tail oligomers, which is mandatory for bona fide RNase activity *in vitro* (Yokogawa et al., 2016). The before-mentioned CCCH-zinc finger is highly conserved among different species and Regnase family member genes and the ZnF of Regnase-1 is engaged in direct RNA interaction but is not essential for mRNA degradation (Matsushita et al., 2009; Yokogawa et al., 2016). The C-terminal PRR in Regnase-1 could serve as a protein-protein-interaction surface as it was reported for other PRR-containing proteins before (Yokogawa et al., 2016). In accordance, the carboxy terminus in human Regnase-1 enables oligomerization of multiple Regnase-1 proteins therefore facilitating cleavage of pre-miRNAs and antagonizing Dicer function (Suzuki et al., 2011). However, a later study claimed that miRNAs are not targeted for Regnase-1-mediated degradation since Regnase-1 deficient MEF cells did not show elevated abundance of several miRNAs in comparison to WT MEF cells (Mino et al., 2015).

As mentioned before, Regnase-1 is capable of recognizing stem loop structures mainly localized in 3'-UTRs and thus facilitating degradation of its target mRNAs. These target mRNAs encode for co-stimulatory receptors like Ox40, Icos and Ctla-4, cytokines like IL-2, IL-6 or IL-12 $\beta$  or transcription factors such as c-Rel, Irf4 or I $\kappa$ B $\zeta$  and I $\kappa$ B $\eta$ . RNA regulation requires the RNase catalytic center in the PIN-domain of Regnase-1, since a point mutation of Asp141 to Asn (D141N) abrogates the mRNA degradation capacity (Behrens et al., 2018; Jeltsch et al., 2014; Mino et al., 2015; Uehata et al., 2013). The degradation of target mRNAs was reported to be independent of the CCCH ZnF, but NMR studies showed that the ZnF can indeed bind //6 mRNA (Yokogawa et al., 2016). Additionally, Regnase-1 directly cleaves circular and linear //6 mRNA, whereas the recognition of a stem loop is mandatory for degradation, indicating that Regnase-1 acts as an endonuclease (Mino et al., 2015).

On the one hand Regnase-1 facilitates the degradation of its target mRNAs by direct cleavage dependent on its RNase catalytic center (Lipert et al., 2017; Matsushita et al., 2009). On the other hand, Regnase-1 engages with other post-transcriptional gene regulators. The helicase UPF1, which is essential for the induction of NMD, directly interacts with Regnase-1 and its helicase activity is critical for Regnase-1-mediated transcript degradation (Mino et al., 2019; Mino et al., 2015). Not only mRNA degradation, but also inhibition of translation has been attributed to Regnase-1. A conserved translational silencing element (TSE) in the 3'-UTR of human *Nfkbiz* is targeted for degradation by Regnase-1. Here, two highly conserved SL (SL 4 and 5) structures are targeted by Regnase-1 to induce mRNA decay, whereas three tandem SL structures (SL1-3) are required in addition to SL4 and 5 for translational silencing by Regnase-1 (Behrens et al., 2018). Interestingly, SL4 and SL5 share sequence and structure

similarities with the Roquin-targeted CDE element. These findings indicate that Regnase-1 serves a broad spectrum of molecular functions to guarantee post-transcriptional gene regulation during an acute immune response.

#### **1.3.2.4 Control of Regnase-1 protein expression**

Since the endonuclease Regnase-1 plays important roles in controlling immune responses, its expression needs to be under tight control to facilitate expression of target genes. In macrophages, Regnase-1 is phosphorylated at the canonical DSGXXS (Ser435, Ser439) sequence motif by the inhibitor of transcription factor NF- $\kappa$ B kinase (IKK) complex upon signaling of TLRs or IL-1R stimulation resulting in ubiquitination and degradation of Regnase-1 (**Figure 5**). Interestingly, self-regulation of Regnase-1 has been reported whereby Regnase-1 targets its own transcript for degradation via a stem loop structure in its 3'-UTR (Iwasaki et al., 2011; Mino et al., 2015). These mechanisms facilitate a tightly coordinated expression of Regnase-1 in macrophages and therefore a release of Regnase-1 target genes like *I/6* from mRNA degradation. In T cells, TCR stimulation and co-stimulation triggers cleavage of Regnase-1 by the paracaspase MALT1 at amino acid 111 (Gewies et al., 2014; Jeltsch et al., 2014; Uehata et al., 2013). Intriguingly, the degradation kinetic is analogous to the cleavage of Roquin proteins depending on TCR signal strength (**Figure 5**).

### **1.3.3 The overlapping functions of Roquin and Regnase-1 in the control of immune responses**

In the previous chapter, the role of the RNA-binding proteins Roquin and Regnase-1 in shaping the adaptive immune response and how their molecular function is integrated into an efficient immune response have been discussed. However, by comparing both types of RNA regulators, it becomes clear that they potentially possess overlapping functions. In T cells, the protein abundance of both factors is strictly controlled by T cell stimulation, when MALT1 cleaves both proteins, thereby facilitating release of targeted mRNAs. Additionally, target transcripts of Roquin and Regnase-1 overlap and require a similar stem loop structure for the recognition of either *trans*-acting factor. Most interestingly, mice deficient for Roquin paralogs or Regnase-1 in T cells develop an autoimmune-like phenotype with similar characteristics, emphasizing their importance in controlling the same steps of T cell biology.

Previously, three publications have discussed the possible overlapping roles of Roquin and Regnase-1 and whether they are functionally redundant, non-redundant or if they cooperate in regulating gene expression in immune cells.

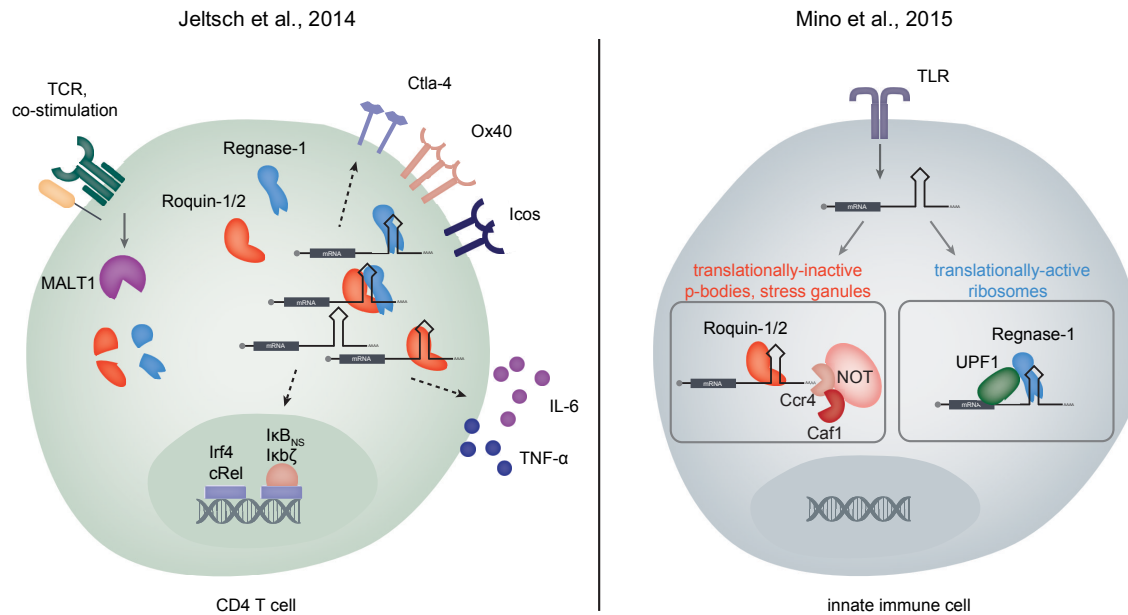


**Figure 6 | Current models of Roquin- and Regnase-1-mediated gene regulation.**

Left side: Jeltsch et al. suggested in 2014 a cooperative gene regulation by Roquin and Regnase-1 in CD4 T cells. Here, Roquin and Regnase-1 regulate target mRNAs with similar stem loop structures and the RNA-binding domain of Roquin is mandatory for mRNA regulation. These target mRNAs involve genes that encode for co-stimulatory receptors (Ctla-4, Icos, Ox40), cytokines (IL-6, TNF- $\alpha$ ), transcription factors (Irf4, cRel) and modulators of transcription factors (I $\kappa$ B<sub>NS</sub>, I $\kappa$ B $\zeta$ ). Upon TCR stimulation and co-stimulation, Roquin and Regnase-1 proteins are cleaved by the paracaspase MALT1 and release targeted mRNAs from repression. Right side: Mino and colleagues published in 2017 a model wherein Roquin and Regnase-1 have spatial-temporally compartmentalized functions. In innate immune cells, Roquin and Regnase-1 control expression of mRNAs that are induced upon toll-like receptor (TLR) stimulation. In bone-marrow-derived macrophages, Roquin is located to P-bodies and in stress granules upon stress induction and regulates translationally-inactive mRNAs by recruiting the Ccr4-Caf1-NOT deadenylation complex. In contrast to that, Regnase-1 was reported to associate with ribosomes and controls translationally-active mRNAs by interaction with the helicase UPF1 and other components of the nonsense-mediated decay pathway.

In 2014, our group identified the first links of a cooperative type of Roquin- and Regnase-1-mediated gene regulation (Jeltsch et al., 2014) (**Figure 6**). Briefly, we identified that Roquin and Regnase-1 control target genes that facilitate T<sub>H</sub>17 differentiation including *Nfkbid*, *Nfkbiz*, *cRel* and *Irf4* in a cooperative manner. We found that Roquin-1/2 and Regnase-1 can downregulate an ICOS-GFP reporter under the control of the *Icos*, *cRel*, *Ctla4*, *Il6* and *Irf4* 3'-UTRs with either overexpression of Roquin in Roquin-deficient or Regnase-1 in Regnase-1-deficient MEF cells. Intriguingly, the repression of a reporter having the CDE of *Tnfa* was only efficient in the presence of the other protein. In addition, this cooperative regulation depends on the RNase activity of Regnase-1 and the RNA-binding capacity of Roquin-1, which we proved by employing a chimeric construct consisting of the ROQ-domain of Roquin fused to Regnase-1. MALT1-induced cleavage of Roquin and Regnase-1 is TCR-signal strength dependent and therefore results in elevated release of Roquin- and Regnase-1 targeted



genes. Collectively, in this study a cooperative mode of gene regulation by these RBPs is suggested, whereby Roquin involves its ROQ-domain for identifying SL structures and the catalytic RNase domain of Regnase-1 is crucial for mediating mRNA degradation.

One year later, the group of Osamu Takeuchi further expanded the knowledge about Roquin and Regnase-1-mediated gene regulation (Mino et al., 2015) (**Figure 6**). However, they suggested a quite different model for post-transcriptional gene regulation.

By performing RNA-immunoprecipitation and sequencing (RIP-Seq) they confirm that Roquin and Regnase-1 target genes significantly overlap in HeLa cells. Interestingly, they identified the mRNA of Regnase-1 itself (*Zc3h12a*) as significantly enriched. Additionally, Regnase-1 predominantly targets py-pu-py triloop stem loops like the CDE and Roquin recognizes SLs in *Tnfa*, *Nfkbiz*, *Ptgs2* and *Il6* in a comparable manner identified by HITS-CLIP (high-throughput sequencing of RNA isolated by crosslinking immunoprecipitation). However, they suggest different subcellular localizations of Roquin and Regnase-1: Here, Regnase-1 localizes to the rough ER-membrane proposing a role in active translation of membrane or secreted proteins, whereas Roquin is found at sites of P-bodies and stress granules upon arsenite treatment in NIH/3T3 mouse cells. In polysomal fractionations, Regnase-1 associates in non-polysomal and polysomal fractions whereas Roquin was only found in fractions with low ribosomal abundance. These data were interpreted that Regnase-1 rather controls mRNAs during active translation and Roquin regulates translationally-inactive transcripts. Additionally, Regnase-1 associates with UPF1, a helicase involved in NMD, and depends on the helicase activity of UPF1, whereas Roquin functions completely independent of UPF1, supporting two distinct regulatory mechanisms by Roquin and Regnase-1. Finally, the authors compared the gene expression of Regnase-1-deficient, *Rc3h1*<sup>san/san</sup> MEF cells and cells with a combined deletion/point mutation upon LPS treatment. Here, the Regnase-1-deficiency affected genes at early timepoints of stimulation, whereas *Rc3h1*<sup>san/san</sup> impacted gene expression at later timepoints and the deletion/point mutation cell line showed an additive and increased expression of the target genes *Il6*, *Tnf* and *Ptgs2*. Together, the authors promoted the concept that Roquin and Regnase-1 are functioning in a spatial- and temporally compartmentalized way.

A third publication claiming that Regnase-1 and Roquin have non-redundant functions was released in 2017 (Cui et al., 2017). Here, the authors generated mice combining the *Rc3h1*<sup>san/san</sup> (*sanroque*) mutation, which is expressed in all cells, with a conditional deletion of Regnase-1 only in T cells (*Zc3h12a*<sup>fl/fl</sup>; *Cd4-cre*) and compared this to either single knockout or *Rc3h1*<sup>san/san</sup> mutant mice. The combined deletion/point mutation mouse mutant showed hyperactivation of T cells tending to differentiate towards T<sub>H</sub>1 shown by high IFN- $\gamma$  production, increased abundance of B cells producing high immunoglobulin levels and cardiac inflammation. All analyzed phenotypes were strongest in the combined deletion/point mutation mouse mutant whereas the single knockout or *sanroque* point mutant revealed a less severe

outcome. mRNA-sequencing of isolated T cells of those mice revealed that T<sub>H</sub>1-signature genes like *Furin* and *Il12rb1* are enriched in deletion/ point mutation mice in comparison to wild-type controls. Here, they claim that the cardiac inflammation seen in deletion/ point mutation mice could be T<sub>H</sub>1-cell related since high IFN- $\gamma$  levels have been reported to promote fibrosis, however the impact of T<sub>H</sub>1 cells in fibrogenesis is still under debate. In addition, the authors addressed the autoregulation of *Zc3h12a* and *Rc3h1/2* mRNA by Roquin and Regnase-1 themselves. Regnase-1 controls *Rc3h1* and *Zc3h12a* mRNA expression while Roquin is not able to regulate Regnase-1-encoding mRNA but can de-stabilize its own transcript in the human T cell line Jurkat.

In summary, all discussed studies share the overlap of Roquin and Regnase-1 target genes and regulation of these targets through RNA stem loops that have comparable structural requirements. Still, the molecular mechanism of Roquin and Regnase-1-mediated gene regulation in T cells remains open as well as the mutual inhibition and autoregulation of Roquin and Regnase-1 is contradictory. Moreover, it is unclear how enhanced phenotypes observed in *Rc3h1*<sup>san/san</sup>; *Zc3h12a*<sup>fl/fl</sup>; *Cd4-cre* mice can be interpreted, since these may either result from nonredundant or cooperative functions in T cells or cooperative effects of Roquin-1 and Regnase-1 in different cell types. Accordingly, it would be of high interest to combine deletion of Roquin-1, Roquin-2 and Regnase-1 in the same cells to analyze the phenotypic consequences of a system lacking these essential RBPs individually and in combination. Therefore, most of this thesis will focus on analyzing the functional association of Roquin-1, Roquin-2 and Regnase-1 and whether these essential mRNA decay factors cooperate in their target gene regulation and consequently together control autoimmunity.

## 2 Aim

The RNA-binding protein Roquin-1 and its paralog Roquin-2 are essential post-transcriptional regulators of mRNAs encoding proteins involved in T cell activation and differentiation. Consequently, mice with a T cell-specific deletion of Roquin-1/2 partially phenocopy the severe autoimmune disease of mice with a single point mutation in Roquin-1 (M199R). Roquin proteins mediate mRNA degradation of target mRNAs by interacting with secondary stem loop structures, the so-called constitutive decay elements (CDE), in 3'-UTRs. However, in the recent years more and more concepts of Roquin-mediated gene regulation have been proposed, suggesting a complex, cooperative network of gene regulation. The aim of this PhD thesis is to unravel the cooperative function of Roquin proteins in controlling mRNA degradation of immune-related mRNAs.

In the first part of this thesis, the cooperation of multiple Roquin proteins on the prototypical Roquin targets *Ox40* and *Nfkbid*, that encode essential factors in CD4 T helper cell fate decisions, were studied in detail. This first required a structural and conservational analysis of *cis*-regulatory elements in the 3'-UTRs of *Ox40* and *Nfkbid* to identify potential new Roquin binding sites. A detailed and complex mutational analysis of Roquin binding secondary structure elements of the *Nfkbid* and *Ox40* 3'-UTRs should uncover a potential cooperativity of multiple Roquin proteins on these prototypical Roquin targets.

The concept of a cooperative gene regulation by Roquin was further extended in the second part of this thesis, which focused on the cooperative gene regulation with the endonuclease Regnase-1. The starting point of this project were the investigations by Jeltsch and colleagues in 2014 who discovered that Roquin and Regnase-1 have overlapping target mRNAs and thus might cooperate in their target gene regulation. The finding that TCR signaling triggers cleavage of both Roquin and Regnase-1 proteins by the paracaspase MALT1 further strengthened this concept. Studies on mouse embryonic fibroblasts with overexpression of Roquin and Regnase-1 confirmed a possible cooperativity in this cell system. However, whether the cooperative regulation is true in CD4 T cells was not proven yet, since further conceptual models were proposed by different groups that rather suggest redundancy and a spatially- and temporally-distinct gene regulation by Roquin and Regnase-1 in immune cells (Cui et al., 2017; Mino et al., 2015). Since deficiency of Roquin proteins and Regnase-1 in T cells caused similar autoimmune-like phenotypes in mice, we generated conditional triple-knockout mice of Roquin-1/2 and Regnase-1 in T cells to identify potential overlapping functions of Roquin and Regnase-1 in controlling autoimmunity. Comparative analysis of all three genotypes should uncover cooperative functions of Roquin and Regnase-1. To further

prove if the phenotypes identified in the conditionally deleted mice are cell-intrinsic, mixed bone marrow chimeric mice were generated with bone marrow from wild-type mice and mice conditionally deleted for Roquin and Regnase-1 in T cells.

To identify if the autoimmune phenotype of these mice is a consequence of an altered RNA expression profile of T cells lacking Roquin and Regnase-1, we performed mRNA-sequencing in CD4 T cells deficient for Roquin-1 and Roquin-2, Regnase-1 and all three genes and compared the differential gene expression pattern. Additionally, reconstitution assays with Roquin or Regnase-1 overexpression on selected target genes in CD4 T cells should help to strengthen the concept of cooperativity. Finally, the physical interaction, which is most likely a requirement for cooperativity, should be tested by co-immunoprecipitation experiments.

### 3 Material and Methods

#### 3.1 Material

##### 3.1.1 Mice

*Rc3h1/2<sup>fl/fl</sup>* mice are transgenic for the Roquin-1-encoding gene *Rc3h1* harboring loxP-sites flanking exon 4 to 6 (Bertossi et al., 2011) as well as the Roquin-2-encoding gene *Rc3h2* with loxP-flanked exon 4 (Vogel et al., 2013). *Zc3h12a<sup>fl/fl</sup>* mice have loxP-sites flanking exon 3 of the Regnase-1-encoding gene *Zc3h12a* (Li et al., 2017). Transgenic *Rc3h1/2<sup>fl/fl</sup>* mice were crossed to *Zc3h12a<sup>fl/fl</sup>* mice to reach the final genotype of *Rc3h1/2<sup>fl/fl</sup>; Zc3h12a<sup>fl/fl</sup>* resulting in six floxed alleles in *Rc3h1*, *Rc3h2* and *Zc3h12a*.

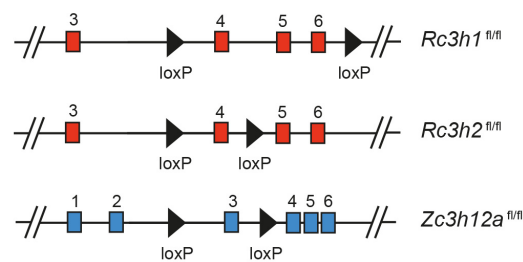


**Figure 7 | Schematic representation of genetically modified alleles of *Rc3h1*, *Rc3h2* and *Zc3h12a*.** Schematic representation of targeting strategy in *Rc3h1*, *Rc3h2* and *Zc3h12a* and position of loxP-flanked sites within the respective genes.

Mice with loxP-flanked genes were crossed to either *Cd4-Cre* (Lee et al., 2001; Sawada et al., 1994) or *Cd4-CreERT2* (Sledzinska et al., 2013) mice to induce recombination of genes. *Cd4-cre* is a transgene that drives Cre recombinase expression under the *Cd4* promoter allowing conditional deletion in the T cell lineage. In *Cd4-CreERT2* transgenic mice, Cre recombinase is fused to estrogen-receptor 2 (ERT2) and is expressed under the CD4 promoter, which induces deletion exclusively in the CD4 T cell subsets by treatment with 4'OH-tamoxifen. In this study this system was used to induce deletion of loxP-flanked alleles either *in vitro* for 24h with 4'OH-tamoxifen or *in vivo* in mice by oral administration of tamoxifen.

*Rc3h1/2<sup>fl/fl</sup>; Cd4-creERT2; rtTA-M2* mice were generated by crossing *Rc3h1/2<sup>fl/fl</sup>; Cd4-creERT2* mice with *Gt(ROSA)26<sup>Sortm1(rtTA\*M2)Jae</sup>* (Hochedlinger et al., 2005). These mice allow expression of an optimized form of reverse tetracycline-controlled transactivator (rtTA-M2) protein, which is compatible with doxycycline-inducible studies utilizing rtTA/tet-ON systems. In this study,

CD4 T cells isolated from these rtTA-expressing mice were *in vitro* retrovirally transduced with a pRetroXTight vector (Takara Clontech) to express a gene of interest under the control of P<sub>Tight</sub>, a modified Tet-responsive promoter that is blocked in the presence of rtTA-M2 and transcription can be induced by administration of doxycycline. All mice were bred on a C57/Bl6 background and housed in a special pathogen-free barrier facility at Helmholtz Zentrum München or Biomedical Center Munich in accordance with the Helmholtz Zentrum München and Biochemical Center Munich institutional, state and federal guidelines.

**Table 1 | Mouse lines utilized in this thesis.**

Mouse line	Name
<i>Cd4-cre</i>	WT
<i>Cd4-creERT2</i>	WT
<i>Rc3h1/2<sup>fl/fl</sup>; rtTA-M2</i>	WT, rtTA
<i>Rc3h1/2<sup>fl/fl</sup>; Cd4-cre</i>	DKO <sup>T</sup>
<i>Rc3h1/2<sup>fl/fl</sup>; Cd4-creERT2</i>	iDKO
<i>Rc3h1/2<sup>fl/fl</sup>; Cd4-creERT2; rtTA-M2</i>	iDKO, rtTA
<i>Rc3h1/2<sup>fl/fl</sup>; Zc3h12a<sup>fl/fl</sup>; Cd4-cre</i>	TKO <sup>T</sup>
<i>Rc3h1/2<sup>fl/fl</sup>; Zc3h12a<sup>fl/fl</sup>; Cd4-creERT2</i>	iTKO
<i>Zc3h12a<sup>fl/fl</sup>; Cd4-cre</i>	KO <sup>T</sup>
<i>Zc3h12a<sup>fl/fl</sup>; Cd4-creERT2</i>	iKO

### 3.1.2 Cell Culture and cell lines

*Rc3h1/2<sup>fl/fl</sup>; creERT2* mouse embryonic fibroblasts (MEF) were generated from *Rc3h1/2<sup>fl/fl</sup>; creERT2* mice (Vogel et al., 2013) and *Rc3h1/2<sup>-/-</sup>* MEF cells were generated from *Rc3h1/2<sup>fl/fl</sup>* mice stably transduced with Cre recombinase to delete the respective exons (**Table 1**).

To produce *Rc3h1/2<sup>-/-</sup>; rtTA3* MEF cells, *Rc3h1/2<sup>-/-</sup>* MEFs were stably transduced with a retrovirus encoding rtTA3 (**Table 2**). Media used for cultivating cell lines (DMEM supplemented with 10% FCS, 1% Pen-Strep and 1% HEPES) and primary T cells (DMEM supplemented with 10% FCS, 1% Pen-Strep, 1% HEPES, 1% non-essential amino acids and  $\beta$ -Mercaptoethanol) are described in **Table 3**.

**Table 2 | Cell lines utilized in this study.**

Cell Line	Species
HEK293	<i>Homo sapiens</i>
<i>Rc3h1/2<sup>fl/fl</sup>; creERT2</i> MEF	<i>Mus musculus</i>
<i>Rc3h1/2<sup>-/-</sup>; rtTA3</i> MEF	<i>Mus musculus</i>

**Table 3 | Cell Culture components and media for mouse embryonic fibroblast (MEF) and T cell culture.**

<b>MEF cell culture medium</b>	<b>Supplier</b>
DMEM (Dulbecco's modified eagle medium + 4,5 g/l D-Glucose + L-Glutamine + Pyruvate)	Thermo Fisher Scientific
10% FCS	PAN Biotech
1% Penicillin-Streptomycin (10.000 U/ml)	Thermo Fisher Scientific
1% HEPES-Buffer pH 7.4 (1 M)	Thermo Fisher Scientific
<b>T cell culture medium</b>	<b>Supplier</b>
DMEM (Dulbecco's modified eagle medium + 4,5 g/l D-Glucose + L-Glutamine + Pyruvate)	Thermo Fisher Scientific
10% FCS	PAN Biotech
1% Penicillin-Streptomycin (10.000 U/ml)	Thermo Fisher Scientific
1% HEPES-Buffer pH 7.4 (1M)	Thermo Fisher Scientific
1 mM $\beta$ -Mercaptoethanol (50 mM)	Sigma-Aldrich
1x MEM non-essential amino acids (100x)	Thermo Fisher Scientific

### 3.1.3 Oligonucleotides

Oligonucleotides were purchased from MWG Eurofins or IDT DNA. DNA Oligonucleotides were salt-free purified and oligonucleotides used in real-time qPCR were HPLC-purified.

**Table 4 | DNA oligonucleotides for cloning.**

Mutations inserted by QuikChange II XL Site directed mutagenesis are shown in bold letters.

<b>Name</b>	<b>Sequence (5' - 3')</b>	<b>Application</b>
<i>Nfkbid</i> (1-263) for	GACCGAAACCCAGAACCTGGAC	cloning
<i>Nfkbid</i> (1-263) rev	CTAGAGTGTTCACAGAAACAATCAAG-	cloning
<i>Nfkbid</i> (1-559) for	TAGCTACAGGGATACACAGACCAA	cloning
<i>Nfkbid</i> (1-559) rev	TGAGGCCAAATTGAGTTTAATTGG	cloning
<i>Nfkbid</i> (1-410) for	ATCGATGGACCGAAACCCAGAACCTG	cloning
<i>Nfkbid</i> (1-410) rev	GGCCTTAATGGCCTCTCAGGGGTGTGGGTCC	cloning
<i>Nfkbid</i> (112-559) for	ATCGATGAGGGTCTTACATTAATACTCCA	cloning
<i>Nfkbid</i> (112-559) rev	GGCCTTAATGGCCTGAGGCCAAATTGAGTTTAATG	cloning
<i>Nfkbid</i> (209-559) for	ATCGATGCTAGGTGATTTCTGTGAAATC	cloning
<i>Nfkbid</i> (209-559) rev	GGCCTTAATGGCCTGAGGCCAAATTGAGTTTAATG	cloning
<i>Nfkbid</i> SL1 LM for	AAACCCAGAACCTGGACTG <b>CAAAAA</b> CAGTCCCCACCGTCCCGTG	QC mutagenesis
<i>Nfkbid</i> SL1 LM rev	CACGGGACGGTGGGGACTG <b>TTTTT</b> GCAGTCCAGGTT CTG GGT TT	QC mutagenesis
<i>Nfkbid</i> SL2 LM for	ACTGATTTTCCAGTCCCCAC <b>GCAGGG</b> GTGGGACAGTC AGCGTATGCT	QC mutagenesis
<i>Nfkbid</i> SL2 LM rev	AGCATACGCTGACTGTCCCAC <b>CCCTGC</b> GTGGGGACTGGAATCAGTC	QC mutagenesis
<i>Nfkbid</i> SL3 LM for	TATCCTGCCATTAGGGTCTTA <b>ACG</b> TAAATACTCCA AAGTGGCACGGG	QC mutagenesis
<i>Nfkbid</i> SL3 LM rev	CCCGTGCCACTTTGGAGTTT <b>ACG</b> TAAAGACCCTAATGGCAGGATAT	QC mutagenesis
<i>Nfkbid</i> SL4 LM for	GGGAGGTGAGCAGTCTCCAA <b>AC</b> ATTGGGGTCTGTGACAC	QC mutagenesis
<i>Nfkbid</i> SL4 LM for	GTGTCACAGACCCCAAT <b>G</b> TTTGGAGACTGCTCACCTCCC	QC mutagenesis

<i>Nfkbid</i> SL5 LM for	AGGGGCTTTCTAGGTGATTTC <b>GTG</b> GAAATCGAGC CCTTTGATTG	QC mutagenesis
<i>Nfkbid</i> SL5 LM rev	CAATCAAGTGGGCTCGATTTC <b>CAC</b> GAAATCACCT AGAAAGCCCCT	QC mutagenesis
<i>Nfkbid</i> SL6 LM for	TCGAGCCCACTTGATTGTTTC <b>CAC</b> AGAAACACTCT AGGGCCATTAA	QC mutagenesis
<i>Nfkbid</i> SL6 LM rev	TTAATGGCCCTAGAGTGTTTCT <b>GTG</b> AAACAATCA AGTGGGCTCGA	QC mutagenesis
<i>Nfkbid</i> SL1 SM for	ACCGAAACCCAGAACCTG <b>CTGT</b> GATTTTCCAGTC CCCA	QC mutagenesis
<i>Nfkbid</i> SL1 SM rev	CGTGGGGACTGGAAAATCA <b>CAG</b> CAGGTTCTGGG TTTCGGT	QC mutagenesis
<i>Nfkbid</i> SL2 SM for	ACTGATTTTCCAGTCC <b>GGT</b> CCGTCCCGTGGGAC AG	QC mutagenesis
<i>Nfkbid</i> SL2 SM rev	CTGTCCACGGGACGG <b>ACCG</b> GACTGGAAAATCA GT	QC mutagenesis
<i>Nfkbid</i> SL3 SM for	AATATATGTGTAATATCCTGCA <b>AACTC</b> ATCTTAC ATTAAACTCCAAAG	QC mutagenesis
<i>Nfkbid</i> SL3 SM rev	CTTTGGAGTTTTAATGTAAGAT <b>GAGG</b> TTTGCAGG ATATTACACATATATT	QC mutagenesis
<i>Nfkbid</i> SL4 SM for	AGTGGCACGGGGGGGAGGTGAT <b>GTCTGGG</b> CAA TATTTGGGGTCTGTGACA	QC mutagenesis
<i>Nfkbid</i> SL4 SM rev	TGTCACAGACCCCAAATATTG <b>CCAGAC</b> ATCACC TCCCCCGTGCCACT	QC mutagenesis
<i>Nfkbid</i> SL5 SM for	CTACAAGGGGCTTTCTAGGT <b>CT</b> ATTCTGTGAAAT CGAGCCAC	QC mutagenesis
<i>Nfkbid</i> SL5 SM rev	GTGGGCTCGATTTCACAGAAT <b>AGAC</b> CTAGAAAGC CCCTTGTAG	QC mutagenesis
<i>Nfkbid</i> SL6 SM for	CTGTGAAATCGAGCCCACTTGAT <b>AC</b> ATTCTGTGA AACACTCTAGGG	QC mutagenesis
<i>Nfkbid</i> SL6 SM rev	CCCTAGAGTGTTTCACAGAAT <b>GT</b> ATCAAGTGGGC TCGATTTACAG	QC mutagenesis
<i>Nfkbid</i> SL1 hexa-tri LM for	CCAGAACCTGGACTG <b>TG</b> TCAGTCCCCACCGTCC	QC mutagenesis
<i>Nfkbid</i> SL1 hexa-tri LM rev	5GGACGGTGGGGACTG <b>ACAC</b> AGTCCAGGTTCTG G	QC mutagenesis
<i>Nfkbid</i> SL2 hexa-tri LM for	CCAGTCCCCACT <b>GTGT</b> GGGACAGTC	QC mutagenesis
<i>Nfkbid</i> SL2 hexa-tri LM rev	CAGTGTCCAC <b>ACAG</b> TGGGGACTGG	QC mutagenesis
<i>Nfkbid</i> SL5 tri-hexa LM for	GGGCTTTCTAGGTGATTTC <b>ATTTTC</b> GAAATCGAG CCCACTTGAT	QC mutagenesis
<i>Nfkbid</i> SL5 tri-hexa LM rev	ATCAAGTGGGCTCGATTTC <b>GAAAAT</b> GAAATCACC TAGAAAGCCC	QC mutagenesis
<i>Nfkbid</i> SL1 Reverse Stem Mutation for	CCAGAACCTG <b>CTGT</b> GATTTTCCAC <b>CAG</b> CCACCGT CCCG	QC mutagenesis
<i>Nfkbid</i> SL1 Reverse Stem Mutation rev	CGGGACGGTGGG <b>CTGT</b> GGAAAATCA <b>CAG</b> CAGGT TCTGG	QC mutagenesis
<i>Nfkbid</i> SL2 Reverse Stem Mutation for	GTCC <b>GGT</b> CCGTCCCG <b>ACCG</b> ACAGTCAGCGTATG	QC mutagenesis
<i>Nfkbid</i> SL2 Reverse Stem Mutation rev	CATACGCTGACTG <b>TGGG</b> ACGGGACGGT <b>CCCG</b> AC	QC mutagenesis
<i>Nfkbid</i> SL5 Reverse Stem Mutation for	AAGGGGCTTTCTAGGT <b>CT</b> ATTCTGTGAAT <b>AGG</b> AG CCCACTTGATTG	QC mutagenesis
<i>Nfkbid</i> SL5 Reverse Stem Mutation rev	CAATCAAGTGGGCT <b>CCT</b> ATTACAGAAT <b>AGAC</b> CT AGAAAGCCCCTT	QC mutagenesis
<i>Nfkbid</i> boxB (1-263) Gibson Cloning Insert for	TCCACTGTGGAATTCGCCCTTCGATGGACCGAA	Gibson cloning



<i>Nfkbid</i> boxB (1-263) Gibson Cloning Insert rev	GCTGGGTCGAATTCGCCCTTGGCCTTAATGGCC	Gibson cloning
<i>Nfkbid</i> boxB (1-263) Gibson Cloning vector for	CGAATTCGACCCAGCTTTCTTGT	Gibson cloning
<i>Nfkbid</i> boxB (1-263) Gibson Cloning vector rev	GAATTCCACAGTGGATATCAAGC	Gibson cloning
$\lambda$ N-Roquin-p2A-mCherry cloning insert for	GGCGGCTCAGGCGGCCCTGTACAAGCTCCACAA TGG	Gibson cloning
$\lambda$ N-Roquin-p2A-mCherry cloning insert rev	GGCTCCGGAACCTGAGGGAGCAGAATTGGAAAC AACTC	Gibson cloning
$\lambda$ N-Roquin-p2A-mCherry cloning vector for	TCAGGTTCCGGAGCCACGAA	Gibson cloning
$\lambda$ N-Roquin-p2A-mCherry cloning vector rev	GCCGCCTGAGCCGCCT	Gibson cloning
<i>Nfkbid</i> boxB (283-559) Gibson Cloning Vector for	CTTGTACAAAGTGGTTCGATGACGG	Gibson cloning
<i>Nfkbid</i> boxB (283-559) Gibson Cloning Vector rev	TTACTTGTACAGCTCGTCCATGCCG	Gibson cloning
Roquin-1 Y250A for	CATGTTGTTTCAGCTCCTC <b>GCC</b> AGAGCCTCCTGCT TCAA	QC mutagenesis
Roquin-1 Y250A rev	TTGAAGCAGGAGGCTCT <b>GGC</b> GAGGAGCTGAACA ACATG	QC mutagenesis

**Table 5 | DNA oligonucleotides and probes from the Universal Probe Library (UPL) system (Roche) used for RT-qPCR analyses.**

Name	Sequence (5' - 3')	UPL probe
<i>Bcl2l1</i> for	TGACCACCTAGAGCCTTGGA	2
<i>Bcl2l1</i> rev	GCTGCATTGTTCCCGTAGA	2
<i>Cd69</i> for	AACGGAAAATAGCTCTTCACATCT	29
<i>Cd69</i> rev	TCCTTCATGATGCTTCTCAAAA	29
<i>Cebpd</i> for	GAGAGTGCAGGAACCTTCTTGGT	4
<i>Cebpd</i> rev	GACCCCATGGCTTTCTCTC	4
<i>cKit</i> for	GATCTGCTCTGCGTCTGT	15
<i>cKit</i> rev	CTTGCAGATGGCTGAGACG	15
<i>cRel</i> for	TTGCAGAGATGGATACTATGAAGC	93
<i>cRel</i> rev	CACCGAATACCCAAATTTTGAA	93
<i>D1ertd622e</i> for	GGAACCTTGACAGTGACATCAT	64
<i>D1ertd622e</i> rev	GGTACTTCTGGAATCCCCATTT	64
<i>Hprt</i> for	TCCTCCTCAGACCGCTTTT	95
<i>Hprt</i> rev	CCTGGTTCATCATCGCTAATC	95
<i>Hdac2</i> for	CTCCACGGGTGGTTCAGT	45
<i>Hdac2</i> rev	CCCAATTGACAGCCATATCA	45
<i>Icos</i> for	AACCTTAGTGGAGGATATTTGCAT	33
<i>Icos</i> rev	CTACGGGTAGCCAGAGCTTC	33
<i>Irf4</i> for	AGCACCTTATGGCTCTCTGC	3
<i>Irf4</i> rev	TGACTGGTCAGGGGCATAAT	3
<i>Nfkbid</i> for	TTTCTACCCTCCGTCAGACC	9
<i>Nfkbid</i> rev	TACAGCCGGGTATCCAGAGA	9
<i>Nfkbiz</i> for	GAGTCCCGTCCCAGAGGT	27
<i>Nfkbiz</i> rev	TTCACGCGAACACCTTGA	27
<i>Rc3h1</i> for	GAGACAGCACCTTACCAGCA	22
<i>Rc3h1</i> rev	GACAAAGCGGGACACACAT	22
<i>Rc3h2</i> for	TTGTCAGCCACCGAATGAC	98
<i>Rc3h2</i> rev	TTCAAATGACCACAAGGTTCC	98
<i>Stat5a</i> for	TTGACGTTTCTTACCTGCAAAG	70
<i>Stat5a</i> rev	GCTCCTGACGGCTCTTGA	70
<i>Tnfrsf4</i> for	GCTTGGAGTTGACTGTGTTCC	79
<i>Tnfrsf4</i> rev	GGGTCTGCTTTCCAGATAAGG	79
<i>Tnfrsf8</i> for	AAGATGGAGCAGACAGATTCT	5
<i>Tnfrsf8</i> rev	TCAACTTGTGTCCCGTGCT	5
<i>Ywhaz</i> for	CGCTAATAATGCAGTTACTGAGAGA	2
<i>Ywhaz</i> rev	TTGGAAGGCCGGTTAATTTT	2
<i>Zc3h12a</i> for	GAAGCAATGTGGCCATGAG	76
<i>Zc3h12a</i> rev	CCTCGCTCCAGAAACCAG	76

### 3.1.4 Chemicals and consumables

**Table 6 | Chemicals and consumables.**

Description	Supplier
1.5 ml, 2 ml centrifuge tubes	Eppendorf, Beckmann
2-Isopropanol	Roth
4'OH-tamoxifen	Sigma-Aldrich
5 ml FACS tubes	Falcon
15 ml, 50 ml tubes	Sarstedt
25 cm <sup>2</sup> 75 cm <sup>2</sup> cell culture flask 175 cm <sup>2</sup>	BD
96-well plate V- bottom	Roth
96-well plate qPCR Lightcycler	4titude
100 mm cell culture dish 150 mm	BD VWR
384-well plate qPCR Lightcycler	4titude
Acrylamide 4K (30%)	AppliChem
Agarose	Biozym
Album Fraction V	Roth
Ammonium-peroxide sulfate (APS)	Roth
Ampicillin	AppliChem
Barrier food wrap	Saran
β-Mercaptoethanol	Roth Invitrogen
Bradford Reagent	Bio-Rad
Brefeldin A	Sigma
BSA (98%)	Sigma
Calcium chloride	Roth
CASY cups	Ols-bio
CASY ton	Ols-bio
Cell culture plates	Falcon
Cell strainer 40 µM Cell strainer 100 µM	Falcon
Centrifuge Maxtract	Qiagen
Chloroform	Sigma
Chloroquine	Sigma
Complete Protease Inhibitor Cocktail Tablets	Roche
Corn Oil	Sigma
Cryo Tubes	Thermo Scientific
Dextran sulphate Amersham	Biosciences
DMSO	Sigma
DNase/ RNase-free H <sub>2</sub> O	Invitrogen
dNTP	Fermentas
Doxycycline-hyclat	Sigma
DTT (Dithiothreitol)	AppliChem
Dulbecco's Modified Eagle Medium (DMEM) low glucose	Invitrogen
Dynabeads Protein A Dynabeads Protein G	Invitrogen
ECL reagent	GE Healthcare Invitrogen
EDTA	Roth
Ethanol (100%)	Roth
Ethanol (denatured)	Roth
Ethidium bromide	Roth
Fetal Calf Serum (FCS)	Sigma

Filter paper Whatman 3mm	Whatman
Filter tips Sarstedt	Molecular BioProducts
Fixable blue Indo-1 viability dye	Thermo Fisher
Fixation and Developing Solution	Agfa
Formaldehyde (37%)	VWR
Glass pipettes 5 ml, 10 ml	Hirschmann ®
Glassware	Schott
Glycerol	Roth
Halt™ Phosphatase Inhibitor	Thermo Fisher
HEPES Buffer (1M)	Invitrogen
Immobilon PVDF Membrane	Merck Millipore
Ionomycin	Calbiochem
Isopropanol bucket	Merck
Kanamycin	Roth
Laboratory film	Parafilm®
LB Agar	Applichem
LB Medium (Miller)	Roth
Methanol	Roth
Milk powder	Roth
MgCl <sub>2</sub> solution (25 mM)	PCR Perkin Elmer
MilliQ water	Millipore
Neubauer Counting Chamber	Roth
NP-40	Sigma
Parafilm	Fleischhacker
Pasteur pipettes	Brand
PCR tubes	Thermo
Penicillin / Streptomycin (Pen-Strep)	Thermo Fisher
Petri Dishes	Greiner
Pipette tips	Rainin
PMA (Phorbol-12-myristate-13-acetate)	Calbiochem
Polybrene	Sigma
Proteinase K	Sigma
RNasin®	Promega
Saponin	VWR
SBA Clonotyping System-AP	Southern Biotech
Sodium acid (NaN <sub>3</sub> )	Roth
Sodium dodecyl sulfate (SDS)	Roth
Spectinomycin	Roth
Syringe filter 0,45 µM	VWR
Tamoxifen	Sigma
Temed	Roth
Tris-HCl pH 7,5	Invitrogen
Triton X-100	Sigma
Trizol	Ambion
Trypan blue	Roth
Trypsin/Ethylenediaminetetraacetic acid (EDTA) (0,05%)	Invitrogen
Tween-20	AppliChem
Whatman-membrane	VWR
X-ray films	Röntgen Bender

### 3.1.5 Kits, markers and enzymes

**Table 7 | Kits and markers.**

<b>Kit/ Marker</b>	<b>Supplier</b>
BD Cytofix/Cytoperm	BD Biosciences
DNA 2-log-ladder	Biolabs
DNA ladder 1 kb	Fermentas
EasySep™ Mouse CD4+ T Cell Isolation Kit	Stem Cell Technologies
EasySep™ Mouse Naïve CD4+ T Cell Isolation Kit	Stem Cell Technologies
Foxp3 staining buffer set	eBioscience
Gene Ruler 1 kb DNA ladder	Invitrogen
In-Fusion® HD Cloning Kit	Takara Clontech
Light Cycler® 480 probes master	Roche
Nucleobond® Xtra Midi/Maxi	Macherey-Nagel
NucleoSpin Gel and PCR Clean Up Kit	Macherey-Nagel
NucleoSpin RNA	Macherey-Nagel
peqGold Protein Marker IV	Peglab
Protein Marker VI prestained 10-245 kDa	AppliChem
PureYield Plasmid Miniprep System	Promega
QIA®quick gel extraction Kit	Qiagen
Quantitect Reverse Transcriptase Kit	Qiagen
QuikChange II XL Site-Directed Mutagenesis Kit	Agilent Technologies
RevertAid Reverse Transcriptase	Thermo
RNeasy® Mini Kit	Qiagen
Universal Probe Library	Roche

**Table 8 | Enzymes.**

<b>Enzyme</b>	<b>Supplier</b>
Gateway® BP clonase enzyme mix	Life technologies
Gateway® LR clonase II enzyme mix	Life technologies
RevertAid Reverse Transcriptase	Qiagen
SUPERase IN	Promega
Taq Polymerase	Invitrogen NEB

### 3.1.6 Buffers

**Table 9 | Buffers.**

Description	Composition
Blocking solution	5% Milk powder TBS
Cell culture freezing medium	FCS 10% DMSO
Citrate-Phosphate Buffer	4,7g Citric Acid 9,2 g Na <sub>2</sub> HPO <sub>4</sub> ·2H <sub>2</sub> O pH 5.0
FACS buffer	2% FCS 0,01% NaN <sub>3</sub> PBS
HBS (2x) pH 6,95 – 7.0	280 mM NaCl 50 mM HEPES 1.5 mM Na <sub>2</sub> HPO <sub>4</sub>
Laemmli loading buffer (5x)	314 mM Tris 50% Glycerol (v/v) 5% SDS (v/v) 5% β-Mercaptoethanol (v/v) 0.01% Bromophenol blue (w/v), adjust buffer to pH 6.8
LB agar	LB medium 1.5% Bacto agar (w/v)
LB Medium	1.0% Tryptone (w/v) 0.5% Yeast extract (w/v) 1.0% NaCl (w/v)
Meister Lysis buffer	20 mM Tris-HCl pH 7.5 150 mM NaCl 0,25% NP-40 1.5 mM MgCl <sub>2</sub>
NP40 lysis Buffer (5x)	250 mM HEPES, pH 7.5 750 mM KCl 10 mM EDTA 5 mM NaF 2,5% (v/v) NP-40
PBS	137 mM NaCl 2.7 mM KCl 10 mM Na <sub>2</sub> HPO <sub>4</sub> , pH 7.4
Saponin buffer	0,5 % Saponin 1% BSA PBS
SDS running buffer	20 mM Tris 200 mM Glycine 0,1 % SDS
TAC lysis buffer	13 mM Tris 140 mM NH <sub>4</sub> Cl, pH 7.2
TBE (1x)	89 mM Tris-borate 2 mM EDTA, pH 8.0
TBS (1x)	50 mM Tris-HCl, pH 8.0 150 mM NaCl
TBS-T	TBS with 0,05% Tween-20
T cell buffer	2% FCS 1 mM EDTA PBS
Transfer buffer for WB	25 mM Tris 39 mM Glycine 20% Methanol (v/v)

### 3.1.7 Antibodies

**Table 10 | Antibodies used for flow cytometry, immunoblotting and T cell cultures.**

Antibody	Clone	Source	Application	Dilution/ Concentration
α-CD3	2C11	E. Kremmer	T <sub>H</sub> 1 culture	0,25 µg/ml
α-CD4	GK1.5	eBioscience	Flow Cytometry	1:200
α-CD5	53-7.3	eBioscience	Flow Cytometry	1:200
α-CD8a	53-6.7	eBioscience	Flow Cytometry	1:200
α-CD21/CD35	7G6	BD	Flow Cytometry	1:200
α-CD23	B3B4	eBioscience	Flow Cytometry	1:200
α-CD24	M1/69	Biolegend	Flow Cytometry	1:200
α-CD28	37.5N	E. Kremmer	T <sub>H</sub> 1 culture	2,5 µg/ml
α-CD25	PC61.5	eBioscience	Flow Cytometry	1:200
α-CD40L	MR1	eBioscience	Flow Cytometry	1:200
α-CD44	IM7	eBioscience	Flow Cytometry	1:200
α-CD45.2	A20	eBioscience	Flow Cytometry	1:200
α-CD45.2	104	eBioscience	Flow Cytometry	1:200
α-CD45R (B220)	RA3-6B2	eBioscience	Flow Cytometry	1:200
α-CD62L	MEL-14	eBioscience	Flow Cytometry	1:200
α-CD69	H1.2F3	BD	Flow Cytometry	1:200
α-CD90.1	OX-7	BD	Flow Cytometry	1:200
α-CD117 (c-Kit)	ACK2	Fisher Scientific	Flow Cytometry	1:200
α-CD127 (IL-7Rα)	A7R34	eBioscience	Flow Cytometry	1:200
α-CD134 (Ox40)	OX-86	eBioscience	Flow Cytometry	1:200
α-CD152 (Ctla-4)	UC10-4B9	eBioscience	Flow Cytometry	1:200
α-CD185 (Cxcr5)	L138D7	Biolegend	Flow Cytometry	1:50
α-CD196 (Ccr6)	R6H1	eBioscience	Flow Cytometry	1:100
α-CD197 (Ccr7)	4B12	eBioscience	Flow Cytometry	1:100
α-CD278 (Icos)	7E.17G9	eBioscience	Flow Cytometry	1:200
α-CD278 (Icos)	C398.4A	eBioscience	Flow Cytometry	1:200
α-CD279 (PD1)	J43	eBioscience	Flow Cytometry	1:200
α-CD357 (GITR)	DTA-1	eBioscience	Flow Cytometry	1:200
α-cleaved caspase-3	D3EP	Cell signaling	Flow Cytometry	1:200
α-cRel	1RELAH5	Invitrogen	Flow Cytometry	1:200
α-cRel	1RELAH5	eBioscience	Western Blot	1:500
α-CyclinA2	E23.1	Invitrogen	Western Blot	1:500
α-GFP	7.1/13.1	Roche	Immunoprecipitation	25 µg/ µl
α-GFP	3E6	Invitrogen	Western Blot	1:1.000
α-Foxp3	FJK-16S	eBioscience	Flow Cytometry	1:100
α-GAPDH	6C5	Merck Millipore	Western Blot	1:10.000
α-GL-7	GL7	eBioscience	Flow Cytometry	1:200
α-goat-α-rat	MRG2a-8.3	Biolegend	Flow Cytometry	1:200
α-hamster IgG	polyclonal	MP Biochemicals	T cell culture	2.5 mg/ml
α-HDAC2	3F3	Santa Cruz Biotechnology	Western Blot	1:10.000
α-IFN <sub>γ</sub>	XMG1.2.1	In house production	T <sub>H</sub> 17 culture	5 µg/ml
α-IFN <sub>γ</sub>	XMG1.2	eBioscience	Flow Cytometry	1:200
α-IgM	II/41	BD	Flow Cytometry	1:200
α- IκB <sub>ζ</sub>	LK2NAP	eBioscience	Flow Cytometry	1:200
α-IκB <sub>NS</sub>	4C1	In house production	Flow Cytometry	1:100
α-IL-2	JES6-5H4	eBioscience	Flow Cytometry	1:200
α-IL-4	11B11	eBioscience	Flow Cytometry	1:40
α-IL-4	11B11	In house production	T <sub>H</sub> 1 culture	10 µg/ml

$\alpha$ -IL-10	JES5-16E3	eBioscience	Flow Cytometry	1:200
$\alpha$ -IL-12	C17.8	in house production	T <sub>H</sub> 17 culture	10 $\mu$ g/ml
$\alpha$ -Irf4	E34	eBioscience	Flow Cytometry	1:200
$\alpha$ -Ly-6G (Gr1)	RB6-8C5	eBioscience	Flow Cytometry	1:200
$\alpha$ -mouse IgG-HRP		Cell Signaling	Western Blot	1:3.000
$\alpha$ -NK1.1	PK136	eBioscience	Flow Cytometry	1:200
$\alpha$ -rat IgG-HRP		Cell Signaling	Western Blot	1:3.000
$\alpha$ -rabbit IgG-HRP		Biolabs	Western Blot	1:3.000
$\alpha$ -Regnase-1	604421	R&D	Western Blot/ Immunoprecipitation	1:500
$\alpha$ -Regnase-1	15D11	In house production	Western Blot Flow Cytometry	1:10
$\alpha$ -Roquin-1	polyclonal	Bethyl	Western Blot	1:1.000
$\alpha$ -Roquin-1/2	3F12	In house production	Western Blot Flow Cytometry	1:10
$\alpha$ -Streptavidin		eBioscience	Flow Cytometry	1:200
$\alpha$ -TCR $\beta$	H57-597	eBioscience	Flow Cytometry	1:200
$\alpha$ -TCR $\gamma\delta$	eBioGL3	eBioscience	Flow Cytometry	1:200

### 3.1.8 Cytokines

Cytokines applied in T cell differentiations and T cell cultures. For concentrations used in different T cell culture systems see **Table 17**.

**Table 11 | Cytokines used for T cell cultures.**

Antibody	Source	Application
hIL-2	Novartis	T cell culture
rmIL-6	R&D System	T <sub>H</sub> 17 culture
rmIL-12 p79	BD Pharmingen	T <sub>H</sub> 1 culture
rhTGF- $\beta$ 1	R&D System	T <sub>H</sub> 17/ T <sub>reg</sub> culture

### 3.1.9 Plasmids

DNA-plasmids were utilized for retroviral production in HEK293 cells. The retroviral expression plasmids MSCV-hICOS-GFP-*Nfkbid*(1-263)-IRES-Thy1.1 (MSCV-*Nfkbid*(1-263)) and MSCV-hICOS-GFP-*Nfkbid*(1-559)-IRES-Thy1.1 (MSCV- *Nfkbid*(1-559)) were kindly provided by Dr. Sven Brenner.

All modifications within MSCV-*Nfkbid*(1-263) were introduced by QuikChange II XL Site-directed mutagenesis (Agilent Technologies).

The RetroX<sup>TM</sup> Tet-ON<sup>®</sup> advanced inducible expression system was purchased at Takara Clontech. Instead of the puromycin resistance gene in the expression vector pRetroX-Tight-Pur, a chloramphenicol resistance and CcdB gene were introduced, which are flanked by Gateway-cloning-compatible attR1 and attR2 sites. This allows recombination of a gene sequence from a Gateway entry vector into the modified pRetroXTight vector (see section



**3.2.1.2).** Plasmids for expression of doxycycline-inducible GFP-fusion proteins like pRetroXTight-GFP, -GFP-Roquin-1, -GFP-Regnase-1 and -GFP-Regnase-1(D141N) were kindly supplied by Dr. Gesine Behrens and Sascha Wani. The pRetroXTight- $\lambda$ N-fusion proteins and the MSCV-*Nfkbid*(1-263)-boxB constructs were generated by Gibson Assembly utilizing the In-Fusion® HD cloning Kit (Takara Clontech).

**Table 12 | Retroviral expression plasmids.**

Destination vector	Insert	Application
MSCV-hICOS- GFP-CcdB-IRES-Thy1.1	<i>Nfkbid</i> (1-263)	Retroviral expression
MSCV-hICOS- GFP-CcdB-IRES-Thy1.1	<i>Nfkbid</i> (1-263)-SL1LEM	Retroviral expression
MSCV-hICOS- GFP-CcdB-IRES-Thy1.1	<i>Nfkbid</i> (1-263)-SL1LM	Retroviral expression
MSCV-hICOS- GFP-CcdB-IRES-Thy1.1	<i>Nfkbid</i> (1-263)-SL1RSM	Retroviral expression
MSCV-hICOS- GFP-CcdB-IRES-Thy1.1	<i>Nfkbid</i> (1-263)-SL1SM	Retroviral expression
MSCV-hICOS- GFP-CcdB-IRES-Thy1.1	<i>Nfkbid</i> (1-263)-SL2LEM	Retroviral expression
MSCV-hICOS- GFP-CcdB-IRES-Thy1.1	<i>Nfkbid</i> (1-263)-SL2LM	Retroviral expression
MSCV-hICOS- GFP-CcdB-IRES-Thy1.1	<i>Nfkbid</i> (1-263)-SL2RSM	Retroviral expression
MSCV-hICOS- GFP-CcdB-IRES-Thy1.1	<i>Nfkbid</i> (1-263)-SL2SM	Retroviral expression
MSCV-hICOS- GFP-CcdB-IRES-Thy1.1	<i>Nfkbid</i> (1-263)-SL3LM	Retroviral expression
MSCV-hICOS- GFP-CcdB-IRES-Thy1.1	<i>Nfkbid</i> (1-263)-SL3SM	Retroviral expression
MSCV-hICOS- GFP-CcdB-IRES-Thy1.1	<i>Nfkbid</i> (1-263)-SL4LM	Retroviral expression
MSCV-hICOS- GFP-CcdB-IRES-Thy1.1	<i>Nfkbid</i> (1-263)-SL4SM	Retroviral expression
MSCV-hICOS- GFP-CcdB-IRES-Thy1.1	<i>Nfkbid</i> (1-263)-SL5LM	Retroviral expression
MSCV-hICOS- GFP-CcdB-IRES-Thy1.1	<i>Nfkbid</i> (1-263)-SL5SM	Retroviral expression
MSCV-hICOS- GFP-CcdB-IRES-Thy1.1	<i>Nfkbid</i> (1-263)-SL6LM	Retroviral expression
MSCV-hICOS- GFP-CcdB-IRES-Thy1.1	<i>Nfkbid</i> (1-263)-SL6SM	Retroviral expression
MSCV-hICOS- GFP-CcdB-IRES-Thy1.1	<i>Nfkbid</i> (1-263)-SL3+4LM	Retroviral expression
MSCV-hICOS- GFP-CcdB-IRES-Thy1.1	<i>Nfkbid</i> (1-263)-SL5+6LM	Retroviral expression
MSCV-hICOS- GFP-CcdB-IRES-Thy1.1	<i>Nfkbid</i> (1-263)-SL3+4+6LM	Retroviral expression
MSCV-hICOS- GFP-CcdB-IRES-Thy1.1	<i>Nfkbid</i> (1-263)-SL2+3+4+6LM	Retroviral expression
MSCV-hICOS- GFP-CcdB-IRES-Thy1.1	<i>Nfkbid</i> (1-263)-SL2+3+4+5+6LM	Retroviral expression
MSCV-hICOS- GFP-CcdB-IRES-Thy1.1	<i>Nfkbid</i> (1-263)-SL1_boxB	Retroviral expression
MSCV-hICOS- GFP-CcdB-IRES-Thy1.1	<i>Nfkbid</i> (1-263)-SL2_boxB	Retroviral expression
MSCV-hICOS- GFP-CcdB-IRES-Thy1.1	<i>Nfkbid</i> (1-263)-SL5_boxB	Retroviral expression
MSCV-hICOS- GFP-CcdB-IRES-Thy1.1	<i>Nfkbid</i> (1-263)-SL125_boxB	Retroviral expression
MSCV-hICOS- GFP-CcdB-IRES-Thy1.1	<i>Nfkbid</i> (1-263)-SL5_boxB	Retroviral expression
MSCV-hICOS- GFP-CcdB-IRES-Thy1.1	<i>Nfkbid</i> (1-263)-SL125_boxB	Retroviral expression
MSCV-hICOS- GFP-CcdB-IRES-Thy1.1	<i>Nfkbid</i> (1-559)	Retroviral expression
pRetroXTight-CcdB	GFP	Retroviral expression
pRetroXTight-CcdB	GFP-Roquin-1	Retroviral expression
pRetroXTight-CcdB	GFP-Regnase-1	Retroviral expression
pRetroXTight-CcdB	GFP-Regnase-1(D141N)	Retroviral expression
pRetroXTight-CcdB	Roquin-1	Retroviral expression
pRetroXTight-CcdB	Roquin-1(Y250A)	Retroviral expression
pRetroXTight-CcdB	Roquin-1 (K220A+K239A+R260A)	Retroviral expression
pRetroXTight-CcdB	$\lambda$ N-p2A-mCherry	Retroviral expression
pRetroXTight-CcdB	$\lambda$ N-Roquin-1 (K220A+K239A+R260A)-p2A- mCherry	Retroviral expression

**Table 13 | Entry vectors for Gateway cloning.**

Entry vector	Insert
pCR8/GW/TOPO	Roquin-1
pCR8/GW/TOPO	Roquin-1(K220A-K239A-R260A)
pCR8/GW/TOPO	Roquin-1(Y250A)

### 3.1.10 Software and technical devices

**Table 14 | Software.**

Software	Application	Supplier
Adobe Illustrator CS6 Adobe Photoshop CS6	Image processing	Adobe
ApE	Sequence alignment	<a href="http://jorgensen.biology.utah.edu/wayned/apel/">http://jorgensen.biology.utah.edu/wayned/apel/</a>
Endnote X7	Organization of citations	Clarivate analytics
FlowJo 10	Flow cytometry data analysis	Treestar
Microsoft® Excel Microsoft® PowerPoint Microsoft® Word	Data processing	Microsoft
Prism 5.0	Data processing	Graphpad

**Table 15 | Technical devices and instruments.**

Description	Supplier
-80°C freezer	Thermo Scientific
-20°C freezer	Liebherr
4°C fridge	Liebherr
37°C bacterial incubator	Memmert
37°C mammalian cell incubator	New Brunswick
Autoclave (Varioklav)	H+R
BD Canto II	Beckman Dickinson
BD Fortessa 5 Laser	Beckman Dickinson
Cassettes for SDS-PAGE	Life Technologies
Cell counter	Casy Cell Counter, Innovartis
Centrifuges	Eppendorf 5417R (1.5ml reaction tubes) Eppendorf Centrifuge 5810R (15 and 50ml reaction tube) Beckmann-Coulter SS34
Cytoflex	Beckman Dickinson
Developer machine Curix 60	Agfa
Film cassettes	VWR
Fluorescence microscope	Leica
Freezing box Isopropanol	Roth
Gel documentation system	Bio-Rad
Gel electroporation chamber	Bio-Rad
Gel cassettes SDS gel	Bio-Rad
Hood (Tissue Culture)	Clean Air
Ice machine	Scotsman
Incubation shaker	Eppendorf
Light cycler 480®	Roche
Magnet stirrer	IKA
Microscopes	Zeiss
Microwave	LG
Neubauer counting chamber	Brand
pH-Meter	InoLab pH 720

---

Photometer	Eppendorf
Pipetboy	Eppendorf
Pipettes	Rainin
Power supply	Bio-Rad
Rotating wheel	Neolab, VWR
Shaker	Roth
Spectrophotometer	Nanodrop ND100, Peqlab
SD semi-dry transfer cell	Biorad
Thermocycler	Analytic Jena, Biozym
Thermomixer 5436	Eppendorf
Vacuum pump	VWR
Vortexer	IKA
X-ray machine	XStrahl RS225

## 3.2 Methods

### 3.2.1 Molecular biology methods

#### 3.2.1.1 Polymerase chain reaction

Polymerase chain reaction (PCR) allows for exponential amplification of DNA fragments by utilizing gene-specific forward and reverse primers, heat-stable DNA Polymerases and primer- and polymerase-specific cycling temperatures. A standard PCR reaction is shown in **Table 16**. Here, the Taq Polymerase by New England Biolabs was utilized.

**Table 16 | Reagents and PCR-cycle conditions used in a standard PCR reaction.**

reagent	final concentration	50 $\mu$ l reaction
Taq Reaction Buffer (10x)	1x	5 $\mu$ l
dNTPs (10 mM)	200 $\mu$ M	1 $\mu$ l
forward primer (10 $\mu$ M)	0,2 $\mu$ M	1 $\mu$ l
reverse primer (10 $\mu$ M)	0,2 $\mu$ M	1 $\mu$ l
Taq DNA Polymerase	1,25 units	0,25 $\mu$ l
template DNA	1-100 ng	variable
nuclease-free H <sub>2</sub> O		to 50 $\mu$ l

step	temperature	time
Initial denaturation	95°C	30 s
30 cycles	95°C	30 s
	45 – 68 °C	15-60 s
	68°C	1 min/kb
Final extension	68°C	5 min

The reaction mix contained about 1-100 ng DNA as template, 5  $\mu$ l 10x reaction buffer, 1  $\mu$ l dNTP Mix (10 mM each), 1  $\mu$ l MgCl<sub>2</sub> (50 mM), 2  $\mu$ l forward and reverse primer (10 mM each) and 1  $\mu$ l Taq Polymerase. Deionized water was added to reach the final volume of 50  $\mu$ l. The PCR was performed for 30 cycles with denaturation at 95°C for 30 sec, annealing at 52°C for 30 sec and elongation at 72°C for 45 sec. The reaction products were size separated by electrophoresis on a 1.5% (w/v) agarose gel in 1x TBE buffer and visualized by UV light. The band with the correct size was cut, and DNA purified using the QIA®quick gel extraction Kit according to the given instructions.

#### 3.2.1.2 Cloning methods

Different cloning techniques were applied to produce expression plasmids utilized for retroviral transduction (**Table 12**). All primer pairs are given in **Table 4**.

### Gateway® Cloning:

The Gateway® cloning method (Invitrogen) relies on bacteriophage att-site-mediated gene recombination within entry (pCR8/GW/TOPO) and destination vector (MSCV-IRES-Thy1.1 or pRetroXTight) systems (**Table 12** and **Table 13**). For generation of doxycycline-inducible expression plasmids, the pCR8/GW/TOPO plasmid containing the gene of interest flanked by attL-sites was used to integrate the gene of interest into modified pRetroXTight retroviral plasmid harboring attR-recombination sequences via Gateway LR recombination according to manufacturer's protocol.

### QuikChange II XL Site directed mutagenesis:

QuikChange II XL Site-Directed mutagenesis (Agilent Technologies) was used to introduce mutations in retroviral reporter plasmids by PCR amplification with primers containing the mutated sequence flanked by gene-specific sequences 5' and 3' of the mutation and a high-proof-reading Pfu Polymerase. Mutations in *Nfkbid* sequence within the MSCV-ICOS-GFP-*Nfkbid* 3'-UTR-IRES-Thy1.1 reporter were generated using site-directed mutagenesis.

### In-Fusion® HD Cloning:

In-Fusion® HD Cloning (Takara Clontech) relies on the Gibson assembly strategy that allows integration of an insert into a linearized backbone based on complementary 15 nt-overhangs within double-stranded insert and backbone, which are digested by a T5-exonuclease at the 5'-end allowing hybridization of sticky ends. DNA-Polymerase and Ligase then amplify and join insert and backbone. To introduce three or one  $\lambda$ N binding sequences (boxB RNA stem-loops) in the *Nfkbid*(1-263) 3'-UTR, the corresponding DNA constructs were synthesized by IDT and cloned into the MSCV-ICOS-GFP-IRES-Thy1.1 reporter by Gibson assembly using the In-Fusion HD cloning Kit. Cloning of the boxB binding protein  $\lambda$ N-p2A-mCherry or the fusion protein  $\lambda$ N-Roquin(K220A, K239A, R260A)-p2A-mCherry was performed by PCR-amplification followed by Gibson assembly (**Table 12**). These constructs were then sub-cloned into a modified pRetroXTight vector backbone by Gibson assembly.

#### **3.2.1.1 Transformation**

Frozen chemical-competent DH5 $\alpha$  *E. coli* cells (in-house production) were thawed on ice. 50  $\mu$ l of bacteria suspension were gently mixed with plasmid DNA. The solution was incubated on ice for 20 min, subsequently exposed to a heat shock at 42°C for 30 sec and immediately cooled down on ice for 2 min. After addition of 100  $\mu$ l LB media bacteria cells were incubated for 1 h at 37°C. Then cells were plated onto selective LB Plates containing appropriate antibiotics (100  $\mu$ g/ml) and incubated ON at 37°C.

### **3.2.1.2 Bacterial culture and preparation of plasmid DNA**

*E. coli* bacteria were grown in 3 ml of LB medium (small-scale, “mini”-culture) or 250 ml (large-scale, “maxi”-culture) supplemented with the appropriate antibiotic (100 µg/ml ampicillin) at 37°C overnight while constantly shaking with 160 rpm. Cultures were then harvested by centrifugation (4.122 x g, 4°C) and the plasmids were isolated using PureYield Plasmid Miniprep System for small-scale or Nucleobond® Xtra Midi/Maxi kit for large-scale DNA isolation following the manufacturer’s protocol.

### **3.2.1.3 Agarose Gel Electrophoresis**

Size separation of DNA fragments was performed by electrophoresis on agarose gels (0.75% - 1.5% w/v agarose in TBE) containing 0.5 µg/ml ethidium bromide. Bands were visualized under UV light (254 – 366 nm).

## **3.2.2 Cell biology methods**

### **3.2.2.1 Definition of cell numbers**

Cell suspensions isolated from mouse organs were counted by the Casy cell counter according to manufacturer’s instruction. Cell numbers of adherent cell lines were defined by cell counting with a Neubauer counting chamber. Here, cells of a specific density were mixed with Trypan blue. Cells were then distributed onto the Neubauer Counting Chamber and cells in the 4 quadrants were counted. The mean of counted cells was determined and the dilution factor of  $1 \times 10^4$  was included in the calculation to define the final cell concentration.

### **3.2.2.2 Cryo-conservation of cell lines**

Cells were counted as described above and a desired number of cells was centrifuged and washed once in PBS. After another centrifugation step, the cell pellet was taken up in 1 ml FCS + 10% DMSO and immediately frozen at -80°C in an isopropanol freezing bucket.

To thaw frozen cells, the vials were briefly put in a 37°C water bath and cells were quickly taken up in 10 ml of fresh DMEM culture medium. After one centrifugation step, the cells had been cultivated in an appropriate cell culture vessel.

### **3.2.2.3 Cultivation of eukaryotic cell lines**

Adherent cell lines e.g. HEK293 cells and mouse embryonic fibroblasts (MEFs), were cultivated in a 37°C, 10% CO<sub>2</sub> incubator with DMEM cell culture medium containing 10% fetal calf serum (FCS), 1% Penicilin-Streptomycin (Pen-Strep) and 1% HEPES-Buffer (**Table 3**).

Cell lines were splitted each 3 to 4 days until reaching a specific cell density. To avoid overgrowing of adherent cells, the cell culture medium was aspirated, and cells were washed with PBS. After removing PBS, the cells had been relieved from the cell culture plate by incubation with Trypsin-EDTA and taken up again in fresh DMEM cell culture medium and cultivated in the incubator.

### 3.2.2.4 Isolation and cultivation of primary CD4 T cells

For cultivation of primary CD4 T cells, mice were sacrificed at an age of 6-12 weeks by CO<sub>2</sub> euthanasia and cervical dislocation and spleen as well as cervical, axillary, brachial, inguinal and mesenteric lymph nodes were dissected and pooled. To perform phenotypic flow cytometry analysis, spleen, thymus and peripheral as well as mesenteric lymph nodes were taken from sacrificed mice and cells were purified individually. Organs were squished and passed through a 100 µm filter. Erythrocytes were eliminated in spleens by tris-ammonium-chloride (TAC)-lysis. After one additional filtration step through a 150 µm filter, the cell suspension was either directly used for flow cytometry analysis (see 3.2.2.11) or CD4 T cells were isolated by negative selection using Stem Cell Mouse CD4<sup>+</sup> T cell isolation Kit according to manufacturer's protocol. Purified CD4 T cells were then cultured in DMEM T cell culture medium supplemented with 10% FCS, 1% Pen-Strep, 1% HEPES-Buffer, 1% non-essential amino acids (NEAA) and 1 mM β-Mercaptoethanol (**Table 3**).

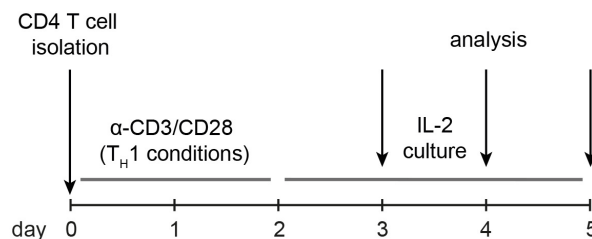


**Figure 8 | Schematic representation of T cell culture under TH1 conditions.**

CD4 T cells were isolated from spleen and lymph nodes and stimulated with α-CD3/ CD28 under TH1 conditions for 2 days (Table 17). Cells were then expanded and cultured with T cell medium containing IL-2 and analysis of cells was performed on day 3, 4 or 5.

To culture primary CD4 T cells, TH1 differentiation was performed. Therefore, 4-5 Mio purified CD4 T cells were taken up in T cell medium containing 0,25 µg/ml α-CD3, 2.5 µg/ml α-CD28, 10 µg/ml α-IL-4 and 10 ng/ml IL-12 (**Table 11**) and cultured on α-hamster IgG pre-coated 6-well culture plates for 40-48h. Cells were cultured in medium supplemented with 20 U/ml hIL-2 in a 10% CO<sub>2</sub> incubator and expanded for 3-4 days, whereas cells were fed with fresh IL-2-containing medium every 24h and cultured at a density of 0.5 - 1 Mio cells/ ml (**Figure 8**).

### 3.2.2.5 *In vitro* deletion of loxP-flanked genes by 4'OH-tamoxifen

Mouse embryonic fibroblasts that express creERT2 and loxP-flanked alleles for Roquin-1 and Roquin-2 (*Rc3h1/2*) were treated with 0.32  $\mu$ M 4'-hydroxy (OH)-tamoxifen for 24h to induce deletion. Purified CD4 T cells from mice that were heterozygous for *Cd4*-creERT2 and expressed loxP-flanked alleles were treated with 1  $\mu$ M 4'OH-tamoxifen for 24h to induce deletion of loxP-flanked genes. Cells were washed once in T cell culture medium and then activated in T cell medium under T<sub>H</sub>1 conditions (**Table 11**) and seeded on a goat- $\alpha$ -hamster IgG pre-coated plate. Cells were further cultured and expanded as described in 3.2.2.4 (**Figure 9**).

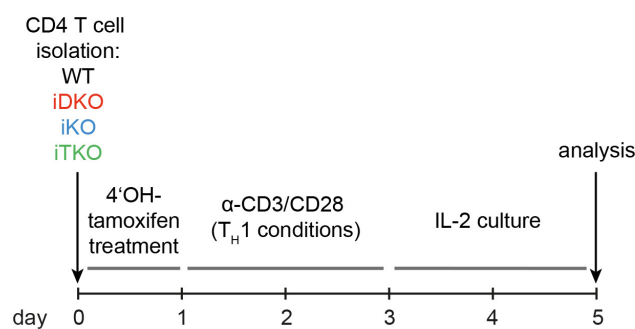


**Figure 9 | Schematic representation of T cell culture under T<sub>H</sub>1 conditions with 4'OH-tamoxifen-induced gene deletion.**

CD4 cells were isolated from *Cd4*-creERT2 (WT), *Rc3h1/2*<sup>fl/fl</sup>; *Cd4*-creERT2 (iDKO), *Zc3h12a*<sup>fl/fl</sup>; *Cd4*-creERT2 (iKO) or *Rc3h1/2*<sup>fl/fl</sup>; *Zc3h12a*<sup>fl/fl</sup>; *Cd4*-CreERT2 (iTKO) mice and deletion of loxP-flanked alleles was induced *in vitro* by 4'OH-tamoxifen treatment for 24h. After T cell stimulation under T<sub>H</sub>1 conditions (Table 17) and IL-2 culture for 2d, cells were used for further analysis.

### 3.2.2.6 Calcium-phosphate-transfection of HEK293 cells and retrovirus production

Retroviral transduction was used to stably integrate transgenes into MEF cells and primary CD4 T cells. Therefore, retrovirus was produced in HEK293 cells by Calcium-phosphate-transfection of plasmids (MSCV=Murine Stem Cell Virus or modified pRetroXTight, **Table 12**) containing an SV-40 promoter and the transgene flanked by long terminal repeat (LTR) sequences together with a pCI-Eco vector expressing viral packaging and envelope genes (*gag-pol* and *env*). In detail, HEK293 cells were seeded at a density of 8 million cells on 15 cm culture dishes one day prior to the experiment. On the day of transfection, the medium was replaced by 17 ml DMEM supplemented with chloroquine (100  $\mu$ M) and incubated for 1h at 37°C, 5% CO<sub>2</sub>. Meanwhile the transfection mix was prepared by mixing 50  $\mu$ g of plasmid DNA with 5  $\mu$ g of the packaging vector pCI-Eco, 125 mM CaCl<sub>2</sub> and H<sub>2</sub>O to reach a final volume of 1250  $\mu$ l. The DNA-CaCl<sub>2</sub> mixture was then supplemented with 1250  $\mu$ l HBS (pH 6.95-7.05) while vortexing. This mix was incubated for 15-20 min at RT and then added dropwise on



HEK293 cells containing chloroquine-medium. 7h after transfection the medium was exchanged with fresh DMEM medium. After 48h, the cell culture supernatant containing retrovirus particles was harvested and passed through a 0.45  $\mu\text{m}$  syringe filter and either used freshly or stored at  $-80^{\circ}\text{C}$ .

### 3.2.2.7 Retrovirus transduction of MEF cells or primary CD4 T cells

For stable integration of transgenes into cell genomes, retroviral infection was performed. MEF cells were seeded at a density of 50.000 cells in a 6-well plate at  $37^{\circ}\text{C}$  for 16-18h. Cells were then spin infected with retrovirus supplemented with 5  $\mu\text{g/ml}$  polybrene in a centrifuge at 300 x g at  $32^{\circ}\text{C}$  for 2hr. After 6h, virus supernatant was removed, and fresh medium was added to the cells. When using MEF cells expressing the reverse tetracycline-dependent transactivator rtTA3 and transduced with pRetroXTight constructs, doxycycline was administered for 16h to induce expression of genes. Transduction efficiency was measured by flow cytometry detecting the marker Thy1.1 (MSCV-reporter) or GFP (pRetroXTight-expression plasmid). Retroviral transduction of primary CD4 T cells expressing rtTA-M2 (*Rc3h1/2*<sup>fl/fl</sup>; rtTA (WT, rtTA) or *Rc3h1/2*<sup>fl/fl</sup>; *Cd4*-creERT2; rtTA-M2 (iDKO, rtTA)) was performed during T cell activation with  $\alpha$ -CD3/CD28. 40h after seeding cells onto pre-coated goat- $\alpha$ -hamster IgG plates (see 3.2.2.4), cell culture medium was replaced by retrovirus-containing medium and 5  $\mu\text{g/ml}$  polybrene. After spin-infection via centrifugation at 2.000 rpm at  $18^{\circ}\text{C}$  for 1h, cells were incubated at  $37^{\circ}\text{C}$ , 5%  $\text{CO}_2$  for 6h. Then virus-containing medium was aspirated and cells were resuspended in T cell culture medium containing hIL-2 and further cultivated as described above. Gene expression was induced by administration of 1  $\mu\text{g/ml}$  doxycycline for 6-16h prior to analysis (Figure 10).

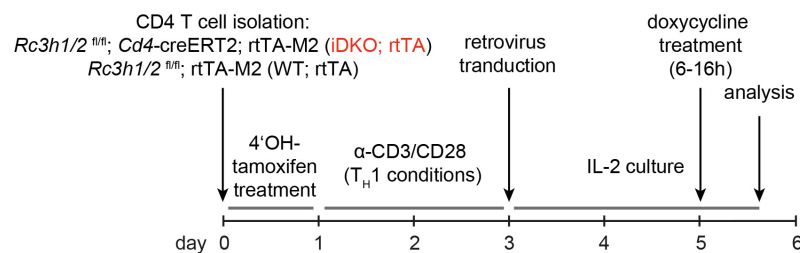


**Figure 10 | Schematic representation of T cell culture under T<sub>H</sub>1 conditions with 4'OH-tamoxifen-induced gene deletion and retroviral transduction.**

CD4 cells were isolated from *Rc3h1/2*<sup>fl/fl</sup>; rtTA-M2 (WT, rtTA) or *Rc3h1/2*<sup>fl/fl</sup>; *Cd4*-creERT2; rtTA-M2 (iDKO, rtTA) both expressing the reverse tetracycline-dependent transactivator rtTA-M2 and deletion of loxP-flanked alleles was induced *in vitro* by 4'OH-tamoxifen treatment for 24h. After 40h of T cell stimulation under T<sub>H</sub>1 conditions (Table 17), cells were transduced with a pRetroXTight retrovirus harboring a doxycycline-inducible cassette. Cells were cultured in IL-2-containing medium for 2 d. Expression of retrovirally integrated plasmids was induced by administration of doxycycline for 6-16h prior to further analysis.

*Rc3h12<sup>-/-</sup>*, rtTA3 MEF cells were first transduced with retroviruses encoding the *Nfkbid* reporter harboring either boxB RNA structures or the wild-type *Nfkbid* reporter. Two days after the first transduction, these cells were super-transduced with retroviruses encoding  $\lambda$ N-Roquin (K220A, K239A, R260A)-p2A-mCherry fusion protein or  $\lambda$ N-p2A-mCherry itself. Overexpression of  $\lambda$ N-constructs was induced by the addition of 1  $\mu$ g/ml doxycycline for 14h two days after superinfection. The infected cells were analyzed by flow cytometry.

### 3.2.2.8 *Ex vivo* stimulation of CD4 T cells with PMA and ionomycin

To measure cytokine expression of *ex vivo* isolated cells from spleen, 1 - 2 Mio splenocytes were taken up in T cell medium containing 20 nM PMA and 1  $\mu$ M ionomycin. PMA and ionomycin stimulation lead to the activation of T cells by inducing different signaling pathways that lead to cytokine secretion of T cells. After an incubation time of 2.5h, cells were supplemented with 10  $\mu$ g/ml Brefeldin A and further incubated for another 2.5h. Brefeldin A inhibits protein transport from the golgi apparatus and thus cytokines remain in the cytoplasm and can be analyzed by flow cytometry. Therefore, cells were intracellularly stained with antibodies against cytokines (see **Table 10**) and analyzed on a flow cytometer.

### 3.2.2.9 Tamoxifen gavage and *in vitro* differentiation of naïve CD4 T cells

To examine the differentiation capacity of naïve T cells with deficiency of Roquin- and Regnase-1 alleles, deletion was induced in mice by oral administration of tamoxifen. Therefore, mice received 50 mg tamoxifen diluted in corn oil on 3 consecutive days whereas on the last day mice got 2 doses of tamoxifen. Mice were sacrificed three days after treatment and naïve T cells were isolated from spleen and LNs by applying the EasySep™ Mouse Naïve CD4+ T Cell Isolation Kit according to manufacturer's protocol.

**Table 17 | Antibody and cytokine concentrations for T helper cell differentiations.**

	<b>T<sub>H</sub>0</b>	<b>T<sub>H</sub>1</b>	<b>T<sub>H</sub>17</b>	<b>T<sub>reg</sub></b>
$\alpha$ -CD3	0,25 ng/ml	0,25 ng/ml	0,25 ng/ml	0,25 ng/ml
$\alpha$ -CD28	2,5 $\mu$ g/ml	2,5 $\mu$ g/ml	2,5 $\mu$ g/ml	2,5 $\mu$ g/ml
$\alpha$ -IFN-g	-	-	5 $\mu$ g/ml	-
$\alpha$ -IL-2	-	-	2,5 $\mu$ g/ml	-
$\alpha$ -IL-4	-	10 $\mu$ g/ml	10 $\mu$ g/ml	-
$\alpha$ -IL-12	-	-	10 $\mu$ g/ml	-
IL-2	-	-	-	100 IE/ml
IL-6	-	-	60 ng/ml	-
IL-12	-	10 ng/ml	-	-
TGF- $\beta$	-	-	10 ng/ml	2 ng/ml

T cells were then activated under  $T_H1$ ,  $T_H17$ ,  $T_{reg}$  or  $T_H0$  conditions (**Table 17**) for 3.5d on a goat- $\alpha$ -hamster IgG pre-coated 96-well plate and split on the 2<sup>nd</sup> day. Cells were restimulated with PMA and ionomycin as described above. Cells were then stained for intracellular cytokine expression and analyzed on a flow cytometer (**Figure 11**).

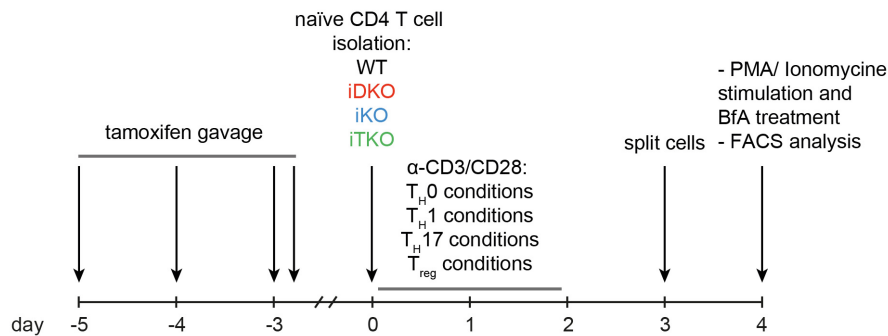


**Figure 11 | Schematic representation of *in vitro* differentiation of naïve T cells deleted by tamoxifen gavage *in vivo*.**

*Cd4*-creERT2 (WT), *Rc3h1/2*<sup>fl/fl</sup>; *Cd4*-creERT2 (iDKO), *Zc3h12a*<sup>fl/fl</sup>; *Cd4*-creERT2 (iKO) and *Rc3h1/2*<sup>fl/fl</sup>; *Zc3h12a*<sup>fl/fl</sup>; *Cd4*-creERT2 (iTKO) mice were treated with tamoxifen on three consecutive days, whereas on the third day mice received two pulses of tamoxifen. Three days later, naïve CD4 T cells were isolated and stimulated under  $T_H0$ ,  $T_H1$ ,  $T_H2$ ,  $T_H17$  and  $T_{reg}$  conditions (Table 17). After a 3 days culture in IL-2-containing medium, cells were split and 24h later cells were restimulated with PMA and ionomycin in the presence of Brefeldin A (BfA) and cytokine expression was analyzed by flow cytometry.

### 3.2.2.10 Generation of mixed bone marrow chimeric mice

Bone marrow cells were isolated from following donor mice:  $CD45.1^+$  WT ( $WT^{CD45.1}$ ),  $CD45.2^+$  *Cd4*-cre ( $WT^{CD45.2}$ ) or  $CD45.2^+$  *Rc3h1/2*<sup>fl/fl</sup>; *Zc3h12a*<sup>fl/fl</sup>; *Cd4*-cre ( $TKO^T CD45.2$ ). Here, femurs and tibias were taken, and bones were rinsed with PBS to isolate bone marrow cells. After one washing step in PBS + 3% FCS, cells were frozen in FCS containing 10% DMSO and stored at -80°C until injected into mice.  $CD45.1/2$  heterozygous recipient mice were lethally irradiated with 5,5 Gy (=550 rad)  $\gamma$ -radiation of a <sup>137</sup>Cs-source twice on two consecutive days. Frozen bone marrow cells were thawed, counted and 2 Mio  $CD45.1^+$  WT cells were either mixed with 2 Mio  $CD45.2^+$  WT cells ( $WT^{CD45.1}/WT^{CD45.2}$ ) or 2 Mio  $CD45.2^+$   $TKO^T$  cells ( $WT^{CD45.1}/TKO^T CD45.2$ ) and diluted in 200  $\mu$ l PBS. 4h after second radiation,  $CD45.1/2$  heterozygous recipient mice received 4 Mio mixed bone marrow cells either  $WT^{CD45.1}/WT^{CD45.2}$  or  $WT^{CD45.1}/TKO^T CD45.2$  by intravenous injection. Mice were treated for two weeks with water supplemented with antibiotics and 9 weeks after irradiation, the reconstituted cells were analyzed by flow cytometry. Irradiation and injection were performed together with Dr. Taku Kureha.

### 3.2.2.11 Antibody staining for flow cytometry and data analysis with FlowJo

To analyze antigen expression by flow cytometry, single-cell suspensions were washed in PBS and stained for viability with a live-dead dye for 20 min at 4°C. After one washing step with FACS Buffer, cell suspensions were stained with antibodies against the appropriate cell surface proteins. Ccr6 and Ccr7 surface staining was performed for 30 min at 37°C, prior to surface staining. For staining of intracellular antigens with in-house produced hybridoma supernatants cells were fixed with 2% formaldehyde at RT for 15 min, washed with Saponin permeabilization buffer and then stained with the appropriate antibody in Saponin Buffer. For commercially available intracellular antibodies cells were fixed with Foxp3 Fixation/Perm Buffer according to manufacturer's protocol for 30 min at 4°C, followed by one washing step in Foxp3 permeabilization Buffer and staining with antibodies diluted in Foxp3 permeabilization Buffer for 40 min at 4°C. Intracellular staining of cleaved caspase-3 was conducted according to Breed et al., 2019. After staining, cells were acquired on different flow cytometer devices: BD Fortessa (5-laser), FACS Canto II (3-laser) or Cytoflex (4-laser). The data were further processed with the software FlowJo (**Figure 12**).

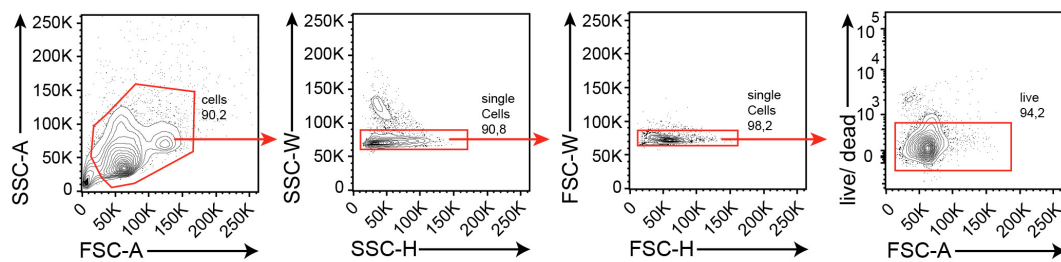


**Figure 12 | Common flow cytometry gating strategy for splenocytes and thymocytes using the software FlowJo.**

This first gating strategy was applied to all cell subsets that were defined by flow cytometry analyses in this thesis. After choosing splenocytes or thymocytes (FSC-A, SSC-A), duplets were excluded by SSC-H and SSC-W and FSC-H and FSC-W discrimination and live cells were gated. (FSC = forward side scatter, SSC = sideward side scatter, A = area, H = height, W = width)

## 3.2.3 Biochemical methods

### 3.2.3.1 Protein extraction, SDS-PAGE and immunoblotting

To analyze protein expression in T cells, cells were harvested, washed once in PBS and subsequently lysed in Meister lysis Buffer supplemented freshly with protease inhibitor (PI) and dithiothreitol (DTT), corresponding to three times the cell pellet size. After incubation for 10 min on ice with repeated mixing, cells were centrifuged at 13.000 g for 15 min to separate the protein-containing lysate from cell debris. Protein concentration was determined using Bio-Rad Protein assay based on the method of Bradford (Bradford, 1976). 30-50 µg protein lysate was

electrophoretically resolved according to the size on 8-10% SDS-polyacrylamide gels. Protein samples were denatured in 5x Laemmli loading buffer, boiled at 95°C for 5 min and loaded next to a pre-stained size marker. After electrophoresis was carried out in SDS running buffer at 110 V, the gels were further used for immunoblotting. Therefore, electrophoretic transfer of resolved proteins from an SDS-PAGE to a PVDF membrane was conducted by wet blotting using the Bio-Rad System. Blotting was either carried out for .,25h at 100V on ice or ON at 40V in the cold room. For immunodetection of distinct proteins, the membrane was first blocked in TBS containing 5% milk powder for 2h. Primary antibody incubations were performed ON at 4°C under constant agitation. Primary antibodies were either diluted in 1% milk powder in TBS-T for hybridoma supernatants (Roquin 3F12 and Regnase-1 15D11) or for commercially available antibodies according to the manufacturer's recommendation. Membranes were washed three times for 10 min with 1% milk powder in TBS-T. Appropriate horseradish peroxidase (HRP)-conjugated secondary antibodies diluted in 1% milk powder in TBS-T were added to the membrane for 1h at room temperature, followed by three additional washing steps with TBS-T. The signals were detected using different ECL substrates for HRP depending on the intensity of the expected bands and subsequently exposed to x-ray films in a dark room.

### **3.2.3.2 Co-Immunoprecipitation (Co-IP)**

To analyze interaction of Roquin and Regnase-1 proteins, co-immunoprecipitation was performed. Therefore, 100 µl Protein-A dynabeads were coupled under constant rotation to 10 µg antibody directed against Regnase-1 (R&D) at 4°C, ON followed by 1h at RT. Cell lysates were prepared as described with Meister lysis buffer supplemented additionally with 0.2 U/ µl RNase inhibitor (RNasin, Promega) and 1x Halt™ Phosphatase inhibitor. After washing of the antibody-coupled beads with Phosphate-Citrate Buffer containing DTT and PI, washed beads were incubated with 15 mg protein lysate in 900 µl Meister Buffer for 4h at 4°C while continuously rotating. Then, beads were washed three times with Meister Buffer supplemented freshly with PI and DTT and resuspended in 40 µl 1x Laemmli Buffer. The samples were boiled at 95°C for 5 min and co-immunoprecipitation was analyzed by polyacrylamide gel separation and immunoblotting with antibodies recognizing Regnase-1 and Roquin.

### **3.2.3.3 Enzyme-linked immunosorbent assay (ELISA)**

Whole blood from mice was taken immediately after CO<sub>2</sub> euthanasia by puncture of the heart from the sternum with a 26Gx1 needle. Blood was directly centrifuged at 10.000 g for 10 min at 4°C to isolate antibody-containing serum from cells. For determination of immunoglobulin concentrations in the blood, enzyme-linked immunosorbent assays (ELISAs) were performed by Elaine Wong using the SBA Clonotyping System-AP according to manufacturer's

recommendation. After addition of substrate, optical density at 405 nm was measured on an ELISA reader and concentrations were calculated by using standard serum as a reference.

### **3.2.4 RNA methods**

#### **3.2.4.1 RNA isolation and cDNA synthesis**

RNA isolation was performed by phenol-chloroform extraction method using Trizol (Ambion) or by column-based RNA isolation utilizing the RNeasy Kit by Macherey-Nagel. Isolation was performed according to manufacturer's protocol. RNA was then transcribed into cDNA by a Reverse Transcriptase, whereas either the Quantitect RT Kit or the RevertAid RT Kit were utilized according to manual.

#### **3.2.4.2 Real-Time qPCR**

To quantify gene expression, the UPL Probe Library System by Roche and the Roche Light Cycler were utilized. This method is based on a combination of gene-specific oligonucleotide amplification and a fluorescent-probe binding to the gene of interest. During amplification cycles the fluorescent signal is measured. This fluorescent intensity is then used to calculate the amount of cDNA in the sample. Oligonucleotides and probes used to amplify gene expression are given in **Table 5**.

#### **3.2.4.3 Polysome profiling**

For the preparation of polysomes,  $1.0 \times 10^7$  CD4 T cells were harvested, washed with PBS containing cycloheximide (0.1 mg/ml) and frozen at  $-80^{\circ}\text{C}$ . Polysome Profiling was performed by Dr. Gesine Behrens and Anneke Doerri in the group of Prof. Dr. Helmut Holtmann at the Medical School Hannover. After centrifugation at  $500 \times g$  for 7 min, pellets were incubated in extraction buffer (20 mM Tris-HCl, pH 8.0, 140 mM KCl, 0.5 mM DTT, 5 mM  $\text{MgCl}_2$ , 0.5% Nonidet-P40, 0.1 mg/ml cycloheximide, and 0.5 mg/ml heparin) for 5 min on ice. Extracts were centrifuged for 10 min at  $12.000 \times g$  and approximately 500  $\mu\text{l}$  of supernatant was layered onto a 12-ml linear sucrose gradient (10–50% sucrose (w/v) in 20 mM Tris-HCl, pH 8.0, 140 mM KCl, 0.5 mM DTT, 5 mM  $\text{MgCl}_2$ , 0.1 mg/ml cycloheximide, and 0.5 mg/ml heparin) and centrifuged at  $4^{\circ}\text{C}$  in an SW40Ti rotor (Beckman, Palo Alto, CA) at 35.000 rpm without brake for 80 min. The gradients were collected in 12 fractions and absorbance profiles at 260 nm recorded (ISCO, UA-6 detector). The samples were supplemented with 0.1 volume of 3 M sodium acetate (pH 5.2) and 1 volume of isopropyl alcohol and precipitated ON at  $-20^{\circ}\text{C}$ . RNA was purified using NucleoSpin RNA Kit (Macherey & Nagel) according to the

manufacturer's protocol. RNA was reverse transcribed into cDNA and genes associated with the ribosome fractions were analyzed by RT-qPCR.

### **3.2.5 Secondary structure prediction of the *Nfkbid* 3'-UTR**

Secondary structure predictions were performed by Anne Hoffman and Dr. Kristin Reiche in the group of Prof Dr. Jörg Hackermüller at the Helmholtz Center for Environmental Research – UFZ Leipzig. Briefly, mRNA and sequence data were acquired from the NCBI Reference Sequence Database (RefSeq) collection release (McGarvey et al., 2015). All mRNAs of *Nfkbid*, which amounted to sequences of 68 mammalian species were extracted. Extracted mRNAs that harbor an incompletely annotated 3'-UTR were re-annotated by 3'-terminally appending the corresponding genomic sequence. The coordinates of the appended genomic sequence, that were resulting from the best BLAT hit, while using BLAT version 3.5 with standard parameter settings (Kent, 2002). To guarantee a minimum quality the resulting elongated mRNAs were subsequently aligned with the corresponding genomic sequences using BLAT. mRNA sequences with an alignment mean pairwise identity greater than 95 percent were retained. To determine sequence and structure conservation of the SL elements over the 68 mammalian genomes, a progressive multiple sequence alignment of the mRNA sequences using T-coffee v 10.00.r1613 was prepared with standard parameter settings (Notredame et al., 2000). Additionally, a blastn search of the mouse SLs against the data set were generated with a word size of 7, an e-value of 100 and applying the blastn-short command (Camacho et al., 2009). Sequence regions of the mRNAs corresponding to the genomic coordinates of the known SL elements were extracted and a five nucleotide long flanking region to the predicted SLs added. Simultaneously local-progressive sequence and structure alignments of the predicted SLs with the known mouse SLs were generated using mLocARNA (Will et al., 2007).

### **3.2.6 Next generation sequencing and bioinformatical analysis**

CD4 T cells were prepared as described in the results section 4.3.3 (Figure 43). After restimulation of T cells, cells were taken up in Trizol Reagent and libraries were prepared and Illumina Next Generation Sequencing was performed by Dr. Stefan Krebs at the LAFUGA platform of Dr. Helmut Blum (Laboratory of functional genome analysis, LMU München). To generate high quality sequence reads the samples were sequenced with a length of 100 bp paired-end and 15 Mio reads/ sample. After sequencing, the bioinformatic analysis was done by Dr. Gergely Csaba from the group of Prof. Dr. Ralf Zimmer at the Institute for Informatics (LMU München).





## 4 Results

### 4.1 Roquin recognizes multiple types of *cis*-elements

The *trans*-acting factors Roquin-1 and its paralog Roquin-2 have been extensively studied in the past for their interaction with stem loop (SL) structures in the 3'-UTRs of their target mRNAs. Binding of the so-called constitutive decay element (CDE) in the *Tnf* 3'-UTR was one of the first breakthroughs in understanding the molecular function of Roquin proteins (Leppek et al., 2013). It was reported that the ROQ domain adopts an extended winged helix fold that recognizes rather the shape of hairpins than the sequence, thereby involving the three amino acids namely Lys220 (K220), Lys239 (K239) and Arg260 (R260). However, the pyrimidine-purine-pyrimidine (py-pu-py loop) sequence is mandatory for Roquin-recognition, since changes to pu-py-pu bases completely abolished gene regulation by Roquin. (Leppek et al., 2013; Schlundt et al., 2016). Besides the CDE, a second *cis*-element was identified in our group by a SELEX (Systematic Evolution of Ligands by Exponential Enrichment) approach and was termed the alternative decay element (ADE), consisting of a hexaloop hairpin structure (Janowski et al., 2016). Moreover, we recently identified a linear binding element (LBE) that was strongly enriched in a PAR-CLIP (Photoactivatable-ribonucleoside-enhanced crosslinking immunoprecipitation) approach in mouse embryonic fibroblasts (Essig et al., 2018). The next chapter will focus on the regulation of different types of *cis*-elements (CDE, ADE and LBE) by Roquin proteins and describe how Roquin contributes to the regulation of the mRNAs by involving multiple regulatory *cis*-elements. The subsequently discussed data on *Ox40* regulation by Roquin were published in 2016 (Janowski et al., 2016) and the gained knowledge about the cooperative regulation of the *Nfkbid* 3'-UTR by multiple Roquin proteins resulted in a manuscript that was published in 2018 (Essig et al., 2018). Dr. Katharina Essig included the latter publication as part of her cumulative PhD thesis.

#### 4.1.1 The ROQ domain of Roquin harbors residues required for *cis*-element recognition in the *Ox40* 3'-UTR

One highly conserved ADE-like as well as one CDE-like structure are found in the *Tnfrsf4* 3'-UTR encoding for the co-stimulatory receptor Ox40 (Janowski et al., 2016), suggesting that Roquin might recognize these structures (**Figure 4**). It was previously described that Roquin targets the *Tnfrsf4* mRNA, but the exact molecular mechanism has not been described, yet

(Jeltsch et al., 2014; Vogel et al., 2013). To identify how Roquin can recognize the novel ADE-like SL structure, the co-crystal structure of the Roquin-1 ROQ domain bound to the ADE-like SL was solved. From this structure, additional amino acid residues (Lys220, Thr240, Lys239, Tyr250, Ser253, Arg260, Leu266) were proposed to form an interaction surface with the 5'-side of the RNA stem within the *Tnfrsf4* ADE-like SL. Mutation of Tyr250 to Ala (Y250A) results in an almost complete loss of binding of the ROQ-domain to the ADE-like SL in electrophoretic mobility shift assays (EMSAs) (Janowski et al., 2016). To prove the contribution of the key residue Y250 in Roquin-1 to *Tnfrsf4* mRNA recognition and regulation, a retroviral reconstitution system in Roquin-deficient CD4 T cells was utilized. Here, *Rc3h1/2<sup>fl/fl</sup>*; *Cd4-creERT2*; rtTA-M2 mice were generated to genetically combine loxP-flanked Roquin-1/2 encoding alleles, a 4'OH-tamoxifen-inducible cre recombinase and the reverse tetracycline-controlled transactivator rtTA-M2. The isolated CD4 T cells were treated *in vitro* with 4'OH-tamoxifen to induce deletion of Roquin-1/2. The cells were then transduced with doxycycline-inducible retroviral vectors to reconstitute Roquin-1 with either wild-type Roquin-1 or mutant forms thereof (Y250A and K220A, K239A, R260A) (**Figure 10**).

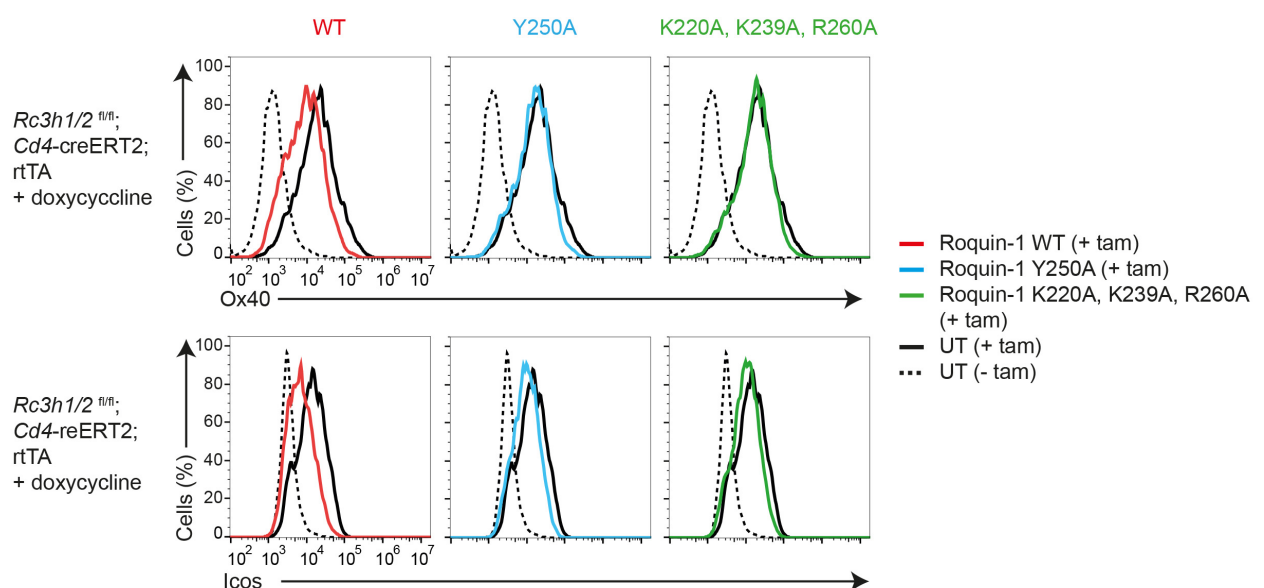


**Figure 13 | Mutational analysis of Roquin-1 for the regulation of Ox40 and Icos.**

Flow cytometry of Ox40 and Icos surface expression on CD4 T<sub>H</sub>1 cells from *Rc3h1/2<sup>fl/fl</sup>*; *Cd4-creERT2*; rtTA-M2 mice treated with 4'OH-tamoxifen (+ tam) to induce Roquin-1/2 deletion or left untreated (- tam). The cells were then either left untransduced (UT) or transduced with retrovirus containing a doxycycline-inducible cassette to express Roquin-1 wild-type (WT), Roquin-1 Y250A or Roquin-1 K220A, K239A and R260A mutants. Data are representative of two independent experiments.

Depletion of Roquin proteins by 4'OH-tamoxifen treatment (+tam) strongly increased surface expression of Ox40 and Icos (**Figure 13**). This increase was partially suppressed in cells with doxycycline-induced reconstitution with Roquin-1 WT protein. No downregulation was similarly observed upon expression of Roquin-1 with the mutation of Y250A, which binds to ADEs or

the K220A, K239A, R260A mutant, which was strongly impaired in CDE SL interactions. Therefore, our analyses showed that the Y250 residue was essential for Roquin interaction and regulation of Ox40, and potentially also for other Roquin targets such as Icos. Since the *Icos* 3'-UTR has a length of about 2500 nt, there is high possibility for hexaloop structures being formed. These data also suggest, that multiple Roquin proteins might potentially recognize several regulatory elements within one 3'-UTR to tightly control gene expression of its target mRNAs. The combination of the inducible knockout system with short-term doxycycline-induced reconstitution allows to analyze short term effects on endogenous target regulation and makes this overexpression a good tool for studying target genes in more depths.

#### **4.1.2 *Nfkbid* is a prototypical Roquin target**

In our previous study, Roquin-1/2-deficient CD4 T cells showed increased expression of the atypical NF- $\kappa$ B inhibitor I $\kappa$ B<sub>NS</sub> and this increase contributed to elevated IL-17A production and increased T<sub>H</sub>17 differentiation (Jeltsch et al., 2014). Additionally, *Nfkbid* was identified in RNA-IP experiments to be directly bound by Roquin and secondary structure predictions revealed that the *Nfkbid* 3'-UTR harbors two CDE elements that could be potentially targeted by Roquin (Leppek et al., 2013). Hence, the control of I $\kappa$ B<sub>NS</sub> expression by Roquin proteins is potentially an important mechanism to specify cell fate decisions in T cells.

The following section focuses on the regulation of the *Nfkbid* 3'-UTR via multiple Roquin proteins binding to six highly conserved stem loops. This multiple binding enables a tight control of the expression of the atypical inhibitor I $\kappa$ B<sub>NS</sub>. Furthermore, this multiple interaction can contribute to a translational inhibition by Roquin. The work in the following section was published in Essig K., Kronbeck N., et al., in 2018 (Essig et al., 2018).

##### **4.1.2.1 The minimal response element of the *Nfkbid* 3'-UTR harbors six conserved stem loops that are targeted by Roquin**

To define a minimal response element in the *Nfkbid* 3'-UTR for Roquin-mediated regulation, we made use of a reporter system. Here, the human ICOS coding-sequence (CDS) was fused to green-fluorescence protein (GFP), whereas the expression of ICOS-GFP was under the control of the 559 nt long *Nfkbid* 3'-UTR (**Figure 14 b**). To analyze the binding motifs of the Roquin-regulated target *Nfkbid* we retrovirally introduced the reporter expressing ICOS-GFP and the 3'-UTR in a MEF cell line (*Rc3h1/2*<sup>fl/fl</sup>; CreERT2) that allows depletion of endogenous Roquin proteins by 4'OH-tamoxifen treatment (iDKO) *in vitro*. The inducible deletion system allowed us to compare the impact of complete deletion of endogenous Roquin-1 and Roquin-2

on the expression of the 3'-UTR reporter without overexpression (**Figure 14 a**). This experimental setup will be utilized throughout section 4.1.2.

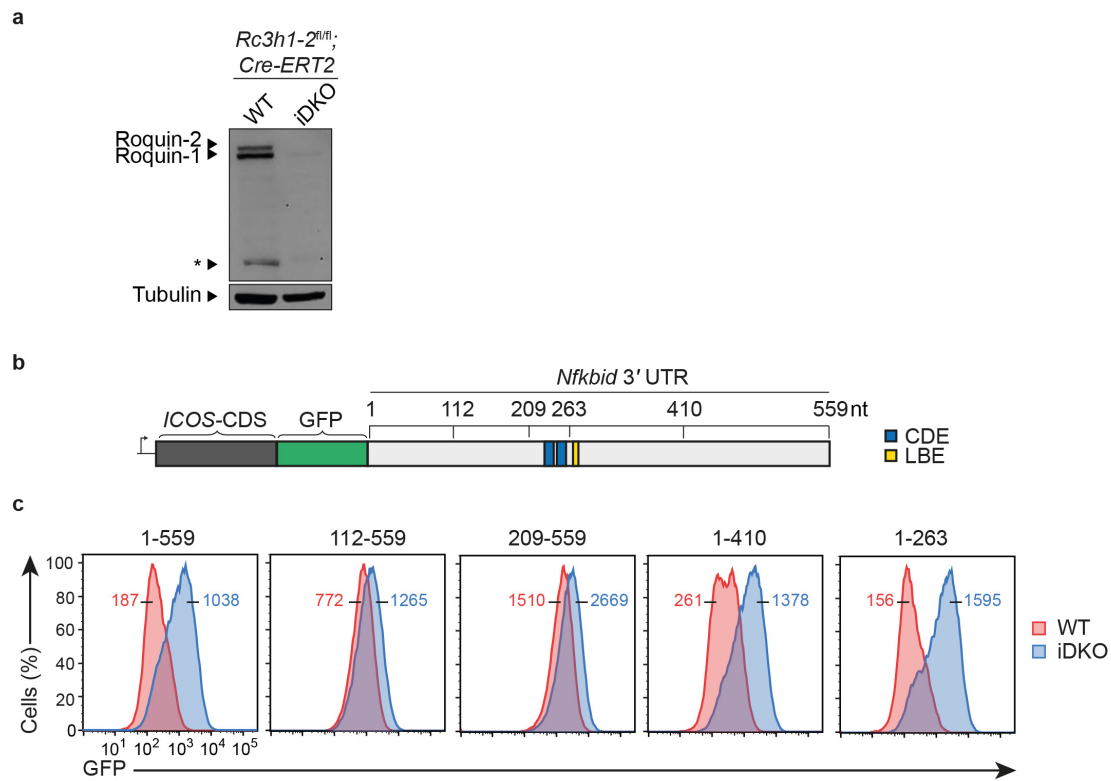


**Figure 14 | Defining the minimal response element of the *Nfkbid* 3'-UTR for Roquin-mediated regulation.**

**a)** Immunoblot analysis of Roquin expression in *Rc3h1/2<sup>fl/fl</sup>; CreERT2* MEF cells treated with 4'-OH-tamoxifen (iDKO) or left untreated (WT). **b)** Schematic overview of the reporter utilized in the following experiment. The human *Icos* CDS (ICOS) is fused to GFP, followed by the full-length *Nfkbid* 3'-UTR (559 nucleotides), which harbors two CDE and one LBE elements or truncated versions thereof. **c)** Flow cytometry analysis of GFP in *Rc3h1/2<sup>fl/fl</sup>; CreERT2* MEF cells retrovirally transduced with the indicated reporter construct, either treated with 4'-OH-tamoxifen (iDKO) or left untreated (WT). Median fluorescent intensities (MFI) of GFP for WT (red) and iDKO (blue) MEF cells are indicated at the corresponding histogram. Data are representative of three (a,c) independent experiments. The immunoblot was performed by Dr. Katharina Essig.

Using deletion mutagenesis of the full length 3'-UTR, we mapped a response element of 1-263 nucleotides, which was required and sufficient to confer strong upregulation of the ICOS-GFP reporter upon induced deletion of Roquin encoding alleles in MEF cells (**Figure 14 c**). Interestingly, the linear U-rich LBE motif did not contribute to the Roquin-mediated repression, although it was highly abundant in our Roquin PAR-CLIP data set and additionally present in an independent PAR-CLIP experiment with human cells (Murakawa et al., 2015).

To our surprise, the two tandem high-affinity CDE elements were not sufficient to confer full regulation when the more 5' located sequences of the minimal response elements were

missing (112-559 and 209-559 nt). These data propose a novel type of gene regulation that requires multiple RNA-binding elements targeted by one or more RBPs.

To prove our hypothesis, we examined if the minimal response element has the potential to form further secondary structures in addition to the two CDE elements.

Therefore, Dr. Jörg Hackermüller, Dr. Kristine Reiche and Anne Hoffmann from the Department of Molecular Systems Biology at the Helmholtz Centre for Environmental Research-UFZ Leipzig performed sequence and structure predictions using the mLocARNA multiple alignment algorithm, which first predicts stem-loop forming sequences and then aligns this sequence for conservation amongst different species (Smith et al., 2010; Will et al., 2007). The conservation analysis of the *Nfkbid* 3'-UTR was performed on 68 mammalian species, resulting in the prediction of six highly conserved stem loops (SL1-6). **Figure 15 a** depicts the individual conserved sequences for each stem loop and how often these conserved sequences differed over the 68 mammalian species. Here, the tandem CDE elements were identified as SL5 and SL6 and one ADE-like element showed the highest sequence conservation in the nucleotides involved in forming the structure (SL1). Additionally, one non-ADE hexaloop (SL2) as well as two triloops (SL3 and SL4) were predicted. The base pairs involved in forming the stems of the consensus CDE SL5 and SL6, but also those forming SL3 are highly conserved, and those of SL1, a bona-fide ADE, are even invariant over 58 species. The consensus *Nfkbid* 3'-UTR structure and conservation of individual nucleotides according to mLocARNA algorithm is depicted in **Figure 15 b**. The structure prediction of these six highly conserved stem loops was utilized for the design of mutations on the individual SL structures in the *ICOS*-CDS-GFP reporter (**Figure 15 c**).

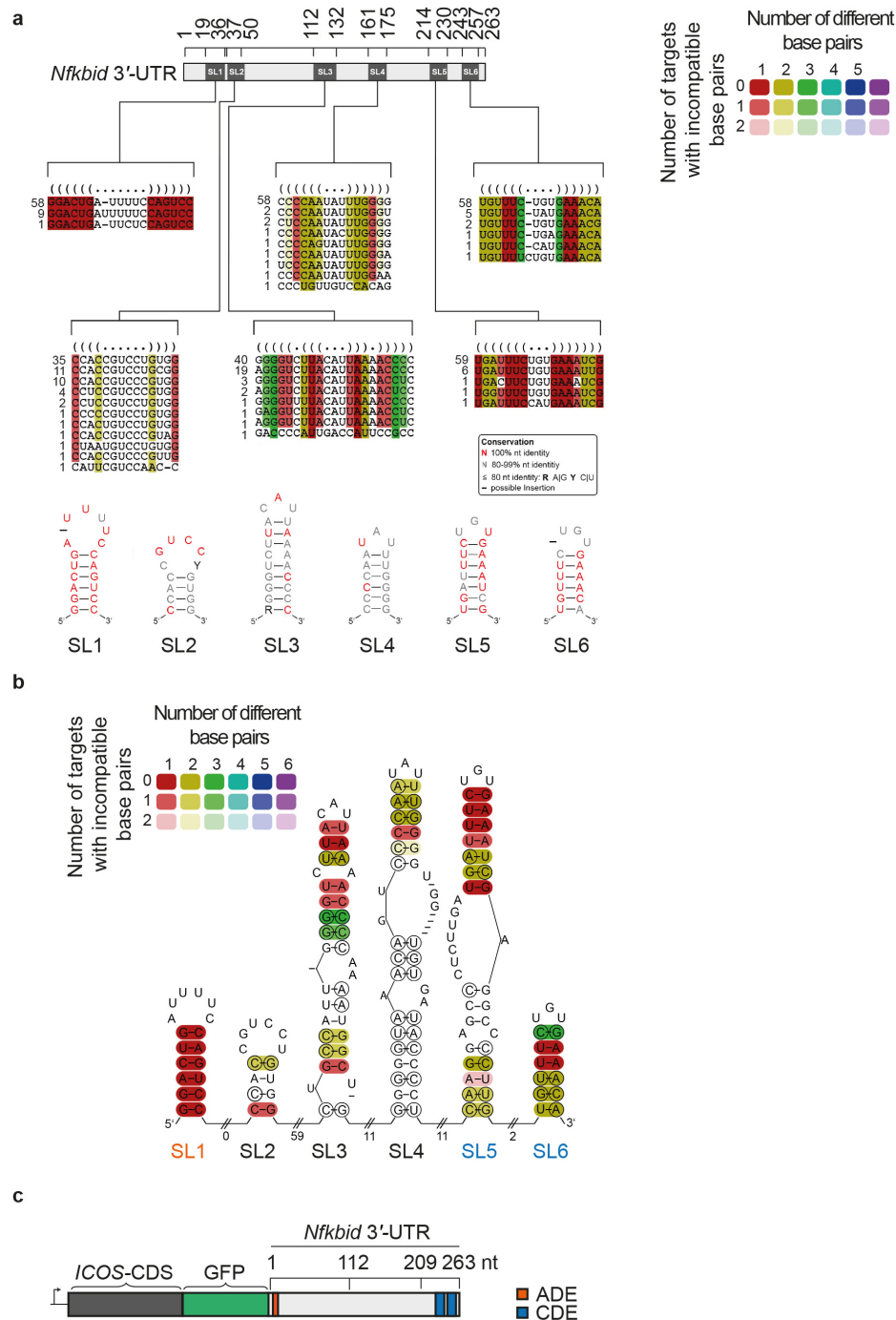


**Figure 15 | The *Nfkbid* 3'-UTR minimal response element harbors six conserved stem loops.**

**a)** Structural and sequential conservation analysis of the minimal response element of the mouse *Nfkbid* 3'-UTR (1-263) by using mLocARNA. Out of 68 analyzed mammalian species the number of species in which the respective sequence occurred is listed to the left of the sequences in the conservation pattern. A conservation model for the consensus secondary structure of the six stem loops (SL) is shown below. Nucleotides are color coded according to their base pair conservation. The graphical representation of a mLocARNA alignment depicts at each site the number of sequences forming a base pair and the number of compensatory mutations (e.g. when base pair AU is mutated to base pair UA or GU or UG or GC or CG). The color code for compensatory mutations is as follows: red=no compensatory mutation; ochre=2 different base pairs, i.e. one compensatory mutation; green, turquoise, blue, and violet highlight base pairs with 2, 3, 4 and 5 compensatory mutations, respectively. The higher the opacity of the color the more sequences form a base pair at this site. **b)** Consensus secondary structure prediction of the

minimal response element of the *Nfkbid* 3'-UTR (1-263) by mLocARNA. Consensus sequences of SL1 (residues 19-36), SL2 (residues 37-50), SL3 (residues 112-132), SL4 (residues 161-175), SL5 (residues 214-230), and SL6 (residues 243-257) are represented. The color code is described in a). c) Schematic representation of the minimal response element and its *cis*-elements ADE and CDE in the *ICOS*-CDS-GFP reporter.

#### 4.1.2.2 Mutational analyses of the *Nfkbid* 3'-UTR for identifying the contributions of single SLs to Roquin-mediated regulation

We then tested the importance of stem loop recognition by converting the nucleotides in the SL sequences in the reporter construct (loop mutation, LM) from purine (pu) to pyrimidine (py) bases and vice versa, since it was shown that the py-pu-py triloop sequence in the CDE is crucial for recognition by Roquin (Leppek et al., 2013). Loop mutations (LM) impacted full regulation of the reporter by Roquin only when located in SL1 and SL2, whereas the sequences in the loops of SL3-6 appeared not essential for the regulation, since they were comparably regulated to the wild-type 1-263 3'-UTR (**Figure 16 a**).

Considering the strong conservation of sequences in SL5 and SL6 (**Figure 15 a**), we hypothesized that both CDEs may compensate for each other's loss-of- function. Indeed, when we combined those mutations in SL5 and SL6 that had no effect when introduced individually (combining SL5 LM with SL6 LM), we observed the same strong impairment of Roquin-mediated regulation as for mutations in the essential SL1 and SL2 (**Figure 16 b**). In addition to loop mutations, we also introduced individual mutations in the stem of the hairpin structures. Thus, we disrupted base-pairing of 3-8 nucleotides in the stem sequences by converting nucleotides to complementary sequences (**Figure 17**). We again identified a strong contribution of SL1, SL2 and SL5, whereas SL3, SL4 and SL6 showed no effect upon stem mutation.

In summary, this mutagenesis revealed that Roquin-mediated regulation of the *Nfkbid* mRNA involves a complex and composite *cis*-element. Its function requires stem loop formation and loop recognition of SL1, SL2 and SL5/SL6, whereas introduction of mutations in SL3 and SL4 had no effect on Roquin-mediated regulation of the reporter.

To check whether the recognition of loop structure was sequence- and shape-specific, we individually exchanged the hexaloop sequence (Loop Exchange, LE) of SL1 or SL2 with the CDE triloop sequence of SL5 and likewise changed the triloop of SL5 to the hexaloop of SL1 and then dissected if Roquin was still able to regulate these reporter constructs (**Figure 18**).

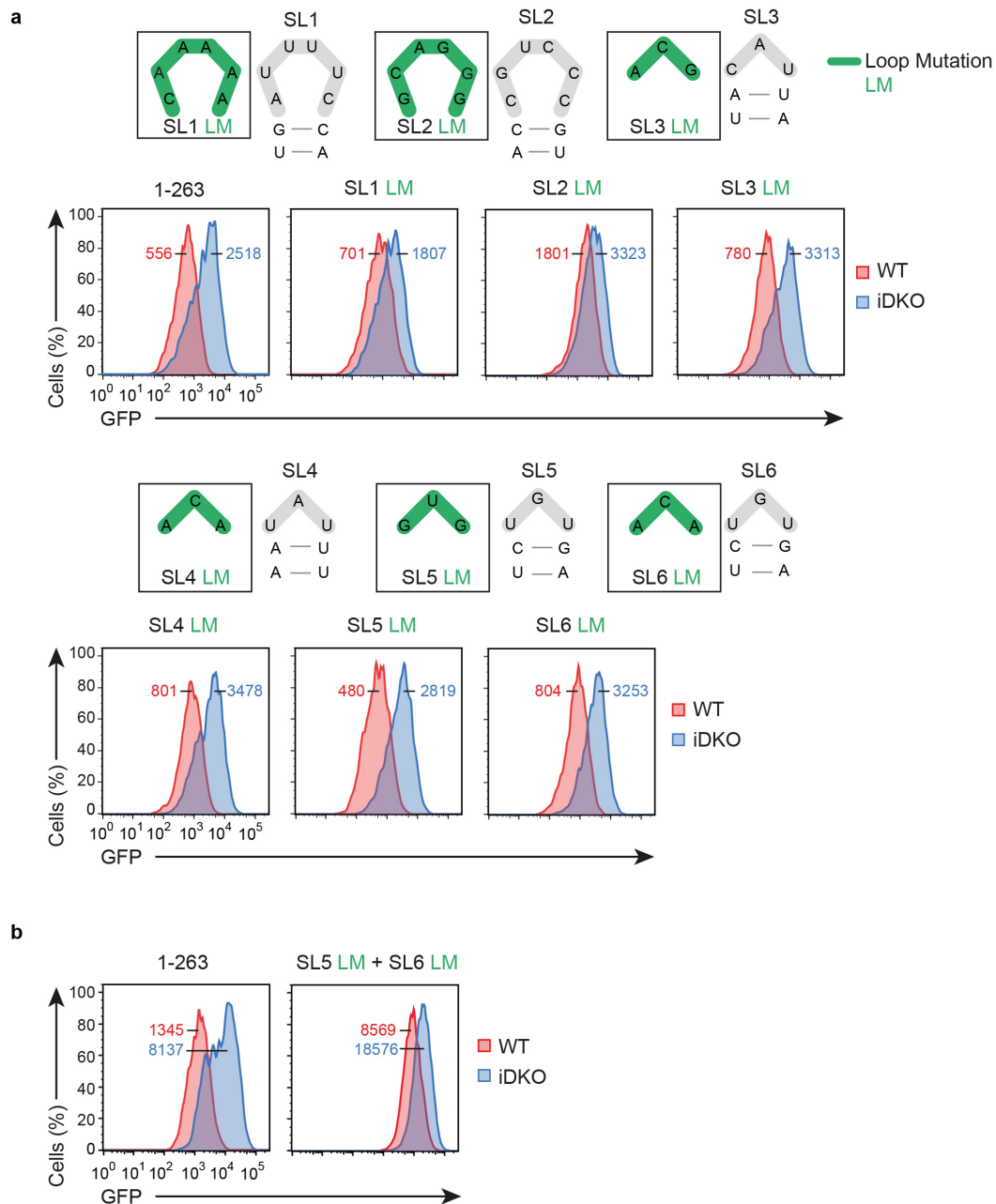


**Figure 16 | Mutational analysis of loop structures within the *Nfkbid* minimal response element.**  
**a)** Schematic representation of the loop sequences from the six conserved SL structures within the 3'-UTR of mouse *Nfkbid*. Wild-type loop structures (grey) of the six SLs were modified by individual loop mutations (LM: change of purine and pyrimidine bases, green). Flow cytometry analysis of GFP in *Rc3h1/2<sup>fl/fl</sup>*; CreERT2 MEF cells retrovirally transduced with the ICOS-GFP-*Nfkbid* 3'-UTR (1-263) reporter without mutation, with individual LMs or with combined LMs (**b**). MEF cells were either treated with 4'OH-tamoxifen (iDKO) or left untreated (WT). Median fluorescent intensities (MFI) of GFP for WT (red) and iDKO (blue) MEF cells are indicated. Data are representative of six (**a**) and three (**b**) independent experiments.



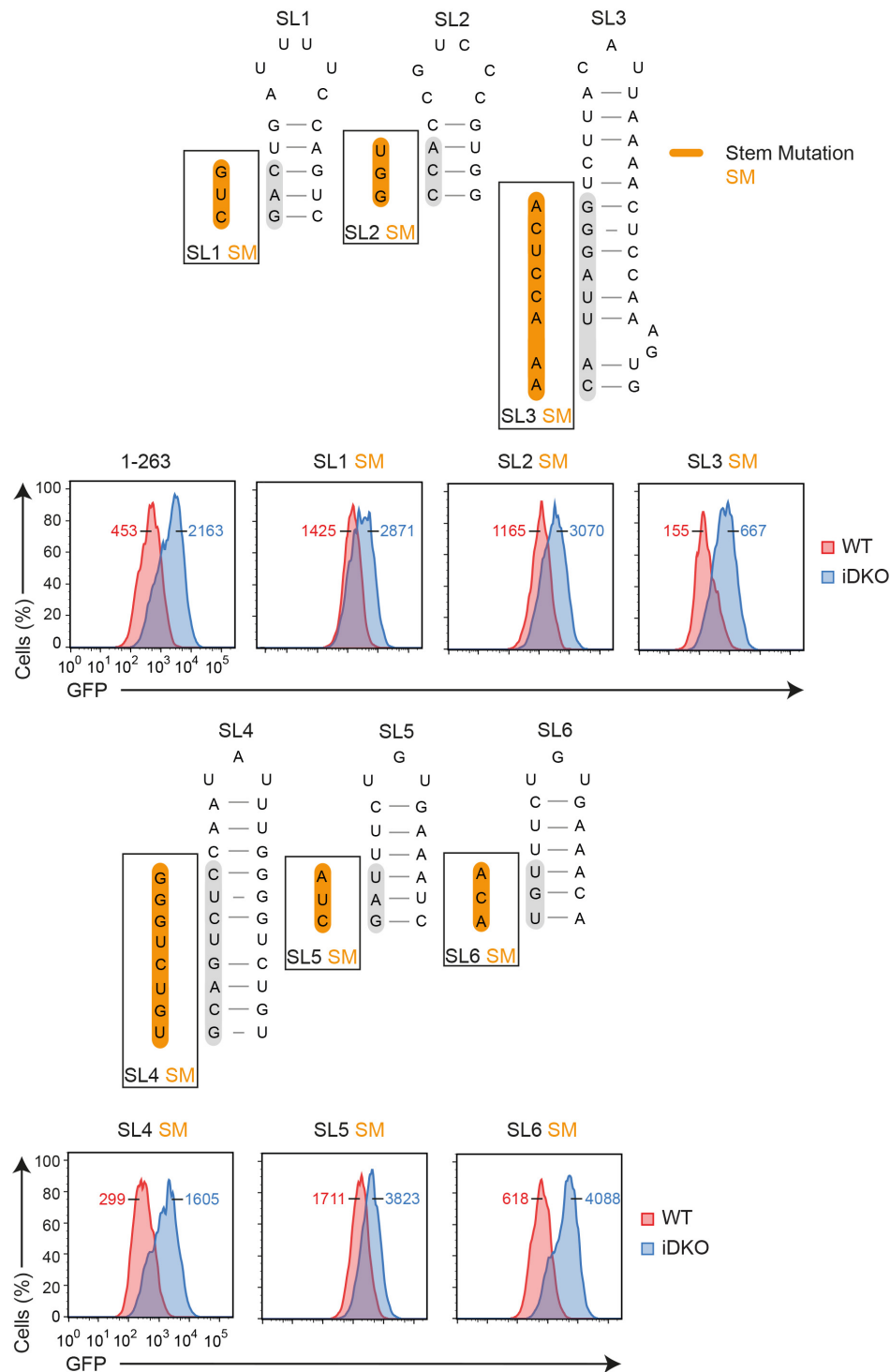


**Figure 17 | Mutational analysis of stem sequence within the *Nfkbid* minimal response element.**

Schematic representation of the six conserved SL structures within the 3'-UTR of mouse *Nfkbid*. Wild-type sequences (grey) of the six conserved SLs were modified by introducing stem mutations (SM, orange) that result in the disruption of base-pairing within the individual stem sequence. Flow cytometry analysis of GFP in *Rc3h1/2<sup>fl/fl</sup>*, CreERT2 MEF cells retrovirally transduced with the ICOS-GFP-*Nfkbid* 3'-UTR (1-263) reporter without mutation or with individual SMs. MEF cells were either treated with 4' OH-tamoxifen (iDKO) or left untreated (WT). Median fluorescent intensities (MFI) of GFP for WT (red) and iDKO (blue) MEF cells are indicated. Data are representative of six independent experiments.

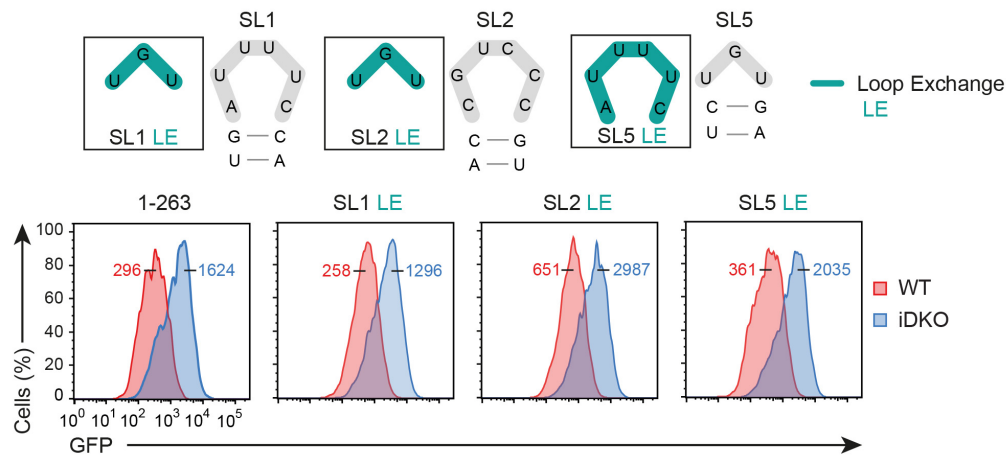


**Figure 18 | Introducing Loop Exchange (LE) mutations in SL1, SL2 and SL5.**

Nucleotide sequences of the loop structures of wild-type mouse *Nfkbid* 3'-UTR stem loops (SL) 1, 2, and 5 (grey) and introduced loop exchange mutations (LE: change of hexa- to tri-loops and vice versa, blue) are depicted above. Flow cytometry analysis of GFP in in *Rc3h1*<sup>2<sup>fl/fl</sup></sup>; CreERT2 MEF cells retrovirally transduced with the ICOS–GFP–*Nfkbid* 3'-UTR (1–263) reporter containing LE mutations in the indicated SLs MEF cells were either treated with 4'OH-tamoxifen (iDKO) or left untreated (WT). MFI of GFP is shown for WT (red) and iDKO (blue) MEF cells. Data are representative of six independent experiments.

The LE mutations were fully functional for Roquin-mediated regulation, suggesting that Roquin has no preference for ADE or CDE loop sequences in the context of the *Nfkbid* 3'-UTR and that SL1, SL2 and SL5 contribute to the full regulation individually. Here, we found that Roquin not solely involves one stem loop structure, but indeed requires multiple stem loop structures to ensure full gene regulation of the *Nfkbid* 3'-UTR.

#### 4.1.2.3 Analyzing cooperativity of multiple Roquin proteins in the regulation of the *Nfkbid* mRNA

We next wanted to address if multiple Roquin proteins contribute to the regulation of the *Nfkbid* mRNA, since single LMs and SMs in SL1, SL2 and SL5 showed a strong impairment in Roquin-mediated regulation. Additionally, we aimed to elucidate the contribution of the non-essential stem loops SL3 and SL4 and therefore progressively combined the LMs with the essential SL1, 2 and 5 (**Figure 19**). Combined mutation of the non-essential SL3, SL4 and SL6 showed a gradual de-repression comparable to the single LM in the crucial SL2. Additional mutation of SL2 and SL6 then resulted in a complete loss of regulation by Roquin. This led us to the hypothesis that multiple Roquin proteins might contribute individually by binding of different stem loops in the *Nfkbid* 3'-UTR.

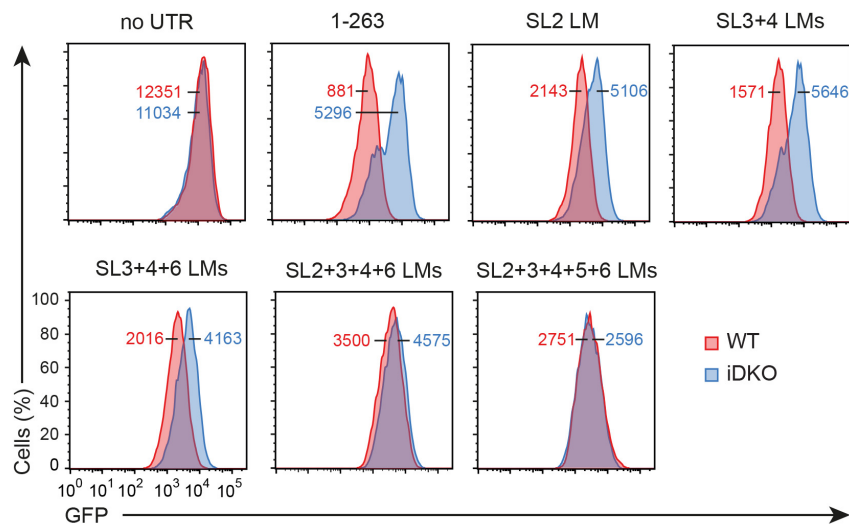


**Figure 19 | Analyzing the contribution of multiple stem loops in the *Nfkbid* 3'-UTR for Roquin-mediated regulation.**

Flow cytometry analysis of GFP in *Rc3h1/2<sup>fl/fl</sup>*; CreERT2 MEF cells retrovirally transduced with the ICOS-GFP-*Nfkbid* 3'-UTR (1–263) reporter without UTR or harboring single or combined LMs as introduced in Figure 16. MEF cells were either treated with 4'OH-tamoxifen (iDKO) or left untreated (WT). MFI of GFP is shown for WT (red) and iDKO (blue) MEF cells. Data are representative of three independent experiments.

To prove whether post-transcriptional regulation of the *Nfkbid* 3'-UTR requires binding of multiple Roquin proteins, we made use of a  $\lambda$ N-boxB-tethering assay system (Gehring et al., 2008). As it was shown in **Figure 13**, mutating Roquin-1 at K220, K239 and R260 reduces the ability to regulate ADE- as well as CDE-containing mRNAs like *Tnfrsf4* and *Icos*. Hence, we mutated Roquin-1 at these three critical amino acids in its ROQ domain (K220A, K239A, and R260A) to weaken physiologic stem loop recognition and fused this mutant protein to a bacteriophage lambda N peptide ( $\lambda$ N) that confers high affinity binding to boxB stem loop structures. We reconstituted *Rc3h1/2<sup>-/-</sup>* MEF cells expressing the reverse-tetracycline-dependent transactivator rtTA3 with  $\lambda$ N-Roquin-1(K220A, K239A, R260A)-p2A-mCherry or  $\lambda$ N-p2A-mCherry alone by doxycycline administration and after retrovirally introducing the ICOS-GFP reporter (**Appendix 1**). In the reporter we substituted the essential SL1, SL2 and SL5 either individually or in combination with boxB structures, which are RNA stem loops that are bound by  $\lambda$ N with high affinity (**Figure 20 a**). The reporter regulation was then analyzed by flow cytometry and the fold-change regulation was calculated (**Figure 20 b**).

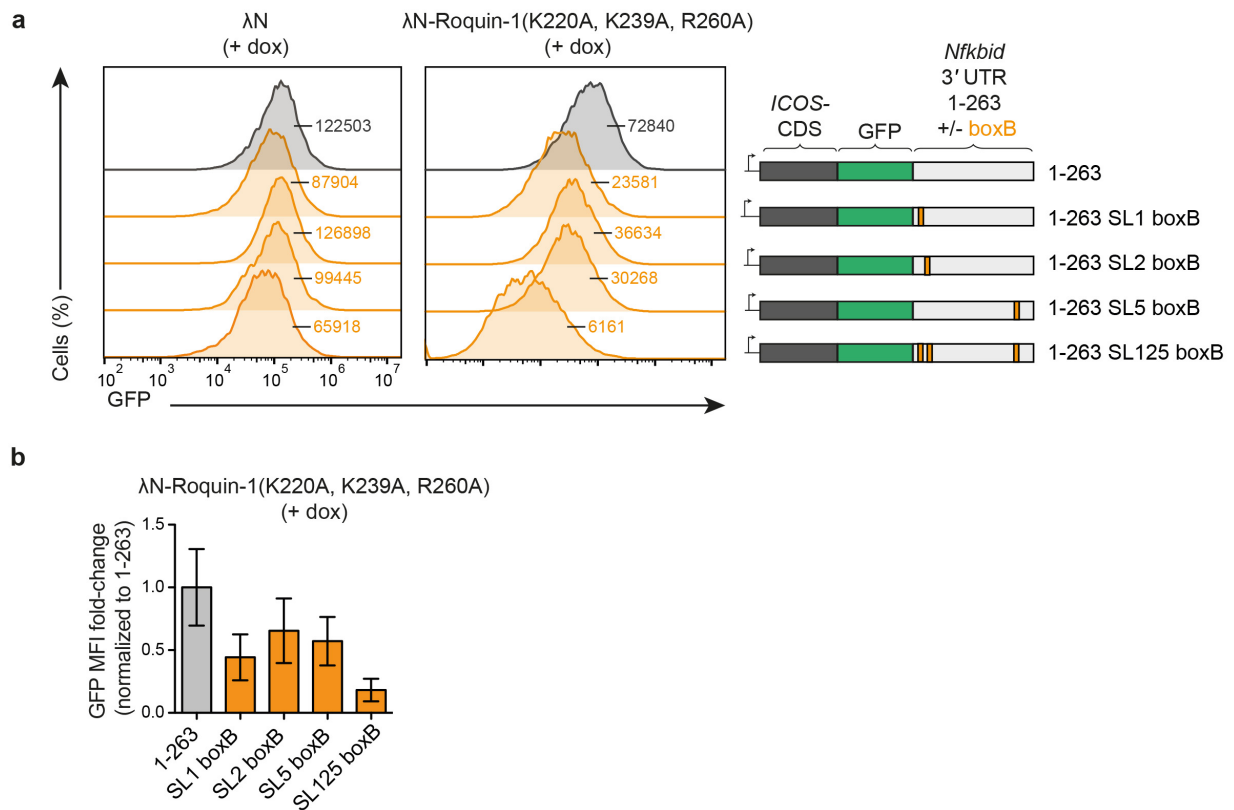


**Figure 20 | *Nfkbid* regulation requires Roquin-1 to interact with at least three SLs.**

**a)** Flow cytometry analysis of GFP in the  $\lambda$ N-boxB-tethering system in *Rc3h1/2<sup>-/-</sup>* MEF cells stably expressing the reverse tetracycline-controlled transactivator rtTA3. MEF cells were first either transduced with a retrovirus containing the ICOS–GFP reporter with the wild-type *Nfkbid* 3'-UTR (1–263) or mutants containing one (at position of SL1, SL2, or SL5) or three (at all positions of SL1, SL2, and SL5) boxB RNA structures. The cells were additionally transduced with a retrovirus encoding for  $\lambda$ N-p2A-mCherry or  $\lambda$ N-Roquin-1(K220A, K239A, R260A)-p2A-mCherry containing a doxycycline-inducible cassette. Overexpression of the  $\lambda$ N-constructs was induced by doxycycline administration for 14h. MFI of GFP for wild-type *Nfkbid* 3'-UTR (1–263) (grey) and boxB mutants (orange) are indicated.

**b)** Fold-change of GFP MFI levels in cells as described in (a) normalized to mean of wild-type *Nfkbid* (1–263). Error bars indicate mean  $\pm$  SEM. Data are representative of three independent experiments.

With this system we were able to tether  $\lambda$ N-fused Roquin-1(K220A, K239A, R260A) to RNA structures in the *Nfkbid* 3'-UTR and thereby elucidate the amount of Roquin proteins that was required for full repression of the reporter.

Introduction of either one or three boxB stem loops at the position of SL1, SL2, or SL5 within the minimal response element induced  $\lambda$ N-Roquin-1-mediated repression of the reporter. However, the three boxB binding sites, that enable simultaneous interactions with three molecules of overexpressed  $\lambda$ N-Roquin-1 protein, lead to a much stronger repression. These findings uncovered that complex and composite Roquin- recognized cis-elements in the 3'-UTR precipitate a strong cooperative repression of target mRNA expression. So far, cooperation of multiple Roquin proteins has not been considered as a type of post-

transcriptional gene regulation. By performing mutational and functional analyses on the *Nfkbid* 3'-UTR, I was able to identify this new type of Roquin-mediated gene regulation.

#### 4.1.2.4 Roquin induces mRNA degradation and translational inhibition

Recruitment of factors involved in mRNA deadenylation (Ccr4-NOT) and decapping (Ddx6/Rck) are mechanisms for Roquin-mediated target repression (Glasmacher et al., 2010; Leppek et al., 2013; Murakawa et al., 2015). However, when we blocked deadenylation and decapping of the *Nfkbid* 3'-UTR-bearing mRNA individually and in combination, Roquin-mediated reporter regulation was not at all or only partially impaired, suggesting that the mRNA degradation pathways of deadenylation and decapping have redundant functions. We consequently interpreted, that the residual regulation of the reporter assay could be due to translational inhibition. Therefore, we performed in collaboration with the group of Prof. Dr. Helmut Holtmann at the MH Hannover polysome profiling, which uses sucrose gradient centrifugation to separate monosomal from polysomal fractions from cell lysates and accordingly RNAs isolated from these fractions were either strongly (polysomes) or weakly (monosomes) translated.

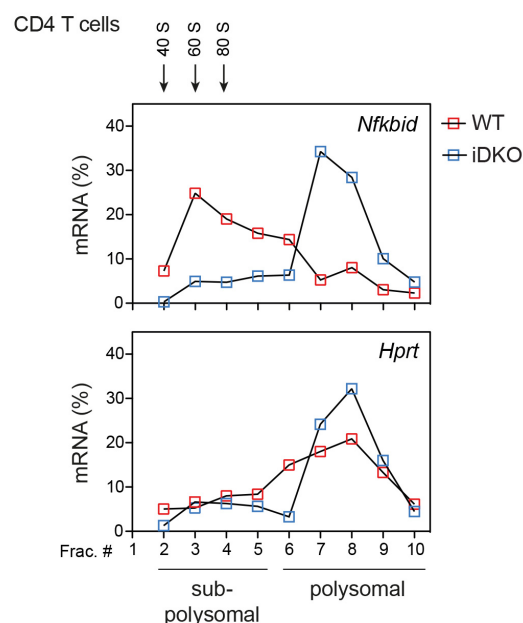


**Figure 21 | Polysome Profiling of *Nfkbid* mRNA in WT and Roquin-deficient CD4 T cells.**

Representative polysome profiles of endogenous *Nfkbid* and *Hprt* in *Rc3h1/2<sup>fl/fl</sup>*; *Cd4-creERT2* CD4 T cells treated with (iDKO) or without (WT) 4'OH-tamoxifen. Cytoplasmic lysates from these cells were fractionated on sucrose gradients. The amount of mRNA in each fraction was analyzed by RT-qPCR and are shown in percent of the sum detected in all fractions (Frac). Fractions 2, 3 and 4 represent the 40S, 60S and 80S ribosomal units. Fractions 2-5 comprise subpolysomal and fractions 6-10 polysomal fractionations. The respective absorbance profile at 260 nm of the gradient fractionation is shown in Appendix 2. Data are representative of two independent experiments.

The presence of the ribosomal subunits 40S, 60S and 80S and polysomes were controlled by absorbance profiles at 260 nm during fractionation of gradients (**Appendix 2**). Indeed, when we analyzed the abundance of ribosomes on the mRNA by performing polysome profiling, we realized that endogenous *Nfkbid* in T cells revealed profound Roquin-induced repression on the level of translation (**Figure 21**). Roquin was able to induce translation inhibition of the *Nfkbid* mRNA, since this mRNA shifted from monosomal to polysomal fractions of sucrose gradients of cell extracts when Roquin encoding alleles were conditionally deleted in CD4 T cells.

My colleague Dr. Katharina Essig and our collaborator Dr. Joao C. Guimaraes (Computational and Systems Biology, Biozentrum, University of Basel), combined ribosome profiling with mRNA-sequencing in Roquin-deficient and Roquin-1-overexpressing MEF cells. The technique of ribosome profiling identifies fragments of RNA that are occupied by ribosomes, which consequently indicates stronger translational activity (Ingolia et al., 2009). By globally comparing the abundance of RNA and the ribosome-protected fragments (RPF), conclusions about translational efficiency can be drawn and we thereby identified that some Roquin target genes show translational inhibition, respectively. Amongst them we identified *Nfkbid*. We found that targets with more Roquin binding sites showed increased regulation of the mRNA and RPFs and that a significantly higher proportion of translationally regulated targets had Roquin-binding sites corresponding to four or more binding elements. In this work we have demonstrated how a complex *cis*-element composed of nonessential and essential binding sites in the *Nfkbid* 3'-UTR responds to Roquin expression by inducing deadenylation, decapping and translational inhibition. Consequently, Roquin facilitates target gene regulation in a cooperative manner: multiple Roquin proteins enable a strong depression of the target mRNA controlling transcript abundance.

## 4.2 Investigating the phenotypic consequences of conditional deletion of Roquin and Regnase-1 in T cells

In the previous chapter I have focused on cooperative and composite *cis*-elements targeted by Roquin proteins. Based on these analyses we found that robust regulation of mRNA transcripts requires several post-transcriptional gene regulators and involves multiple mechanisms including mRNA degradation and translational inhibition.

The following chapters of this thesis will focus on elucidating the cooperative function of the post-transcriptional gene regulators Roquin and Regnase-1. By comparing the phenotypic consequences of conditionally deleting Roquin and/ or Regnase-1 in T cells of mice, I aimed to learn about the physiological functions of Roquin and Regnase-1 for the prevention of autoimmunity. Then, the potential cooperative gene regulation will be studied in more detail by performing a global mRNA-sequencing analysis in inducible knockout T cells and by investigating the molecular mechanism underlying the functional cooperation.

### 4.2.1 Published mouse models of Roquin and Regnase-1

Since Roquin and Regnase-1 mouse models have already been published, I will first summarize the phenotypes of the genetically deleted or mutated mice (**Table 18**). Here, the comparison of hyperactivated CD4 and CD8 T cells, increased differentiation of CD4 T cells to the T<sub>FH</sub> cell lineage and accompanying GC B cells expansion implies an aberrant, lymphoproliferative phenotype.

The production of autoantibodies as well as increased abundance of immunoglobulins of all subtypes (hypergammaglobulinemia) and changes in regulatory T (T<sub>reg</sub>) cell expansion hint towards an autoimmune-like phenotype in the mouse models. The *sanroque* (*Rc3h1*<sup>san/san</sup>) mouse strain shows an aberrant phenotype of all parameters including the production of autoantibodies. In contrast to that, the single knockout of either Roquin-1 or Roquin-2 in T cells shows no alteration in neither of the determinants. Solely, Roquin-1 ablation induces activation of the CD8 T cell compartment. But, a combined deficiency of both paralogs drastically increases the frequency of CD4 and CD8 effector-memory-type T cells, elevated levels of T<sub>FH</sub> and GC B cells as well as T<sub>reg</sub> cells, suggesting that, Roquin deficiency can lead to the onset of autoimmunity. Interestingly, a lack of Regnase-1 in T cells comparably hyperactivates CD4 and CD8 T cells and causes elevated production of autoantibodies as well as immunoglobulin levels of all subtypes. Whether Regnase-1 controls the GC response by influencing T<sub>FH</sub> differentiation and GC B cell expansion like Roquin still needs to be clarified. Overall these

comparisons suggest that Roquin and Regnase-1 have potential overlapping functions in the prevention of autoimmunity.

**Table 18 | Comparison of previously published phenotypes in *sanroque* mice and mice deficient for Roquin-1, Roquin-2 and Regnase-1 in T cells.**

Published phenotypes of *Rc3h1<sup>san/san</sup>* (Vinuesa et al., 2005), *Rc3h1<sup>fl/fl</sup>; Cd4-cre* (Bertossi et al., 2011), *Rc3h2<sup>fl/fl</sup>; Cd4-cre*, *Rc3h1/2<sup>fl/fl</sup>; Cd4-cre* (Vogel et al., 2013) and *Zc3h12a<sup>fl/fl</sup>; Cd4-cre* (Uehata et al., 2013) mice. Comparison of effector-memory (EM) phenotype of CD4 and CD8 T cells, differentiation of follicular helper T cells (T<sub>FH</sub>) and germinal center (GC) B cell formation, autoantibody (ANA) and hypergammaglobulinemia and frequencies of regulatory T cells (T<sub>reg</sub>) in the different knockout situations. –: comparable to WT control mice, +: frequency increased or impairment, ++: strong changes in frequencies or impairment, /: not investigated.

phenotype	<i>Rc3h1<sup>san/san</sup></i> (Linterman et al., 2009; Vinuesa et al., 2005)	<i>Rc3h1<sup>fl/fl</sup>; Cd4-cre</i> (Bertossi et al., 2011)	<i>Rc3h2<sup>fl/fl</sup>; Cd4-cre</i> (Vogel et al., 2013)	<i>Rc3h1/2<sup>fl/fl</sup>; Cd4-cre</i> (Vogel et al., 2013)	<i>Zc3h12a<sup>fl/fl</sup>; Cd4-cre</i> (Uehata et al., 2013)
CD4 EM	+	-	-	+	++
CD8 EM	+	+	-	++	+
T <sub>FH</sub>	+	-	-	+	/
GC B cell formation	+	-	-	+	/
ANA	+	-	-	-	+
hypergammaglobulinemia	+	-	-	-	+
T <sub>reg</sub>	+	-	-	+	-

To investigate the role of Roquin and Regnase-1 proteins in preventing autoimmunity, we generated mice with a conditional deletion of the Roquin-1-, Roquin-2- and Regnase-1-encoding alleles, respectively (**Figure 7**). We utilized the *cre* recombinase under the control of the CD4 promoter, which deletes loxP-flanked alleles *Rc3h1<sup>fl/fl</sup>*, *Rc3h2<sup>fl/fl</sup>* and *Zc3h12a<sup>fl/fl</sup>* during T cell development of CD4<sup>+</sup>, CD8<sup>+</sup>, CD25<sup>lo</sup>, CD44<sup>lo</sup> (DN4) lymphocytes in the thymus (Lee et al., 2001; Sawada et al., 1994). *Rc3h1/2<sup>fl/fl</sup>; Cd4-cre* mice are in the following termed TKO<sup>T</sup> and the phenotype was compared to *Rc3h1/2<sup>fl/fl</sup>; Cd4-cre* (DKO<sup>T</sup>) and *Zc3h12a<sup>fl/fl</sup>; Cd4-cre* (KO<sup>T</sup>) as well as to wild-type controls either *Cd4-cre* or *Rc3h1/2<sup>fl/fl</sup>; Zc3h12a<sup>fl/fl</sup>* mice (WT).

I would like to point out that we did not use the same genetically targeted mouse for deleting Regnase-1-encoding alleles as Uehata et al., 2013 (**Table 18**). The *Zc3h12a<sup>fl/fl</sup>* mouse was provided by Dr. Mingui Fu (Li et al., 2017). As **Figure 7** implies, the loxP sites are flanking exon 3, resulting in cre-mediated deletion of the PIN domain of Regnase-1. In comparison to that, the *Zc3h12a<sup>fl/fl</sup>* generated by Uehata et al. resulted in cre-mediated deletion of exon 4-6 lacking the C-terminal part of the protein and the 3'-UTR.



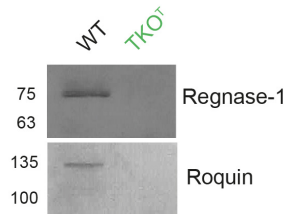


**Figure 22 | Validation of knockouts in *Rc3h1/2<sup>fl/fl</sup>*; *Zc3h12a<sup>fl/fl</sup>*; *Cd4-cre* (TKO<sup>T</sup>) mice.**

Immunoblot analysis of Roquin and Regnase-1 protein expression in CD4 T cells isolated from spleens of *Rc3h1/2<sup>fl/fl</sup>*; *Zc3h12a<sup>fl/fl</sup>*; *Cd4-cre* (TKO<sup>T</sup>) and *Rc3h1/2<sup>fl/fl</sup>*; *Zc3h12a<sup>fl/fl</sup>* (WT) mice. The molecular weight in kDa is depicted at the left. Data are representative of two independent experiments.

The cre-mediated deletion of loxP-flanked alleles in Roquin-1-, Roquin-2- and Regnase-1 encoding alleles in TKO<sup>T</sup> mice was successful as shown in the immunoblot in **Figure 22** on full-length protein levels in CD4 T cells isolated from spleens.

In the following section, the consequences of a phenotypic deletion were compared in TKO<sup>T</sup>, KO<sup>T</sup> and DKO<sup>T</sup> mice by applying flow cytometry. We were aiming to dissect the individual or shared contributions of Roquin and Regnase-1 in shaping T cell-mediated immunity and to uncover a potential cooperativity of these factors.

Due to space limitations I will in the following figures show representative flow cytometry analyses of at least WT and TKO<sup>T</sup> mice, but always include a quantification of all genotypes.

#### 4.2.2 Analyzing thymic T cell development in mice lacking Roquin- and Regnase-1 in T cells

To investigate the components of the adaptive immune system, we started investigating the cell compositions of the thymus, the organ where T cells originate and gain their antigen-specificity. The thymi of TKO<sup>T</sup> and KO<sup>T</sup> mice were drastically reduced in absolute cell numbers, whereas DKO<sup>T</sup> showed no change. This drastic loss of cell numbers can be explained by a strong decline of DP thymocytes (**Figure 23 a-c**). Lymphocytes that were negative for CD4 and CD8 (DN) were decreased in frequencies, but not significantly in cell numbers. DN thymocytes can be further discriminated by CD25 and CD44 expression in DN1-4 (**Figure 23 d-e**). Thymocytes at the DN1 stage were increased in frequency in TKO<sup>T</sup> mice, which was not reflected in total cell numbers of CD44<sup>hi</sup>, CD25<sup>lo</sup> cells. Since important stages in T cell development seemed to be dysregulated, the selection processes and maturation of thymocytes were validated by flow cytometry.

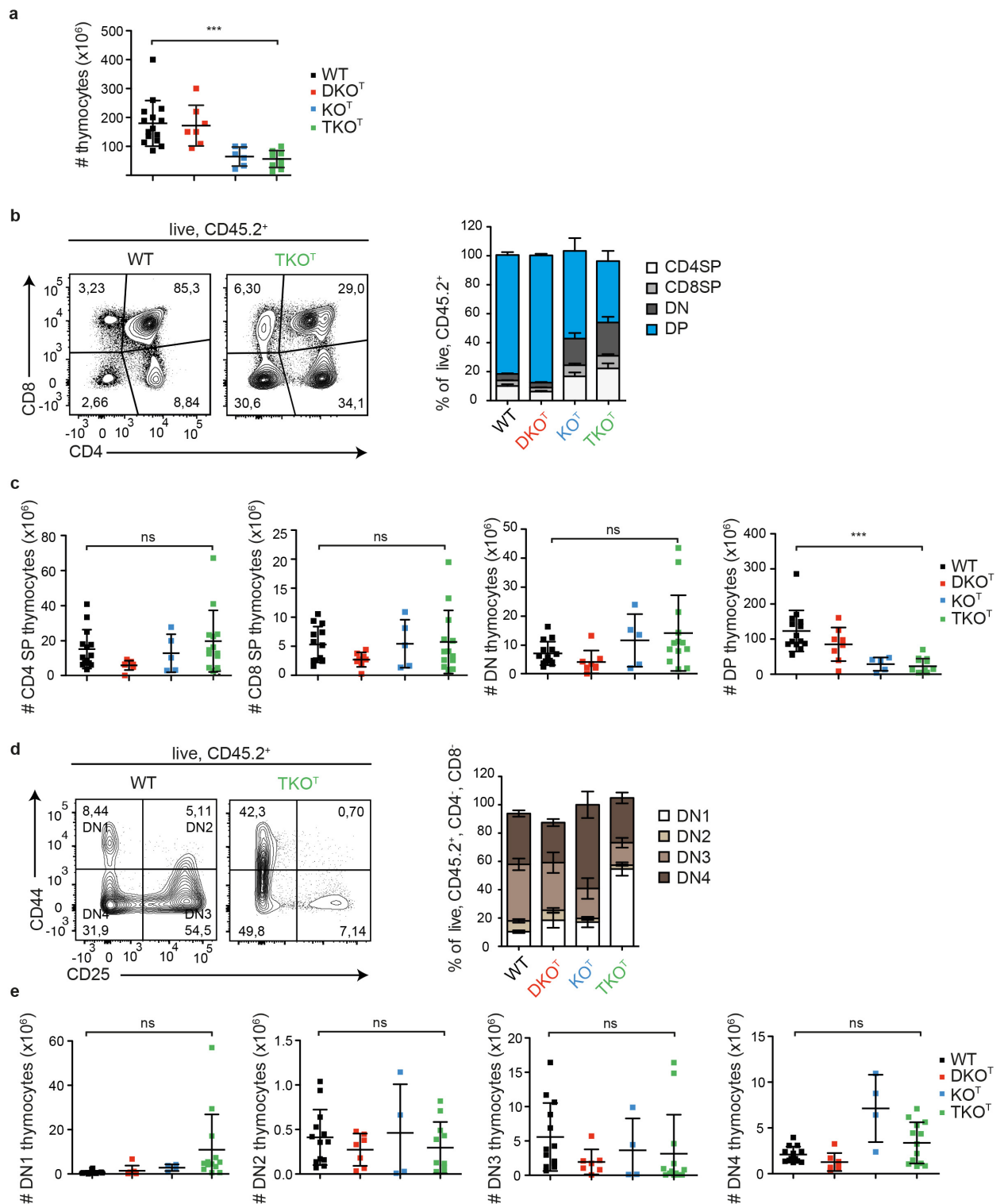


**Figure 23 | Determination of thymic T cell development in Roquin- and Regnase-1-deficient mice.**

Total numbers of thymocytes were defined for WT, DKO<sup>T</sup>, KO<sup>T</sup> and TKO<sup>T</sup> mice (a). The stages of T cell development are determined by flow cytometry analysis of CD4 and CD8 and frequencies (b) and absolute numbers (c) thereof were calculated. Discrimination of maturation stages (DN1-4) of double negative (DN) thymocytes by flow cytometry analysis of CD25 and CD44. Frequencies (d) and absolute numbers (e) of DN1-4 were calculated. The bars represent the mean value in each group and data are representative for 6 (b) and 4 (d) independent experiments. Statistical significances were calculated by one-way analysis of variance (ANOVA) with Bonferroni post test.

In **Figure 24 a-b**, the expression pattern of CD69 and TCR $\beta$  during the process of positive selection resulted in 5 different stages that can be controlled for CD4 and CD8 expression (Fu et al., 2009; Wang et al., 2012).

Population 1 and 2 represented pre-positive selection stages with low CD69 and TCR $\beta$  expression still devoid of CD4 and CD8 SP cells. The expression of CD69 in stage 3 correlated with decreased CD4 and CD8 expression on DP thymocytes and then resulted in CD4 and CD8 SP thymocytes by induced TCR $\beta$  on the cell surface (stage 4). In the post-positive selection stage 5 cells lost CD69 and became mature CD4 and CD8 SP thymocytes. Interestingly, in mice with ablation of Roquin and Regnase-1 DP thymocytes were still strongly detectable in stage 5. The overall frequencies of the different stages revealed that TKO<sup>T</sup> mice showed slightly increased frequencies of thymocytes in stage 4-5, but stronger changes in stage 3. (**Figure 24 b**). This phenotype was not shared by mice deficient for either Roquin-1/2 or Regnase-1 (**Appendix 3**). Calculating the ratio of mature (CD24<sup>lo</sup>, TCR $\beta$ <sup>hi</sup>) to immature (CD24<sup>hi</sup>) thymocytes (right panel), resulted in an elevated proportion of mature CD4 SP cells in TKO<sup>T</sup> mice, whereas mature CD8 SP cells were only slightly affected by conditional deletion of Roquin and Regnase-1 in T cells (**Figure 24 c**). These findings suggested that positive selection and maturation potentially proceeded faster in the absence of Roquin and Regnase-1.

Since the selection process in the thymus results in regulatory T cell formation, we were wondering if the differentiation of thymic-derived T<sub>reg</sub> cells was impaired in TKO<sup>T</sup> mice. In all knockout genotypes we discovered increased frequencies of regulatory T cells in the thymus (**Figure 25 a**), whereas absolute numbers were only elevated in KO<sup>T</sup> and TKO<sup>T</sup> thymi. To rule out that the large frequency of regulatory T cells results from recirculating peripheral T<sub>reg</sub> cells, we determined the expression of the chemokine receptors Ccr6 and Ccr7. Ccr6<sup>+</sup> Ccr7<sup>-</sup> Foxp3<sup>+</sup> CD4 T cells were previously described to re-enter the thymus from the periphery (Cowan et al., 2016). Interestingly, the frequency of Ccr6<sup>+</sup> Ccr7<sup>-</sup> Foxp3<sup>+</sup> cells was not altered in all genotypes, suggesting that the strong induction of regulatory T cells in TKO<sup>T</sup> and KO<sup>T</sup> mice potential arose in the thymi of these mice (**Figure 25 b**). Most of the increase in T<sub>reg</sub> frequencies was caused by an elevation of CD25<sup>-</sup> T<sub>reg</sub> cells (**Figure 25 c**), which have been reported to derive from diverted, potentially autoreactive thymocytes that have less repressive capacity than CD25<sup>+</sup> regulatory T cells and are prone to become T<sub>FH</sub> cells (Zhan et al., 2011).

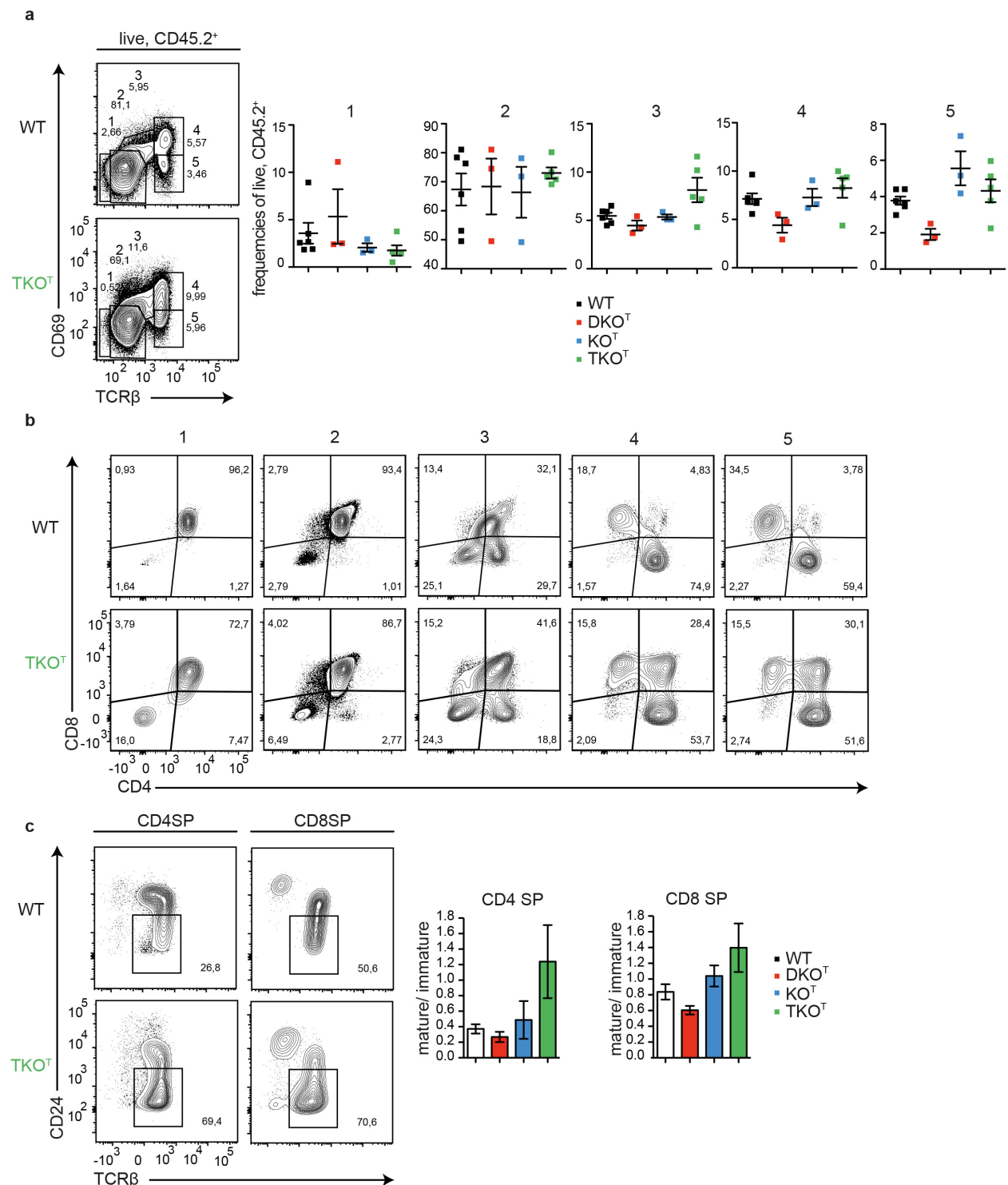


**Figure 24 | Analyzing positive selection and maturation of SP T cells in TKO<sup>T</sup> mice.**

**a)** Positive selection was determined in live, CD45.2<sup>+</sup> cells of thymi from WT, DKO<sup>T</sup>, KO<sup>T</sup> and TKO<sup>T</sup> by CD69 and TCR $\beta$  expression in populations 1-5. Representative flow cytometry analysis is shown in the left panel and frequencies of populations 1-5 are depicted in the right. **b)** CD4 and CD8 expression in the 5 populations defined by TCR $\beta$  and CD69 expression in **a)** of WT and TKO<sup>T</sup> thymocytes. **c)** Flow cytometry analysis of CD24 and TCR $\beta$  in CD4 and CD8 SP thymocytes represents mature (CD24<sup>lo</sup>, TCR $\beta$ <sup>hi</sup>) and immature (CD24<sup>hi</sup>) thymocytes (left contour plot). The ratio of mature to immature T cells was calculated for CD4SP and CD8 SP in WT, DKO<sup>T</sup>, KO<sup>T</sup> and TKO<sup>T</sup> mice (right panels). Genotypes are indicated in the figure and data are representative for 3 (a-c) independent experiments.

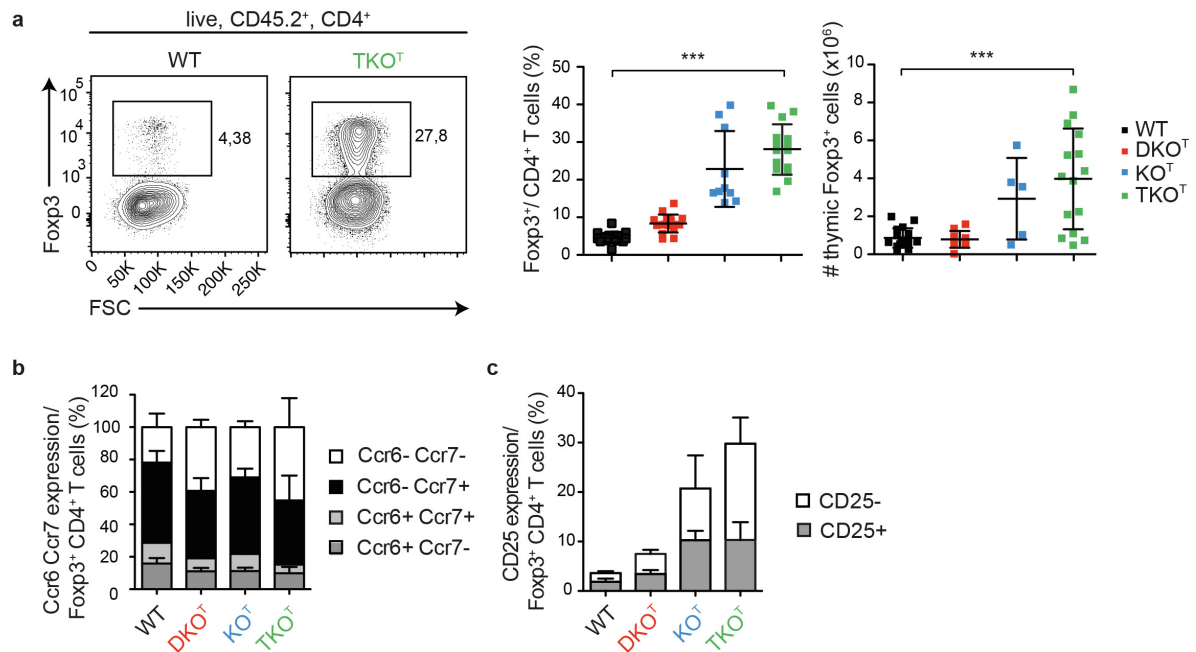


**Figure 25 | Altered thymic T<sub>reg</sub> development in KO<sup>T</sup> and TKO<sup>T</sup> mice.**

**a)** Thymic regulatory T cells (T<sub>reg</sub>) were determined in WT, DKO<sup>T</sup>, KO<sup>T</sup> and TKO<sup>T</sup> CD45.2<sup>+</sup>, CD4<sup>+</sup> T cells by intracellular flow cytometry analysis of Fcpx3 expression. A representative contour plot is shown in the left panel and frequencies and absolute numbers of all genotypes are shown in the right. **b)** Regulatory T cells as defined in a) were investigated for their recirculating capacity by Ccr6 and Ccr7 chemokine receptor expression by flow cytometry and quantifications thereof are shown. **c)** Proportion of CD25 expression on Fcpx3<sup>+</sup> CD4<sup>+</sup> T cells was analyzed by flow cytometry and quantified. Genotypes are indicated in the figure and data are representative of at least 2 (b) and 5 (c) individual mice per genotype.

To further investigate the development of regulatory T cells, we determined the pre-T<sub>reg</sub> stages (I-V) defined by GITR, CD25 and Fcpx3 expression (**Figure 26 a-d**). Maturation of regulatory CD4 T cells occurs via induction of GITR (I: GITR<sup>-</sup> CD25<sup>-</sup>; II: GITR<sup>int</sup> CD25<sup>-</sup>; III: GITR<sup>+</sup> CD25<sup>-</sup>), followed by the expression of the IL-2 receptor CD25 (IV: GITR<sup>+</sup> CD25<sup>+</sup>) upon strong TCR interaction with p:MHC on antigen-presenting cells or epithelial cells in the cortex and medulla of the thymus. When GITR<sup>+</sup> CD25<sup>+</sup> precursor cells encounter IL-2 and IL-15, they induce the expression of Fcpx3 (V: GITR<sup>+</sup> CD25<sup>+</sup> Fcpx3<sup>+</sup>) and become mature T<sub>reg</sub> cells (Burchill et al., 2007; Lio and Hsieh, 2008).

TKO<sup>T</sup> mice had significantly increased numbers of cells in the last stages of T<sub>reg</sub> formation (IV and V). Previous studies showed that these last stages of T<sub>reg</sub> development are impaired in the absence of the atypical NF-κB inhibitor IκB<sub>NS</sub> and the NF-κB transcription factor cRel (Schuster et al., 2012; Schuster et al., 2017). As shown in the previous chapter, the *Nfkbid* gene, encoding for IκB<sub>NS</sub>, and cRel are targets of Roquin and Regnase-1 (Jeltsch et al., 2014; Leppek et al., 2013; Mino et al., 2015; Murakawa et al., 2015; Uehata et al., 2013).

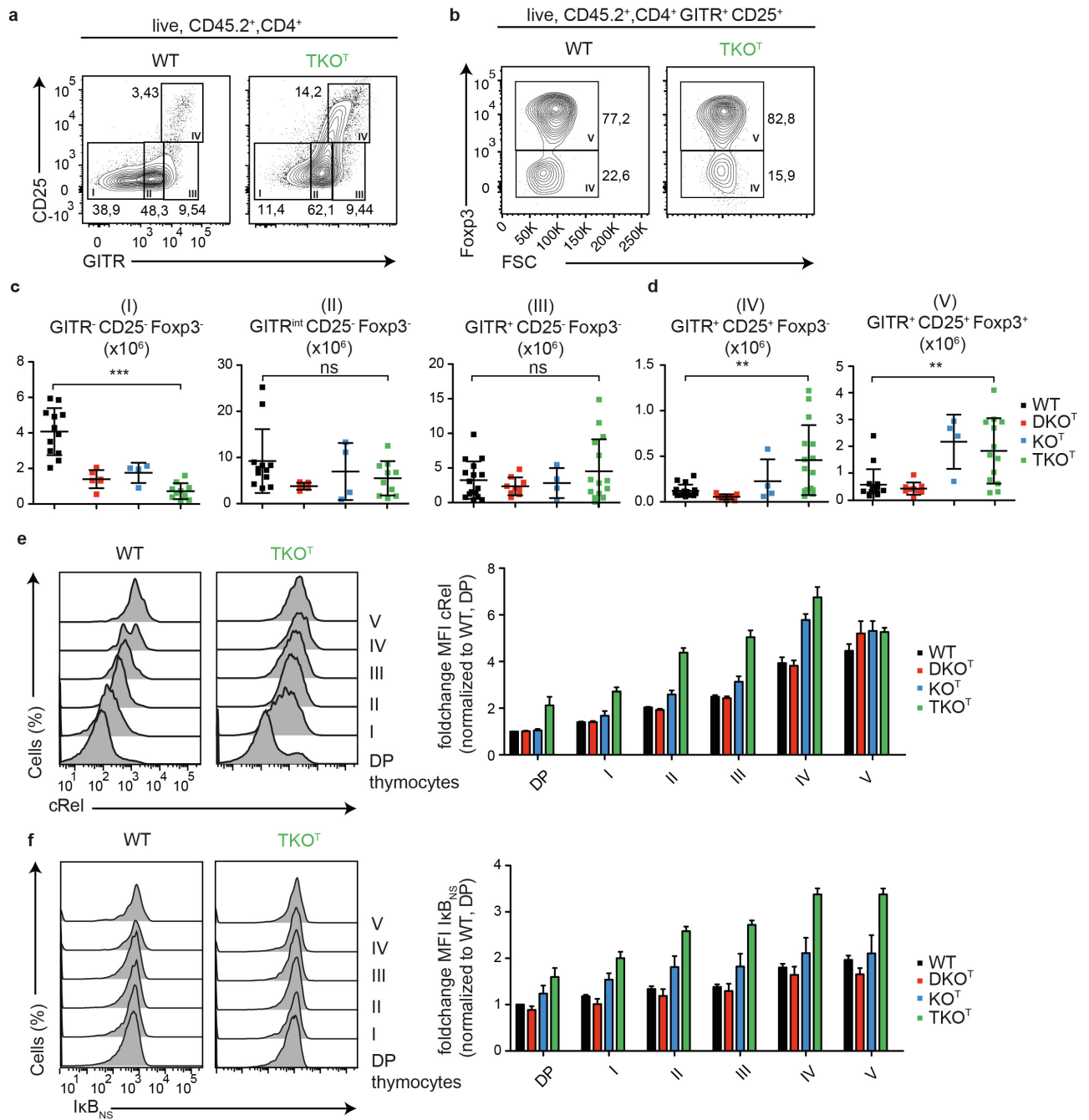


**Figure 26 | Analyzing IκB<sub>NS</sub> and cRel protein expression during thymic T<sub>reg</sub> development.**

Regulatory T cell development in the thymus is defined by step-wise expression of GITR, CD25 and Foxp3: I: GITR<sup>-</sup> CD25<sup>-</sup>, II: GITR<sup>int</sup> CD25<sup>-</sup>, III: GITR<sup>+</sup> CD25<sup>-</sup>, IV: GITR<sup>+</sup> CD25<sup>+</sup>, V: GITR<sup>+</sup> CD25<sup>+</sup> Foxp3<sup>+</sup>. These stages are shown in a representative contour blot of GITR, CD25 (a) and Foxp3 and forward side scatter (FSC) (b) by flow cytometry in CD45.2<sup>+</sup>, CD4<sup>+</sup> T thymocytes of WT and TKO<sup>T</sup> mice. Absolute numbers of populations I, II, III, IV (c) and V (d) were calculated for WT, DKO<sup>T</sup>, KO<sup>T</sup> and TKO<sup>T</sup> mice. Expression of cRel (e) and IκB<sub>NS</sub> (f) were determined by intracellular flow cytometry analysis. Representative histograms of protein expression in WT and TKO<sup>T</sup> mice of DP, I, II, III, IV and V populations are shown in the left panel and at the right the foldchange mean-fluorescence intensity (MFI) of cRel and IκB<sub>NS</sub> in the different stages and genotypes were calculated. MFIs were normalized to WT expression in CD4 and CD8 DP thymocytes. Genotypes are indicated in the figure and data are representative of at least 6 (a-d) and 3 (e-f) individual mice per genotype. Statistical significances were calculated by one-way analysis of variance (ANOVA) with Bonferroni post test.

We therefore investigated the protein expression of I $\kappa$ B<sub>NS</sub> and cRel in WT, DKO<sup>T</sup>, KO<sup>T</sup> and TKO<sup>T</sup> mice in the different stages of T<sub>reg</sub> development as defined in **Figure 26 a-b**. Elevated expression of I $\kappa$ B<sub>NS</sub> and cRel was detected by flow cytometry throughout all stages (**Figure 26 e-f**) in TKO<sup>T</sup> mice, whereas cRel expression was not further increased in the last stage V. Calculating foldchange expression for I $\kappa$ B<sub>NS</sub> and cRel in all analyzed genotypes, revealed that TKO<sup>T</sup> mice showed the strongest induction of I $\kappa$ B<sub>NS</sub> and cRel, whereas the single and double knockouts had weaker effects. These data suggest that Roquin- and Regnase-1-deficiency strongly impacts on I $\kappa$ B<sub>NS</sub> and cRel expression in the thymus and that this could consequently result in aberrant regulatory T cell formation in these mice.

Overall, one can conclude that the thymic T cell development in the thymus was impaired in the TKO<sup>T</sup> mice and this aberrancy was also seen partially in KO<sup>T</sup> mice. Here, there might be a developmental defect during T cell selection, since the TKO<sup>T</sup> mice had less DP thymocytes, whereas the SP CD4 and CD8 proportion was increased.

#### 4.2.3 Investigating cell-intrinsic effects of Roquin- and Regnase-1-deficiency

To prove whether these effects were cell-intrinsic or if the drastic changes in thymic cell compositions resulted from an inflamed microenvironment that induced cytokine storm in the thymus, we next generated mixed bone marrow (BM) chimeric mice. Here, I made use of congenic mouse strains with allelic variants of CD45 (CD45.1, CD45.2 and heterozygous CD45.1/2) to track hematopoietic cells. Either WT (CD45.2) or TKO<sup>T</sup> (CD45.2) BM cells were mixed at a 1:1 ratio with WT (CD45.1) BM cells and intravenously injected into lethally irradiated recipient mice that were heterozygous for both congenic markers (CD45.1/2) (**Figure 27**). After 9 weeks, the reconstitution of the hematopoietic system was completed and the cells were tracked by flow cytometry with antibodies specifically discriminating between CD45.1 and CD45.2. The immune cell compartments were always compared between CD45.1- and CD45.2-expressing cells within the same mouse and mice reconstituted with WT<sup>CD45.1</sup> and WT<sup>CD45.2</sup> BM cells were generated as additional controls.



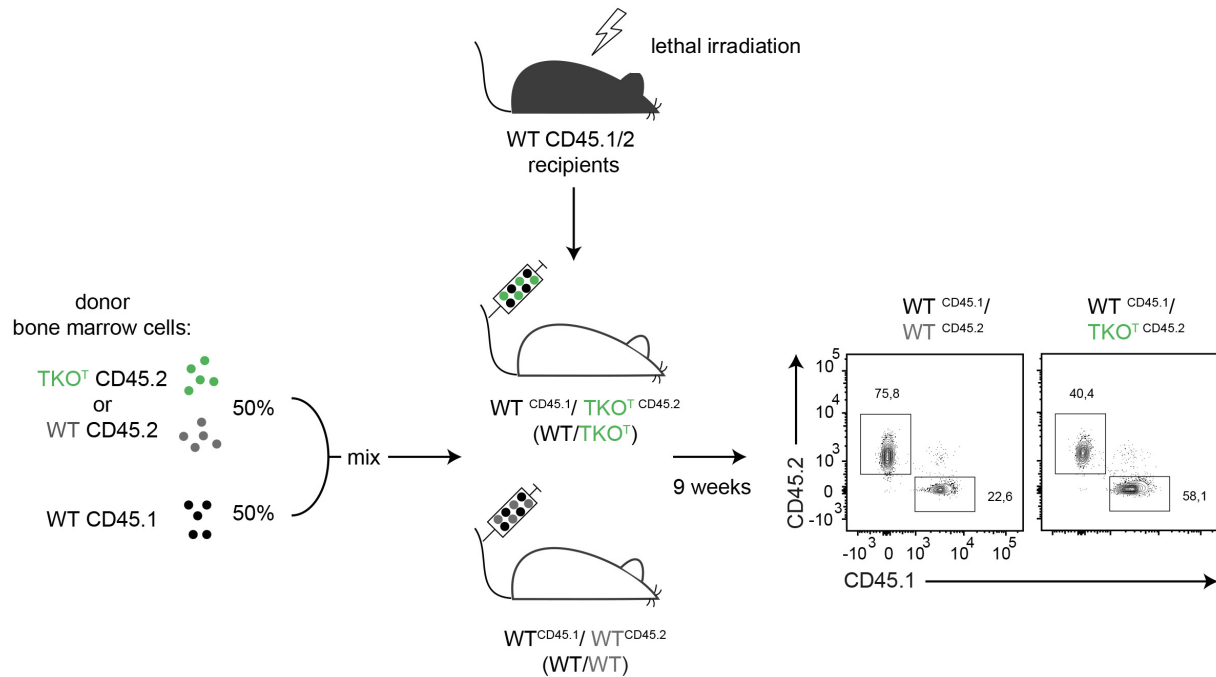


**Figure 27 | Generation of mixed bone marrow chimeric mice.**

WT CD45.1/2 heterozygous recipient mice were lethally irradiated and reconstituted with 4 Mio bone marrow (BM) cells either containing TKO<sup>T</sup> or WT CD45.2 BM mixed at a 1:1 ratio with WT CD45.1 BM cells. After 9 weeks, the reconstituted immune system was analyzed by flow cytometry of thymocytes with monoclonal antibodies identifying either CD45.1 or CD45.2 cells in the recipient mice.

In total, two WT/WT mice (reconstituted with WT<sup>CD45.1</sup> and WT<sup>CD45.2</sup> BM cells) and three WT/TKO<sup>T</sup> mice (reconstituted with WT<sup>CD45.1</sup> and Roquin-1/2- and Regnase-1-deficient TKO<sup>T</sup> CD45.2 BM cells) were generated and analyzed. As shown in **Figure 27**, irradiation and reconstitution were successful, since the CD45.1/2 recipients were devoid of endogenous heterozygous CD45 cells and the mice received CD45.1 and CD45.2 cells. Investigating the thymic T cell development by analyzing CD4 and CD8 expression, revealed that the loss of DP thymocytes as seen in the TKO<sup>T</sup> mice was potentially explained by an extrinsic effect, for example strong inflammation in the thymus, since no aberrant T cell development was seen in the WT<sup>CD45.1</sup> / TKO<sup>T</sup> CD45.2 mixed BM chimeric mice (**Figure 28**). In the following experiments, only representative flow cytometry plots for the WT<sup>CD45.1</sup> / TKO<sup>T</sup> CD45.2 mice are depicted, but total frequencies and ratios are additionally compared to the WT<sup>CD45.1</sup> / WT<sup>CD45.2</sup> control mice.



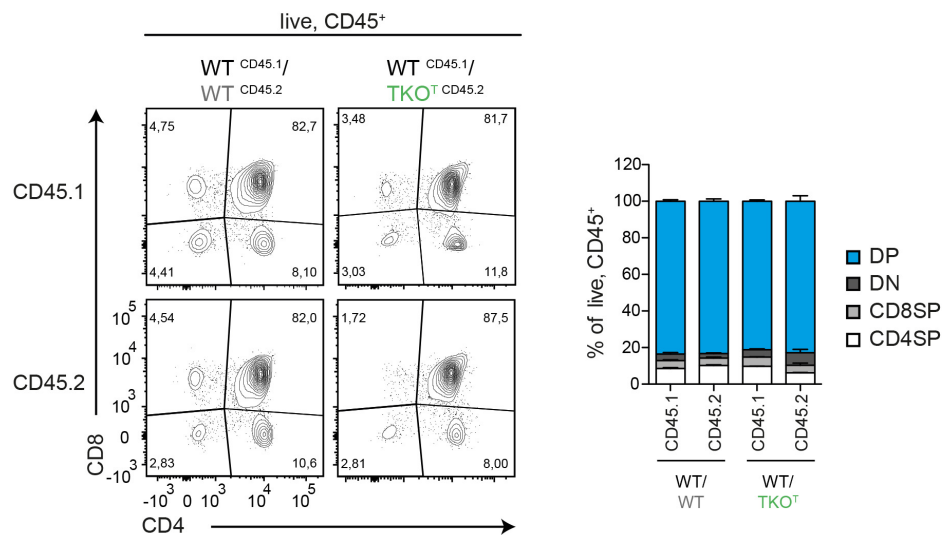


**Figure 28 | T cell development in WT <sup>45.1</sup>/ TKO<sup>T</sup> CD45.2 mixed BM chimera mice.**

Flow cytometry analysis of CD4 and CD8 expression in live, CD45.1<sup>+</sup> or CD45.2<sup>+</sup> cells of WT <sup>45.1</sup>/ WT CD45.2 or WT <sup>45.1</sup>/ TKO<sup>T</sup> CD45.2 mice (left) and frequencies of double-negative (DN), double-positive (DP), CD4 single-positive (SP) and CD8 SP thereof (right panel). Data are representatives of two (WT/WT) and three (WT/TKO<sup>T</sup>) individual mice.

We further investigated if the selection processes in the thymus were impaired in mice that received TKO<sup>T</sup> CD45.2 bone marrow. Therefore, we again analyzed steps of positive selection by comparing CD69 and TCR $\beta$  expression within the CD45.1<sup>+</sup> and CD45.2<sup>+</sup> cells of both WT/WT control and WT/TKO<sup>T</sup> BM chimeric mice (**Figure 29 a**). Here, the frequencies of pre-selected cells (population 1, TCR $\beta$ <sup>lo</sup> and CD69<sup>lo</sup>) were increased, whereas stages 3 and 5 comprising selected cells were reduced in the TKO<sup>T</sup> CD45.2 cell compartment in comparison to WT cells of mixed bone marrow chimeric mice. These data were not consistent with the observed increased frequencies of stages 3-5 in the conditional TKO<sup>T</sup> mice (**Figure 24**). Analyzing the distribution of CD4 and CD8 within these populations in CD45.1<sup>+</sup> and CD45.2<sup>+</sup> cells of WT/TKO<sup>T</sup> BM chimeric mice revealed that the TKO<sup>T</sup> CD45.2 cells had slightly elevated levels of double-positive (DP) thymocytes within population 5 (**Figure 29 b**), which was in accordance with the phenotype of TKO<sup>T</sup> mice (**Figure 24**). However, CD8 single-positive (SP) cells in stage 4 and 5 were reduced in TKO<sup>T</sup> CD45.2 in comparison to the WT CD45.1 compartment. Investigating maturation of CD4 and CD8 SP T cells showed that the ratio of mature to immature T cells was different in all controls (WT CD45.1/WT CD45.2 and WT CD45.2) and the TKO<sup>T</sup> CD45.2 cells (**Figure 29 c**). These data suggest that the competitive mixed bone marrow situation caused strong changes in the phenotype of the TKO<sup>T</sup> CD45.2 cells and therefore no conclusion can be drawn about the cell-intrinsic influence of a conditional knockout of Roquin and Regnase-1 on positive selection.

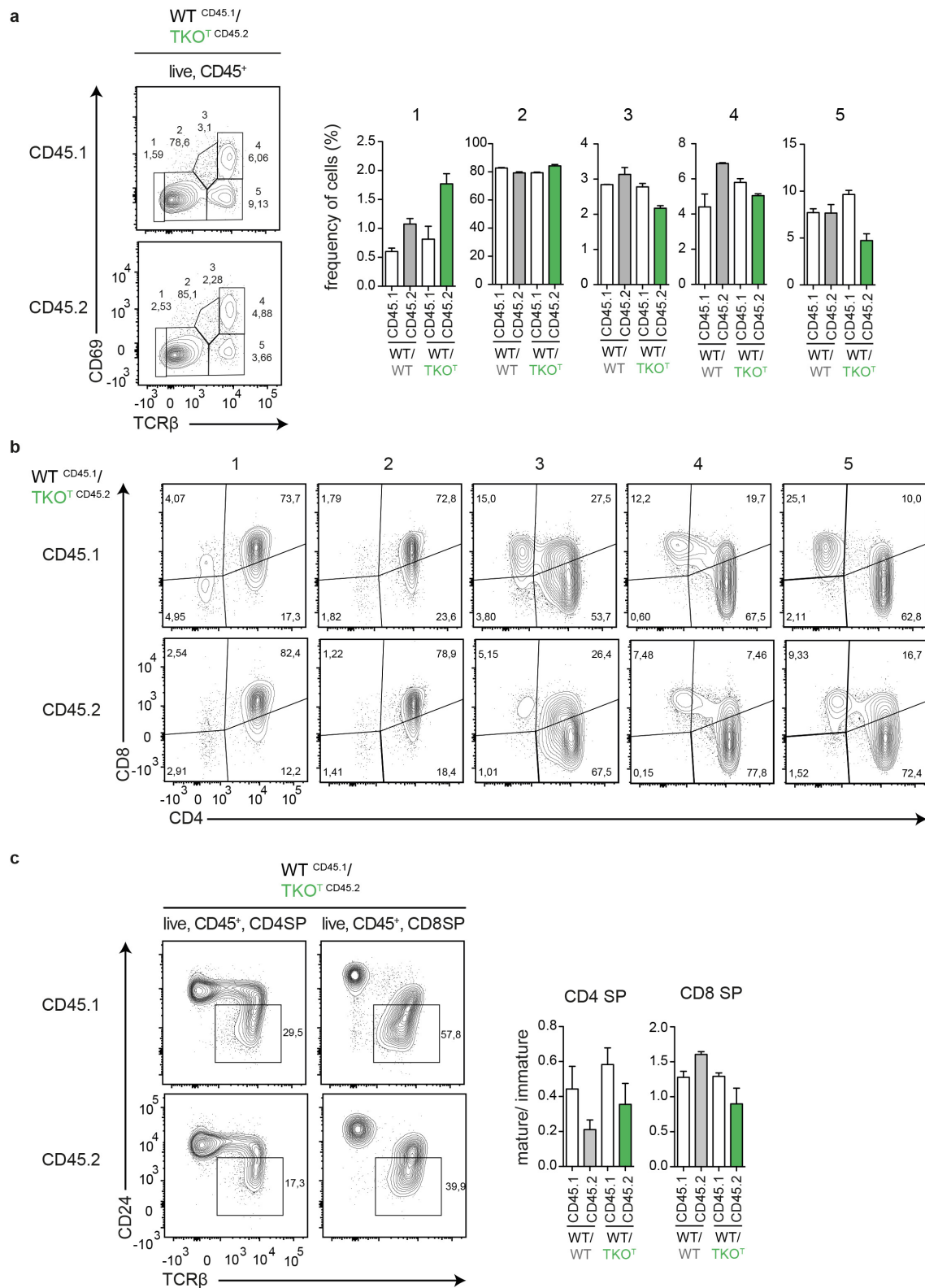


**Figure 29 | Investigating positive selection in thymi of mixed BM chimera mice.**

**a)** Flow cytometry analysis and quantification of CD69 and TCRβ-expressing cells of live, CD45.1<sup>+</sup> and CD45.2<sup>+</sup> cells in WT/TKO<sup>T</sup> and WT/WT mixed BM chimeric mice in populations 1-5. **b)** Flow cytometry of CD4 and CD8 expression in populations 1-5 within CD45.1<sup>+</sup> and CD45.2<sup>+</sup> cells of WT/TKO<sup>T</sup> mice. **c)** Investigation of maturation of CD4 single-positive (SP) or CD8 SP cells within WT/TKO<sup>T</sup> BM chimeric mice by flow cytometry analysis of CD24 and TCRβ (left). Ratio of mature to immature CD4 or CD8 SP

cells between CD45.1<sup>+</sup> and CD45.2<sup>+</sup> cells of WT/WT and WT/TKO<sup>T</sup> mice was calculated (right). Data are representatives of two (WT/WT) and three (WT/TKO<sup>T</sup>) individual mice.

Very recently, a flow cytometry-based assay to measure thymic clonal deletion in the polyclonal repertoire of WT mice was published (Breed et al., 2019). Elimination of self-reactive T cells in the thymus either induces apoptosis due to death by neglect or clonal deletion.

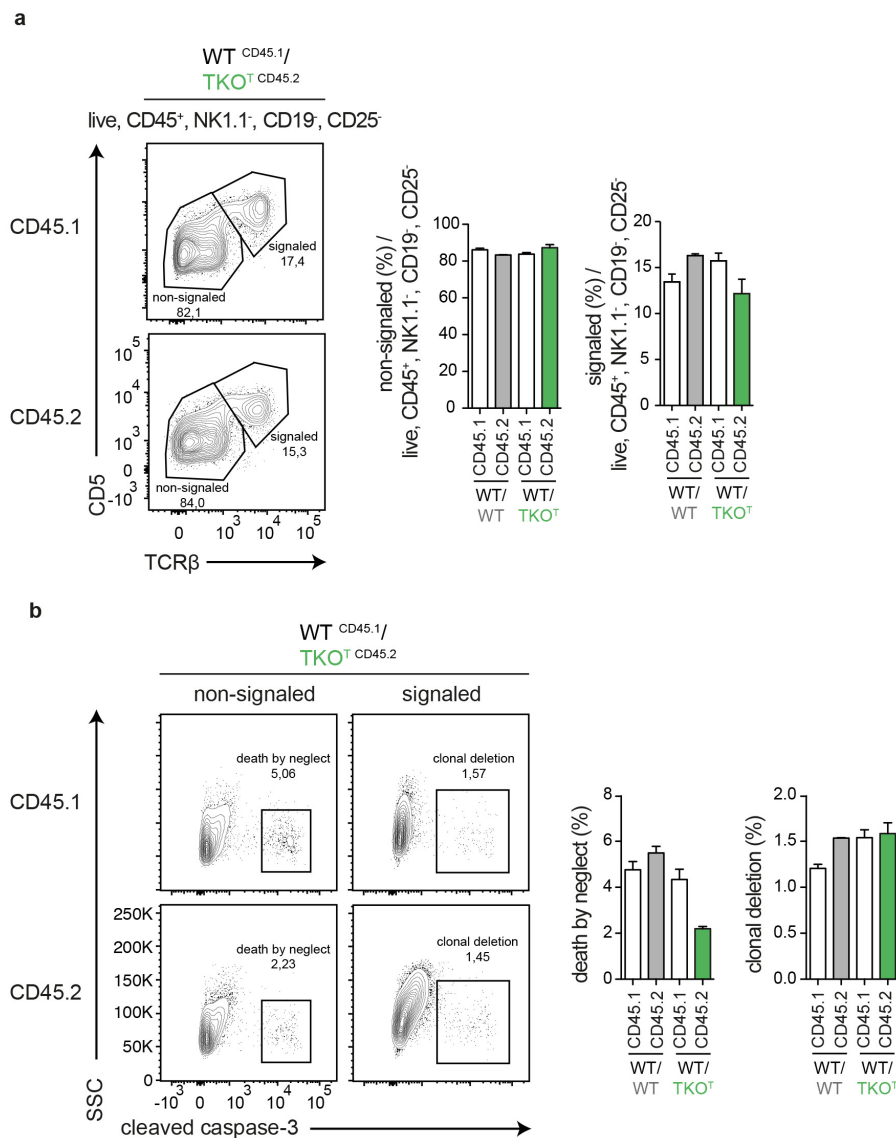


**Figure 30 | Determination of apoptosis in thymi of mixed BM chimeric mice.**

**a)** Flow cytometry analysis of signaled (CD5<sup>hi</sup>, TCRβ<sup>hi</sup>) and non-signaled (CD5<sup>lo</sup>, TCRβ<sup>lo</sup>) CD45.1<sup>+</sup> or CD45.2<sup>+</sup> cells within WT/TKO<sup>T</sup> mixed bone marrow chimeric mice and quantification thereof in comparison to CD45.1<sup>+</sup> and CD45.2<sup>+</sup> cells within WT/WT bone marrow chimeras. **b)** Analyzing cleaved caspase-3 expression by flow cytometry in non-signaled (death by neglect) and signaled (clonal deletion) CD45.1<sup>+</sup> or CD45.2<sup>+</sup> cells within WT/TKO<sup>T</sup> mixed bone marrow chimeric mice (left). Quantification of CD45.1<sup>+</sup> or CD45.2<sup>+</sup> cells either undergoing death by neglect or clonal deletion in WT/WT or WT/TKO<sup>T</sup> mixed BM chimeric mice. Data are representatives of two (WT/WT) and three (WT/TKO<sup>T</sup>) individual mice.

Here the authors measured apoptosis by intracellular antibody-staining of cleaved caspase-3, a marker of induced apoptosis. They combined this with TCR $\beta$  and CD5 to distinguish between cells that have already undergone TCR signaling (signaled, clonal deletion) or cells that have been eliminated due to no or weak p:MHC interaction (non-signaled, death by neglect). Applying this protocol to the mixed BM chimeras, revealed that the TKO<sup>T</sup> CD45.2<sup>+</sup> cells within the WT/TKO<sup>T</sup> mixed BM chimeric mice, showed overall no alteration between signaled and non-signaled cells in comparison to WT<sup>CD45.1</sup> cells (**Figure 30 a**). However, non-signaled cells that undergo death by neglect appeared decreased in the TKO<sup>T</sup> CD45.2<sup>+</sup> cells in comparison to either WT<sup>CD45.1</sup> control within the same mouse or WT/WT mixed BM chimeric mice. In contrast to that, cleaved caspase-3 staining in signaled cells did not show any alterations in cells undergoing clonal deletion (**Figure 30 b**).

Since the generation of regulatory T cells develops alongside with clonal deletion, thus requiring strong p:MHC-TCR interaction, we further wanted to investigate the cell-intrinsic effects on the development of regulatory T cells. Indeed, the frequency of Foxp3-expressing regulatory T cells in TKO<sup>T</sup> CD45.2<sup>+</sup> mixed bone marrow chimeras phenocopies the abnormal generation of T<sub>reg</sub> cells seen in mice with a conditional deletion of Roquin and Regnase-1 in T cells (**Figure 25**). The frequency of Foxp3-expressing CD4 T cells in TKO<sup>T</sup> CD45.2<sup>+</sup> was drastically increased in comparison to WT<sup>CD45.1</sup> cells as well as to WT/WT mixed BM chimeric controls (**Figure 31 a**).

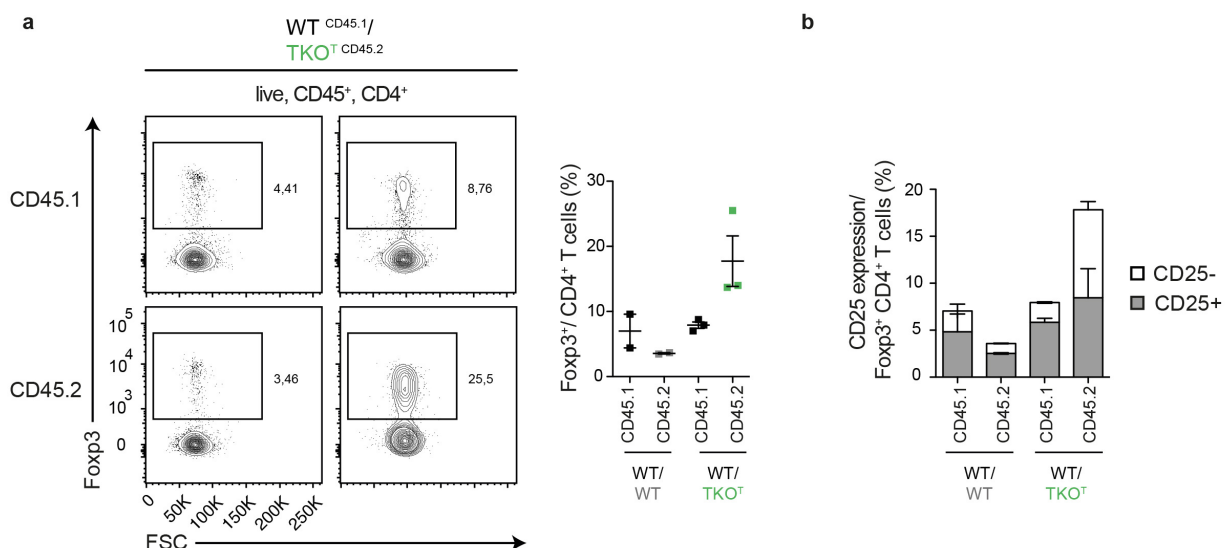


**Figure 31 | Altered frequencies of regulatory T cells in thymi of mixed bone marrow chimeric mice.**

Flow cytometry analysis of Foxp3 expression in CD45.1<sup>+</sup> or CD45.2<sup>+</sup> cells within WT/TKO<sup>T</sup> mixed bone marrow chimeric mice and quantification thereof in comparison to CD45.1<sup>+</sup> and CD45.2<sup>+</sup> cells within WT/WT bone marrow chimeras. **b**) Quantification of CD25 expression within Foxp3<sup>+</sup> CD4<sup>+</sup> T cells in CD45.1<sup>+</sup> or CD45.2<sup>+</sup> cells of WT/TKO<sup>T</sup> or WT/WT mixed bone marrow chimeric mice. Data are representatives of two (WT/WT) and three (WT/TKO<sup>T</sup>) individual mice.

The proportion of CD25<sup>+</sup> cells of Foxp3<sup>+</sup> CD4 T cells was drastically elevated in the TKO<sup>T</sup> CD45.2 cells in comparison to WT controls in accordance with the data generated in conditional TKO<sup>T</sup> mice. Since the development of regulatory T cells was impaired potentially due to aberrant I $\kappa$ B<sub>NS</sub> or cRel expression in the conditionally deleted mice (**Figure 25**), we next sought to investigate if this phenotype was cell-intrinsic. Indeed, mixed BM chimeric mice that lack Roquin and Regnase-1 in their CD45.2 (TKO<sup>T</sup> CD45.2) compartment, showed drastically increased expression of Foxp3 in the early stages of T<sub>reg</sub> development (**Figure 32 a-b**). Interestingly, T<sub>reg</sub> cells from TKO<sup>T</sup> CD45.2 cells had elevated I $\kappa$ B<sub>NS</sub> expression when directly compared to the WT<sup>CD45.1</sup> counterpart in the same mouse (**Figure 32 c**).

In summary these data revealed that the overall dramatic changes in thymic T cell development seen in the TKO<sup>T</sup> mice and partially in KO<sup>T</sup> mice was not cell-intrinsic. However, the selection processes, especially clonal deletion, were impaired in the CD45.2<sup>+</sup> counterpart of the WT/TKO<sup>T</sup> mice which lacks Roquin and Regnase-1 in T cells. Cells deficient for Roquin and Regnase-1 revealed less apoptosis, which rather suggests a support of anti-apoptotic mechanisms. Additionally, the development of regulatory T cells occurred faster, since already early stages of T<sub>reg</sub> development with low CD25 levels had high expression of Foxp3. This could be due to the impact of Regnase-1 and Roquin-deletion on target genes that impaired T cell selection or T<sub>reg</sub> development such as I $\kappa$ B<sub>NS</sub>. One further possibility therefore could be that T cells lacking Roquin and Regnase-1 had higher TCR signal strength that then results in impaired selection processes.

Since, clonal deletion as well as thymic regulatory T cell development was strongly influenced by Roquin and Regnase-1 cell-intrinsically, we next addressed the phenotypic consequences of conditional deletion in the periphery especially focusing here on phenotypes linked to autoimmunity and aberrant T cell activation.

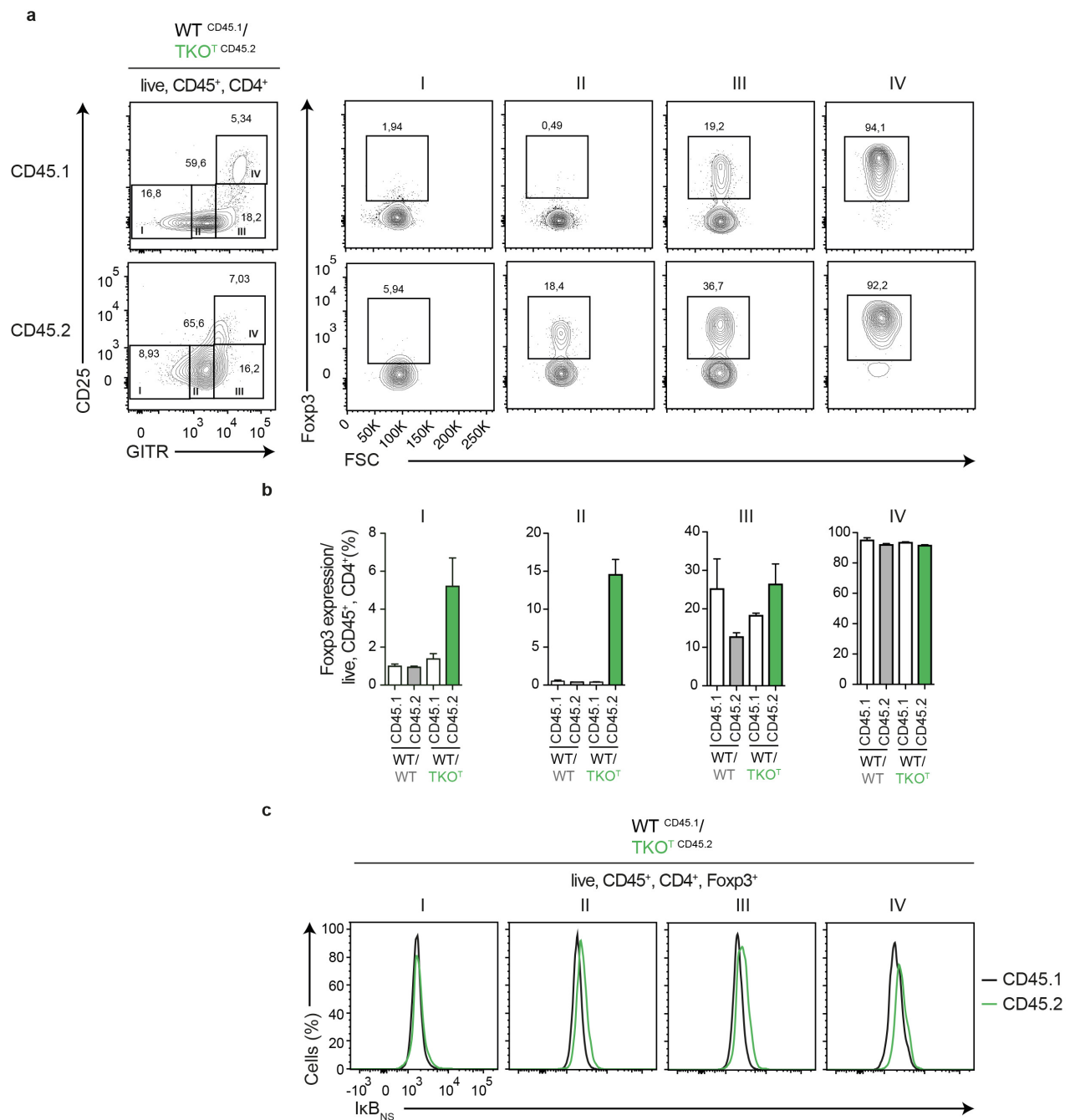


**Figure 32 | Impaired T<sub>reg</sub> development in TKO<sup>T</sup> <sup>CD45.2</sup> cells of mixed BM chimeric mice.**

**a)** Investigating regulatory T cell development in the thymus by flow cytometry of step-wise expression of GITR, CD25 and Foxp3: I: GITR<sup>-</sup> CD25<sup>-</sup>, II: GITR<sup>int</sup> CD25<sup>-</sup>, III: GITR<sup>+</sup> CD25<sup>-</sup>, IV: GITR<sup>+</sup> CD25<sup>+</sup>. The stages are shown in a representative contour blot of GITR, CD25 (left) and Foxp3 and forward side scatter (FSC) by flow cytometry (right) in CD45.1<sup>+</sup> or CD45.2<sup>+</sup> cells within WT/TKO<sup>T</sup> mixed bone marrow chimeric mice. **b)** Frequencies of Foxp3 expression in I, II, III and IV of CD45.1<sup>+</sup> and CD45.2<sup>+</sup> cells within WT/WT and WT/TKO<sup>T</sup> mixed BM chimeric mice. **c)** Expression of IkB<sub>NS</sub> within I, II, III and IV determined by intracellular flow cytometry analysis in CD45.1<sup>+</sup> or CD45.2<sup>+</sup> cells of WT/TKO<sup>T</sup> or WT/WT mixed bone marrow chimeric mice. Data are representatives of two (WT/WT) and three (WT/TKO<sup>T</sup>) individual mice.

#### 4.2.4 T-cell-specific deletion of Roquin and Regnase-1 induces autoimmunity in mice

Both, Roquin-1/2 and Regnase-1 deficiency in T cells resulted in an autoimmune-like phenotype in mice (**Table 18**). Therefore, we investigated whether a deletion of all three genes in mouse T cells would recapitulate or even amplify the phenotype. All analyzed mice were sacrificed at an age of 6 weeks, because  $\text{TKO}^{\text{T}}$  mice showed signs of illness with increased volume of the abdomen. The reason for this enlarged abdomen became clear when measuring the size of spleens. The mice developed splenomegaly and lymphadenopathy of all peripheral (pLN) as well as the abdominal mesenteric lymph nodes (mLN).

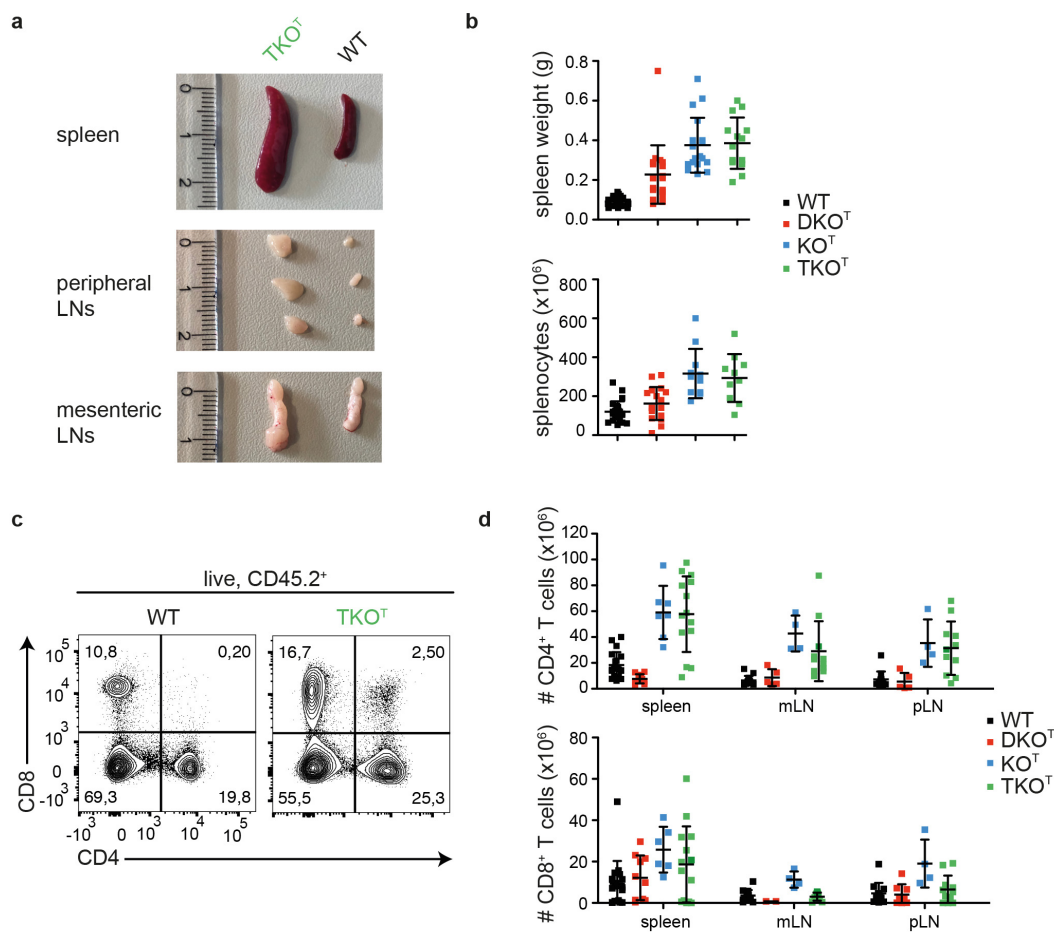


**Figure 33 | Analysis of the T cell composition in spleens and lymph nodes of mice with a T cell-specific deletion of Roquin and Regnase-1.**

**a)** Representative image of spleen, peripheral and mesenteric lymph nodes from WT and  $\text{TKO}^{\text{T}}$  mice. **b)** Spleen weight and number of splenocytes in WT,  $\text{DKO}^{\text{T}}$ ,  $\text{KO}^{\text{T}}$  and  $\text{TKO}^{\text{T}}$  mice. **c)** Representative contour plots of frequencies of CD4 and CD8 populations in live,  $\text{CD45.2}^+$  splenocytes of WT and  $\text{TKO}^{\text{T}}$  mice and absolute numbers thereof and of mesenteric LNs (mLN) and peripheral lymph nodes (pLN) **(d)** in WT,  $\text{DKO}^{\text{T}}$ ,  $\text{KO}^{\text{T}}$  and  $\text{TKO}^{\text{T}}$  mice. Genotypes are indicated in the figure and data are representative of at least 14 (b) and 3 (c-d) individual mice per genotype.



Augmented spleen weights correlated with elevated numbers of total splenocytes (**Figure 33 a-b**). Splenomegaly of  $\text{TKO}^{\text{T}}$  and  $\text{KO}^{\text{T}}$  mice was most severe, whereas  $\text{DKO}^{\text{T}}$  mice showed a less prominent expansion of cells in spleens. Analyzing frequencies of total CD4 and CD8 T cells indicated increased absolute numbers of CD4 T cells in spleens, mLN and pLN in  $\text{KO}^{\text{T}}$  and  $\text{TKO}^{\text{T}}$ , whereas  $\text{DKO}^{\text{T}}$ , at this age, showed comparable numbers to WT mice. CD8 T cells were expanded in  $\text{DKO}^{\text{T}}$ ,  $\text{KO}^{\text{T}}$  and  $\text{TKO}^{\text{T}}$  in spleens, but only  $\text{KO}^{\text{T}}$  mice had elevated numbers of CD8 cells in pLNs and mLNs (**Figure 33 c-d**).

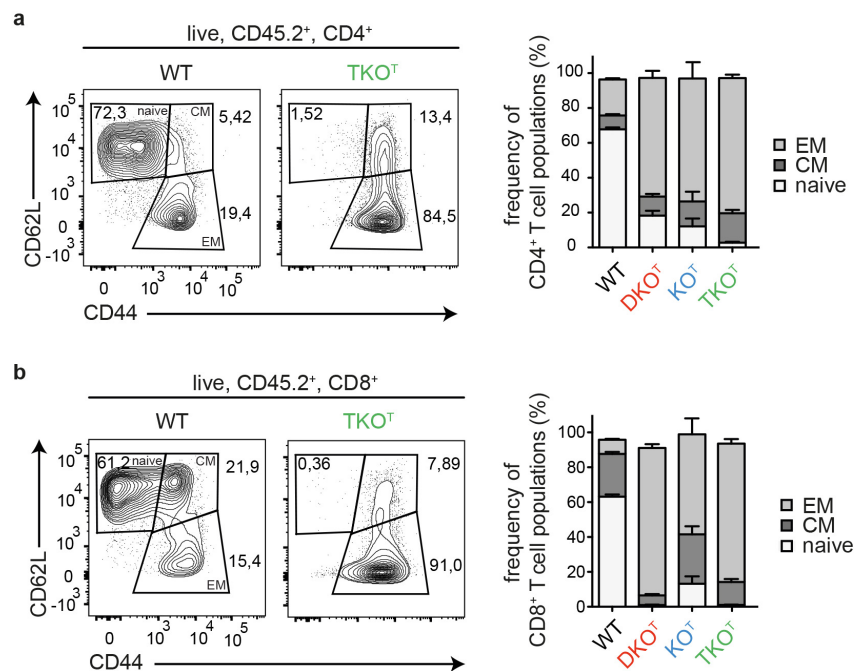


**Figure 34 | Discrimination of naïve, central-memory and effector-memory T cells in mice with a T cell-specific ablation of Roquin and Regnase-1.**

Representative contour plot (left panel) and frequencies (right panel) of naïve ( $\text{CD62L}^{\text{hi}} \text{CD44}^{\text{lo}}$ ), effector memory-like (EM,  $\text{CD62L}^{\text{lo}} \text{CD44}^{\text{hi}}$ ) and central memory-like (CM,  $\text{CD62L}^{\text{hi}} \text{CD44}^{\text{hi}}$ ) CD4 (a) and CD8 T cells (b). Genotypes are indicated in the figure and data are representative of at least 4 (a-b) individual mice per genotype.

The activation status of these T cells revealed that  $\text{DKO}^{\text{T}}$ ,  $\text{KO}^{\text{T}}$  and  $\text{TKO}^{\text{T}}$  CD4 T cells showed gradually higher frequencies of an effector memory-like (EM,  $\text{CD62L}^{\text{lo}} \text{CD44}^{\text{hi}}$ ) and central-memory like (CM,  $\text{CD62L}^{\text{hi}} \text{CD44}^{\text{hi}}$ ) phenotype, which in turn resulted in a relative decrease in naïve ( $\text{CD62L}^{\text{hi}} \text{CD44}^{\text{lo}}$ ) CD4 T cells (**Figure 34 a**). The increase of CD8 T cells in double knockout animals was ameliorated in the triple knockout, particularly on the level of total cell numbers. Excessive EM formation and loss of naïve T cells was apparent in CD8 T cells of  $\text{DKO}^{\text{T}}$  and  $\text{TKO}^{\text{T}}$  mice and was less pronounced in WT and  $\text{KO}^{\text{T}}$  CD8 T cells (**Figure 34 b**).

The highly activated CD4 and CD8 T cells in  $\text{TKO}^{\text{T}}$  mice prompted us to investigate the functionality and differentiation of CD4 T cells. Since an autoimmune-like phenotype was



described for DKO<sup>T</sup> and T cell specific knockout of Regnase-1 (**Table 18**), the germinal center response in spleens was analyzed.

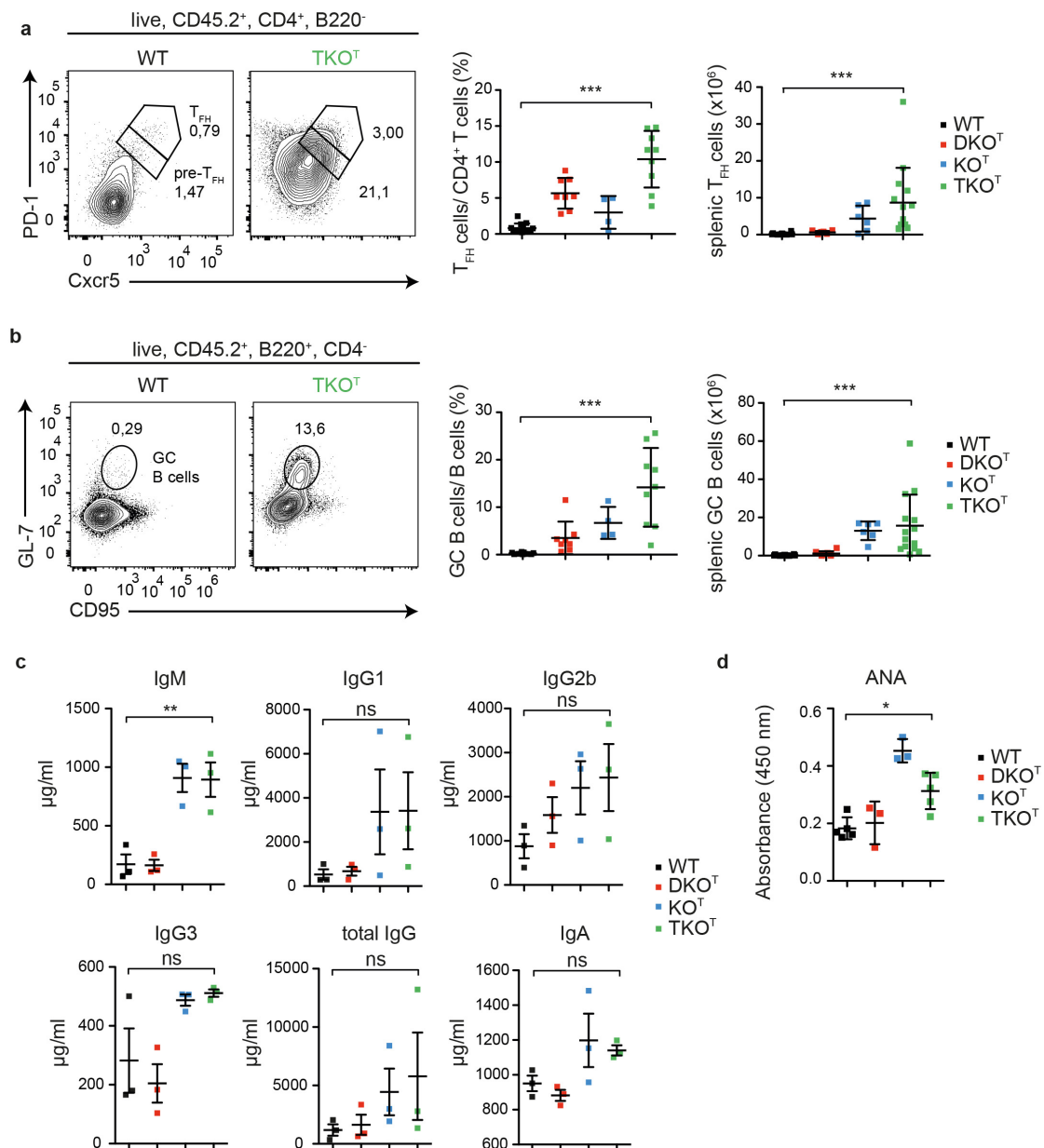


**Figure 35 | Analyzing the GC reaction and antibody response of mice with T cell-specific deletion of Roquin and Regnase-1.**

**a)** Pre-T<sub>FH</sub> and T<sub>FH</sub> cells were determined by flow cytometry analysis of Cxcr5 and PD-1 in live, CD45.2<sup>+</sup>, CD4<sup>+</sup> cells in the indicated genotypes. Representative contour blots are shown in the left panel and calculated frequencies and absolute numbers are given in the right. **b)** Live, CD45.2<sup>+</sup>, B220<sup>+</sup>, CD4<sup>-</sup> cells were determined as germinal center (GC) B cells by the expression of CD95 and GL-7. Contour blots of WT and TKO<sup>T</sup> mice are shown in the left and the frequencies and absolute numbers of GC B cells for all analyzed genotypes are given in the right panel. Serum levels of different immunoglobulin subclasses (IgM, IgG1, IgG2b, IgG3, IgA and total IgG) (**c**) as well as anti-nuclear autoantibodies (**d**) were defined by enzyme-linked-immunosorbant assay (ELISA) in WT, DKO<sup>T</sup>, KO<sup>T</sup> and TKO<sup>T</sup> mice. Data are representative of at least 4 (a-b) and 3 (c-d) individual mice per genotype. Statistical significances were calculated by one-way analysis of variance (ANOVA) with Bonferroni post test.

Frequencies and numbers of  $T_{FH}$  cells, characterized by the expression of *Cxcr5* and PD-1, were significantly elevated in  $TKO^T$  mice, whereas a significant increase was also detected for  $DKO^T$  and  $KO^T$  mice (**Figure 35 a**). This observation was in line with increased numbers and frequencies of GC B cells ( $B220^+$ ,  $GL-7^+$  and  $CD95^+$ ) and aberrant concentrations of immunoglobulins in sera of the mice (**Figure 35 b-c**). Here, IgM was significantly enhanced in  $KO^T$  and  $TKO^T$  mice, whereas total IgG and IgA as well as subtypes IgG1 and IgG2b had a mild increase in  $KO^T$  and  $TKO^T$ . The Roquin  $DKO^T$  only caused slightly raised levels of IgG2b. The autoimmune phenotype in  $TKO^T$  mice was supported by the secretion of anti-nuclear autoantibodies (ANAs) (**Figure 35 d**), which is highly elevated in  $KO^T$  and  $TKO^T$  mice, but not prominent in  $DKO^T$  mice. The large increase in  $T_{FH}$  cells prompted us to further investigate if these cells have the character of follicular regulatory T ( $T_{FR}$ ) cells by the expression of the transcription factor *Foxp3*. Indeed, we identified a significant abundance of  $T_{FR}$  cells in  $TKO^T$  mice (**Figure 36 a**). In addition, the frequency of regulatory T cells showed a drastic increase in all knockout-genotypes, whereas this was only represented in absolute numbers by  $KO^T$  and  $TKO^T$  mice (**Figure 36 b**).

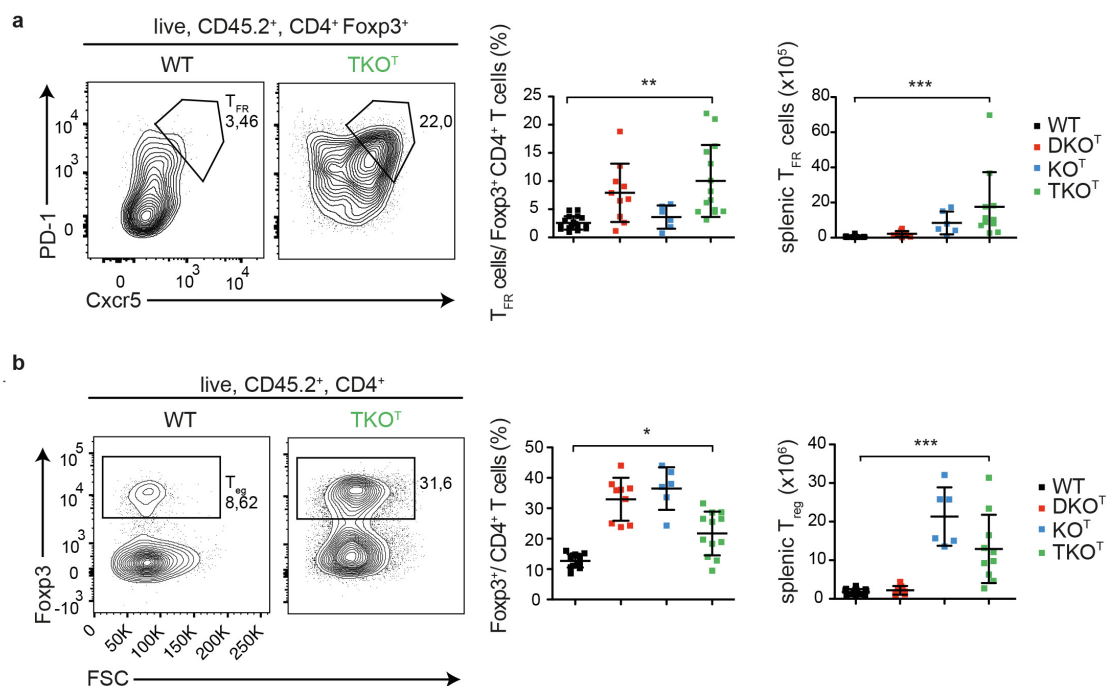


**Figure 36 | Determining frequencies and absolute numbers of Foxp3-expressing CD4 T cells in mice conditionally deleted for Roquin and Regnase-1 in T cells.**

**a**) Contour blot showing follicular regulatory T cells ( $T_{FR}$ ) by expression of PD-1 and *Cxcr5* in live, CD45.2<sup>+</sup>, CD4<sup>+</sup>, Foxp3<sup>+</sup> T cells of WT and  $TKO^T$  mice (left panel) and corresponding frequencies and absolute numbers, thereof. **b**) Foxp3 levels in live, CD45.2<sup>+</sup>, CD4<sup>+</sup> cells in WT and  $TKO^T$  mice shown as representative contour plot and frequencies and absolute numbers in WT,  $DKO^T$ ,  $KO^T$  and  $TKO^T$  mice. Genotypes are indicated in the figure and data are representative of at least 4 (a) and 6 (b) individual mice per genotype. Statistical significances were calculated by one-way analysis of variance (ANOVA) with Bonferroni post test.

In summary, the phenotypes of the  $\text{TKO}^T$  mice were in most analyzed T cell subsets reasoned in a cooperative effect of Roquin and Regnase-1 deficiency. This was especially seen for the hyperactivation of CD4 T cells or frequencies of  $\text{T}_{\text{FH}}$  and GC B cells. The cellular phenotypes of mice lacking either Roquin-1/2 or Regnase-1 were almost comparable, but in some cases the deficiency of Regnase-1 in T cells exhibited a more severe phenotype such as the production of autoantibodies. Interestingly, mice ablated for Roquin and Regnase-1 in T cells were less prone to develop autoantibodies. Additionally, as seen in the thymus, regulatory T cells were significantly increased in all analyzed genotypes and the proportion of  $\text{T}_{\text{FR}}$  cells was drastically elevated in peripheral lymphoid organs.

The mixed bone marrow chimeric mice that were described in **section 4.2.3** to partially have a cell-intrinsic thymic phenotype, were additionally analyzed for their capacity to form follicular T helper cells, regulatory T cells, regulatory follicular T helper cells and the effector-memory phenotype of CD4 and CD8 T cells.

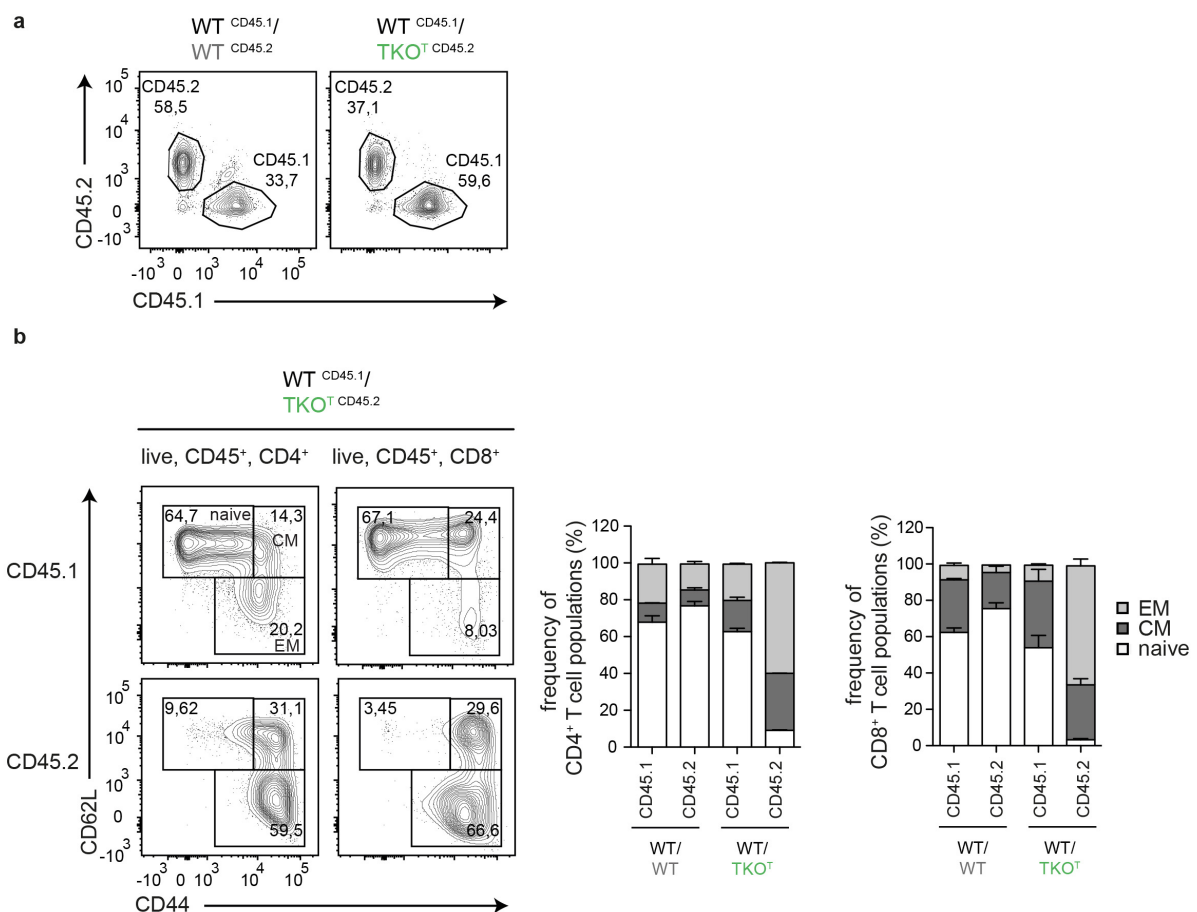


**Figure 37 | Flow cytometry analysis of splenocytes from mixed bone marrow chimeric mice.**

**a)** Flow cytometry analysis of CD45.1 and CD45.2 expression in live cells of  $\text{WT}^{\text{CD45.1}}/\text{WT}^{\text{CD45.2}}$  or  $\text{WT}^{\text{CD45.1}}/\text{TKO}^T \text{CD45.2}$  mice. **b)** Representative contour blots of CD4 and CD8 naive, central-memory- (CM) and effector-memory-like (EM) CD4 and CD8 T cells in live,  $\text{CD45}^+$  and  $\text{CD4}^+$  T cells of  $\text{WT}^{\text{CD45.1}}/\text{TKO}^T \text{CD45.2}$  mice and quantification thereof and  $\text{WT}^{\text{CD45.1}}/\text{WT}^{\text{CD45.2}}$  mixed bone marrow chimeric mice. Data are representatives of two (WT/WT) and three (WT/ $\text{TKO}^T$ ) experiments.

The reconstitution of CD45.1 and CD45.2 cells in the periphery of mixed bone marrow chimeric mice is depicted in **Figure 37 a**. Indeed, mice that received bone marrow from mice lacking Roquin and Regnase-1 developed hyperactivated EM-like CD4 and CD 8 T cells and increased central-memory-like CD4 T cells (**Figure 37 a**).

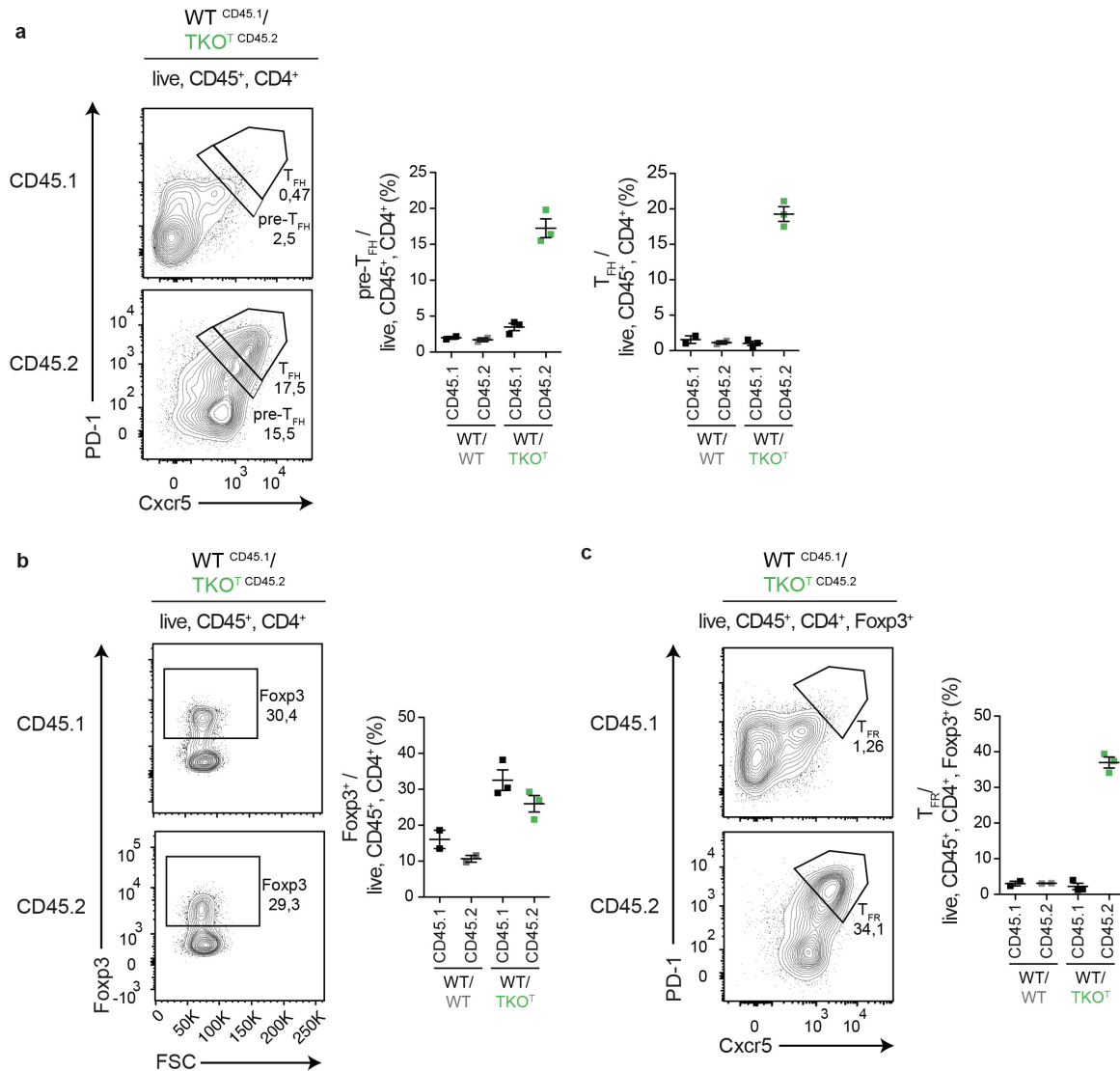


**Figure 38 | Analyzing T<sub>FH</sub>, T<sub>FR</sub> and T<sub>reg</sub> populations in splenocytes from mixed bone marrow chimeric mice.**

**a)** Representative contour blot of pre-T<sub>FH</sub> and T<sub>FH</sub> cells of live, CD45<sup>+</sup> and CD4<sup>+</sup> T cells of WT<sup>CD45.1/</sup> TKO<sup>T</sup> CD45.2 mice and quantification thereof and WT<sup>CD45.1/</sup> WT<sup>CD45.2</sup> mixed bone marrow chimeric mice. **b)** Representative contour blot of Fcpx3<sup>+</sup>, live, CD45<sup>+</sup> and CD4<sup>+</sup> T cells of WT<sup>CD45.1/</sup> TKO<sup>T</sup> CD45.2 mice and quantification thereof and WT<sup>CD45.1/</sup> WT<sup>CD45.2</sup> mixed bone marrow chimeric mice. **c)** Representative contour blot of T<sub>FR</sub> cells of live, CD45<sup>+</sup>, CD4<sup>+</sup> and Fcpx3<sup>+</sup> cells of WT<sup>CD45.1/</sup> TKO<sup>T</sup> CD45.2 mice and quantification thereof and WT<sup>CD45.1/</sup> WT<sup>CD45.2</sup> mixed bone marrow chimeric mice. Data are representatives of two (WT/WT) and three (WT/TKO<sup>T</sup>) experiments.

Additionally, mice receiving bone marrow devoid of Roquin and Regnase-1 showed a strong differentiation towards T<sub>FH</sub> and T<sub>FR</sub> cells (**Figure 38 a, c**). Different from the thymic phenotype,

the  $\text{TKO}^{\text{T}} \text{CD45.2}$  mixed bone marrow chimeric mice only had a mild increase in the peripheral  $\text{T}_{\text{reg}}$  compartment (**Figure 38 b**).

Overall these data suggest that the cellular phenotype in the  $\text{TKO}^{\text{T}}$  mice characterized by strongly activated effector-memory CD4 and CD8 T cells and an elevated germinal center response due to the formation of  $\text{T}_{\text{FH}}$  and  $\text{T}_{\text{FR}}$  cells, is cell-intrinsic and a result of Roquin and Regnase-1 deficiency.

#### 4.2.5 Roquin and Regnase-1 proteins control T cell activation and differentiation

T helper cell subsets are defined by a unique pattern of master transcription factor expression and cytokine secretion and have distinctive functions in host defense (**Figure 1**). Roquin and Regnase-1 were already described to control  $\text{T}_{\text{H}}17$  differentiation by influencing gene expression of  $\text{T}_{\text{H}}17$ -related genes such as  $\text{I}\kappa\text{B}_{\text{NS}}$  or  $\text{I}\kappa\text{B}\zeta$ . Additionally, the highly activated CD4 T cells identified in  $\text{DKO}^{\text{T}}$ ,  $\text{KO}^{\text{T}}$  as well as  $\text{TKO}^{\text{T}}$  mice, prompted us to further investigate, whether these cells have the tendency to differentiate into distinct T helper cell subsets.

By *ex vivo* stimulation of CD4 T cells with PMA (Phorbol-myristate-acetate) and ionomycin in the presence of Brefeldin A, we were able to analyze intracellular cytokine production of CD4 T cells, which then can uncover predispositions for certain differentiation programs (**Figure 39**). All cytokines were significantly elevated in  $\text{TKO}^{\text{T}}$  in comparison to WT cells.  $\text{IFN-}\gamma$  levels were augmented in  $\text{DKO}^{\text{T}}$ ,  $\text{KO}^{\text{T}}$  and  $\text{TKO}^{\text{T}}$  mice, whereas the changes were overall not significant. The signature cytokine of  $\text{T}_{\text{H}}17$  cells IL-17A was significantly increased in all analyzed knockout (**Figure 39 a-d**), whereas IL-4 was augmented only in  $\text{TKO}^{\text{T}}$  mice (**Figure 39 b-d**).  $\text{T}_{\text{reg}}$  cells are characterized by the expression of CD25 and were reported to secrete IL-10. IL-10 production in  $\text{CD25}^+$ ,  $\text{CD4}^+$  T cells was enhanced in  $\text{DKO}^{\text{T}}$  and  $\text{TKO}^{\text{T}}$  mice (**Figure 39 c-d**).

To further validate these findings, we utilized an inducible deletion system by crossing  $\text{Rc3h1/2}^{\text{fl/fl}}$  (iDKO),  $\text{Zc3h12a}^{\text{fl/fl}}$  (iKO) and  $\text{Rc3h1/2}^{\text{fl/fl}}; \text{Zc3h12a}^{\text{fl/fl}}$  (iTKO) mice with  $\text{Cd4-creERT2}$  mice (**Figure 7**). Here, we made use of the  $\text{Cd4-creERT2}$  system, which enables deletion of loxP-flanked sites with a cre-recombinase that is fused to the estrogen receptor 2 (ERT2), which, upon administration of tamoxifen, enters the nucleus and induces deletion of loxP-flanked genes by its cre activity.  $\text{Cd4-creERT2}$  was generated by a knock in of the fusion protein into the CD4 locus, thus these mice can only be bred with heterozygous expression of the transgene. To induce the deletion of loxP-flanked alleles in CD4-expressing cells *in vivo*, mice were treated with tamoxifen by oral gavage (**Figure 40 a**). 3 days after the last treatment

with tamoxifen, naïve CD4 T cells were isolated and stimulated towards T<sub>H</sub>1, T<sub>H</sub>17 or T<sub>reg</sub> with cytokine and antibody mixes (**Table 17**).

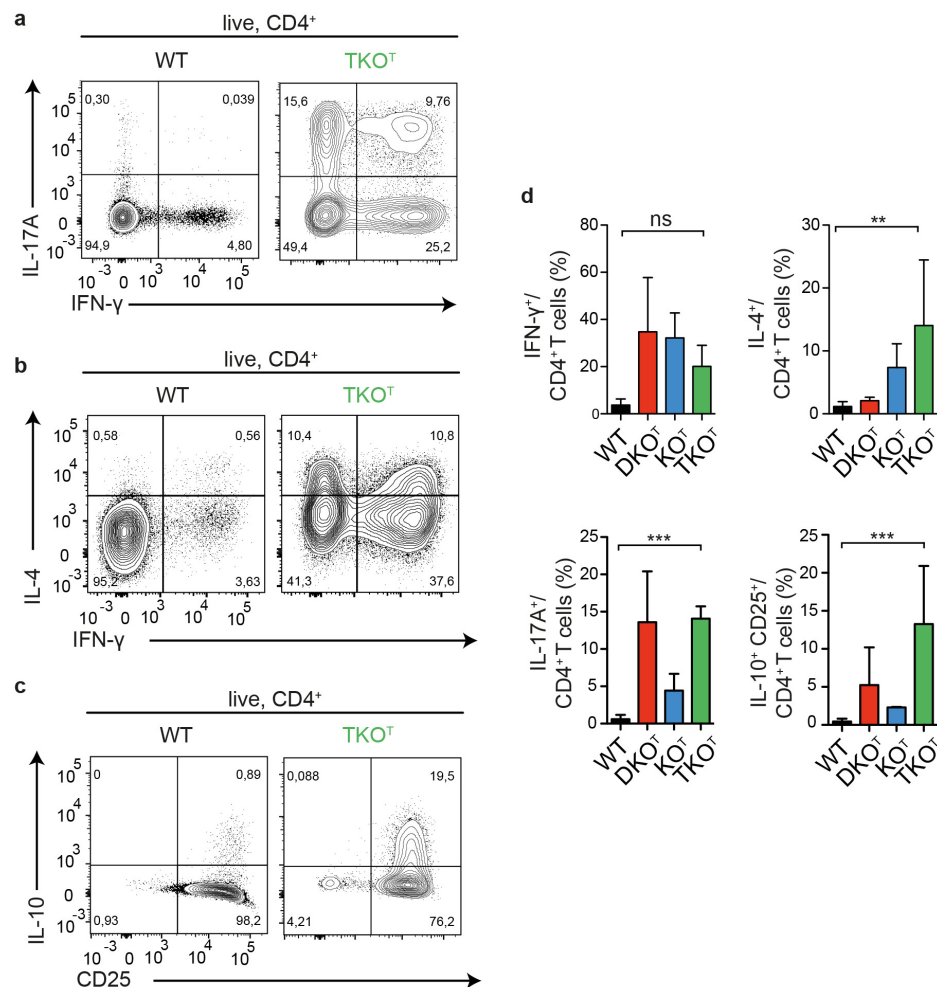


**Figure 39 | Ex vivo cytokine expression levels of CD4 T cells from WT, DKO<sup>+</sup>, KO<sup>+</sup> and TKO<sup>+</sup> mice.**

Total CD4 T cells from WT, DKO<sup>+</sup>, KO<sup>+</sup> and TKO<sup>+</sup> cells were isolated and stimulated with PMA (Phorbol-myristate-acetate) and ionomycin in the presence of Brefeldin A to evaluate intracellular cytokine expression. Flow Cytometry analysis of CD4<sup>+</sup> cells for their expression of IL-17A and IFN-γ (**a**), IL-4 and IFN-γ (**b**) and IL-10 and CD25 (**c**). Frequencies thereof were calculated in **d**). Genotypes are indicated in the figure and data are representative of at least 2 mice per genotype. Statistical significances were calculated by one-way analysis of variance (ANOVA) with Bonferroni post test.

The expression of the T helper cell specific cytokines was validated by flow cytometry analyses for IFN-γ on T<sub>H</sub>1 cells and IL-17A for cells differentiated towards T<sub>H</sub>17 (**Figure 40**). T<sub>reg</sub> cells were validated according to CD25 and Foxp3 expression. Naïve CD4 T cells of iTKO mice showed a higher capacity to differentiate into the T<sub>H</sub>17 lineage (**Figure 40 c**). Elevated production of the T<sub>H</sub>17 cytokine IL-17A was also partially visible in iDKO and iKO mice.



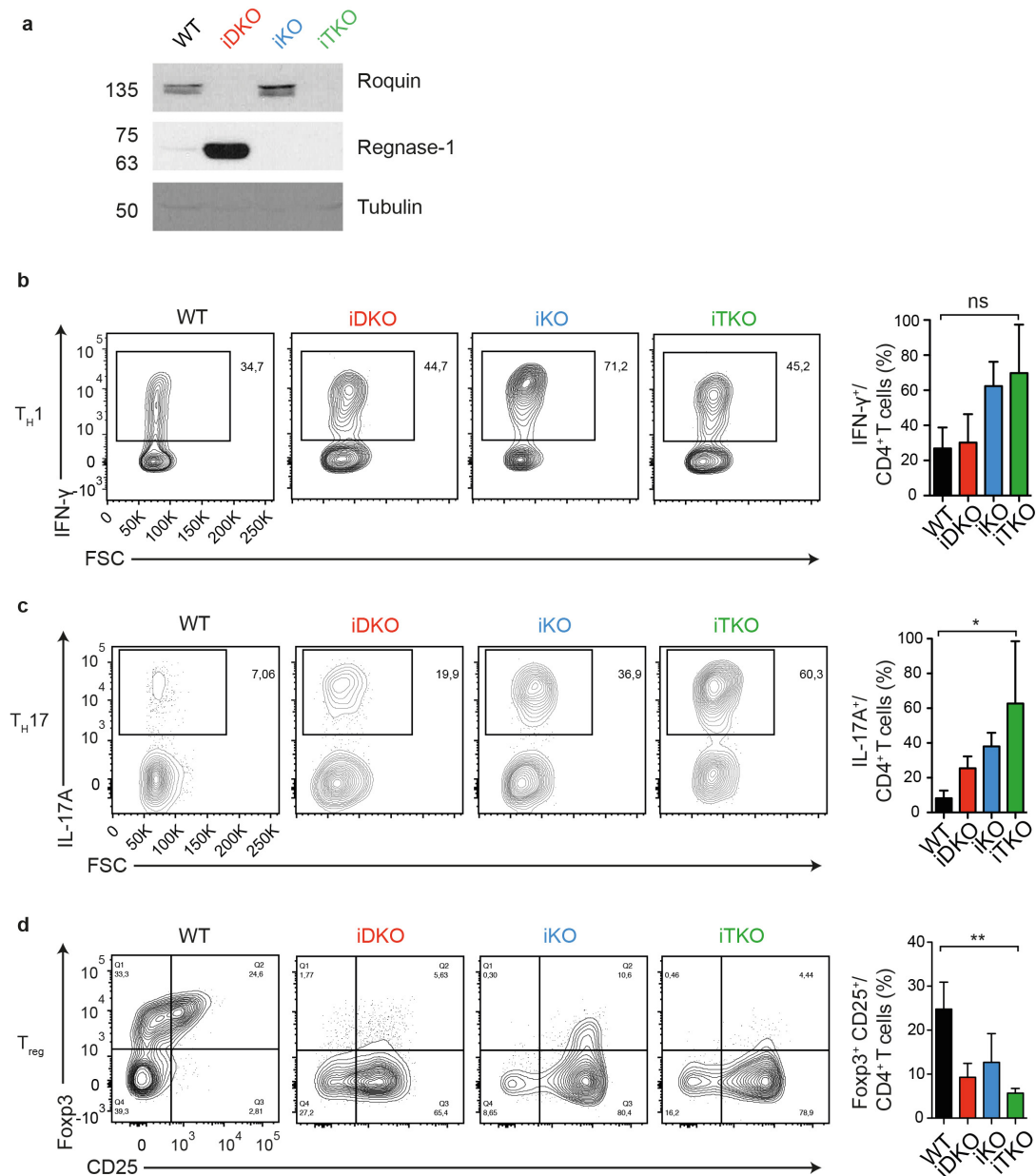


**Figure 40 | Flow cytometry analysis of naïve CD4 T cells from WT, iDKO, iKO and iTKO mice differentiated into  $T_H1$ ,  $T_H17$  and  $T_{reg}$  cells.**

WT, iDKO, iKO and iTKO mice were treated with tamoxifen orally and naïve CD4 T cells were isolated from these mice and stimulated under  $T_H1$ ,  $T_H17$  and  $T_{reg}$  conditions. **a**) Immunoblot analysis of Roquin and Regnase-1 expression in WT, iDKO, iKO and iTKO CD4 T cells. Flow cytometry analysis of IFN- $\gamma$  on  $T_H1$  differentiated cells (**b**), IL-17A for cells differentiated towards  $T_H17$  (**c**) and Foxp3 and CD25 on cells differentiated towards  $T_{reg}$  cells (**d**). The left panel shows a representative contour plot and the right a quantification of all genotypes. The molecular weight in kDa is depicted at the left of the immunoblot. Genotypes are indicated in the figure and data are representative of 3 individual experiments. Statistical significances were calculated by one-way analysis of variance (ANOVA) with Bonferroni post test.

Naïve CD4 T cells from iTKO mice were impaired in iT<sub>reg</sub> differentiation and the differentiation capacity decreased with loss of Regnase-1 (iKO) and Roquin (iDKO) expression. Interestingly, all knockout genotypes had higher expression of CD25 (**Figure 40 d**). IFN- $\gamma$  levels were

different in all three inducible knockout mice, but the alteration was not statistically significant (**Figure 40 b**). These data support the observations in **Figure 39**, suggesting that Roquin and Regnase-1 proteins control T helper cell differentiation of naïve T cells. Especially the differentiation towards the T<sub>H</sub>17 lineage was regulated by both Roquin and Regnase-1, suggesting that this differentiation program was under the influence of shared target genes. Thus, the reciprocal differentiation programs of T<sub>H</sub>17 and T<sub>reg</sub> were under control of Roquin and Regnase-1 and T cells lacking Roquin and Regnase-1 were biased to differentiate towards T<sub>H</sub>17.



### 4.3 Analyzing the functional cooperativity of Roquin and Regnase-1 proteins in T cell differentiation

To analyze whether the different phenotypes in individual and combined knockouts correlate with augmented RNA expression levels we investigated the mRNA targets of Roquin and Regnase-1.

#### 4.3.1 Roquin and Regnase-1 share a mRNA target set in immune cells

The role of the post-transcriptional gene regulators Roquin and Regnase-1 has been extensively studied in the past years and various mRNA targets have been identified so far in different cell types. **Table 19** gives an overview of the identified Roquin and Regnase-1 mRNA targets in studies analyzing their function in immune cells.

**Table 19 | Previously published Roquin-1/2, *sanroque* and Regnase-1 target genes in cells of the immune system.**

Data of target genes identified in immune cells were obtained from the indicated publications. Genes that were described as potential targets of Roquin and/or Regnase-1 proteins are depicted. Genes potentially targeted by both Roquin and Regnase-1 are shown in bold letters.

Gene name	<i>Rc3h1/2</i>	<i>Rc3h1<sup>san/san</sup></i>	<i>Zc3h12a</i>
<i>A20</i>	(Murakawa et al., 2015)	-	-
<b><i>Acta2</i></b>	-	(Cui et al., 2017)	(Cui et al., 2017)
<i>Bmpr1a</i>	(Leppek et al., 2013)	-	-
<i>Calcr</i>	-	-	(Matsushita et al., 2009)
<b><i>Ccr4</i></b>	(Cui et al., 2017)	-	(Cui et al., 2017)
<b><i>Ccr5</i></b>	(Cui et al., 2017)	-	(Cui et al., 2017)
<b><i>Ccr6</i></b>	(Cui et al., 2017)	-	(Cui et al., 2017)
<i>Ccl20</i>	-	-	(Nakatsuka et al., 2018)
<i>Ccl28</i>	-	-	(Nakatsuka et al., 2018)
<i>Cd40lg</i>	-	-	(Uehata et al., 2013)
<i>Cd69</i>	-	-	(Uehata et al., 2013)
<i>Cebpd</i>	-	-	(Lipert et al., 2017)
<b><i>Csf3</i></b>	(Braun et al., 2018)	-	(Nakatsuka et al., 2018)
<i>Col22a1</i>	-	-	(Mino et al., 2015)
<b><i>Ctla4</i></b>	(Jeltsch et al., 2014)	-	(Uehata et al., 2013) (Jeltsch et al., 2014)
<i>Cxcl1</i>	-	-	(Mino et al., 2015)
<i>Cxcl2</i>	-	-	(Mino et al., 2015)
<i>Cxcl3</i>	-	-	(Mino et al., 2015)
<i>Cxcl5</i>	-	-	(Nakatsuka et al., 2018)
<b><i>Cxcl10</i></b>	-	(Cui et al., 2017)	(Cui et al., 2017)
<i>Cxcl17</i>	-	-	(Nakatsuka et al., 2018)
<i>Cxcr3</i>	-	-	(Cui et al., 2017)
<b><i>Furin</i></b>	-	(Cui et al., 2017)	(Cui et al., 2017)
<i>Hmgxb3</i>	(Leppek et al., 2013) (Tan et al., 2014)	-	-
<b><i>Icos</i></b>	(Glasmacher et al., 2010) (Vogel et al., 2013) (Pratama et al., 2013) (Jeltsch et al., 2014) (Schlundt et al., 2014) (Rehage et al., 2018)	(Vinuesa et al., 2005) (Yu et al., 2007) (Linterman et al., 2009) (Cui et al., 2017)	(Uehata et al., 2013) (Jeltsch et al., 2014) (Cui et al., 2017)

<i>Id1</i>	-	-	(Mino et al., 2015)
<i>Ier3</i>	(Leppek et al., 2013)	-	(Mino et al., 2015)
<i>Ifng</i>	(Lee et al., 2012; Pratama et al., 2013)	-	(Matsushita et al., 2009) (Cui et al., 2017)
<i>Il2</i>	-	(Cui et al., 2017)	(Cui et al., 2017)
<i>Il12p40</i>	-	-	(Matsushita et al., 2009)
<i>Il2ra</i>	-	-	(Uehata et al., 2013)
<i>Il6</i>	(Tan et al., 2014) (Jeltsch et al., 2014)	(Mino et al., 2015) (Cui et al., 2017)	(Matsushita et al., 2009) (Iwasaki et al., 2011) (Uehata et al., 2013) (Jeltsch et al., 2014) (Mino et al., 2015) (Cui et al., 2017)
<i>Irf4</i>	(Vogel et al., 2013) (Jeltsch et al., 2014)	-	(Jeltsch et al., 2014)
<i>Itch</i>	(Essig et al., 2018)	-	-
<i>Mafk</i>	(Mino et al., 2015)	-	(Mino et al., 2015)
<i>Metap1</i>		-	(Mino et al., 2015)
<i>Nfkbia</i>	(Murakawa et al., 2015)	-	-
<i>Nfkbid</i>	(Leppek et al., 2013) (Jeltsch et al., 2014) (Murakawa et al., 2015) (Essig et al., 2018)	-	(Mino et al., 2015)
<i>Nfkbiz</i>	(Leppek et al., 2013) (Jeltsch et al., 2014)	-	(Mino et al., 2015) (Behrens et al., 2018)
<i>Ptgs2</i>	-	-	(Mino et al., 2015)
<i>Pten</i>	(Essig et al., 2018)	-	-
<i>Rc3h1</i>	(Leppek et al., 2013) (Cui et al., 2017)	-	(Cui et al., 2017)
<i>Rc3h2</i>	(Leppek et al., 2013)	-	-
<i>Rel</i>	(Jeltsch et al., 2014)	-	(Uehata et al., 2013) (Jeltsch et al., 2014)
<i>Shcbp1l</i>	-	-	(Mino et al., 2015)
<i>Sprr2f</i>	-	-	(Matsushita et al., 2009)
<i>Sprr2h</i>	-	-	(Matsushita et al., 2009)
<i>Sprr2j</i>	-	-	(Matsushita et al., 2009)
<i>Sprr2k</i>	-	-	(Matsushita et al., 2009)
<i>Tgfb</i>	-	(Cui et al., 2017)	(Cui et al., 2017)
<i>Tm2d3</i>	(Braun et al., 2018)	-	(Mino et al., 2015)
<i>Tnf</i>	(Leppek et al., 2013) (Pratama et al., 2013) (Jeltsch et al., 2014) (Schludt et al., 2014) (Braun et al., 2018)	(Mino et al., 2015) (Cui et al., 2017)	(Jeltsch et al., 2014) (Mino et al., 2015) (Cui et al., 2017)
<i>Tnfrsf1b</i>	-	-	(Uehata et al., 2013)
<b>Ox40</b> <b>(Tnfrsf4)</b>	(Vogel et al., 2013) (Schludt et al., 2014) (Janowski et al., 2016)	-	(Uehata et al., 2013)
<i>Ucp3</i>	(Braun et al., 2018)	-	-
<b>Zc3h12a</b>	(Braun et al., 2018) (Cui et al., 2017) (Jeltsch et al., 2014) (Mino et al., 2015)	-	(Iwasaki et al., 2011) (Mino et al., 2015) (Cui et al., 2017)

The classified mRNA targets of the Roquin paralogs are displayed together, because both proteins have redundant functions in T cells (Vogel et al., 2013). *Rc3h1*<sup>san/san</sup> (*sanroque*) targets are depicted in a separate column, since the function of the M199R mutation in Roquin-1 has not been fully elucidated yet.

One must mention here, that the cited publications used distinctive cell types (mouse T cells, human Jurkat T cells, HeLa cells, HEK cells and bone-marrow-derived macrophages) and

consequently analyzed different species (human and mouse). Moreover, various techniques have been utilized for discovering the mRNA targets, e.g. mRNA expression analysis in wild-type vs. knockout cells, luciferase and reporter assays, global analyses (mRNA-sequencing), CDE predictions, RNA-immunoprecipitations and global binding profiles (CLIP experiments). Not all genes can be considered as direct targets, but nevertheless can provide insights about overlapping functions of Roquin and Regnase-1. Some genes have been described to be targeted by Roquin and Regnase-1 (shown in bold in **Table 19**). Amongst them are the co-stimulatory receptors Icos (*Icos*), Ctla-4 (*Ctla4*) and Ox40 (*Tnfrsf4*) as well as proinflammatory cytokines like IL-6 (*Il6*), TNF- $\alpha$  (*Tnfa*) and IFN- $\gamma$  (*Ifng*). Several chemokine receptors have been proposed to be targeted by Roquin and Regnase-1 as well as transcription factors like cRel (*Rel*) and Irf4 (*Irf4*) and modulators of transcription factors as I $\kappa$ B<sub>NS</sub> (*Nfkbid*) and I $\kappa$ B $\zeta$  (*Nfkbiz*). Interestingly, Regnase-1 (*Zc3h12a*) itself has been identified as Roquin and Regnase-1 target gene.

#### 4.3.2 Roquin and Regnase-1 control overlapping immune-associated target mRNAs

To validate already described target genes of Roquin and Regnase-1 that were described in the literature, we utilized inducible knockout mice as described in the previous chapter (4.2.5). CD4 T cells of WT, iKO and iDKO mice were isolated, and knockouts were induced by administration with 4'OH-tamoxifen or cells were left untreated as wild-type controls.

Analyzing protein expression of Roquin and Regnase-1 target genes revealed that the induced knockout of Roquin and Regnase-1 led to an increased expression of cRel, I $\kappa$ B $\zeta$ , Ctla-4 and Icos. Whereas, I $\kappa$ B<sub>NS</sub>, Irf4 and Ox40 are mainly affected upon ablation of the Roquin paralogs. A20, which was described as a Roquin-1 target gene (Murakawa et al., 2015), showed almost no change on protein expression upon inducible Roquin or Regnase-1 knockout (**Figure 41 a-b**). A comparable type of expression was detectable on RNA level. Here, *Zc3h12a*, *Tnfrsf4*, *Irf4* and *Ctla4* were mainly upregulated in the absence of Roquin-1 and Roquin-2. In turn, a knockout of Regnase-1 affected *Icos*, *Nfkbiz* and slightly *Ctla4* expression (**Figure 41 c**). Interestingly, Regnase-1 showed a robust upregulation on protein and mRNA level upon knockout of Roquin-1 and Roquin-2, suggesting it to be a strong Roquin target gene. The expression of Ox40 being exclusively altered upon inducible Roquin knockout was in line with the data shown in chapter 4.1.

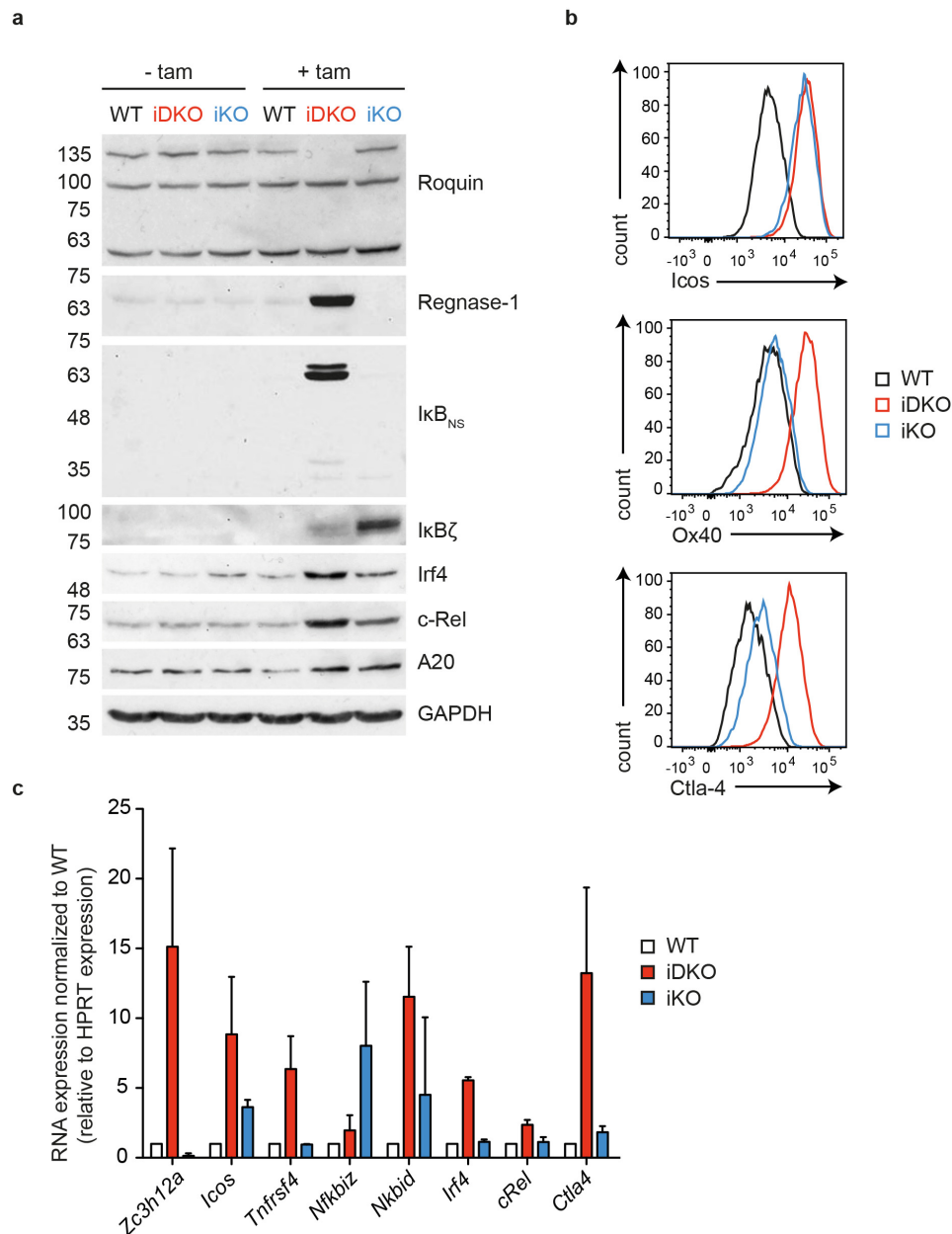


**Figure 41 | Protein and RNA expression levels of known Roquin and Regnase-1 targets in WT, iDKO and iKO CD4 T cells.**

CD4 T cells were isolated from *Rc3h12<sup>fl/fl</sup>*; *Cd4-creERT2* (iDKO), *Zc3h12a<sup>fl/fl</sup>*; *Cd4-creERT2* (iKO) and *Cd4-creERT2* (WT) mice and treated with 4'OH-tamoxifen (+tam) for 24h *in vitro* to induce deletion of loxP-flanked genes or left untreated (-tam). After 2d of IL-2 culture under T<sub>H</sub>1 conditions, cells were analyzed for target protein expression by immunoblotting (a) or flow cytometry (b) and RNA expression was measured by RT-qPCR (c). The molecular weight in kDa is depicted at the left of the immunoblot. Data are representative of 3 (a-c) individual experiments.

Overall these data showed that prototypic target genes were influenced by Roquin and Regnase-1, whereas all targets were increased upon Roquin knockout and some only reacted weakly or not at all on Regnase-1 deficiency. Especially, *Nfkbid* and *Nfkbiz* expression was selectively controlled by Roquin and Regnase-1 proteins, respectively.

### 4.3.3 Global mRNA-sequencing analysis in Roquin and Regnase-1-deficient CD4 T cells

Observing exclusive and cooperative gene regulation on selected targets made us question how Roquin and Regnase-1 regulate mRNA expression on a global scale and if different modes of gene regulation exist.

#### 4.3.3.1 Design of the mRNA-sequencing experiment

In order to define the types of regulation, it was crucial to compare CD4 T cells of the single knockout of Regnase-1 (iKO) and the double knockout of Roquin-1 and Roquin-2 (iDKO) to cells deficient for all three proteins. For this reason, we generated *Rc3h1/2<sup>fl/fl</sup>*; *Zc3h12a<sup>fl/fl</sup>*; *Cd4-creERT2* mice that can be *in vitro* deleted for their expression of Roquin-1, Roquin-2 and Regnase-1 by administration of 4'OH-tamoxifen. For validation of the inducible triple-knockout (iTKO), CD4 T cells from these mice were isolated and activated under T<sub>H</sub>1 conditions for 40h, cultured for 2d with IL-2 and then analyzed for the knockouts on protein level by flow cytometry and immunoblotting (**Figure 9**). As a comparison iDKO and iKO T cells were included in the analyses (**Figure 42**).

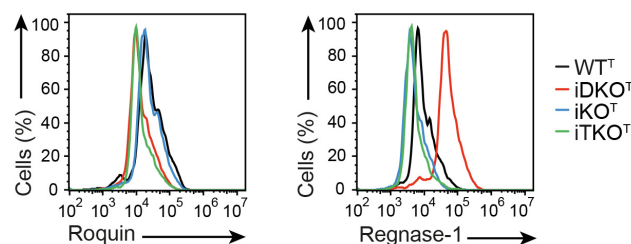


**Figure 42 | Validation of the inducible triple knockout (iTKO) of Roquin and Regnase-1.**

CD4 cells were isolated from *Cd4-creERT2* (WT), *Rc3h1/2<sup>fl/fl</sup>*; *Cd4-creERT2* (iDKO), *Zc3h12a<sup>fl/fl</sup>*; *Cd4-creERT2* (iKO) and *Rc3h1/2<sup>fl/fl</sup>*; *Zc3h12a<sup>fl/fl</sup>*; *Cd4-creERT2* (iTKO) mice and deletion of loxP-flanked alleles was induced *in vitro* by 4'OH-tamoxifen treatment. After T cell stimulation under T<sub>H</sub>1 conditions and IL-2 culture for 2d, knockouts were confirmed by flow cytometry with monoclonal antibodies specific for Roquin and Regnase-1. Data are representatives of three independent experiments.

Flow Cytometry analysis with Roquin and Regnase-1-specific monoclonal antibodies confirmed a successful knockout in *Rc3h1/2<sup>fl/fl</sup>*; *Zc3h12a<sup>fl/fl</sup>*; *Cd4-creERT2* (iTKO) CD4 T cells (**Figure 42**). iDKO and iTKO cells were devoid of Roquin expression and iKO cells expressed Roquin at comparable levels to WT cells. Regnase-1 expression was completely diminished in iKO and iTKO cells, whereas iDKO cells showed an increase in 1.5 log levels of Regnase-1 protein levels, suggesting that Regnase-1 itself is a strong target for Roquin-mediated regulation.

After evaluation of successful knockouts in T cells, we performed mRNA-sequencing to compare the gene expression patterns of WT, iDKO, iKO and iTKO CD4 T cells. Therefore, four replicates of WT, iDKO, iKO and iTKO T<sub>H</sub>1 cells were prepared by inducing deletion of loxP-flanked genes *in vitro* with 4'OH-tamoxifen and stimulation with  $\alpha$ -CD3/CD28 under T<sub>H</sub>1 conditions. After IL-2 culture, cells were restimulated with  $\alpha$ -CD3/CD28 for 1, 2 and 4h or left unstimulated (0h) (**Figure 43**).

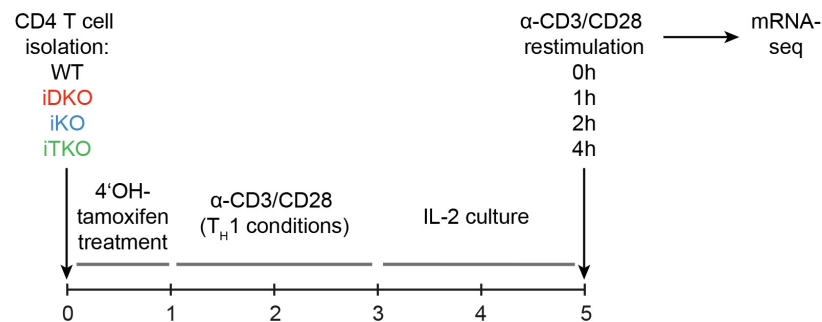


**Figure 43 | Schematic overview of T<sub>H</sub>1 cell culture for mRNA-sequencing experiment.**

CD4 cells were isolated from *Cd4-creERT2* (WT), *Rc3h1/2<sup>fl/fl</sup>*; *Cd4-creERT2* (iDKO), *Zc3h12a<sup>fl/fl</sup>*; *Cd4-creERT2* (iKO) and *Rc3h1/2<sup>fl/fl</sup>*; *Zc3h12a<sup>fl/fl</sup>*; *Cd4-creERT2* (iTKO) mice and deletion of loxP-flanked alleles was induced *in vitro* by 4'OH-tamoxifen treatment. After T cell stimulation with  $\alpha$ -CD3/CD28 under T<sub>H</sub>1 conditions and IL-2 culture for 2d, cells were restimulated with  $\alpha$ -CD3/CD28 for 1, 2 and 4h or left unstimulated (0h). Cells were resuspended in Trizol Reagent and submitted to Dr. Stefan Krebs for library preparation and mRNA-sequencing.

Most of the known Roquin and Regnase-1 target genes are associated with T cell differentiation and activation. Therefore, we included restimulated T cells in the analyses to identify genes involved in T cell activation. After restimulation, RNA of cells was preserved by Trizol reagent and submitted to Dr. Stefan Krebs from the group of Dr. Helmut Blum at the Laboratory of functional genome analysis (LAFUGA, LMU München), who prepared the library and performed deep sequencing. After sequencing, the bioinformatic analysis was conducted by Dr. Gergely Csaba from the group of Prof. Dr. Ralf Zimmer at the Institute for Informatics (LMU München).

#### 4.3.3.2 Global mRNA-sequencing analysis of CD4 T cells deficient for Roquin and Regnase-1

Global mRNA-sequencing in Roquin-1/2-deficient (iDKO), Regnase-1-deficient (iKO) and cells devoid of Roquin-1/2 as well as Regnase-1 (iTKO) was performed to identify gene expression patterns and consequently learn about a potential cooperative, molecular mechanism of Roquin- and Regnase-1-mediated gene regulation. To validate differentially expressed genes in the three different knockout situations, genes in unstimulated wild-type cells (WT, 0h) were

taken as a reference to calculate foldchange (FC) gene expression of iDKO, iKO and iTKO over the analyzed timepoints of T cell stimulation (0h, 1h, 2h and 4h).

First, we sought to determine the overall global gene expression pattern in the different knockout situation. **Figure 44** shows heatmaps of absolute numbers of genes significantly upregulated (**a**) or downregulated (**b**) in the knockouts at indicated timepoints in comparison to WT, 0h. Here, only significantly expressed genes ( $p\text{-value} \leq 0.05$ ) and genes with a minimum foldchange-expression of  $\log_2(\text{FC}) \geq 1$  (upregulated) and  $\log_2(\text{FC}) \leq 1$  (downregulated) were considered.

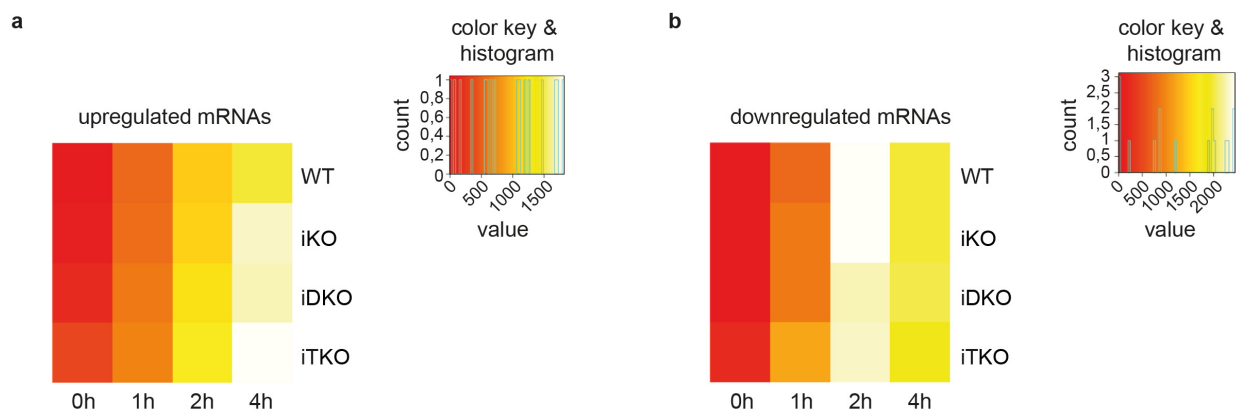


**Figure 44 | Quantitative analysis of the overall gene expression in unstimulated and restimulated WT, iDKO, iKO and iTKO CD4 T cells.**

Heatmap showing absolute numbers of significantly upregulated (**a**) or downregulated (**b**) genes in WT, inducible Roquin-1/2 double knockout cells (iDKO), inducible Regnase-1 knockout cells (iKO) and inducible Roquin-1/2 and Regnase-1 triple knockout cells (iTKO) without stimulation (0h) or restimulated for 1, 2 or 4h with  $\alpha$ -CD3/CD28. Here, significantly expressed genes with a  $p\text{-value}$  of  $\leq 0.05$  and a  $\log_2(\text{FC}) \geq 1$  (upregulated) and  $\log_2(\text{FC}) \leq 1$  (downregulated) are depicted. The color key shows the numbers of expressed genes and corresponding color code. Count represents how often these numbers of genes occurred over all analyzed samples.

Comparing the quantity of significantly upregulated genes in the different knockout situations revealed that equally more genes in iKO and iDKO T cells were expressed in comparison to WT during all timepoints of T cell stimulation, whereas knockout of Roquin and Regnase-1 (iTKO) in CD4 T cells resulted in an even stronger increase in the overall gene expression which reached the highest number of genes with 4h of stimulation (approximately 2000 genes) (**Figure 44 a**).

The amount of significantly downregulated genes strongly increased during T cell stimulation and reached a maximum at 2h (approximately 2000-2200 genes) of stimulation and declined with 4h (**Figure 44 b**). Here, only a weak difference between the knockouts was detectable and overall the number of downregulated genes in the three knockout situations was comparable to wild-type during all investigated timepoints.

This first expression analysis revealed that there were quantitative differences of upregulated genes expressed in iKO, iDKO and iTKO CD4 T cells, which were most prominent in iTKO at 0, 1, 2 and 4h of stimulation. Overall within downregulated genes, the number of genes was comparable between the knockouts and wild-type. Here, solely T cell stimulation changed the overall abundance of genes independent of the knockout.

To further characterize concordant regulation of the genes in the knockout cells, Dr. Gergely Csaba performed cluster analysis to identify dominant patterns of gene regulation. The aim was to identify genes that significantly changed in the knockout T cells in comparison to WT(0h) and characterize them according to their molecular function and biological process with the help of gene ontology (GO).

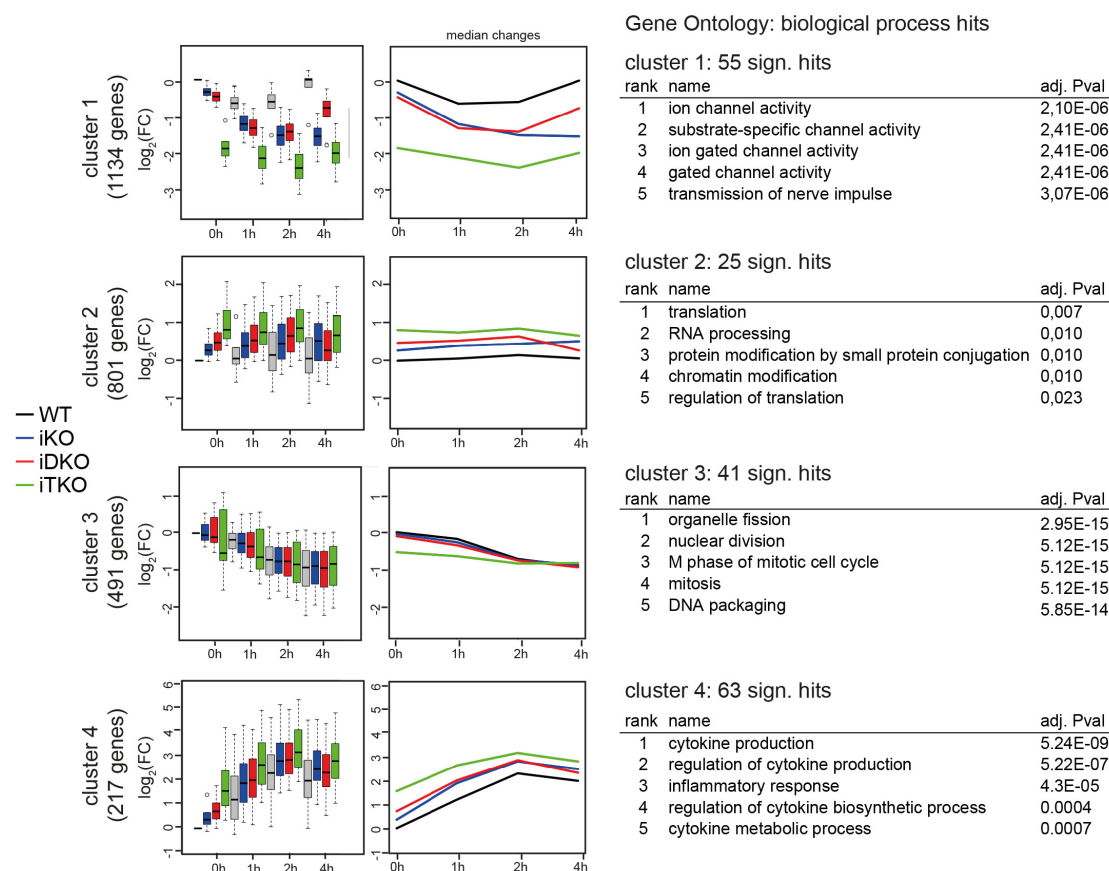


**Figure 45 | Cluster analysis of genes identified by mRNA-sequencing in WT, iDKO, iKO and iTKO CD4 T cells.**

Significantly expressed genes in WT, iDKO, iKO and iTKO during stimulation and without stimulant were considered to define 4 major clusters of gene regulation: Cluster 1 consisted of 1134 genes that showed 55 significant gene ontology (GO) hits in ion channel activity. 801 genes were summarized as cluster 2, consisting of genes involved in translation and chromatin modification with 25 significant GO hits. Cluster 3 was defined by 491 genes involved in mitosis and cell division (41 significant GO hits). Immune-response related genes were comprised by cluster 4, including 217 significantly expressed genes within 63 significant GO hits. In the left panel box plots of  $\log_2(\text{FC})$  expression of all genes within the respective cluster normalized to WT(0h) are shown and the right plot represents the median change thereof. On the right, the top five biological process gene ontology (GO) hits and respective p-values are depicted.



Here, 2913 differentially expressed genes were described by four clusters: Cluster 1 included 1134 genes, cluster 2 801 genes, cluster 3 491 genes and cluster 4 consisted of 217 genes. Cluster 1 and 3 represented downregulated genes, whereas cluster 2 and 4 comprised upregulated genes in all genotypes. In the following, the single clusters will be discussed in detail:

#### Cluster 1 and 3:

Overall genes identified by cluster 1 and cluster 3 were downregulated in the three different knockout situations in comparison to WT(0h) genes during T cell stimulation. In cluster 1 this pattern was maintained during T cell stimulation and the knockout of Roquin-1/2 (iDKO) as well as Regnase-1 deficiency (iKO) lead to a prominent decrease in gene expression in comparison to WT, whereas the knockout of Roquin-1/2 and Regnase-1 (iTKO) consequently resulted in a downregulation of 2-3 log<sub>2</sub> fold-changes (FC). Stimulation for 4h altered gene expression in all samples in comparison to shorter stimulation, which suits to the global pattern of negatively regulated genes (**Figure 44 b**). GO analysis revealed genes in this cluster to be associated with ion channel signaling.

Even though differentially expressed genes in cluster 3 were downregulated, the pattern was distinct to cluster 1: the expression just slightly declined during stimulation and solely a combined deficiency of Roquin and Regnase-1 affected total gene expression without stimulation or with stimulation for 1h. Genes identified in this cluster were associated with DNA replication and cell division.

Since a negative effect on gene expression has not been reported for Roquin and Regnase-1 yet, we were wondering if these downregulated genes might appear due to an elevated abundance of genes encoding for transcriptional repressors or epigenetic modulators in the inducible knockout situations. Therefore, we screened bioinformatically for transcription factors significantly changed in iDKO, iKO and iTKO vs. WT(0h) and again performed cluster formation to find patterns of upregulated transcription factors that could explain the expression pattern of cluster 1 or cluster 3. The transcription factor cluster analyses resulted in overall 9 clusters with unique gene expression patterns (data not shown).

We were not able to identify transcriptional repressors or epigenetic modifiers that could explain the regulation of ion channel associated genes in cluster 1. Considering readcounts of genes in cluster 1, we realized that the amplified readcounts in the mRNA-sequencing analysis was overall quite low for genes in cluster 1. Suggesting that these genes might only be weakly expressed and therefore sequencing depths would have to be increased to make a reliable statement, here.

One transcription factor cluster, which positively correlated with cluster 3 is shown in **Figure 46 a**. This cluster contained 9 genes that expressed transcriptional modulators, amongst them the histone deacetylase 2 (Hdac2). Histone deacetylases on the one hand function as

epigenetic regulators by catalyzing removal of acetyl functional groups from lysine residues of histone and non-histone proteins and thereby impact on the chromatin status of DNA in cells (Seto and Yoshida, 2014). On the other hand, Hdac2 and its family member Hdac1 have been characterized as transcription factors by being recruited to DNA as corepressors (Yang et al., 1996). Moreover, a knockout of Hdac2 and Hdac1 in mouse embryonic fibroblasts, causes an elevated expression of genes associated with cell cycle and reduced proliferation (Yamaguchi et al., 2010). Analyzing the  $\log_2(\text{FC})$  expression of *Hdac2* in the different knockout situations in comparison to WT(0h) in the mRNA-seq data showed a slight induction upon Roquin and Regnase-1 knockout (iTKO) in comparison to WT(0h) and a weak increase in gene expression upon TCR stimulation (**Figure 46 b**).

The expression pattern of *Hdac2* identified in the mRNA-seq experiment was validated by RT-qPCR in unstimulated WT, iDKO, iKO and iTKO CD4 T cells (**Figure 46 b**). Analyzing cell cycle associated genes from Cluster 3 of the mRNA-seq data (**Figure 45**) like *Cdk1*, *Ccna2* and *Cdca8* (encoding for cyclin-dependent kinase 1, Cyclin A2 and cell division cycle associated 8) revealed a gene regulation pattern which is inversely correlating to the differential gene expression of *Hdac2* in the knockout situations vs. WT(0h) (**Figure 46 c**). Interestingly, these cell cycle-associated genes have already been described to be affected by an inhibition of HDACs in breast cancer cell lines (Borbely et al., 2015). Immunoblot analysis of Hdac2 and Cyclin A2 protein expression in WT, iDKO, iKO and iTKO CD4 T cells mirrored the mRNA expression: T cells deficient for Roquin and Regnase-1 showed induced Hdac2 expression, whereas the protein abundance of its potential target Cyclin A2 was decreased in iTKO cells (**Figure 46 d**). Consequently, an upregulation of *Hdac2* expression upon knockout of Roquin-1/2 and Regnase-1 could explain the inverse correlating gene expression pattern of downregulated genes such as *Ccna2* in cluster 3.

Overall, these data support the idea that epigenetic remodelers or repressors, which could be directly or indirectly targeted by Roquin and Regnase-1, influence the negative differential gene expression in cluster 1 and 3.

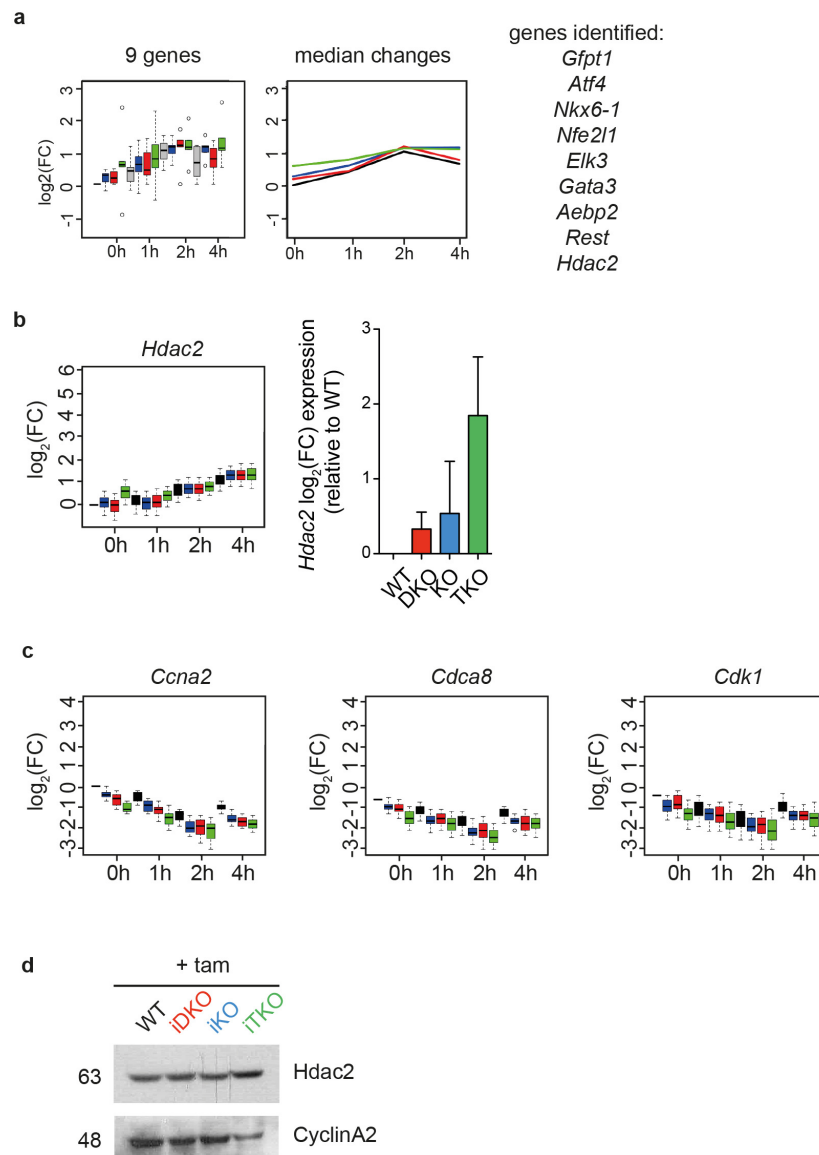


**Figure 46 | Analyzing gene expression of *Hdac2* and potential target genes thereof in cluster 3.**

Cluster analysis of differentially expressed genes encoding for transcription factors resulted in nine different clusters. **a)** One transcription factor cluster consisting of nine genes showed a gene expression pattern that inversely correlated to the gene expression pattern in the previously defined cluster 3 (Figure 45). **b)** mRNA-sequencing analysis of the differential gene expression of *Hdac2* in iDKO, iKO and iTKO cells in comparison to WT(0h) unstimulated or restimulated for 1, 2 and 4h (left panel) and qPCR validation of *Hdac2* expression in WT, iDKO, iKO and iTKO CD4 T cells *in vitro* deleted with 4'OH-tamoxifen and cultured under T<sub>H</sub>1 conditions for 2d (right panel). **c)** Differential gene expression plots of *Ccna2*, *Cdca8* and *Cdk1* as in b. **d)** Immunoblot analysis of *Hdac2* and *CyclinA2* in WT, iDKO, iKO and iTKO CD4 T cells *in vitro* deleted with 4'OH-tamoxifen and cultured under T<sub>H</sub>1 conditions for 2d.

### Cluster 2:

Cluster 2 was comprised of genes that were upregulated upon Roquin and Regnase-1-deficiency. The gene expression of T cells from iKO and iDKO were gradually increased with a median  $\log_2(FC)$  of 1, whereas knockout of all three genes (iTKO) again caused the strongest change in gene expression. The mild changes in gene expression during stimulation implied

that the majority of genes was not induced upon T cell stimulation and potentially not involved in T cell differentiation or rather stably expressed during T cell activation. This was reflected by the top five GO biological process hits, suggesting these genes to rather function in common processes like translation and control of gene expression.

**Table 20 | Differential expressed genes identified in cluster 2.**

Top 20 list of differentially expressed genes from cluster 2 in iTKO, iDKO and iKO vs. WT without stimulation (0h) and stimulated (1,2,4h) rated according to the highest  $\log_2(\text{FC})$  in iTKO at 0h. Red color indicates high  $\log_2(\text{FC})$  up to 2.8 and white color basal gene expression of 0, whereas blue represent negative  $\log_2(\text{FC})$  values down to -1.44.

Gene	0h				1h				2h				4h			
	WT	KO	DKO	TKO	WT	KO	DKO	TKO	WT	KO	DKO	TKO	WT	KO	DKO	TKO
Klk1b27	0,00	0,00	0,78	3,07	0,00	0,00	2,10	2,93	0,00	0,00	1,37	1,79	0,00	0,00	0,00	0,26
Pkdcc	0,00	0,00	0,00	2,76	0,00	0,00	0,00	0,00	0,00	0,00	0,00	0,00	0,00	0,00	0,00	0,00
Hap1	0,00	0,05	1,15	2,73	0,00	0,00	0,33	1,55	-0,20	0,00	0,93	1,06	0,00	-0,60	0,00	0,00
Rims3	0,00	1,22	1,14	2,71	-0,11	1,51	0,99	2,36	-0,49	0,76	0,40	2,04	-0,97	0,83	-0,31	1,39
1100001G20Rik	0,00	0,00	0,00	2,61	0,00	0,00	0,00	2,47	0,00	0,00	0,00	2,52	0,00	0,00	0,00	2,60
Nme4	0,00	0,39	0,84	2,60	0,00	1,11	1,44	2,57	-0,08	0,91	1,27	2,17	0,14	1,42	1,34	2,47
Adap1	0,00	1,10	1,70	2,60	0,00	1,00	1,40	2,09	0,01	0,88	1,18	1,84	-0,07	0,96	0,57	1,53
Clip3	0,00	1,10	1,48	2,59	0,00	1,64	1,73	2,27	-0,81	0,20	0,65	1,37	-0,93	-0,09	0,02	1,32
Ctla4	0,00	0,67	1,56	2,58	-0,16	0,94	1,77	2,76	-1,08	0,40	0,71	1,63	-1,24	0,29	0,09	1,50
Klk1b11	0,00	0,00	0,42	2,56	0,00	0,00	1,30	1,96	0,00	0,00	0,00	1,71	0,77	0,00	0,00	1,14
Plcd1	0,00	0,21	1,06	2,51	-0,71	0,22	1,47	2,30	-0,46	0,06	0,83	1,76	-0,69	-0,54	0,00	1,26
Dmwd	0,00	0,24	1,19	2,51	0,19	0,20	1,37	2,49	-0,24	-0,36	1,16	2,31	0,00	0,71	1,23	2,35
Tmem121	0,00	0,61	1,18	2,51	0,00	0,00	1,14	1,97	0,00	0,00	0,00	0,00	0,23	0,68	0,26	2,10
Sqrdl	0,00	0,22	0,74	2,50	-0,51	0,00	0,45	2,07	-0,55	-0,34	0,16	1,55	-0,50	-1,18	-0,44	0,96
H1fx	0,00	0,34	0,00	2,47	0,00	1,09	0,00	2,32	0,00	1,30	0,00	2,51	0,00	0,00	0,00	0,82
Kynu	0,00	0,09	0,75	2,47	-0,64	-0,16	1,10	2,62	-0,61	-0,62	0,14	1,29	-0,45	-0,75	0,00	1,19
Pnpla3	0,00	0,44	1,62	2,47	0,08	0,00	2,04	2,38	0,02	0,00	1,42	1,31	0,42	0,29	1,70	1,18
Asb2	0,00	0,84	1,42	2,42	0,00	1,26	1,32	2,25	0,25	1,09	0,93	1,33	-1,42	-0,65	-0,87	0,01
Zbtb18	0,00	1,65	1,23	2,41	0,09	2,14	1,23	2,17	0,23	2,00	1,13	1,63	-0,45	0,68	0,00	0,45
6430571L13Rik	0	0,59	1,99	2,39	0,46	0,62	1,44	1,54	0,53	0,45	1,54	0,91	0,12	0	0,97	1,03

**Table 20** represents the top 20 genes with the strongest differential expression in cluster 2. Besides Ctla4, this cluster did not contain already described Roquin and Regnase-1 target genes (Jeltsch et al., 2014; Uehata et al., 2013).

#### Cluster 4:

Most interestingly, cluster 4 comprised genes involved in immune processes such as cytokine production and inflammatory response. The global gene expression pattern of genes in WT T cells changed with the duration of T cell stimulation, emphasizing the importance of these genes for T cell differentiation and stimulation. T cells deficient for Regnase-1 (iKO) showed a slight increase in gene expression in comparison to WT during T cell stimulation. Comparably, deletion of Roquin-1/2 (iDKO) influenced the gene expression pattern like the Regnase-1 knockout. Most interestingly, knockout of Roquin-1/2 and Regnase-1 (iTKO) affected gene

expression during all timepoints the most, hinting towards an additive influence of Roquin-1/2 and Regnase-1 on the overall mRNA expression in this cluster.

**Table 21 | Differential expressed genes identified in cluster 4.**

Top 20 list of differentially expressed genes from cluster 4 in iTKO, iDKO and iKO vs. WT without stimulation (0h) and stimulated (1,2,4h) rated according to the highest  $\log_2(\text{FC})$  in iTKO at 0h. Red color indicates high  $\log_2(\text{FC})$  up to 6.69 and white color basal gene expression of 0, whereas blue represent negative  $\log_2(\text{FC})$  values down to -2.72.

	0h				1h				2h				4h			
Gene	WT	KO	DKO	TKO	WT	KO	DKO	TKO	WT	KO	DKO	TKO	WT	KO	DKO	TKO
Gm15987	0,00	3,45	1,28	5,48	0,14	3,98	2,28	5,03	0,07	4,81	3,14	5,19	0,00	4,08	2,29	4,46
Cebpd	0,00	1,25	0,72	5,46	0,00	2,46	1,32	5,40	0,00	5,20	3,26	6,78	0,80	5,15	2,73	5,83
Kit	0,00	1,98	1,93	4,98	1,76	4,70	3,81	5,68	1,88	4,99	3,51	5,53	0,59	3,51	1,30	4,58
Tnfrsf8	0,00	0,65	2,14	4,79	-0,28	0,53	2,80	4,72	-0,72	1,61	2,51	4,84	-0,28	2,15	1,90	4,32
Dlk1	0,00	0,16	0,42	4,76	0,00	0,00	1,09	4,87	0,00	0,00	0,42	4,98	0,57	0,00	1,58	4,75
Tlr9	0,00	1,30	2,45	4,64	0,09	3,30	3,10	4,45	0,00	2,99	2,32	3,52	0,00	1,60	1,41	2,22
Wnt10b	0,00	0,00	1,20	4,56	1,32	2,00	3,39	4,82	2,45	3,37	5,19	6,69	2,22	2,84	3,89	5,98
Gm14718	0,00	1,72	2,01	4,51	1,78	4,20	3,89	5,22	2,07	4,29	4,28	5,04	1,05	4,24	3,13	4,73
Zcchc18	0,00	2,60	2,68	4,37	0,10	3,24	3,05	4,27	-1,30	2,72	2,32	3,52	-2,72	1,56	0,32	2,11
Fam43a	0,00	0,79	1,19	4,36	-0,22	2,54	1,98	5,67	0,29	2,23	1,37	4,05	0,72	0,78	0,22	2,93
Ebi3	0,00	0,97	3,28	4,13	0,25	1,75	4,08	4,54	-0,42	1,48	3,72	4,50	0,00	0,97	2,43	4,05
Tox2	0,00	0,37	1,56	4,06	-0,45	0,68	1,63	4,04	0,63	2,07	2,23	3,65	0,33	1,25	0,83	1,86
Ppic	0,00	1,76	1,36	3,99	0,99	2,76	1,86	4,36	1,11	3,17	2,21	4,65	1,13	3,40	1,99	4,68
Prickle1	0,00	2,17	1,07	3,88	-0,50	4,28	2,61	5,43	0,17	4,81	3,20	5,30	0,19	4,11	2,78	4,23
Fcrl1	0,00	0,98	0,71	3,67	-0,15	1,51	0,99	3,70	1,05	2,65	1,67	3,92	1,95	2,85	1,18	2,64
Icos	0,00	1,87	2,37	3,55	0,03	2,18	2,29	3,38	0,15	2,36	1,69	2,75	0,00	1,90	0,79	2,24
Mpzl1	0,00	1,10	0,94	3,51	-0,25	1,03	0,16	3,21	0,47	2,13	0,81	3,38	1,29	2,70	1,89	3,72
Cpd	0,00	1,04	1,84	3,42	1,23	2,78	3,35	4,20	2,41	4,18	4,12	4,95	3,06	4,03	3,74	4,31
Csn2	0,00	0,47	0,00	3,40	0,00	2,16	0,00	4,40	0,00	2,87	0,00	4,29	0,00	2,88	0,00	3,64
Lmna	0,00	0,35	1,56	3,34	2,30	2,71	3,42	4,58	2,06	2,24	3,02	4,45	0,83	1,30	1,37	3,49

Since we already identified that Roquin and Regnase-1 might have an additive or even cooperative function in the prevention of autoimmunity in mice, we further aimed to validate these immune related target genes in cluster 4 for their regulation by these RNA-binding proteins. **Table 21** depicts the genes of cluster 4 with the highest  $\log_2(\text{FC})$  expression in iTKO T cells. Interestingly, amongst the top 20 list we found genes that have already been defined as targeted by Regnase-1 and Roquin such as *Cebpd* and *Icos*. In addition, we performed hierarchical clustering of genes expressed in cluster 4 to gain insights about similarities in gene expression by Roquin and Regnase-1 (**Figure 47**).

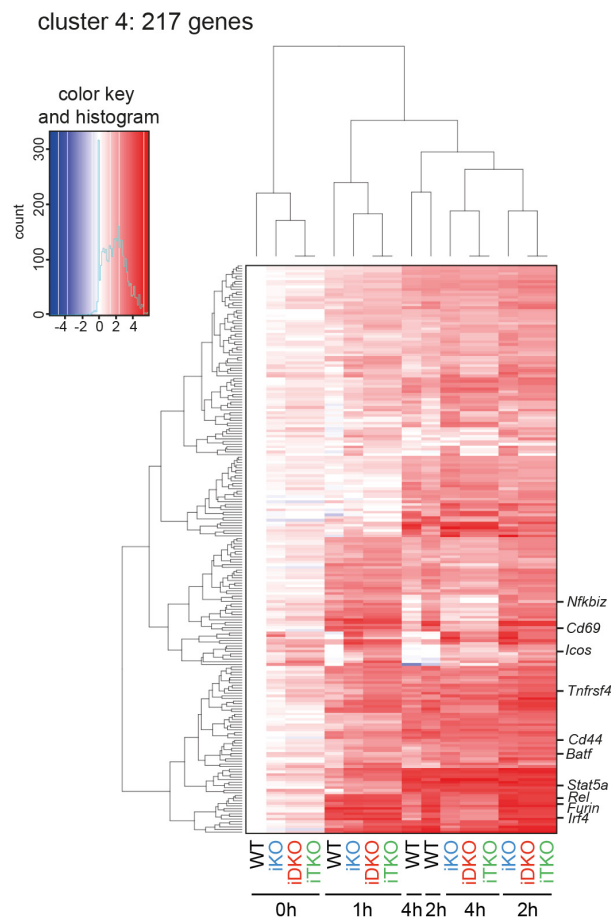


**Figure 47 | Hierarchical clustering of genes identified in cluster 4.**

Hierarchical cluster heat map of genes identified in cluster 4 from WT, iDKO, iKO and iTKO CD4 T cells unstimulated or stimulated for 1, 2 and 4h with  $\alpha$ -CD3/CD28. Color code represents  $\log_2(\text{FC})$  expression of knockout genes relative to WT(0h) and the histogram in the legend represents the numbers of counts with the respective  $\log_2(\text{FC})$ . Known Roquin and Regnase-1 target genes are indicated at the right side of the heatmap.

This analysis revealed the highest similarity of gene expression in iDKO and iTKO, followed by iKO genes, which is maintained during stimulation. Genes of WT samples showed strongest divergency from genes in knockouts at all analyzed timepoints. But with 2h and 4h of stimulation the overall gene expression in WT CD4 T cells was retained, suggesting that gene expression reached a plateau with 2h of TCR stimulation. Interestingly, cluster 4 contained already described target genes of Roquin and Regnase-1: *Batf*, *Cd44*, *Cd69*, *Furin*, *Icos*, *Irf4*, *Nfkbiz*, *Rel*, *Stat5a*, *Cebpd* and *Tnfrsf4* (Ox40) (**Table 19**).

We then validated the mRNA-sequencing data of genes we found significantly enriched in cluster 4 by RT-qPCR of T cells isolated from the respective genotypes that were cultured in the same way as the cells used for mRNA-sequencing (**Figure 48**).

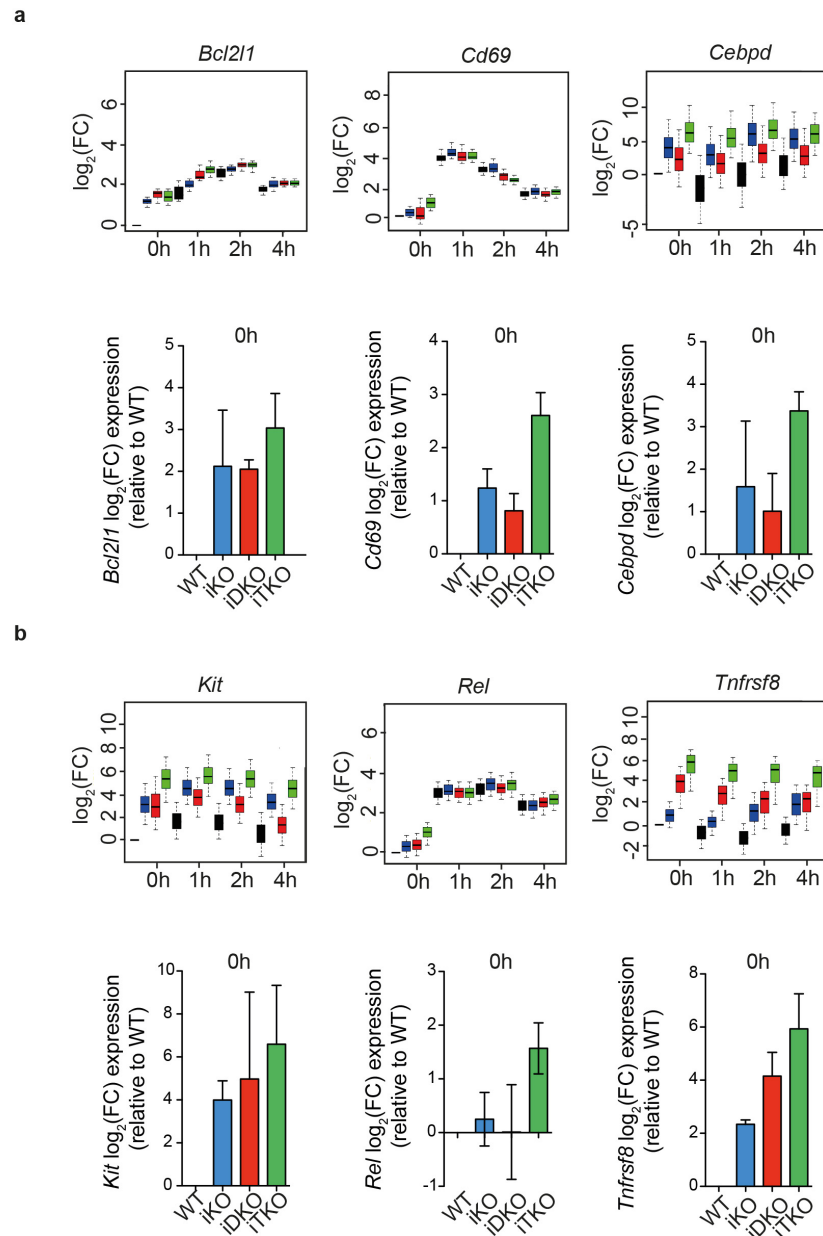


**Figure 48 | Genes identified by mRNA-sequencing in Cluster 2 and 4 and RT-qPCR validation thereof.**

The upper panel of each gene represents the gene expression data obtained by mRNA-sequencing in WT, iDKO, iKO and iTKO T cells unstimulated (0h) or stimulated for 1, 2 or 4h with  $\alpha$ -CD3/CD28. Shown is the  $\log_2(\text{FC})$  regulation in comparison to WT(0h). The lower panel of each gene represents RT-qPCR validation in WT, iDKO, iKO and iTKO cells in unstimulated (0h) condition. Gene expression pattern of *Bcl2l1*, *Cd69*, and *Cebpd* (**a**) and *Kit*, *Rel* and *Tnfrsf8* (**b**). RT-qPCR experiments are representatives of at least two individual experiments.

Amongst them were the transcription factor cRel encoded by *Rel* and the transcriptional activator Cebpd (*Cebpd*), the activation markers CD30 (*Tnfrsf8*) as well as CD69 (*Cd69*) and the anti-apoptotic factor Bcl-X<sub>L</sub> (*Bcl2l1*) and the surface tyrosine-protein kinase cKit encoded by *Kit*. *Cebpd*, *cKit*, and *Tnfrsf8* belonged to the top 20 genes identified in cluster 4 and *Cd69*, *Rel* and *Bcl2l1* were previously identified target genes of Roquin and Regnase-1 (**Table 19**).

By RT-qPCR analysis we could indeed verify the differential gene expression pattern identified by mRNA-sequencing analysis of WT, iDKO, iKO and iTKO T cells.

#### 4.3.3.3 Identifying different types of post-transcriptional gene regulation by Roquin and Regnase-1

Since we found an overlap of genes differentially expressed in the knockout situations, we were wondering if this gene expression analysis can serve as a tool to identify different modes of gene regulation by Roquin and Regnase-1. To prove if Roquin and Regnase-1 cooperatively regulate most of their target mRNAs or if genes that were exclusively targeted by Roquin or Regnase-1 exist, we combined the upregulated genes in cluster 2 and cluster 4 and analyzed the respective 1018 genes by their foldchange expression in the different knockout situations in comparison to WT. We proposed the following types of post-transcriptional gene regulation by Roquin and Regnase-1 proteins: cooperative, Roquin exclusive, Regnase-1 exclusive and redundant. Here, we utilized gene expression of unstimulated (0h) samples to determine the mode of regulation, since Roquin and Regnase-1 are functionally expressed (**Figure 41**).

**Table 22 | Definition of different types of gene regulation by Roquin and Regnase-1 by  $\log_2(\text{FC})$  expression in mRNA-sequencing analyses.**

Cooperative, Roquin exclusive, Regnase-1 exclusive and redundant gene regulation in genes identified in cluster 2 and cluster 4 were defined according to their  $\log_2(\text{FC})$  expression in unstimulated (0h) iDKO, iKO or iTKO cells in comparison to WT(0h). Cooperative target genes have a  $\log_2(\text{FC}) \geq 0.35$  in iDKO and iKO vs. WT(0h) and a  $\log_2(\text{FC}) \geq 0.7$  in iTKO T cells. In addition, the difference of  $\log_2(\text{FC})$  regulation between iTKO and iDKO or iKO must be higher than 25% ( $\log_2(\text{FC})(\text{iTKO}/\text{iDKO}) \geq 1.25$  and  $\log_2(\text{FC})(\text{iTKO}/\text{iKO}) \geq 1.25$ ). Roquin or Regnase-1 exclusive target genes show per definition a  $\log_2(\text{FC}) \geq 0.35$  in the respective knockout and in the iTKO, whereas the other knockout must have a  $\log_2(\text{FC}) < 0.35$ . In Roquin exclusive target genes the  $\log_2(\text{FC})$  expression of iTKO is less than 25% higher in comparison to iDKO target genes ( $\log_2(\text{FC})(\text{iTKO}/\text{iDKO}) \leq 1.25$ ). Accordingly, Regnase-1 exclusive targets have a  $\log_2(\text{FC})(\text{iTKO}/\text{iKO})$  that is less than 25% different to iTKO ( $\log_2(\text{FC})(\text{iTKO}/\text{iKO}) \leq 1.25$ ). Redundant target genes have per definition a  $\log_2(\text{FC}) \leq 0.35$  in iDKO and iKO T cells in comparison to WT(0h), whereas the  $\log_2(\text{FC})$  expression in iTKO v. WT is  $\geq 0.7$ . Here the difference between iTKO and iDKO and iKO should be higher than 25% ( $\log_2(\text{FC})(\text{iTKO}/\text{iKO}) \geq 1.25$  and  $\log_2(\text{FC})(\text{iTKO}/\text{iDKO}) \geq 1.25$ ). Applying these definitions we identified 294 to be cooperatively regulated by Roquin and Regnase-1, 87 and 9 genes to be exclusively regulated by Roquin or Regnase-1 and 52 genes to have a redundant type of post-transcriptional gene regulation.

type of regulation	$\log_2(\text{FC})$ vs. WT (0h)			$\log_2(\text{FC})$ (TKO/DKO)	$\log_2(\text{FC})$ (TKO/KO)	genes identified
	DKO	KO	TKO			
cooperative	$\geq 0.35$	$\geq 0.35$	$\geq 0.7$	$\geq 1.25$	$\geq 1.25$	294
Roquin exclusive	$\geq 0.35$	$< 0.35$	$\geq 0.35$	$\leq 1.25$		87
Regnase-1 exclusive	$< 0.35$	$\geq 0.35$	$\geq 0.35$		$\leq 1.25$	9
redundant	$\leq 0.35$	$\leq 0.35$	$\geq 0.7$	$\geq 1.25$	$\geq 1.25$	52



**Table 22** gives an overview of the thresholds and calculations we defined to determine cooperative, Roquin or Regnase-1 exclusive and redundant target transcripts.

Cooperative target genes were per definition regulated by both Roquin and Regnase-1 proteins, therefore they were expected to be highly abundant in iDKO and iKO in comparison to WT, but showed an even higher expression in iTKO CD4 T cells. Therefore, cooperatively regulated target genes were defined to have a  $\log_2(\text{FC})$  expression  $\geq 0.35$  in iDKO and iKO in comparison to WT(0h) and the  $\log_2(\text{FC})$  expression in iTKO should exceed 0.7. In addition, we wanted to verify that the expression of each cooperatively regulated gene has a 25% higher  $\log_2(\text{FC})$  expression in iTKO than in iDKO and iKO, consequently we included  $\log_2(\text{FC})(\text{iTKO}/\text{iDKO})$  and  $\log_2(\text{FC})(\text{iTKO}/\text{iKO}) \geq 1.25$ . By applying these calculations, we identified 294 potentially cooperative target genes.

We described Roquin or Regnase-1 exclusive target genes as strongly expressed in either iDKO or iKO with a comparably high expression in iTKO cells. Therefore, we applied following definitions to Roquin and Regnase-1 exclusive target genes: The  $\log_2(\text{FC})$  expression in iDKO and iTKO in comparison to WT(0h) should exceed 0.35 in a Roquin exclusive target gene and the  $\log_2(\text{FC})$  in iKO T cells should be  $< 0.35$ . Correspondingly, Regnase-1 exclusive target genes revealed a  $\log_2(\text{FC}) \geq 0.35$  in iKO and iTKO, whereas the iDKO should not influence the mRNA expression by owing a  $\log_2(\text{FC}) < 0.35$ . To verify that the expression of the single knockouts did not vary from the inducible triple knockout more than 25%, we further applied a  $\log_2(\text{FC})(\text{iTKO}/\text{iDKO}) \leq 1.25$  to define Roquin exclusive targets and  $\log_2(\text{FC})(\text{iTKO}/\text{iKO}) \leq 1.25$  to define Regnase-1 exclusive target genes. We identified 87 genes to be exclusively targeted by Roquin, but surprisingly, only 9 mRNAs revealed Regnase-1 exclusivity.

Redundancy was per definition, a mode of gene regulation that implies that only the absence of all three proteins influences the gene expression. Therefore, the  $\log_2(\text{FC})$  of mRNAs in iDKO and iKO vs. WT(0h) was expected to be  $< 0.35$ , whereas loss of Roquin and Regnase-1 in iTKO T cells should result in a  $\log_2(\text{FC}) \geq 0.7$ . Further, the differential gene expression in iTKO T cells should be at least 25% higher than in iDKO and iKO cells, which is determined by  $\log_2(\text{FC})(\text{iTKO}/\text{iDKO})$  and  $\log_2(\text{FC})(\text{iTKO}/\text{iKO}) \geq 1.25$ . In consideration of these definitions, we found 52 genes to be redundantly regulated by Roquin and Regnase-1. A complete list of the genes is attached in the appendix (**Appendix 4-7**).

With the help of these differential gene expression analysis, we were able to identify that most genes showed a cooperative type of gene regulation, in turn almost no Regnase-1 exclusive target genes were found. We further wanted to verify these findings by selecting exemplified target genes and study the mode of gene regulation in detail.

As a cooperative target gene, I chose *Icos*, since this is an already well-studied Roquin target and it appeared in the top 20 list of cluster 4. The gene regulation of *Ox40* (*Tnfrsf4*) has already

been investigated in this thesis (chapter 4.1.1) and thus we wanted to further extend and verify our knowledge about this prototypic Roquin exclusive target gene. Amongst the 9 Regnase-1 exclusive target genes we hardly found interesting candidates. Therefore, I decided to select the cooperative target gene *D1ertd622e* for further investigations, because it showed strong Regnase-1 requirement. In contrast, *Ctla4* was chosen as an additional cooperative target gene that in turn strongly depended on Roquin. Indeed, we were able to verify the gene expression pattern identified by mRNA-sequencing with real-time qPCR analysis of T cells from WT, iDKO, iKO and iTKO mice (**Figure 49**).

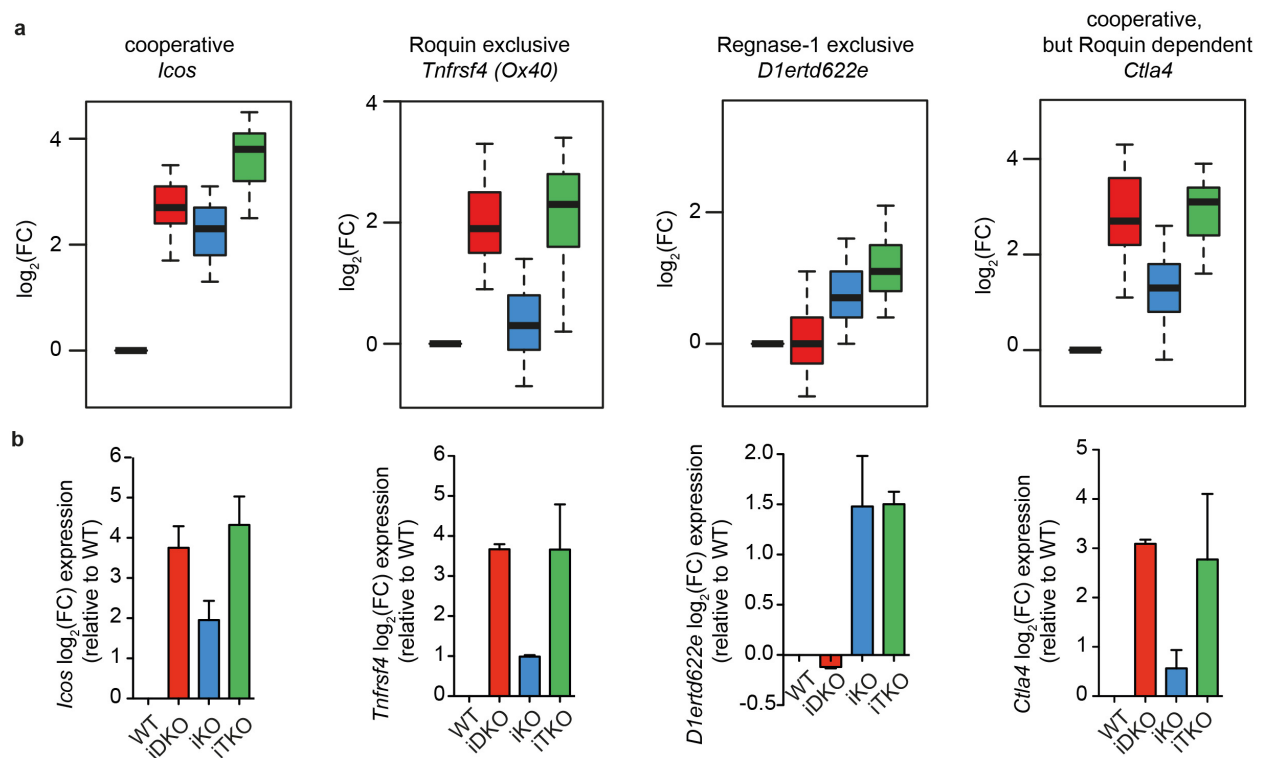


**Figure 49** | *Icos*, *Ox40*, *D1ertd622e* and *Ctla4* expression in Roquin- and Regnase-1-deficient CD4 T cells.

Genes identified by mRNA-sequencing (a) were further confirmed by RT-qPCR (b) in CD4 cells isolated from *Cd4-creERT2* (WT), *Rc3h1/2<sup>fl/fl</sup>*, *Cd4-creERT2* (iDKO), *Zc3h12a<sup>fl/fl</sup>*; *Cd4-creERT2* (iKO) and *Rc3h1/2<sup>fl/fl</sup>*; *Zc3h12a<sup>fl/fl</sup>*; *Cd4-creERT2* (iTKO) mice *in vitro* deleted for loxP-flanked alleles by 4'OH-tamoxifen treatment, stimulated with  $\alpha$ -CD3/CD28 under T<sub>H</sub>1 conditions and cultured in IL-2-containing medium for 2d. RNA was isolated, transcribed into cDNA and RT-qPCR was performed using probe-based gene-specific amplification. Data are representatives of two independent experiments (b).

The expression of the cooperative target *Icos* was under the control of Roquin and Regnase-1, whereas the effect upon Roquin-deficiency was stronger. *Ox40* expression was only affected by Roquin-deficiency (iDKO) and iTKO, whereas *D1ertd622e* was influenced by a loss of all three proteins (iTKO) and Regnase-1 (iKO). Therefore, these genes were verified as Roquin

and Regnase-1 exclusive target genes. In turn, *Ctla4* was more affected by a loss of Roquin and was therefore defined as a more Roquin-dependent mRNA.

#### 4.3.4 Analyzing the functional cooperativity of Roquin and Regnase-1

For identifying direct mRNA targets of RNA-binding proteins, CLIP (crosslinked-immunoprecipitation) experiments are the common method of choice. Briefly, mRNAs are crosslinked by UV irradiation of a specific wavelength to the RBP, followed by immunoprecipitation, RNA radiolabeling with [ $\gamma^{32}\text{P}$ ]-ATP, Proteinase K digest of the protein bound to RNA and library preparation and next generation sequencing of the immunoprecipitated RNA. CLIP experiments with overexpressed Roquin or Regnase-1 in mouse embryonic fibroblasts or HEK293 cells have been described previously (Essig et al., 2018; Mino et al., 2015). For identifying the physiological cooperation of Roquin and Regnase-1 on the mRNA, I tried to establish PAR-CLIP with endogenous Regnase-1 in primary CD4 T cells. CLIP experiments highly depend on the abundance of protein to be immunoprecipitated to obtain enough RNA for appropriate library preparation and deep sequencing. Due to relatively low expression of endogenous Regnase-1 in comparison to the so far established PAR CLIP experiments with overexpressed proteins, my PAR-CLIP experiments were not successful. Therefore, alternative methods were established to prove the functional interaction and cooperation of Roquin and Regnase-1 proteins in T cells.

##### 4.3.4.1 Validation of target genes *ex vivo* in *Cd4-cre* mice

To validate the defined types of gene regulation we found in cluster 2 and 4, flow cytometry analysis of the encoded proteins was performed in splenocytes of WT, DKO<sup>T</sup>, KO<sup>T</sup> and TKO<sup>T</sup> mice. Under these more physiological conditions, Roquin and Regnase-1 target genes should also be elevated in the conditional T-cell-specific knockout situations (**Figure 50**).

Indeed, flow cytometry analysis of endogenous protein expression of the target genes supported the *in vitro* generated mRNA-sequencing data. Icos and *Ctla-4* were defined as more cooperative target genes, which was proven in the *ex vivo* flow cytometry analysis. Here, TKO<sup>T</sup> showed a strong derepression on protein level, but deficiency of Regnase-1 (KO<sup>T</sup>) and Roquin-1/2 (DKO<sup>T</sup>) influenced protein expression in comparison to WT levels. Ox40, comparably to the *in vitro* expression and the previously published data, represented a Roquin exclusive target gene, since loss of Roquin-1/2 (DKO<sup>T</sup>) and the deficiency of all three genes (TKO<sup>T</sup>) caused an upshift of Ox40 protein levels. For *C5orf30* homolog, encoded by *D1ertd622e*, no flow cytometry antibody is commercially available and therefore the protein expression in the knockout T cells could not be further verified.

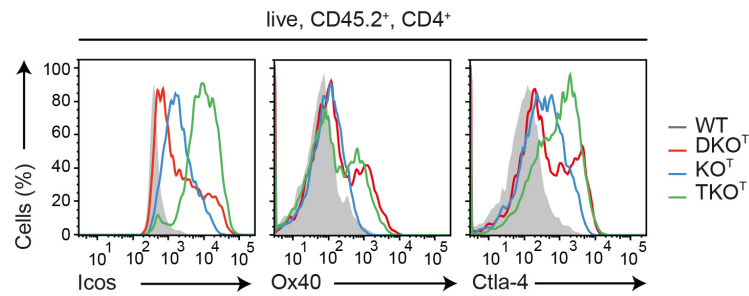


**Figure 50 | Flow cytometry analysis of Roquin and Regnase-1 targets in splenocytes of WT, KO<sup>T</sup>, DKO<sup>T</sup> and TKO<sup>T</sup> mice.**

Flow cytometry analysis of Icos, Ox40 and Ctlα-4, in CD45.2<sup>+</sup>, CD4<sup>+</sup> splenocytes of *Rc3h1/2<sup>fl/fl</sup>; Zc3h12a<sup>fl/fl</sup>* (WT), *Rc3h1/2<sup>fl/fl</sup>; Cd4-cre* (DKO<sup>T</sup>), *Zc3h12a<sup>fl/fl</sup>; Cd4-cre* (KO<sup>T</sup>) and *Rc3h1/2<sup>fl/fl</sup>; Zc3h12a<sup>fl/fl</sup>; Cd4-cre* (TKO<sup>T</sup>) mice. Data are representatives of three experiments.

In summary, the *ex vivo* protein levels correlated with the findings of the mRNA-sequencing analyses and the mRNA expression data, supporting the existence of different types of Roquin- and Regnase-1-induced gene regulation in CD4 T cells.

#### 4.3.4.2 Reconstitution experiments to prove cooperativity of Roquin and Regnase-1

Because the obtained gene expression profiles do not represent direct engagement of the RNA to Roquin or Regnase-1 and could also partially represent indirectly affected genes (as seen for Cluster 3), we used a reconstitution experiment to identify if Regnase-1 requires Roquin for repressing target mRNAs and whether Regnase-1 can function in the absence of Roquin. We hypothesize that binding of the RNA is facilitated via the ROQ domain of Roquin whereas degradation of the mRNA can either be induced via Regnase-1-mediated degradation (e.g. endonucleolytic cleavage), which depends on its catalytic center comprised by Asp141 (D141) or via recruitment of factors involved in decapping, deadenylation or translational inhibition by Roquin proteins (Essig et al., 2018; Glasmacher et al., 2010; Leppek et al., 2013; Murakawa et al., 2015). To test our hypothesis, we reconstituted either wild-type or Roquin-1/2-deficient CD4 T cells with doxycycline-inducible Roquin-1, Regnase-1 or the loss-of-function mutant Regnase-1(D141N) fused to GFP and checked for protein expression of targets. Briefly, CD4 T cells from *Rc3h1/2<sup>fl/fl</sup>; Cd4-creERT2*; rtTA-M2 mice (iDKO, rtTA) were treated with 4'OH-tamoxifen to induce Roquin-1/2 deletion or cells from *Rc3h1/2<sup>fl/fl</sup>; rtTA-M2* (WT, rtTA) mice were used as WT controls (**Figure 10**). After activation with α-CD3/CD28, CD4 cells were transduced with a doxycycline-inducible retrovirus expressing the GFP-fusion constructs. Cells were cultured in IL-2-containing medium, expression of retrovirally integrated genes was induced by doxycycline administration and subsequently targets were analyzed by flow cytometry (**Figure 51**).

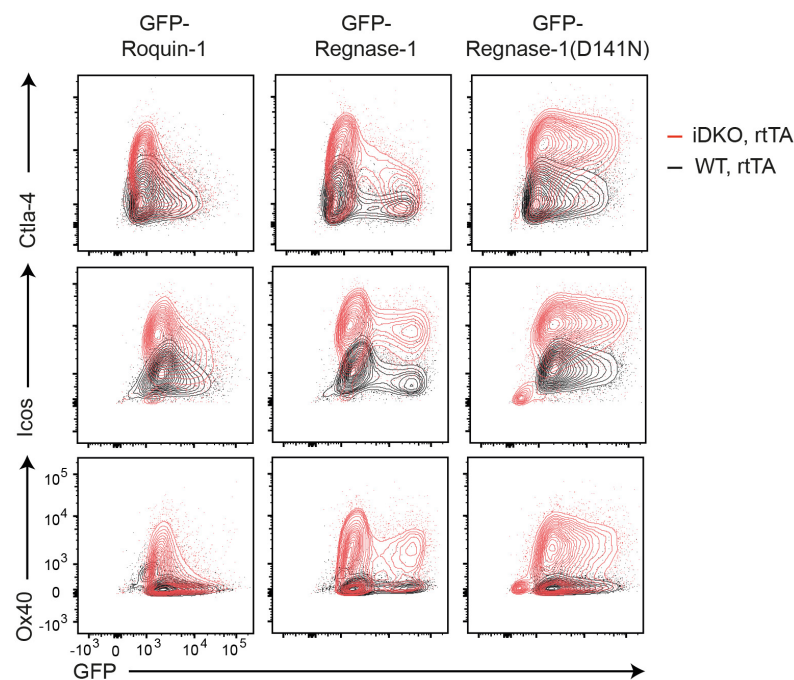


**Figure 51 | Reconstitution of Roquin and Regnase-1 in WT and Roquin-deficient CD4 T cells.**

CD4 T cells from *Rc3h1/2<sup>fl/fl</sup>*; *Cd4-creERT2*; rtTA-M2 mice (iDKO, rtTA) or *Rc3h1/2<sup>fl/fl</sup>*; rtTA-M2 mice (WT, rtTA) were treated with 4'OH-tamoxifen to induce Roquin-1/2 deletion in cre-positive mice. Cells were cultured under T<sub>H</sub>1 conditions and transduced with a retrovirus containing a doxycycline-inducible cassette to express GFP-Roquin-1, GFP-Regnase-1 or GFP-Regnase-1(D141N). After 1.5 d of IL-2 culture, cells were treated with doxycycline for 6h and protein expression of GFP, Ctla-4, Icos and Ox40 was measured by flow cytometry. The experiment was performed together with Dr. Gesine Behrens. These results are representatives of two independent experiments.

Protein expression of Ctla-4 was fully repressed by Roquin-1 reconstitution in Roquin-deficient T cells. Interestingly, GFP-Regnase-1 downregulated Ctla-4 even in the absence of Roquin and this depended on the RNase activity of Regnase-1, suggesting that Regnase-1 can downregulate Ctla-4 independent of Roquin. Different from that, Icos protein levels were influenced by Roquin-1 and Regnase-1 overexpression in WT and iDKO situations. Here, GFP-Regnase-1 only slightly regulated Icos and cRel expression in the absence of endogenous Roquin. Contrary, in the wild-type situation, Regnase-1 altered Icos expression and these effects were diminished with the loss-of-function mutant of Regnase-1. GFP-Roquin-1 alone only partially rescued Roquin-1/2-deficiency, proposing that here Roquin-1 and Regnase-1 might depend on the presence of Roquin-2. As an exemplary Roquin exclusive target, Ox40 was chosen for reconstitution experiments. Here, GFP-Regnase-1 wild-type or D141N overexpression had no effect either in the presence nor in the absence of Roquin, whereas Roquin-1 overexpression in iDKO cells fully reduced Ox40 expression to protein levels comparable to WT. These data strongly support the findings in previous experiments

showing strong Roquin-dependency for *Ox40* gene regulation, but no effect upon Regnase-1 deficiency (**Figure 13** and **Figure 41**) (Janowski et al., 2016).

As shown in **Figure 41**, Regnase-1 protein and mRNA levels were drastically increased in Roquin-deficient T cells proposing that Regnase-1 itself is strongly targeted by Roquin proteins. Since autoregulation of Regnase-1 was suggested by several independent studies, we were wondering if Regnase-1 itself can repress its own target mRNA and if this autoregulation depends on the presence of Roquin proteins. The fact that Roquin-deficient T cells had enormous amounts of Regnase-1, made us hypothesize that Regnase-1 itself is not able to repress its own expression and is therefore a high affinity cooperatively targeted gene. To get insights about the regulation of Regnase-1 itself, we reconstituted Roquin-deficient (iDKO, rtTA) and wild-type (WT, rtTA) T cells as described above with either GFP-Roquin-1 or GFP-Regnase-1 and analyzed endogenous Regnase-1 expression levels in these cells. Since flow cytometry analysis was performed with a monoclonal antibody against Regnase-1, this antibody recognizes endogenous as well as overexpressed GFP-Regnase-1 simultaneously. To avoid a mixed signal here, we mutated the amino acids that form the epitope as such that the antibody was incapable of identifying overexpressed GFP-Regnase-1 (GFP-Regnase-1<sup>invisible</sup>) and consequently the signal measured by flow cytometry resulted exclusively from endogenous Regnase-1.

As a positive control for proving full functionality of GFP-Regnase-1<sup>invisible</sup> protein, Ctla-4 was included in the measurement. Ctla-4 was comparably repressed by GFP-Regnase-1 and GFP-Regnase-1<sup>invisible</sup> demonstrating that the mutation did not influence the activity of Regnase-1. The results in **Figure 52** clearly state that Regnase-1 was only capable to regulate its own expression in the presence of Roquin proteins, since overexpression in Roquin-deficient CD4 T cells had no impact on Regnase-1 expression. Taken together, Roquin as well as Regnase-1 overexpression results in downregulation of many targets including endogenous Regnase-1. However, Regnase-1 requires the presence of Roquin and therefore represents a first target with mandatory cooperative regulation.

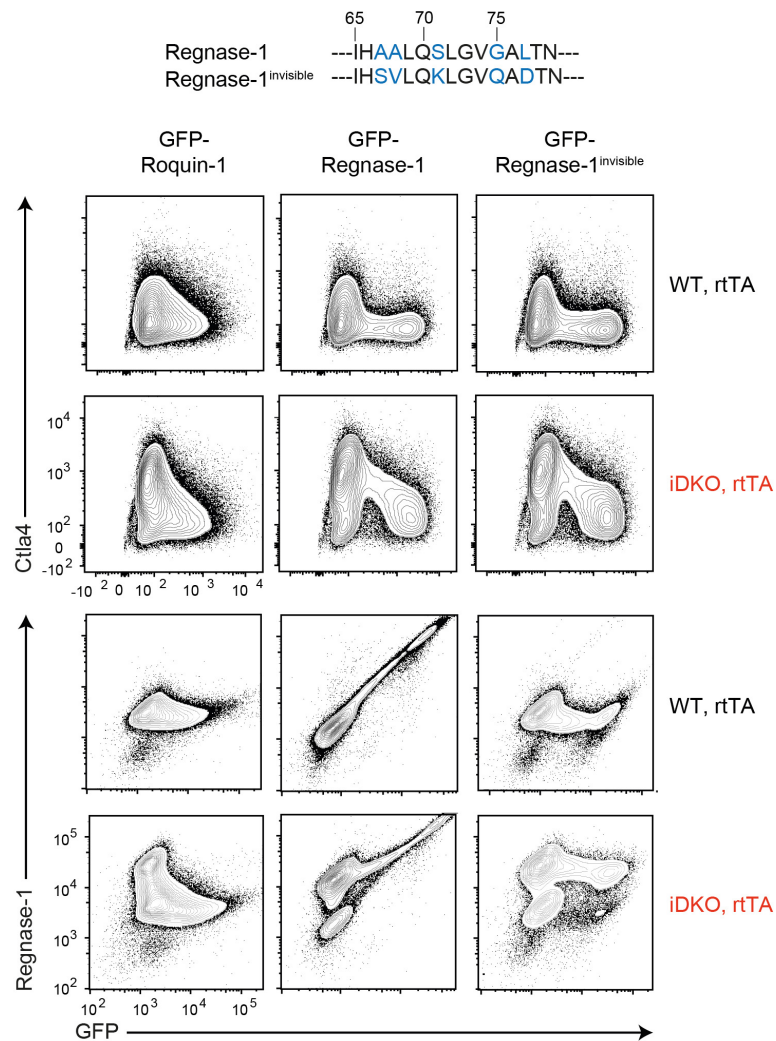


**Figure 52 | Reconstitution of Regnase-1 in WT and Roquin-deficient CD4 T cells.**

CD4 T cells from *Rc3h1/2<sup>fl/fl</sup>*; *Cd4-creERT2*; rtTA-M2 mice (iDKO) or *Rc3h1/2<sup>fl/fl</sup>*; rtTA-M2 mice (WT, rtTA) were treated with 4'OH-tamoxifen to induce Roquin-1/2 deletion in cre-positive mice. Cells were cultured under T<sub>H</sub>1 conditions and transduced with retrovirus containing a doxycycline-inducible cassette to express GFP-Roquin-1, GFP-Regnase-1 or GFP-Regnase-1<sup>invisible</sup>. After 1.5 d of IL-2 culture, cells were treated with doxycycline for 6h and protein expression of GFP, Regnase-1 and Ctla-4 was measured by flow cytometry. The amino acid sequence of the GFP-Regnase-1<sup>invisible</sup> mutant in comparison to wild-type Regnase-1 is depicted above. This experiment was performed by Dr. Gesine Behrens and the results are representatives of three independent experiments.

The reconstitution experiments clearly demonstrated the dependency of Regnase-1 and Roquin in post-transcriptional gene regulation in CD4 T cells. By utilizing this reconstitution system, we were able to distinguish between Roquin exclusive target genes like Ox40, but, in addition, separate cooperative target genes that clearly depend on the presence of both proteins (Regnase-1) from targets that are regulated by both Roquin and Regnase-1 but more in an independent fashion like Ctla-4.

#### 4.3.4.1 Co-Immunoprecipitation of Roquin and Regnase-1

To prove cooperation of Roquin and Regnase-1 proteins, we were wondering if the proteins physically interact and therefore conducted co-immunoprecipitations. Since until now there was no proof for a direct interaction of Roquin and Regnase-1 yet, we first established the co-immunoprecipitation with overexpressed Regnase-1 in WT CD4 T cells.

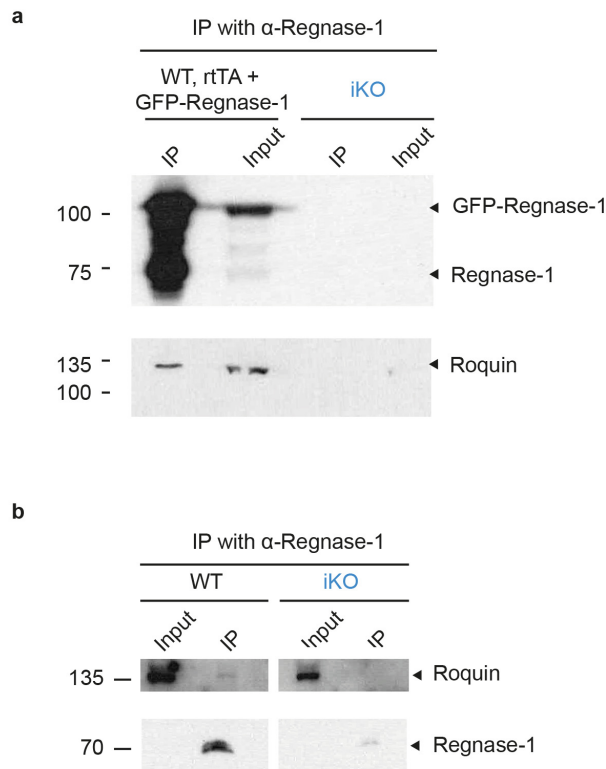


**Figure 53 | Proving direct interaction of Roquin and Regnase-1 by co-immunoprecipitation.**

**a)** CD4 T cells were isolated from *Zc3h12a<sup>fl/fl</sup>*; *Cd4-creERT2* (iKO) or *Rc3h1/2<sup>fl/fl</sup>*; rtTA-M2 mice (WT, rtTA), treated with 4'OH-tamoxifen to induce deletion in iKO cells, activated under  $T_H1$  condition with  $\alpha$ -CD3/CD28 and cultured in IL-2 containing medium for 2d. WT cells were transduced with a doxycycline-inducible retrovirus expressing GFP-Regnase-1. Expression was induced after 2d of IL-2 culture with doxycycline for 16h. **b)** CD4 T cells of *Zc3h12a<sup>fl/fl</sup>*; *Cd4-creERT2* (iKO) or *Zc3h12a<sup>fl/fl</sup>* mice (WT) that were treated with 4' OH-tamoxifen to induce deletion in iKO cells, activated under  $T_H1$  condition with anti-CD3/CD28 and cultured in IL-2-containing medium for 3d. Immunoprecipitation of **a)** and **b)** was performed with a polyclonal antibody against Regnase-1 (R&D) coupled to Protein-A-dynabeads. 50  $\mu$ g protein input and immunoprecipitate (IP) were analyzed on an SDS gel and Roquin and Regnase-1 protein expression were measured by immunoblotting with specific antibodies.

Therefore, CD4 T cells were isolated from *Rc3h1/2<sup>fl/fl</sup>*; rtTA-M2 (WT, rtTA) or *Zc3h12a<sup>fl/fl</sup>*; *Cd4-creERT2* mice (iKO). After 4'OH-tamoxifen-induced deletion, cells were activated with  $\alpha$ -CD3/CD28 and transduced with a doxycycline-inducible retrovirus expressing GFP fused to Regnase-1. Cells were expanded in IL-2-culture medium and expression of GFP-Regnase-1 was induced by doxycycline (**Figure 10**). Co-immunoprecipitation of cell lysates was performed with a monoclonal antibody against Regnase-1 (R&D) in the presence of RNase



inhibitors and phosphatase inhibitors, followed by immunoblotting to control for co-immunoprecipitated Roquin proteins (**Figure 53 a**). Since, we successfully immunoprecipitated Roquin with overexpressed GFP-Regnase-1, we further tested an endogenous interaction of Roquin and Regnase-1 proteins. Immunoprecipitation was performed with protein extracts from CD4 T cells isolated from *Zc3h12a<sup>fl/fl</sup>*; *Cd4-creERT2* (iKO) or *Zc3h12a<sup>fl/fl</sup>* mice (WT), treated with 4'OH-tamoxifen to induce deletion in iKO cells, activated with  $\alpha$ -CD3/CD28 and cultured with IL-2. Co-immunoprecipitation was performed with the same monoclonal anti-Regnase-1 antibody and pulldown of Roquin was tested by immunoblotting (**Figure 53 b**). Even though the abundance of enriched Roquin with endogenous Regnase-1 was rather weak, we were able to prove interaction of both proteins on endogenous levels in WT CD4 T cells. In summary, I was able to show that Roquin and Regnase-1 proteins were not only functionally cooperating in the gene regulation of their shared target genes, but that the underlying molecular mechanism involves a physiologic interaction of both proteins.



## 5 Discussion

In this research project, the cooperative roles of the post-transcriptional gene regulators Roquin-1 and Roquin-2 together with the endonuclease Regnase-1 in controlling autoimmunity were studied.

The first part of this thesis concentrated on the control of complex *cis*-regulatory elements by Roquin proteins. Here, I was, on the one hand, able to show that Roquin not only recognizes a triloop CDE-like element, but also an integrated hexaloop ADE structure to control expression of its mRNA target *Ox40*. On the other hand, I demonstrated that multiple Roquin proteins enable full regulation of the *Nfkbid* 3'-UTR in a cooperative manner, thereby targeting complex *cis*-regulatory elements consisting of triloop CDE-like and hexaloop ADE-like structures. This complex regulatory mechanism induces several degradation pathways: We found that an mRNA harboring the *Nfkbid* 3'-UTR can be degraded via decapping and deadenylation in a redundant manner, and, in addition, be translationally inhibited by Roquin. The focus of the second part of this work was to elucidate the possible cooperative role of Roquin with the endonuclease Regnase-1 in controlling T cell immunity. First, the generation of mice with a conditional deletion of Roquin and Regnase-1 in T cells, helped to gain insights into the overlapping functions of Roquin and Regnase-1 in controlling autoimmunity. Comparing the phenotypes of the triple-knockout mice to either double-knockouts of Roquin encoding genes or Regnase-1 single knockouts, supported the idea of a cooperative regulation. In addition, global mRNA-sequencing analysis of T cells deficient for either Roquin-1/2, Regnase-1 or all three proteins revealed that mRNAs are targeted by both Roquin and Regnase-1, which has the potential to enable a robust and strong gene regulation in T cells to control autoimmunity.

### 5.1 Binding of multiple Roquin proteins enables a cooperative post-transcriptional gene regulation of complex *cis*-regulatory elements

#### 5.1.1 Roquin-mediated regulation involves *cis*-elements with multiple binding sites

As described in the introduction, RNA binding proteins recognize specific *cis*-elements mostly located in the 3'-UTRs of their target mRNAs by involving RNA-binding domains such as zinc

fingers. The RNA-binding protein Roquin involves its ROQ-domain to recognize stem loop structures in its target transcripts. Initially, the CDE element was identified as a high affinity binding element for Roquin-mediated regulation. The repertoire for Roquin-targeted cis-elements was expanded by a novel U-rich hexaloop element termed ADE (alternative decay element). This element was found in an unbiased manner by performing SELEX (Systematic Evolution of Ligands by Exponential Enrichment), which basically enriches RNAs from a random oligonucleotide library bound to a biotinylated N-terminal fragment of the Roquin-1 protein. A homologous ADE-like sequence was identified in the *Ox40* 3'-UTR, which is positioned 5' to another, CDE-like, stem loop structure. The recognition of ADE and CDE element is similarly mediated by residues located in the ROQ-domain of Roquin, whereas, for the hexaloop binding, Roquin additionally involves the amino acid Tyr250, which is not needed for CDE triloop interaction. By introducing wild-type and mutated versions of Roquin-1 into CD4 T cells lacking the Roquin paralogs, I was able to show that the regulation of endogenous *Ox40* requires Tyr250, but additionally involves Lys220, Lys239 and Arg260, which have also been reported to be mandatory for CDE recognition (Figure 13). This publication contained the first proof that Roquin involves multiple binding sites in its *cis* regulatory elements, namely CDE and ADE-like in *Ox40* to ensure full target regulation.

The knowledge about the robustness of this system was further extended by investigating the 3'-UTR of the prototypic Roquin target *Nfkbid* (Jeltsch et al., 2014). Comparing a reporter system under the control of the *Nfkbid* 3'-UTR in wild-type and Roquin-deficient MEF cells, I identified a minimal response element within the 3'-UTR that is highly upregulated upon induced depletion of endogenous Roquin proteins. In a PAR-CLIP approach our group identified even another binding motif, a linear binding element (LBE), which is present in the *Nfkbid* 3'-UTR as well. Intriguingly, in MEF cells Roquin did not require this LBE for full regulation of the minimal response element (Figure 14). Even though this sequence motif is bound by Roquin via its ROQ-domain and is highly abundant in Roquin targets, it had no influence on regulation of the reporter and, in addition, it is a rather low-affinity binding element. Therefore, we would speculate that this motif serves as an element that may either support regulation of lower affinity targets or enable regulation in a more specialized cellular context. To identify possible secondary structure elements within the *Nfkbid* 3'-UTR, we performed mLocARNA secondary structure predictions together with RNAalifold in collaboration with the group of Dr. Jörg Hackermüller. This method enables detection of evolutionary conserved structural motifs based on multiple sequence alignment in combination with secondary structure predictions and is therefore a useful tool to reveal RNA secondary structures with conserved functions (Will et al., 2007). Overall, we identified six highly conserved tandem stem loops within the 263 nucleotides minimal response element of *Nfkbid* of which two had prototypic CDE structures (SL5, SL6) and the highest conservation was seen for an ADE-like

U-rich hexaloop element (SL1) (Figure 15). In a comprehensive mutational analysis of the six conserved SL structures in the *Nfkbid* reporter construct, I was able to distinguish essential and non-essential stem loops for Roquin-mediated regulation. Essential stem loops already affected Roquin-mediated gene regulation when either stem or loop mutations were introduced in the individual stem-loop (SL1, SL2). Interestingly, the CDE-type SL structures 5 and 6 exhibited redundant functions, since reporter expression was only affected with double-mutants thereof. Mutating the non-essential SLs 3 and 4 reduced reporter regulation only in combination with mutation of one of the redundant SLs 5 or 6 (Figure 16). Mutating five of six SLs abolished Roquin-mediated reporter repression completely (Figure 19). This mutational analysis suggests that Roquin prefers specific loop structures over others and that multiple Roquin proteins are required to enable robust and strong regulation. We hypothesize that even the non-essential SLs could contribute, potentially by forming a higher order structure or by supporting correct folding of the RNA. We further excluded the possibility that one Roquin protein might interact with two SLs simultaneously by introducing long, random sequences between tandem SL1 and 2, which did not affect the regulation by Roquin (data not shown). Since we exchanged up to 8 nucleotides within SL structures in our mutational analysis, we asked whether the folding of the other SL structures is not influenced by introducing non-canonical nucleotides into individual SLs. Therefore, Anne Hoffmann from the group of Dr. Jörg Hackermüller investigated during her master thesis the structural components of the *Nfkbid* 3'-UTR. She calculated realization probabilities that predicted how exchanges of nucleotides on one stem loop influence folding of the residual five stem loops of *Nfkbid*. Consequently, I designed the mutations in stems and loops according to her predications to avoid misfolding of the whole minimal response element.

The fact that multiple highly conserved stem loop structures are strongly responding to the presence of Roquin, made us question if several Roquin proteins are indeed involved in this complex regulation. Therefore, I performed a tethering assay where I introduced boxB RNA SL structures at the positions of the essential SLs 1, 2 and 5 and artificially tethered  $\lambda$ N-Roquin to these high-affinity boxB elements in MEF cells that lacked endogenous Roquin-1 and Roquin-2 (Figure 20). These experiments clearly demonstrated that with a gradual increase of boxB elements and therefore Roquin proteins on the RNA, the repression of the reporter was enhanced, emphasizing that simultaneous binding of multiple Roquin proteins enables stronger gene regulation.

### 5.1.2 Roquin controls mRNA stability by integrating multiple decay pathways

We furthermore identified that Roquin redundantly induced either deadenylation or decapping of the *Nfkbid* 3'-UTR. This could be explained by Roquin independently interacting with the deadenylation machinery i.e. the Ccr4-Not complex or factors of decapping including Ddx6/Rck via its carboxy- or amino-terminal region, respectively (Glasmacher et al., 2010; Leppek et al., 2013; Murakawa et al., 2015). In addition, we found that Roquin enables inhibition of translation of the *Nfkbid* mRNA as determined by polysome profiling (Figure 21). This finding was further supported by a global approach. Here, my colleague Dr. Katharina Essig compared global mRNA-sequencing with sequencing of ribosome-protected fragments in MEF cells with overexpressed Roquin-1. In these experiments, we found some target genes that have reduced translational efficiency upon overexpression of Roquin-1, amongst them *Nfkbid*. By further investigating the structural features of these translationally-inhibited target genes, we identified an enrichment of mRNAs containing 4 or more Roquin binding sites in their 3'-UTRs. Altogether these analyses suggest, that Roquin, in addition to mRNA decay, also induces translational repression of some target genes in a 3'-UTR-specific manner resulting from its simultaneous interaction with multiple binding sites. However, how this translational inhibition is induced by Roquin is still not solved. One possibility could be that Roquin requires multiple and mutually exclusive interactions with other post-transcriptional repressors or with effector proteins that can inhibit ribosomal occupancy or processivity.

Very recently, the 3'-UTR of the atypical NF- $\kappa$ B inhibitor I $\kappa$ B $\zeta$ , encoded by *Nfkbiz*, was investigated for its post-transcriptional gene regulation by Regnase-1 (Behrens et al., 2018). Here, the authors identified a translational silencing element (TSE) of the human *NFKBIZ* which forms a very similar structure to the mouse *Nfkbid* 3'-UTR. The TSE consists of five conserved stem loop structures, whereas SL4 and SL5 show strong conservation and are defined as CDE elements. SL4 and 5 effectively induce mRNA degradation, but translational silencing by Regnase-1 is only mediated upon additional presence of SL1-3 in the reporter assays. However, the mechanism of Regnase-1-mediated translational silencing is still under debate. Strikingly, the expression of both *Nfkbid* and *Nfkbiz* are tightly regulated not only on the level of mRNA decay, but also on the level of translational inhibition ensuring controlled protein expression of I $\kappa$ B $\zeta$  and I $\kappa$ B<sub>NS</sub>. The cooperation of Roquin and Regnase-1 in regulating overlapping target mRNAs by translational inhibition could be one potential way how translational silencing is achieved for *Nfkbiz* and *Nfkbid*. Since I $\kappa$ B $\zeta$  and I $\kappa$ B<sub>NS</sub> have high sequence homology and were reported to have overlapping functions in controlling T<sub>H</sub>17 differentiation, the post-transcriptional gene regulation by RNA-binding proteins conferred via complex *cis*-elements, is an important mechanism to control T cell-driven immune responses.

In the future, it would be of high interest to identify the complex regulatory network of RNA-binding proteins, translational silencers, mRNA decay factors and stabilizing factors on mRNAs such as *Nfkbid*. An interesting tool to study this would be a combination of the  $\lambda$ N-boxB tethering assay with an approach termed BioID. BioID utilizes a biotin ligase (BirA), which biotinylates proteins based on proximity (Roux et al., 2018). By tethering BirA- $\lambda$ N to boxB structures in the *Nfkbid* 3'-UTR one could identify the regulatory protein network present at an approximal 10 nm labelling radius of a CDE or ADE element. Experiments to reach this goal are currently under way in our laboratory.

In conclusion, this detailed analysis of the *Nfkbid* 3'-UTR has expanded our knowledge about post-transcriptional gene regulation. Induction of deadenylation, decapping and translational inhibition by interaction with non-essential and essential binding sites enables a cooperative gene regulation by multiple Roquin proteins on the same target mRNA. Of course, interaction with other post-transcriptional gene regulators could contribute to robustness of regulation. It ensures tight regulation of mRNA abundance in immune cells and therefore prevents an imbalance of gene expression that can result in failures of the immune system.

## **5.2 The cooperative molecular function of Roquin and Regnase-1 in T cells**

The first part of this thesis proved a cooperative concept of gene regulation by multiple Roquin proteins bound on complex *cis*-elements. This concept was further expanded by investigating another level of cooperativity by Roquin proteins: the interaction and molecular cooperation with the endonuclease Regnase-1.

Many research groups have studied the role of RNA-binding proteins in the past, establishing many methods to identify direct mRNA target sites and novel potential mRNA target sets globally. The method of choice is CLIP (UV cross-linking and immunoprecipitation), that isolates short RNA fragments cross-linked to RNA-binding proteins via specific immunoprecipitation and analysis by mRNA-sequencing. More and more advanced and further developed CLIP methods have been established in the last years such as PAR-CLIP (Photoactivable ribonucleoside-enhanced CLIP), HITS-CLIP (High-throughput sequencing of RNA isolated by CLIP) and iCLIP (Individual-nucleotide resolution CLIP) (Lee and Ule, 2018). mRNA targets of Roquin and Regnase-1 have been globally identified by PAR-CLIP and HITS-CLIP experiments in the past (Essig et al., 2018; Mino et al., 2015). However, these experiments involved overexpression systems in non-immune cells. My goal was to assess the cooperation of Roquin and Regnase-1 in the most physiological condition. Therefore, I aimed to establish several methods to validate direct mRNA targets of Roquin and Regnase-

1 in a cooperative setting. I tried to establish PAR-CLIP with endogenous Regnase-1 in primary CD4 T cells, which was not successful due to insufficient read numbers. Additionally, I overexpressed Roquin-1 for PAR-CLIP experiments in Roquin-deficient cells, because these cells have high levels of Regnase-1 and thus I wanted to improve immunoprecipitation of endogenous protein. But, already small overexpression of Roquin-1 almost completely reduced endogenous Regnase-1, which made an identification of cooperative target genes impossible. Finally, I performed RNA-immunoprecipitations with endogenous Regnase-1 and subsequently analyzed the RNA by RT-qPCR. Unfortunately, again, only unspecific RNAs and low RNA amounts were detectable, indicating a need for improved technology. In sum, I was not able to verify a cooperative mRNA regulation by Roquin and Regnase-1 proteins under physiological conditions in primary T cells. There might be several reasons to explain this: First, Regnase-1 could endonucleolytically cleave its bound mRNA targets and thus the RNA is rapidly degraded and not detectable. Second, Regnase-1 itself is not capable of binding mRNAs on its own and thus requires an additional factor, such as Roquin or UPF1 that mediates RNA-interaction or unwinds the mRNA stem loop. Third, the physiological complex of Roquin, Regnase-1 and the mRNA is dynamically formed, short-lived or unstable and is therefore hard to detect in immunoprecipitation experiments.

Finally, we decided to globally capture mRNAs that are expressed under wild-type conditions and compare this mRNA set to the global mRNA expression of inducible Roquin-1/2 (iDKO), Regnase-1 (iKO) and Roquin-1/2 and Regnase-1 knockout (iTKO) CD4 T cells by performing mRNA-sequencing.

### **5.2.1 Identifying new target genes of Roquin and Regnase-1**

The analysis of differentially expressed genes in T cells lacking Roquin (iDKO), Regnase-1 (iKO) and all three genes (iTKO) in comparison to the mRNA expression of wild-type (WT) T cells helped us to gain more insights into the gene regulation by Roquin and Regnase-1. By performing cluster analyses in combination with gene ontology we were able to identify already known direct targets in cluster 4 and therefore assumed that this cluster might contain the majority of direct target genes.

Surprisingly, I identified two gene clusters (cluster 1 and 3) that were downregulated upon inducible knockout of Roquin and Regnase-1 (Figure 45). These downregulated genes probably represent genes that were indirectly affected by an inducible knockout of Roquin and Regnase-1, since so far, no directly stabilizing effect by Roquin and Regnase-1 on mRNA has been reported.

A possible explanation for the slight downregulation of genes in cluster 3 has already been put forward in the results section 4.3.3.2. We propose that Roquin and Regnase-1 might together



repress genes encoding for regulators of gene expression including transcription factors or translational repressors but also epigenetic modifiers that then influence expression of genes identified in cluster 3. As exemplified in Figure 46, we found the epigenetic regulator Hdac2 as potential direct or indirect target of Roquin and Regnase-1 since the upregulated pattern of *Hdac2* observed in cells that lack Roquin and Regnase-1 inversely correlated with the gene expression in the mRNA-sequencing data of already described Hdac2 target genes we found in cluster 3 such as *Ccna2* or *Cdk1*. Thus, the influence of Roquin and Regnase-1 on target genes consequently impacted on downstream genes that we detected in the global mRNA-sequencing approach.

As mentioned in the results section 4.3.3.2, the ion-channel-associated genes in cluster 1 could be connected to the sequencing depth. The read counts of the genes in this cluster were low and therefore increasing the sequencing depth could help to further support the regulation within this cluster, but more importantly, protein expression of the candidate genes would have to be analyzed to infer a biological function to this regulation. Nevertheless, the differential gene expression showed a significantly increased expression in an inducible triple-knockout in comparison to Roquin- and Regnase-1-deficiency alone and thus the effect could be triple-knockout-specific. Remarkably, overexpression of the anti-apoptotic factor Bcl-2 accelerates the downregulation of potassium channel genes such as *Kcna1*, *Kcna5*, and *Kcnb1* in vascular smooth muscle cells (Ekhterae et al., 2001). Thus, the direct regulation of Bcl-2 family genes by Roquin and Regnase-1, which will be discussed in more detail later, might be another potential way to negatively influence ion channel associated genes.

As expected, we identified prominent upregulation of genes upon knockouts of Roquin and Regnase-1, which are represented in 2 clusters (cluster 2 and 4). Interestingly, we found already described target genes such as *Nfkbiz*, *Icos*, *Ox40*, *cRel* and *Ctla4* in both clusters, which made us combine the genes and further investigate these two clusters (Figure 48).

Besides validation of already known target transcripts, I moreover identified very interesting new candidate target genes in these clusters.

The negative regulators of the mitochondrial apoptotic pathway *Bcl2a1* (Bcl2-related protein A1) and *Bcl2l1* (Bcl-X<sub>L</sub>) have been reported independently as Regnase-1 and Roquin target candidates. Regnase-1 overexpression promotes death of breast cancer cells by selectively enhancing mRNA degradation of anti-apoptotic gene transcripts, such as *Bcl2l1*, *Bcl2a1*, *RelB*, *Birc3* and *Bcl3* (Lu et al., 2016). In addition, a former PhD student in our lab identified Bcl-2 protein family genes (*Bcl2a1a*, *Bcl2a1b*, *Bcl2a1d* and *Bcl2l1*) significantly upregulated in Roquin-deficient T cells (unpublished data). But so far, no correlation of Roquin and Regnase-1 working together to ensure gene regulation of anti-apoptotic factors was made. Concordantly, in the mRNA-sequencing data I identified *Bcl2l1* expression significantly

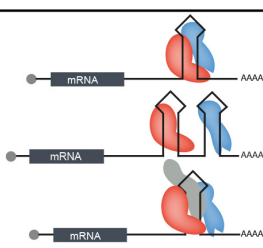


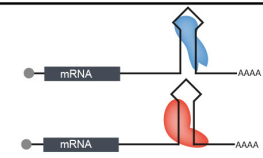
elevated upon knockout of Roquin-1/2 (iDKO), Regnase-1 (iKO) and combined Roquin-1/2 and Regnase-1 (iTKO) in Cluster 4 (Figure 48).

One of the highest differential expressed genes was *Kit* encoding for the transmembrane receptor tyrosine kinase cKit, which interacts with stem cell factor (SCF) produced by stromal cells (Table 21). cKit is expressed in germ cells, hematopoietic stem cells, early hematopoietic progenitors such as double-negative thymocytes (DN1 and DN2) and mast cells. Its expression is lost during cellular differentiation as it is seen for double-negative thymocytes (Waskow et al., 2002). The high differential expression of cKit in T cells lacking Roquin and Regnase-1 ( $\log_2(\text{FC})$  of 5) is very exciting, because so far, its expression on mature T cells was neither reported nor investigated. Very recently, a study on human CD8 T cells and cKit was published (Frumento et al., 2019). Briefly, the authors identified that upon T cell activation cKit expression is induced on CD8 T cells. Thus, cKit expression is linked to TCR signaling and it is conceivable that a TCR-dependent cleavage of Roquin and Regnase-1 by MALT1 releases cKit from being repressed (Jeltsch et al., 2014). Still, the authors did not identify cKit expression on CD4 T cells and all experiments were performed with human T cells. However, this study was a first link between cKit and mature lymphocytes. For future perspectives it would be exciting to test whether Roquin and Regnase-1 together function in dampening the cKit expression on double-negative thymocytes, where cKit is highly expressed. In T cells lacking Roquin and Regnase-1, I saw a remarkable expression of cKit in mature CD4 and CD8 T cells, but I was not able to study their function in early hematopoietic precursors, since *Cd4-cre* deletes loxP-flanked alleles between the late DN and DP stage. One option would be to cross *Rc3h1/2; Zc3h12a<sup>fl/fl</sup>* mice to *vav-cre* mice to achieve deletion in hematopoietic cells and study the function of Roquin and Regnase-1 on cKit expression there. However, this would most probably increase the risk of lethality of these mice. Therefore, it would also be possible to consider an inducible deletion system, such as transgenic mice expressing cre-ERT2 in combination with loxP-flanked alleles of Roquin and Regnase-1. Isolation of the respective cell types such as mast cells or DN thymocytes from these mice and *in vitro* 4'OH-tamoxifen-induced deletion would represent a good tool to study the role of Roquin and Regnase-1 on endogenous cKit expression.

### 5.2.2 Roquin and Regnase-1 enable distinct ways of cooperativity

Since we identified around 1018 genes in cluster 2 and 4, we were wondering if we can identify the major mode of gene regulation by Roquin and Regnase-1. To do so, we compared the differentially expressed genes in the different knockouts with wild-type gene expression. By setting specific thresholds of  $\log_2(\text{FC})$  differential expression (Table 22), I defined four possible major types of gene regulation by Roquin and Regnase-1: cooperative, Regnase-1 exclusive, Roquin exclusive and redundant (**Figure 54**). By applying these definitions, we indeed

identified that the main way of gene regulation by Roquin and Regnase-1 is cooperativity, since 294 genes out of 1018 genes showed this kind of gene expression pattern (Table 22).

	Regnase-1 iKO vs. WT (0h)	Roquin-1/2 iDKO vs. WT (0h)	Roquin-1/2, Regnase-1 iTKO vs. WT (0h)	
 cooperative	+	+	++	
 Roquin-exclusive	-	+	+	
 Regnase-1 exclusive	+	-	+	
 redundant	-	-	+	

- low diff. expr.  
 + intermediate diff. expr.  
 ++ high diff. expr.

**Figure 54 | Schematic representation of different types of regulation by Roquin and Regnase-1.** Modes of gene regulation by Roquin and Regnase-1 are defined by  $\log_2(\text{FC})$  differential gene expression of iDKO, iKO and iTKO vs. WT in unstimulated cells (0h). -: low  $\log_2(\text{FC})$ ; +: intermediate  $\log_2(\text{FC})$  and ++: high  $\log_2(\text{FC})$ . In cooperative target genes, knockout of Regnase-1 and Roquin-1/2 results in increased differential gene expression (+), whereas iTKO gene shows stronger differential expression (++). Roquin and Regnase-1 exclusive target genes are high in the respective knockout (+), not increased in the other knockout situation (-) and similarly high expressed in iTKO vs. WT (+). Redundant target genes are exclusively elevated in the absence of Roquin-1/2 and Regnase-1 (+).

Cooperativity of a *trans*-acting factor, as it was studied in chapter 4.1 for the Roquin targets *Ox40* and *Nfkbid*, can occur on multiple stem loop structures. Since it was reported that Regnase-1 and Roquin interact with similar RNA hairpin structures (Leppek et al., 2013; Mino et al., 2015; Uehata et al., 2013), binding of the same stem loop by Roquin and Regnase-1 or even an interaction of these proteins with each other on the target mRNA could be possible, although a direct interaction has not been reported yet. Studies with chimeric constructs that harbor the ROQ-domain of Roquin fused to Regnase-1 in either Roquin- or Regnase-1-deficient MEF cells, revealed that the RNA-binding domain of Roquin is sufficient to repress an UTR-reporter if artificially fused to Regnase-1 (Jeltsch et al., 2014). Therefore, a functional cooperativity of Roquin and Regnase-1 either on one stem loop or on multiple stem loop structures is possible. We cannot exclude, that additional factors are involved in the mRNP

complex and thus help to induce mRNA degradation. Regnase-1 has been reported to interact with the helicase UPF1 (Mino and Takeuchi, 2015), but an interaction of Roquin with UPF1 has not been described so far. Within cooperatively regulated genes, we identified already described target genes such as *Icos*, *Cebpd*, *Ctla4*, *Furin* and *Nfkbiz* (Appendix 4).

Redundancy and cooperativity are functionally distinct from each other, but experimentally difficult to discriminate. We defined redundant target genes as only de-repressed in the absence of Roquin and Regnase-1, therefore interaction of either one of the RBPs shall be sufficient to confer full regulation. By applying this definition to our target set we identified 52 redundant target genes. Surprisingly, we found only 9 Regnase-1 exclusive target genes, but 87 Roquin exclusive targets.

We tried to also determine the mode of regulation with reconstituted Roquin and Regnase-1 GFP-fusion proteins in WT and inducible Roquin knockout (iDKO) CD4 T cells and could indeed prove different degrees of cooperativity for several of the targets. By comparing GFP-Regnase-1 overexpression to the functionally impaired GFP-Regnase-1(D141N) mutant, conclusions about the dependency on the RNase activity of Regnase-1 can be drawn. We proved our hypothesis on 4 target genes of Roquin and Regnase-1 (Figure 51): *Icos*, *Ctla4*, *Ox40* and *Zc3h12a*.

*Icos* is one of the best-studied Roquin target genes and was identified as cooperatively regulated gene. *Icos* protein expression strongly reacted to Roquin-overexpression in WT and iDKO T cells, but the effect of Regnase-1 overexpression on *Icos* strongly depended on the presence of Roquin and the enzymatic activity of Regnase-1. Consequently, Regnase-1 and Roquin-1 can cooperatively repress *Icos* expression.

*Ctla-4* expression also showed Roquin- and Regnase-1-cooperativity, but in a distinct way as *Icos*. Roquin and Regnase-1 both regulated *Ctla-4* expression, but Regnase-1 functioned independently from Roquin, but required its catalytic activity, suggesting that Roquin and Regnase-1 might target different stem loop structures in the *Ctla4* 3'-UTR.

Intriguingly, Regnase-1 is known to negatively control its own mRNA (Iwasaki et al., 2011; Mino et al., 2015), but Regnase-1 itself also appears as one of the best cooperative target genes, which we already assumed by detecting tremendous amounts of Regnase-1 in Roquin deficient T cells (Figure 41). If Regnase-1 would autoregulate its own expression independently from Roquin proteins as it was described in several studies, it could efficiently downregulate its own mRNA in Roquin-deficient T cells. Indeed, when we overexpressed Regnase-1 in Roquin-deficient cells, the endogenous Regnase-1 expression levels were stable, suggesting that Regnase-1 required Roquin expression to repress its own mRNA (Figure 52). These results disproved the findings of Cui et al., which suggested that Roquin is not able to regulate Regnase-1 and strongly supported our hypothesis of a mandatory cooperative gene regulation by Roquin and Regnase-1.

Analyzing Ox40 regulation by Roquin proteins (chapter 4.1.1), showed that Ox40 is exclusively regulated by Roquin, since knockout of Regnase-1 did not affect Ox40 protein or mRNA expression (Figure 41). This was also verified in the reconstitution experiments: Neither Regnase-1 overexpression nor the Regnase-1(D141N) mutant affected Ox40 expression.

Of the 9 Regnase-1 exclusive target genes, we hardly found a candidate that we could link to T cell immunity. Therefore, I validated *D1ertd622e* encoding for C5orf30 homolog, which we identified per definition as cooperative target gene, but appears much more Regnase-1-dependent (Figure 49). Little is known about the mouse C5orf30 ortholog with regards to T cell immunity or autoimmunity, but human C5orf30 was reported to be highly expressed in rheumatoid arthritis synovial fibroblasts (RASf), which contribute to cartilage damage in RA and loss of C5orf30 commits to the pathology of arthritis (Muthana et al., 2015). Supporting a direct association with Regnase-1, Mino and colleagues enriched C5orf30 in RIP-Seq experiments performed with overexpressed Regnase-1(D141N) in human HeLa cells. Thus, most likely the mouse and human orthologs of C5orf30 are direct target genes of Regnase-1. To prove the impact of Regnase-1 on these target genes it is crucial for future analysis to determine the effect in mice deficient for Regnase-1. For this reason, we are currently generating *Zc3h12a<sup>fl/fl</sup>*; *Cd4-creERT2*; rtTA-M2 (iKO, rtTA) mice to perform inducible reconstitution assays in the absence of Regnase-1.

Hence, most likely Roquin and Regnase-1 exclusive targets do exist as suggested previously (Mino et al., 2015), but cooperatively targeted transcripts are much more abundant.

Recently, a counterplayer of Roquin and Regnase-1, Arid5a has been identified to interact with the ADE-like SL structure in the *Ox40* mRNA and thereby competing with Roquin and Regnase-1 and stabilizing the transcript in T<sub>H</sub>17 cells. Thus, the observed changes upon Roquin and Regnase-1 depletion on mRNA target expression could even appear enhanced due to more accessible binding sites and Arid5a-mediated stabilization (Hanieh et al., 2018; Masuda et al., 2013). However, it is at the moment unclear, whether Arid5a also exerts direct effects on target mRNA expression or whether it only neutralizes Roquin/Regnase-1 effects.

### **5.2.3 The physical interaction of Roquin and Regnase-1 supports the concept of cooperativity**

A most exciting question was whether Roquin and Regnase-1 directly interact with each other, since the widespread cooperativity that we observe may be the result of direct contact. Co-immunoprecipitations with Regnase-1 successfully confirmed that Roquin is bound to Regnase-1, although the signal was weak when compared to the input amount. Nevertheless, this was the first confirmation that Roquin and Regnase-1 physically interact in T cells. In future experiments it would be exciting to validate which domains within Roquin and Regnase-1 are

responsible for the interaction and if this association requires the presence of RNA. Preliminary data generated by my colleague Dr. Gesine Behrens revealed that the *sanroque* mutation of Roquin-1 might be embedded in a putative Regnase-1 interaction surface. Finally, confirming such a molecular function for the M199R mutation, meaning the disruption of Roquin/Regnase-1 binding, may explain how the mutation causes a severe autoimmune phenotype. This would be a breakthrough in understanding the function of Roquin proteins in autoimmunity and a final proof for the importance of the cooperation with the endonuclease Regnase-1, which has been established in this thesis.

### **5.3 Roquin and Regnase-1 are essential regulators of T cell-mediated immune responses**

The cooperation of Roquin and Regnase-1 on the molecular level was also studied by analyzing phenotypic consequences of conditionally deleting Roquin-1, Roquin-2 and Regnase-1 in T cells of mice. These experiments were designed to better understand the cellular processes that are controlled by Roquin and Regnase-1 in the prevention of autoimmunity.

#### **5.3.1 Deficiency of Regnase-1 in T cells affects the cellular composition in the thymus due to cell-extrinsic effects**

I investigated the consequences of a T cell-intrinsic deletion of Roquin and Regnase-1 with respect to the thymic cell composition. The thymus is the organ of T cell development from bone marrow-derived hematopoietic precursors into mature lymphocytes that carry individual antigen-specific TCRs. Several selection processes in the thymus ensure that TCRs recognize their cognate antigen presented on the MHC of an antigen-presenting cell and are self-tolerant to prevent autoimmunity.

The thymi of mice lacking Roquin and Regnase-1 (TKO<sup>T</sup>) showed a drastic reduction in size and absolute numbers. Comparably, Regnase-1 deficiency (KO<sup>T</sup>) alone was already enough to decrease thymocyte numbers. By analyzing the development of CD4 and CD8 single-positive (SP) thymocytes, we realized that the absolute numbers of double-positive (DP) thymocytes was drastically reduced, which was accompanied by elevated double-negative (DN) thymocytes in KO<sup>T</sup> and TKO<sup>T</sup> mice (Figure 23). The development of DN thymocytes into DP is defined by four stages with an initial expression of CD44 in DN1 and DN2, which is replaced by CD25 expression in DN2 and DN3 and then finally lost in DN4. TKO<sup>T</sup> mice have an elevated abundance of DN1 thymocytes. This was unexpected, since *Cd4*-cre-driven

deletion of loxP-flanked alleles occurs between DN4 and the DP stage (Sawada et al., 1994). Therefore, we would rather suggest that this is either a T-cell-extrinsic effect, since the frequency of DN cells was comparable in mixed bone marrow chimeric mice that received TKO<sup>T</sup> bone marrow (Figure 28), or an inappropriate CD44 expression on CD25 negative cells (i.e. on DN4 cells). *Cd44* itself was found as a Regnase-1 target gene and consequently, deletion of Regnase-1 and Roquin-1/2 in DN4 could raise CD44 protein expression and therefore cells that appear as DN1 in flow cytometry due to their high expression of CD44 are actual DN4 cells lacking Roquin and Regnase-1.

The overall loss of size and cellularity has features of thymic involution or thymic atrophy. Thymic involution is a physiological process that arises naturally with aging or stress. In contrast, thymic atrophy can occur either systemically or locally. Local effects occur due to direct infections of the thymus, whereas systemic refers to the consequences of infections outside the thymus that cause thymic atrophy by soluble factors such as glucocorticoids and pro-inflammatory cytokines reaching the thymus through the blood stream (Nunes-Alves et al., 2013). During an acute infection, high glucocorticoids levels can induce rapid apoptotic cell death of DP thymocytes and secretion of pro-inflammatory cytokines such as TNF or IFN- $\gamma$  upon infections can lead to deletion of DP thymocytes mediated by excessive peripheral T cell activation (Deobagkar-Lele et al., 2013). Additionally, stromal cells such as thymic epithelial cells (TECs) are the major source of cytokines in the thymus and can in turn influence thymic atrophy. Aging-associated thymic involution can be sped up by infections, autoimmune diseases and cancer.

Thus, this phenotype could be a result of extrinsic effects due to increased abundance of pro-inflammatory cytokines in the thymus caused by an autoimmune- or autoinflammatory phenotype in the periphery of mice lacking Roquin and Regnase-1 in T cells. To test cell-extrinsic effects, I generated mixed bone marrow chimeric mice (Figure 27). Here, I reconstituted irradiated recipient mice with mixed bone-marrow cells from TKO<sup>T</sup> mice and wild-type mice. Indeed, cells that lack Roquin and Regnase-1 neither showed changes in the total thymocyte numbers nor altered frequencies of the developmental stages of T lymphocytes. This proved that the thymic atrophy in the TKO<sup>T</sup> and KO<sup>T</sup> mice resulted from cell-extrinsic effects such as pro-inflammatory cytokine storm in the thymus which are highly influenced by a loss of Regnase-1.

### 5.3.2 Roquin and Regnase-1 control T cell development

The most striking phenotype of both bone marrow chimeric mice that received Roquin- and Regnase-1-deficient bone marrow and mice with a T cell-conditional deletion of Roquin and

Regnase-1, was the tremendous abundance of regulatory T cells in the thymi of these mice. What are the underlying mechanisms for this aberrant T<sub>reg</sub> development in the thymus?

### 5.3.2.1 Roquin and Regnase-1 affect thymic selection

As described in the introduction, the affinity hypothesis of T cell selection in the thymus suggests that autoreactive T cells with high affinity for self-peptide presented on MHC are clonally deleted, whereas cells without or only very low affinity are prone to die by neglect due to apoptosis. The development of regulatory T cells depends on self-peptide affinity which resembles an intermediate stage between cells receiving normal signal – that then are positively selected and can enter the periphery – and high affinity TCR that undergo clonal deletion (Klein et al., 2014).

I compared the thymic phenotypes of mice conditionally deleted for Roquin and/or Regnase-1 in T cells with the mixed bone marrow chimeric mice to exclude cell-extrinsic effects. The changes of positive selection as well as maturation observed in the conditionally deleted mice were not reproduced in the mixed bone marrow chimeric system (Figure 24 and Figure 29). Nevertheless, we identified tremendous changes in the T<sub>reg</sub> population in both conditionally deleted and mixed bone marrow chimeric mice.

We further assessed if the processes of clonal deletion or apoptosis due to death by neglect are aberrant in the mixed bone marrow chimeric mice. By flow cytometry analysis of intracellular cleaved-caspase 3 in “signaled” and “non-signaled” cells, we indeed found that cells depleted for Roquin and Regnase-1 showed a reduced frequency of death by neglect in comparison to WT cells in the same mouse, whereas clonal deletion of signaled cells was not affected (Figure 30). Hence, we conclude that deficiency of Roquin and Regnase-1 could affect apoptosis during early selection processes in a cell-intrinsic manner. As described in the previous section of the discussion, several anti-apoptotic *Bcl2* genes were identified in the global mRNA-sequencing analysis as potential targets of Roquin and Regnase-1. Intriguingly, apoptosis of thymocytes strongly depends on the pro-apoptotic Bcl-2 family of proteins (Tischner et al., 2010). Here, the pro-apoptotic Bcl-1 homology domain 3 (BH3) only protein Bim promotes apoptosis by binding and inhibiting anti-apoptotic Bcl-2 proteins such as Bcl-2, Bcl-X<sub>L</sub> and Mcl-1 which further directly suppress Bax and Bak that disrupt mitochondrial membrane integrity (Youle and Strasser, 2008). Mice systemically devoid of Bim develop a SLE-like autoimmune disease, indicative of a breakdown in tolerance due to a loss of apoptotic events (Bouillet et al., 1999). Interestingly, *Bcl2l1* is a direct target of the transcription factor c-Rel and upregulated in cells expressing a paracaspase-inactive MALT1 point mutant (Gewies et al., 2014). Therefore, upregulation of *Bcl2l1* or *Bcl2a1* might be a downstream effect of increased canonical NF-κB activity by cRel, which is strongly induced in Roquin and Regnase-



1-deficient T cells, since *cRel* itself is a target for Roquin- and Regnase-1-mediated mRNA decay (Jeltsch et al., 2014). Whether pro-apoptotic genes such as *Bcl2/1* are direct target transcripts of Roquin and Regnase-1 or whether the altered expression is due to an increase of the target *cRel* is not proven yet. However, negative selection - a process that also involves apoptosis - seemed to be unchanged in the mixed bone marrow chimeric mice receiving Roquin- and Regnase-1-deficient bone marrow. It was reported that a balance between pro-apoptotic and anti-apoptotic factors governs the degree of apoptosis. Negative selection is induced upon strong TCR stimulation which causes translocation of Nur77 and Nor-1 from the nucleus to the mitochondria. Here, these proteins bind Bcl2 resulting in the exposure of Bcl2's BH3 domain, which promotes inhibition of anti-apoptotic factors such as Bcl-X<sub>L</sub> (Kolluri et al., 2008; Thompson and Winoto, 2008). Thus, this signal could outcompete the increased anti-apoptotic Bcl-X<sub>L</sub> expression in Roquin- and Regnase-1-deficient T cells. Consequently, the effect of Roquin and Regnase-1 on apoptosis could become only visible in a non- or low-TCR signaling situation such as death by neglect.

#### **5.3.2.2 Deregulation of cRel and I $\kappa$ B<sub>NS</sub> correlates with altered T<sub>reg</sub> development**

The remarkable changes of gene expression in CD4 T cells lacking Roquin and Regnase-1 as shown by global mRNA-sequencing supports the idea that altered gene expression highly influences T cell immunity and development.

As outlined in Figure 26 and Figure 31, the expression of the Roquin and Regnase-1 target genes *cRel* and *Nfkbid* is highly elevated during T<sub>reg</sub> developmental stages in the thymus of mice lacking Roquin and Regnase-1 as well as in the mixed bone marrow chimeric mice. Many studies have investigated the direct influence of cRel on the induction of the master transcription factor Foxp3. Besides binding to its conserved non-coding regions (CNS) within the *Foxp3* locus thereby triggering demethylation of CNS2, recruitment of a cRel-enhanceosome at the Foxp3 promoter and direct binding to CNS3 and causing TCR and co-stimulatory signals to induce *Foxp3* expression have been reported (Long et al., 2009; Zheng et al., 2010). Supporting evidence therefore is the loss of regulatory T cells by deleting *cRel* in mice (Ruan et al., 2009). Studies on *cRel*- and *Nfkbid*-deficient mice have demonstrated that both factors are mandatory for the development of regulatory T cells in the thymus (Schuster et al., 2012; Schuster et al., 2017). Therefore, Roquin and Regnase-1 together are likely to shape thymic T<sub>reg</sub> development by regulating their target genes *cRel* and *Nfkbid* post-transcriptionally. Upon loss of function of both post-transcriptional regulators we hypothesize derepression of their targets in thymocytes, which would normally become conventional T cells

after positive selection in the thymus. However, mis-expression of  $I\kappa B_{NS}$  and  $cRel$  in these cells may switch their fate and make them become  $T_{reg}$  cells.

### 5.3.2.3 Model for clonal selection in the thymus under the control of Roquin and Regnase-1

The model in Figure 55 is a hypothesis that I assembled according to the observations I made in the mixed bone marrow chimeric mice. The mixed bone marrow chimeras that received Roquin-and Regnase-1-deficient bone marrow showed less frequencies of cells that die by neglect and a tremendous gain of thymic regulatory T cells.

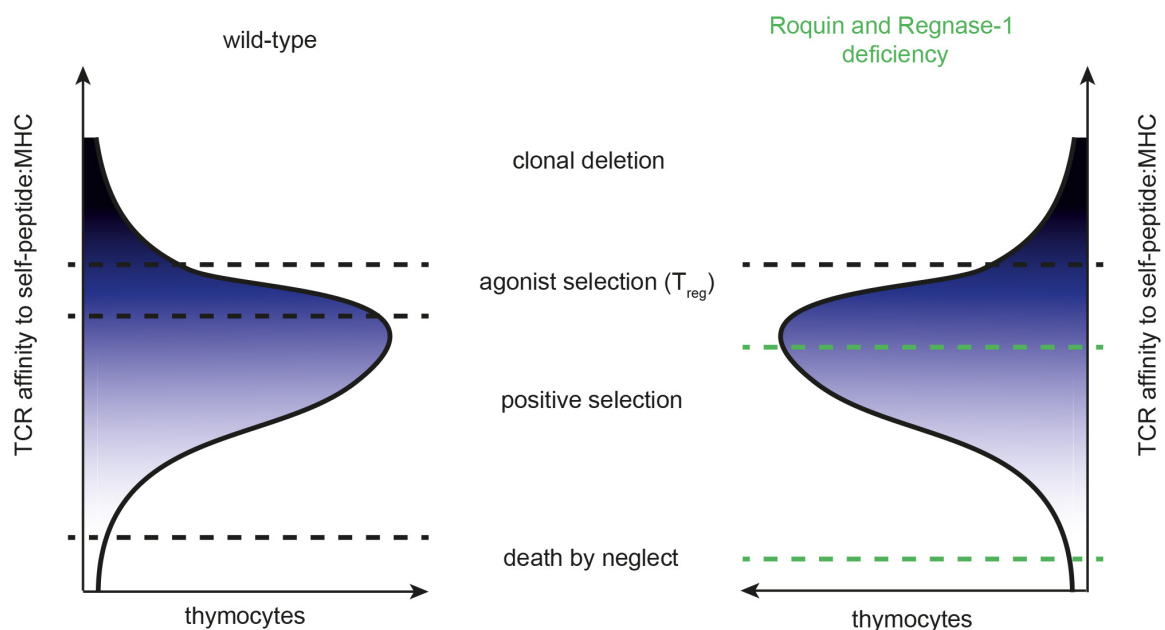


**Figure 55 | Model for changes in the selection processes in mice with a T-cell-intrinsic deletion of Roquin and Regnase-1.**

The left model shows the general affinity hypothesis which proposes that the reactivity of TCRs for self-peptide:MHC defines cell fates of thymocytes. Cells without a TCR or a TCR with very low affinity die by neglect due to apoptosis, whereas double positive thymocytes that have low affinity undergo positive selection and become mature CD4 or CD8 T cells. Strong affinity to self-peptide presented on MHC results in clonal deletion by apoptosis to avoid self-reactivity of thymocytes. However, the agonist selection of self-reactive regulatory T cells occurs in a window of positively and negatively selected thymocytes. T cells depleted for Roquin and Regnase-1 have reduced frequencies of cells that die by neglect, but show a higher proportion of thymic-derived regulatory T cells and no difference for clonal deletion (right model).

In summary, Roquin and Regnase-1 could influence clonal selection by several mechanisms including target gene regulation such as *cRel*, *Nfkbid* or *Bcl2a1* directly affecting  $T_{reg}$  development or apoptosis. This could on the one hand reduce apoptosis in non-signaled cells and on the other hand force positively selected conventional T cells in the thymus to become regulatory T cells in mice deficient for Roquin and Regnase-1. Consequently, conventional T

cells with normal TCR affinity might convert to regulatory T cells. Thus, the repertoire of regulatory T cells is diluted resulting in less self-reactive TCRs that might be incapable of suppressing autoreactive T cells in the periphery.

Of course, changes in the TCR repertoire with altered TCR affinity could explain the drastic abundance of regulatory T cells in the thymus. Many autoimmune diseases have been linked to alterations in the TCR repertoire and this may be one explanation for the break of peripheral tolerance. In contrast to a healthy, normal individual with randomly rearranged TCRs, the TCRs in an autoimmune-prone environment is biased in its distribution. The reason therefore might be the exposure of autoantigens and epitope expansion (Jia et al., 2018).

However, the influence of Roquin and Regnase-1 on V(D)J-recombination is rather unlikely. The possibility that deficiency of Roquin and Regnase-1 causes changes in the TCR repertoire needs to be further proven. One option to validate the TCR repertoire is to perform single-cell next-generation sequencing, which provides information on paired alpha and beta chains of individual cells. An additional possibility would be to cross the  $\text{TKO}^T$  mice to a Nur77-GFP reporter mouse. *Nur77* is an immediate early gene expressed upon TCR stimulation in T cells and would allow to track TCR signaling throughout clonal selection in mice lacking Roquin and Regnase-1. To test whether Roquin and Regnase-1 influence downstream TCR signaling, one could isolate CD4 or CD8 thymocytes of these mice and stimulate the cells *ex vivo* with anti-CD3 and anti-CD28 and check for signaling strength of downstream pathways such as ERK signaling.

### 5.3.3 Roquin and Regnase-1 cooperatively prevent autoimmunity

Another focus of this thesis was to investigate the influence of Roquin and Regnase-1 on T cell functions in the periphery. Comparing the phenotypes of peripheral lymphoid organs in the conditional knockout mice with the data obtained by mixed bone-marrow chimeras, revealed that Roquin and Regnase-1 influence activation of CD4 and CD8 T cells and the germinal center reaction resulting in increased formation of  $T_{FH}$ ,  $T_{FR}$  and GC B cells. Interestingly, these features display multiple characteristics of systemic lupus erythematosus (SLE). Due to diverse phenotypes of patients suffering from SLE, it was proposed that SLE is a polygenic disease (Lohr et al., 2005). The previously described *sanroque* mouse is an outstanding mouse model thereof and underscores the importance of the RNA-binding protein Roquin-1. However, the exact mechanism of how a single point mutation in the ROQ-domain weakens the control over autoimmunity by Roquin-1 is not elucidated, yet. Interestingly, mice lacking Roquin and Regnase-1 together in T cells also reveal a comparable SLE-like autoimmune phenotype. A critical issue was whether Roquin and Regnase-1 together control autoimmunity in a cooperative manner.

### 5.3.3.1 Roquin and Regnase-1 reduce the activation threshold of T cells in a cooperative manner

Splenomegaly and lymphadenopathy are characteristics of SLE-like autoimmune diseases. We identified that mice devoid of Regnase-1 ( $\text{KO}^T$ ) and Roquin-1/2 and Regnase-1 ( $\text{TKO}^T$ ) in T cells had a drastic gain of spleen and lymph node sizes in comparison to WT mice, which was less severe in  $\text{DKO}^T$  mice (Figure 33).  $\text{TKO}^T$  mice developed hyperactivated CD4 and CD8 T cells, whereas the effector-memory phenotype of CD4 T cells depended on both Roquin and Regnase-1 equally, but the activation of CD8 T cells was more under the control of Roquin (Figure 34). Thus, CD8 T cell activation seems to be more dependent on the presence of Roquin, which is further supported by the phenotype of mice devoid of Roquin-1 only in T cells having more activated CD8 T cells (Table 18).

Overall, the accumulation of highly activated T cells could be a consequence of potentially non-functional regulatory T cells in combination with inappropriate co-stimulation which could select these T cells for aberrant T cell activation and subsequent T helper cell differentiation. In the following, the co-stimulatory receptors that potentially influence the hyperactivation of T cells in mice devoid of Roquin and Regnase-1 in T cells are discussed.

The co-stimulator *Icos* is one of the best-studied target genes of Roquin and Regnase-1 and has been reported by several studies to confer essential roles in T cell activation, proliferation, cytokine production and humoral immune responses (Dong et al., 2001). I identified *Icos* in the mRNA-sequencing analysis as cooperative target gene of Roquin and Regnase-1 (Figure 49 and Figure 50). The aberrant *Icos* expression both on protein and RNA level in mice lacking Roquin, Regnase-1 and all three proteins suggests that *Icos* co-stimulatory signaling might strongly influence T cell activation. The post-transcriptional control over *Icos* expression by Roquin and Regnase-1 proteins is further supported by mixed bone-marrow chimeric mice that were reconstituted with a mix of cells lacking Roquin and Regnase-1 and wild-type cells that exhibit a huge increase in frequencies of activated CD4 and CD8 T cells and T follicular helper cells (Figure 37).

Besides *Icos*, *Ox40* is important for the survival of T effector cells (Weinberg, 2010). Constitutive *Ox40* expression through transgenic expression of *Ox40L* on T cells results in a massive induction of effector-like CD4 T cells (Murata et al., 2002). The mRNA-sequencing and flow cytometry data revealed that *Ox40* exhibits exclusive gene regulation by Roquin both on mRNA and on protein level (Figure 49 and Figure 50). Thus, the impairment of regulating *Ox40* both in  $\text{DKO}^T$  as well as  $\text{TKO}^T$  mice contributed to the effector-memory phenotype of CD4 T cells in these mice. Next to *Ox40*, another TNF-receptor family protein, *CD30*, was

identified by mRNA-sequencing as a new potential cooperative target gene of Roquin and Regnase-1 (Figure 48). Intriguingly, deficiency of *Ox40* and *CD30* in *scurfy* mice deficient for *Foxp3* rescued those mice from developing autoimmunity (Gaspal et al., 2011). Thus, an aberrant synergistic expression of CD30 and Ox40 on the surface of T cells in mice depleted for Roquin and Regnase-1 could contribute to the development of autoimmunity.

Mice deficient for Roquin and Regnase-1 in T cells have high abundance of Ctla-4, suggesting that Roquin and Regnase-1 together control its degradation and thereby confirm a functional T cell activation. Nevertheless, high Ctla-4 levels on T cells deficient for Roquin and Regnase-1 are in contradiction to the strong T cell activation, since Ctla-4 dampens T cell activation by competitive binding to CD80/CD86 thereby preventing CD28 activation. Ctla-4 is primarily an intracellular protein, stored in intracellular vesicles, and its surface expression is under strict control since minor changes of surface expression highly impact T cell activation (Tai et al., 2012). Therefore, it is likely that the major Ctla-4 levels measured by flow cytometry are intracellular and therefore not functioning on the surface. Or, Ctla-4 expression on the surface is not sufficient to dampen T cell activation and is thus outcompeted by strong expression of co-stimulatory receptors such as Icos and Ox40 that in turn induce strong activation of T cells. The impact of Roquin and Regnase-1 on CD8 T cell function and activation now involves a potential of the Roquin/Regnase-1-dependent CD8 T cells in anti-tumor immunity, and in response to the CTLA-4 blocking antibodies used in the clinics, which will be investigated in a new research project of our lab.

Based on these observations it is reasonable that loss of Roquin-1, Roquin-2 and Regnase-1 can cause a reduction of the activation threshold of T cells by controlling the expression of several co-stimulatory receptors. Since almost all of the polyclonal T cells become activated upon loss of Roquin/Regnase-1 expression, it appears likely that activation occurs in the absence of cognate antigen recognition. This is in line with the observed phenotype in the thymus, where death by neglect is potentially evaded due to a lower activation threshold (Figure 55).

#### **5.3.3.2 Roquin and Regnase-1 cooperativity is essential for the humoral immune response**

My data support the idea that Roquin and Regnase-1 together control the germinal center (GC) reaction, since a knockout of either Roquin or Regnase-1 or all three proteins in T cells resulted in a drastic increase in T follicular helper cell frequencies (Figure 35). In accordance with that, the frequency of B cells in the germinal centers correlated with T<sub>FH</sub> accumulation.

Altered expression of Icos in T<sub>FH</sub> cells is observed in several autoimmune diseases such as SLE and its expression is mandatory for the generation and function of T<sub>FH</sub> formation, for their

help during GC formation and antibody class switching (Odegard et al., 2008). Consequently, the drastic induction of  $T_{FH}$  cells and GC B cells in mice lacking Roquin and Regnase-1 conditionally in T cells could be explained by an abnormal surface expression of Icos. Blocking the interaction of Icos with its ligand on B cells by using a monoclonal antibody directed against Icos-L has been reported to inhibit  $T_{FH}$  development and reduce anti-dsDNA antibody titers in the NZB/NZW (New Zealand Black and New Zealand White) autoimmune mouse model, suggesting a mandatory and also a driving role for Icos on the surface of follicular T helper cells (Hu et al., 2009). However, deleting *Icos* in *sanroque* mice, did not rescue the strong  $T_{FH}$  cell accumulation. Instead, it was later shown that an excessive production of  $IFN-\gamma$  causes the formation of  $T_{FH}$  cells in *sanroque* mice which is accompanied by a bias towards  $T_H1$  cell differentiation (Lee et al., 2012). A systemic  $IFN-\gamma$  production was similarly observed upon deletion of Regnase-1 in T cells (Cui et al., 2017). Interestingly, the Ox40L-Ox40 axis on T cells positively influences  $T_{FH}$  cell formation and the generation of autoantibodies in humans (Ueno and Blanco, 2015), suggesting that elevated levels of Ox40 on T cells deficient for Roquin and Regnase-1 might contribute to the formation of T follicular helper cells.

Besides a tremendous induction of  $T_{FH}$ , GC B cells and  $T_{reg}$  cells in the periphery of  $TKO^T$  mice, I identified that T cells lacking Roquin and Regnase-1 also adapt a T follicular regulatory T ( $T_{FR}$ ) cell phenotype in a cell-intrinsic manner (Figure 35 and Figure 38). Again, the high Icos expression on T cells deficient for Roquin and Regnase-1 might in addition contribute to the conversion of regulatory T cells to  $T_{FR}$  cells. Intriguingly, deficiency of  $T_{FR}$  cells has been associated with the development of autoimmunity and enhanced autoantibody production, suggesting that  $T_{FR}$  cells dampen humoral autoimmunity (Fu et al., 2018). In Sjogren's syndrome patients, elevated  $T_{FR}$  and  $T_{FH}$  cells correlated with disease severity (Fonseca et al., 2018).

Surprisingly, hypergammaglobulinemia was only partially seen in mice lacking Roquin in T cells, whereas the greatest effects appeared in mice devoid of Regnase in either  $KO^T$  or  $TKO^T$  mice. Significant changes were only detectable for the immunoglobulin subclass IgM. Interestingly, elevated serum IgM levels are associated to several autoimmune diseases such as SLE or RA (Nguyen and Baumgarth, 2016) and could thus be a consequence of Roquin- and Regnase-1-deficiency-driven autoimmunity.

To our surprise, autoantibodies against ds-DNA were massively abundant in mice deficient for Regnase-1 in T cells, whereas  $TKO^T$  mice had less profound autoantibody secretion and mice with depletion of Roquin were completely devoid of autoantibodies which is in line with previously published data (Jeltsch et al., 2014). Why is the production of autoantibodies stronger in mice with a Regnase-1-deficiency in T cells than mice with a T cell-driven depletion of Roquin and Regnase-1? One explanation might be that  $TKO^T$  mice have a higher abundance of  $T_{FR}$  cells that could potentially dampen autoantibody production. Additionally,

the severity of autoimmunity is weaker than in mice with a T cell-specific deficiency of Regnase-1 alone, which correlates with the production of autoantibodies. Notably, our group found that serum from conditional Roquin-deficient mice contains antibodies reactive to pancreatic antigens, suggesting that these mice have the potential to produce autoantibodies (Jeltsch et al., 2014). However, the differences in the autoantibody productions cannot be explained on the basis of the GC reaction, since we did not observe a positive correlation between activation of T cells,  $T_{FH}$  differentiation and the abundance of GC B cells. From the mRNA-sequencing data in CD4 T cells, we know that deficiency of Roquin and Regnase-1 together and depletion of Roquin alone causes strong perturbations in the gene regulation, whereas Regnase-1-deficiency only mildly affects gene expression (Figure 45). Potentially, the strong alterations in gene expression in mice deficient for Roquin and Regnase-1 ( $TKO^T$ ) and Roquin ( $DKO^T$ ) in T cells might exceed a tolerated threshold for the production of autoantibodies, which is not reached in  $KO^T$  mice, yet.

#### **5.3.4 Roquin- and Regnase-1-deficiency causes expansion of non-functional $T_{reg}$ cells in the periphery**

Interestingly, when I analyzed the mixed bone marrow chimeric mice that received bone marrow from WT and  $TKO^T$  mice, I realized that the abundance of regulatory T cells is unchanged for those cells lacking Roquin and Regnase-1 when compared to wild-type cells within the same mouse (Figure 38). This was different to the data obtained in the  $TKO^T$  mice, where I observed a strong increase in the regulatory T cell compartment in spleens of  $TKO^T$  mice, but  $DKO^T$  and  $KO^T$  mice showed an even higher frequency of peripheral regulatory T cells. Why is there a discrepancy between the phenotypes of the mixed bone marrow chimeric mice and the conditionally deleted mice?

I would hypothesize that the expansion of regulatory T cells in the periphery of conditionally deleted mice is rather a result of inflammatory conditions, which is supported by the mixed bone marrow chimera experiment representing a non-inflamed situation. Due to the mixed bone marrow situation, regulatory T cells originated from wild-type bone marrow dampen inflammations, which potentially prevents the expansion of  $T_{reg}$  cells from  $TKO^T$  bone marrow in the same mouse. Under inflammatory conditions the conversion of  $T_{reg}$  cells to  $T_H17$ -like  $T_{reg}$  cells has been reported (Voo et al., 2009). However, whether the regulatory T cells in the conditionally deleted mice express the  $T_H17$  transcription factor ROR- $\gamma$ T or secrete IL-17 must be addressed in future experiments.

One important question still is why the tremendous abundance of regulatory T cells cannot rescue the autoimmune phenotype in T cell specific Roquin- and Regnase-1-deficient mice.

There are several possibilities that could explain these observations.

First, the  $T_{reg}$  cells might not have the correct TCR specificity to neutralize the autoreactive T cells in the  $TKO^T$  mice. If we assume that conventional T cells in the thymus with a potentially lower TCR-affinity become  $T_{reg}$  cells as described above, these regulatory T cells would not be able to suppress autoreactive T cells in the periphery. This can to date not be excluded and therefore, the TCR repertoire needs to be determined in future experiments.

The latter hypothesis is supported by studies that have demonstrated that regulatory T cells with reduced CD25 expression are completely unfunctional due to the requirement of IL-2R-signaling for functional programming and activity of regulatory T cells and that these mice are prone to develop autoimmunity (Chinen et al., 2016; Toomer et al., 2019). Thus, the suppressive capacity of the regulatory T cells from mice with a T cell-specific loss of Roquin and Regnase-1 is attenuated due to a higher proportion of  $CD25^- T_{reg}$  cells with an inappropriate functionality (Figure 31). This was already proven for Roquin-deficient regulatory T cells, since these cells were incapable of protecting mice from T cell-transfer-induced colitis in comparison to wild-type control  $T_{reg}$  cells when injected together with naïve CD4 T cells (Essig et al., 2017).

And finally, regulatory T cells originated in mice lacking Roquin and Regnase-1 could be instable or have an altered plasticity. The strong regulatory T cell abundance in the thymus was not reflected in the periphery of mixed bone marrow chimeric mice receiving  $TKO^T$  bone marrow cells (Figure 38). Appropriately, the frequencies of  $T_{FR}$  cells were drastically increased in the mixed bone marrow chimeric mice, proposing that thymic derived regulatory T cells rather adapted a follicular regulatory T cell phenotype in the absence of Roquin and Regnase-1. I noticed that regulatory T cells lacking CD25 already in the thymus are highly abundant in mice that were reconstituted with bone marrow devoid of Roquin and Regnase-1 expression in comparison to wild-type bone marrow cells (Figure 31). This is in line with a previously published study, where mice with a  $T_{reg}$ -specific deletion of the Roquin paralogs lost CD25 and rather adapted a  $T_{FR}$ -phenotype (Essig et al., 2017). Indeed, it has been reported that  $CD25^-$ ,  $Foxp3^+$  T cells can adapt a highly flexible phenotype and develop into germinal center-resident  $T_{FR}$  cells (Wing et al., 2017). The fact that  $T_{FR}$  cells differentiate from thymic-derived naïve  $Foxp3^+$  precursors (Linterman et al., 2011), further support the hypothesis that the thymic regulatory T cells in the  $TKO^T$  mice adopt a  $T_{FR}$  phenotype in the periphery.

### 5.3.5 The fate of $T_H17$ cells is under control of Roquin and Regnase-1

The tremendous activation of T cells prompted us to also investigate the bias of T cells lacking Roquin and Regnase-1 to differentiate towards the T helper cell lineages (Figure 1).



We assessed expression of the signature cytokines and transcription factors of T<sub>H</sub>1 (IFN- $\gamma$ ), T<sub>H</sub>2 (IL-4), T<sub>H</sub>17 (IL-17A) or T<sub>reg</sub> (CD25 and Foxp3) CD4 T cells in either CD4 T cells of mice depleted of Roquin or Regnase-1 in T cells (Figure 39) or naïve CD4 T cells from inducible knockout mice, that have been deleted *in vivo* by administration of tamoxifen and were differentiated towards T<sub>H</sub>1, T<sub>H</sub>17 and T<sub>reg</sub> *in vitro* (Figure 40).

The relatively low bias towards IFN- $\gamma$  producing T<sub>H</sub>1 T cells that we observed in Roquin-deficient T cells is in accordance with previous investigations we made in our laboratory (Jeltsch et al., 2014; Vogel et al., 2013). There was a strong trend towards high IFN- $\gamma$  expression of all knockouts in comparison to wild-type, but was not significant. As mentioned previously, increased IFN- $\gamma$  production was linked to autoimmunity in *sanroque* mice and caused accumulation of T<sub>H</sub>1 cells. Moreover, conditional deletion of Regnase-1 in T cells either alone or in combination with the *sanroque* mutation induced IFN- $\gamma$ -expressing cells that infiltrated into multiple organs (Cui et al., 2017). Some studies suggested that Roquin regulated the expression of the *Ifng* mRNA, but whether this effect is direct or indirect is still not solved (Li et al., 2007; Vinuesa et al., 2005; Yu et al., 2007).

Especially, IL-17 showed strong Roquin-dependency, since the increase in expression was comparable in T cells from TKO<sup>T</sup> and DKO<sup>T</sup> mice, but milder in Regnase-1-deficient KO<sup>T</sup> mice. Recent literature already suggests that Roquin and Regnase-1 control T<sub>H</sub>17 differentiation by regulating genes that confer essential roles in this differentiation pathway (Jeltsch et al., 2014). The atypical NF- $\kappa$ B inhibitor I $\kappa$ B<sub>NS</sub> and I $\kappa$ B $\zeta$  and the NF- $\kappa$ B transcription factor cRel and Irf4 are required for efficient T<sub>H</sub>17 differentiation and their function influence susceptibility to murine autoimmune diseases such as experimental autoimmune encephalomyelitis (Annemann et al., 2015; Brustle et al., 2007; Chen et al., 2011; Kobayashi et al., 2014). Since Roquin knockout had a stronger effect on IL-17A expression than the single Regnase-1-deficiency, I would assume that the robust regulation of I $\kappa$ B<sub>NS</sub> as it was discussed in section 4.1.2 by Roquin dominantly influences the effect on T<sub>H</sub>17 differentiation, since the expression of several cytokines such as IL-17A, IL-17F and IL-10 is dependent on I $\kappa$ B $\zeta$  and additionally I $\kappa$ B<sub>NS</sub>. Nevertheless, in T cells from TKO<sup>T</sup> mice, the abundance of IL-17-producing cells was still higher in both analyzed systems. Therefore, I would suggest that a combination of de-repressed Roquin and Regnase-1 target genes might strongly influence T<sub>H</sub>17 differentiation and prevent autoimmunity, since aberrant expansion of T<sub>H</sub>17 cells has been linked to autoimmunity such as multiple sclerosis.

The cell fate decision of either T<sub>H</sub>17 or T<sub>reg</sub> cells is reciprocal since both T cell subsets are induced in the presence of TGF- $\beta$ . T<sub>H</sub>17 differentiation is favored together with pro-inflammatory cytokines such as IL-6 or IL-21, whereas regulatory T cell differentiation in the periphery occurs in the absence of these pro-inflammatory signals, but is promoted by IL-2

(Bettelli et al., 2006). The balance of  $T_H17$  and  $T_{reg}$  differentiation is critical in many autoimmune diseases such as RA and MS and a mis-regulation thereof can cause autoimmunity. Consistent with increased  $T_H17$  differentiation, we found in the *in vitro* differentiation system that regulatory T cell fate is decreased in T cells lacking Roquin and Regnase-1. This loss of CD25 and Foxp3 expression is gradually decreasing with Roquin and Regnase-1 deletion, which is also in accordance with our previously published data showing that Roquin-deficient T cells differentiate less efficiently into  $iT_{reg}$  (Jeltsch et al., 2014). CD4 T cells from  $TKO^T$  mice that were stimulated *ex vivo* showed increased expression of IL-10 and CD25. This result is in contradiction to the data obtained by direct  $T_{reg}$  differentiation *in vitro*. The cytokine IL-10 is produced by a variety of T helper cell subsets and is therefore not an ideal signature cytokine for  $T_{reg}$  determination. Therefore, the data obtained by *in vitro* differentiated T cells are more revealing and the Foxp3 expression in the *ex vivo* data will have to be addressed in future experiments. Thus, I would conclude that Roquin- and Regnase-1-deficient CD4 T cells receiving signals in the periphery rather favor to differentiate into the  $T_H17$  cell fate than into the reciprocal fate of regulatory T cells, which is supported by the cytokine expression profiles in the knockout mice, and that the elevated frequencies of  $T_{reg}$  cells in the  $TKO^T$  mice is rather a result of strong inflammation in these mice.

The expression of the  $T_H2$  signature cytokine IL-4 was assessed in *ex vivo* isolated T cells since the *in vitro* differentiation of  $T_H2$  cells was not efficient. The elevated expression of IL-4 in T cells from mice lacking Roquin and Regnase-1 was rather influenced by Regnase-1, since Regnase-1-deficient T cells also expressed higher levels of IL-4, whereas Roquin-deficiency did not alter IL-4 production. Cui et al. investigated the expression of  $T_H2$  signature genes such as *Ii4* and *Gata3* and found that Regnase-1-deficiency caused upregulation of these genes, whereas gene expression in *sanroque* T cells was unchanged. Therefore, an exclusive function for Regnase-1 in controlling  $T_H2$  differentiation is possible.

Collectively, I demonstrated that Roquin and Regnase-1 control T cell activation and differentiation, since the absence of Roquin and Regnase-1 in T cells causes an unphysiological expression of several cytokines and subset-specifying transcription factors. Roquin and Regnase-1 cooperatively control peripheral  $T_H17$  and potentially thymic  $T_{reg}$  cell fate decisions, whereas Regnase-1 might additionally contribute to  $T_H2$  responses. TCR activation triggers MALT1-induced cleavage of Roquin and Regnase-1 proteins during T cell activation, which emphasizes the importance of these RNA-binding proteins during T cell fate decisions. How TCR signaling strength influences the expression of Roquin and Regnase-1 target genes is addressed by a colleague in a different research project.

### 5.3.6 Summarizing the phenotypes of different Roquin and Regnase-1 mouse models

Table 23 summarizes the phenotypes observed in mice deficient for Regnase-1 ( $KO^T$ ), the Roquin paralogs ( $DKO^T$ ) and a triple-knockout of Roquin and Regnase-1 ( $TKO^T$ ) in T cells in comparison to WT mice. To distinguish between cell-intrinsic and -extrinsic effects, I generated mixed bone marrow chimeric mice that were irradiated and reconstituted with mixed bone marrow from wild-type or Regnase-1-/Roquin-1/2-T-cell-deficient mice ( $TKO^T$   $CD45.2$ ).

Intriguingly, most observed phenotypes in the thymus were stronger in T cells devoid of Regnase-1 in comparison to Roquin-deficient mice. One explanation therefore might be that all mice were analyzed at an age of 5-6 weeks, since the  $KO^T$  and  $TKO^T$  mice became sick. At this point, Roquin-deficient mice were still healthy and therefore it might be interesting to analyze thymic development in older mice. Additionally, Regnase-1 was described to interact with the helicase UPF1 to induce mRNA degradation. UPF1 is an essential factor in nonsense-mediated decay, a process in which transcripts with a pre-mature stop codon are targeted for degradation. UPF1 itself was described to play an important role during T cell development, whereby impaired function of UPF1 and UPF2 proteins cause reduced thymocyte development due to a stabilization of out-of-frame transcripts (Frischmeyer-Guerrero et al., 2011).

**Table 23 | Comparing phenotypes of *Cd4*-cre driven deletions of Roquin and Regnase-1 mouse models and mixed bone marrow chimeric mice.**

Summary of phenotypes in mice conditionally devoid of Regnase-1 ( $KO^T$ ), Roquin-1/2 ( $DKO^T$ ) and Roquin and Regnase-1 ( $TKO^T$ ) in T cells compared to cells from mixed bone marrow chimeric mice reconstituted with wild-type and bone marrow from  $TKO^T$  mice ( $TKO^T$   $CD45.2$ ). -: no change in relation to wild-type control, --: reduced frequency in comparison to wild-type, +: increased frequency in comparison to wild-type control, ++: very strong increase in frequency in comparison to wild-type control and /: not analyzed.

		$KO^T$	$DKO^T$	$TKO^T$	$TKO^T$ $CD45.2$
thymus	T cell development	+	-	+	-
	death by neglect	/	/	/	--
	positive selection	-	-	+	--
	nT <sub>reg</sub>	++	+	++	++
	negative selection	/	/	/	-
periphery	EM CD4	+	+	++	++
	EM CD8	+	++	++	++
	T <sub>FH</sub>	+	+	++	++
	GC B cells	+	+	++	/
	hypergammaglobulinemia	+	-	+	/
	autoantibodies	++	-	+	/
	T <sub>FR</sub>	+	+	++	++
	iT <sub>reg</sub>	++	++	+	-
cytokine expression	iT <sub>reg</sub>	+	+	-	/
	T <sub>H</sub> 1	-	-	-	/
	T <sub>H</sub> 2	+	-	+	/
	T <sub>H</sub> 17	+	++	++	/

Indeed, we do see cell-intrinsic effects such as hyperactivation of T cells or thymic regulatory T cell accumulation in the mixed bone marrow chimeric mice that received Roquin- and Regnase-1-deficient bone marrow, but we cannot distinguish if the effect solely derived from lacking Regnase-1 in T cells or if Roquin additionally contributed. Therefore, addressing the single contributions of Roquin and Regnase-1 in bone marrow chimeric mice with mixed bone marrow from wild-type and either DKO<sup>T</sup> or KO<sup>T</sup> mice would be one interesting future experiment.

Mice with Roquin- and Regnase-1-deficiency in T cells developed a strong autoimmune phenotype in the periphery, suggesting that Roquin and Regnase-1 cooperatively function in the control of autoimmunity, especially by tightly regulating the step of T cell activation and T helper cell fate commitment. Here, cooperative control by both Roquin and Regnase-1 was observed for T<sub>H</sub>17 differentiation and T<sub>H</sub>1 differentiation was also slightly affected. The strong abundance of regulatory T cells in the periphery of TKO<sup>T</sup>, DKO<sup>T</sup> and KO<sup>T</sup> mice is most probably due to inflammatory conditions resulting in an expansion of peripheral T<sub>reg</sub> cells.

The phenotypes of the Roquin and Regnase-1 mouse models support our hypothesis that Roquin and Regnase-1 have overlapping functions in the immune system by cooperatively controlling transcript expression that regulates not only the activation and differentiation of CD4 and CD8 T cells, but in addition the GC reaction. However, individual contributions of Roquin and Regnase-1 are also possible, since some phenotypes exclusively depend on Regnase-1 (T<sub>H</sub>2 differentiation) and Roquin (CD8 T cell activation).

In summary, this research project helped to gain novel insights into the cellular functions of Roquin and Regnase-1. I was able to identify that Roquin and Regnase-1 strongly impact on regulatory T cell development in the thymus, the activation threshold of T cells and the germinal center reaction controlling humoral immune response and autoimmunity and most of these phenotypes equally depended on Regnase-1 and Roquin.

### **5.3.7 Can we connect the mouse phenotypes with the global mRNA expression data?**

Strikingly, Regnase-1-abrogation in T cells caused a strong autoimmune phenotype in these mice characterized by an enormous induction of autoantibodies (Figure 35). However, mRNA-sequencing analysis of Regnase-1-deficiency in CD4 T cells revealed only a very mild change in the overall gene expression (Figure 44).

Since the mRNA-sequencing analysis was only performed on *in vitro* cultured T<sub>H</sub>1 cells, the strong autoimmunity could still result from other T cell subsets such as T<sub>reg</sub> cells or CD8 T cells or might only be detectable *in vivo*. Although the effect on CD8 activation was stronger in mice lacking Roquin than those devoid of Regnase-1 in T cells and therefore this might be unlikely.

However, the impact of CD8 T cells on the production of autoantibodies is still uncertain and therefore the absence of autoantibodies could be reasoned in hyperactivated CD8 T cells that lack Roquin. Additionally, I could imagine that the strong effect of Regnase-1 on the pro-inflammatory cytokine IL-6 might severely impact the immunological environment. Excessive IL-6 production induces a life-threatening complication, termed cytokine storm, and causes chronic autoimmune diseases such as RA (Kishimoto, 2005). This could in addition also explain the strong thymic atrophy apparent in mice  $KO^T$  and  $TKO^T$  mice.

The concept of cooperativity by Roquin and Regnase-1 is further proven by the dramatically increased Regnase-1 expression on protein and mRNA level in mice deficient for Roquin in T cells (Figure 40). If Regnase-1 or Roquin would bind and regulate the mRNAs in a mutually exclusive and compartmentalized fashion as suggested by Mino et al. and Cui et al., we would not expect any autoimmune phenotype in Roquin double-knockout mice, since the tremendous amounts of Regnase-1 could substitute for Roquin.

### **5.3.8 How does the observed cooperativity of Roquin and Regnase-1 fit with recent concepts?**

Finally, an important aspect is, if we can connect the data generated in this thesis with the previously published papers by Jeltsch et al., Mino et al. and Cui et al. (Figure 6).

These previously reported studies used different cell lines and mouse models and this might highly influence the conceptual outcome. While Jeltsch et al., analyzed Roquin- and Regnase-1-deficient mouse embryonic fibroblasts (MEFs) and mouse T cells, the studies of Mino et al. and Cui et al. switched between human and mouse systems by utilizing MEF cells, bone-marrow-derived macrophages, HeLa cells, HEK cells, Jurkat cells and NIH/3T3 cells. Although Roquin and Regnase-1 are highly conserved in human and mouse, we saw that Regnase-1 is hardly expressed in MEF cells (data not shown) and it is commonly accepted that MEF cell clones are highly variable. Therefore, I performed all experiments exclusively in primary T cells either under well-established *in vitro* conditions or directly *ex vivo* by flow cytometry. Thus, all experiments are highly comparable and reflect the physiological function of Roquin and Regnase-1 in T cells. Though Cui et al. used primary T cells, the genetic combination of T-cell-specific Regnase-1 deletion and *sanroque* mutation is difficult to interpret, since to date the functional and mechanistical role of the M199R mutant of Roquin-1 is still unsolved and therefore the interpretation of the phenotypic consequences is questionable. Moreover, *sanroque* mice still express wild-type Roquin-2, which is not addressed in these studies at all, even though it can compensate for the loss-of-function of Roquin-1.

The major claim in the study by Mino and colleagues is that Roquin and Regnase-1 are spatially separated in P-bodies and endoplasmatic reticulum and functionally distinct from each

other, since Roquin acts on translationally-inactive and Regnase-1 controls the expression of translationally-active mRNAs. However, by analysis of the *Nfkbid* mRNA we were able to show that Roquin inhibits translation of some mRNA targets (section 4.1.2) and so does Regnase-1 for the *Nfkbiz* mRNA. Therefore, at least in T cells, the distinction of Roquin and Regnase-1 by controlling translationally inactive or active mRNAs is not informative. Even though Mino et al., claimed that Roquin and Regnase-1 are spatially distinct from each other, their polysomal fractionations show that Roquin and Regnase-1 proteins were both present in non-polysomal fractions, suggesting that indeed these proteins may be able to function together. Although Mino and colleagues did not see association of Regnase-1 in P-bodies, this localization has already been described previously (Suzuki et al., 2011).

Finally, Cui et al., suggested a strong autoregulation of Regnase-1 that is independent of Roquin in human Jurkat T cells. Unlike this, I identified a strong de-repression of Regnase-1 in the absence of Roquin and the regulation of Regnase-1 was highly dependent on both Roquin and Regnase-1 (Figure 42 and Figure 52). The differences here might be explained by the different cell systems and species being used, however, our data have been obtained in primary T cells.

Collectively, the data I generated in this thesis can expand the current models: The major mode of gene regulation by Roquin and Regnase-1 in T cells is cooperativity and less exclusivity or redundancy. But, Roquin and Regnase-1 exclusive target genes in T cells most likely exist. Roquin and Regnase-1 directly interact, which is in contradiction to a suggested spatial compartmentalization. Additionally, Roquin indeed regulates translational active mRNAs such as *Nfkbid* and, at least in T cells, Regnase-1 is not capable of auto-regulating its own expression and depends on the presence of Roquin-1. The involvement of other factors such as UPF1 or members of the deadenylation or decapping machinery in a huge post-transcriptional network is likely and thus enables a tightly controlled gene regulation which is required to prevent autoinflammation and autoimmunity.

## 5.4 Conclusions, model and future perspectives

A strong evidence for the importance of post-transcriptional gene regulation by RNA-binding proteins comes from a very recent study that uncovers a human patient with a homozygous nonsense mutation of Roquin-1 (Tavernier et al., 2019). The patient suffers from hyperinflammation and uncontrolled cytokine secretion such as TNF, IL-2 and IL-17A characterized as hemophagocytic lymphohistiocytosis (HLH). Interestingly, the R687\* variant of this patient phenocopies aspects of the *sanroque* point mutation by causing aberrant immune cell activation and increased cytokine release.

In this thesis, I was able to prove the concept of a cooperative post-transcriptional gene regulation in CD4 T cells by the RNA-binding protein Roquin on several levels (**Figure 56**).

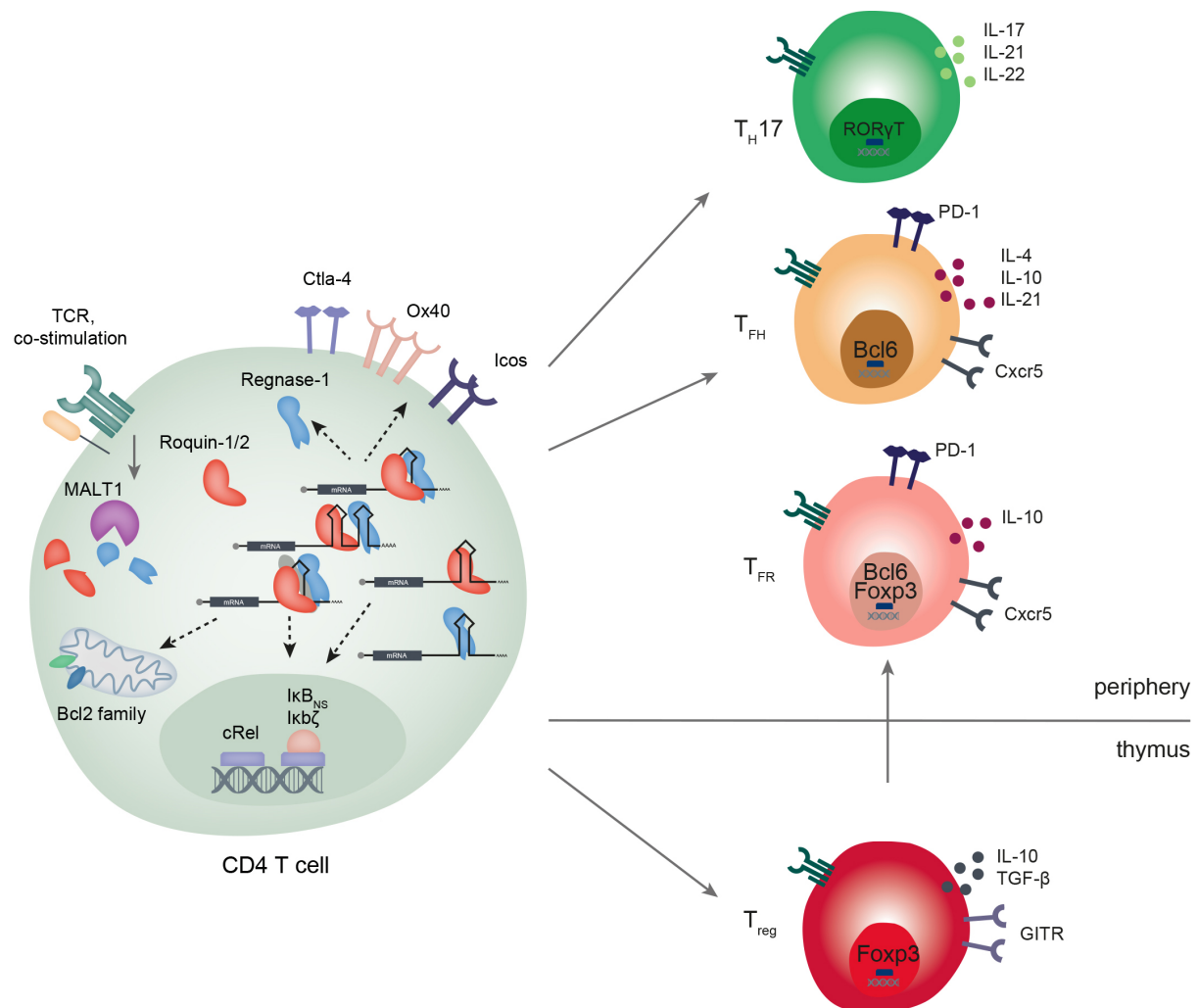


**Figure 56 | Model for Roquin- and Regnase-1-mediated gene regulation in CD4 T cells.**

Roquin and Regnase-1 have overlapping target genes in CD4 T cells. These target mRNAs involve genes that encode for co-stimulatory receptors (Ctla-4, Icos, Ox40), transcription factors (cRel), modulators of transcription factors ( $\text{IkB}_{\text{NS}}$ ,  $\text{IkB}\zeta$ ) and mitochondrial anti-apoptotic members of the Bcl2 family such as Bcl-X<sub>L</sub>. Upon TCR stimulation and co-stimulation, Roquin and Regnase-1 proteins are cleaved by the paracaspase MALT1 and release targeted mRNAs from repression. Roquin and Regnase-1 target mRNAs can be regulated in several ways: Roquin exclusive ( $\text{IkB}_{\text{NS}}$ , Ox40), cooperative by Roquin and Regnase-1 interacting with the same stem loop structure (Icos) or on two distinct stem loop structures (Ctla-4) and the involvement of additional post-transcriptional regulators on the RNA is possible (grey symbol). The repression of Roquin and Regnase-1 targeted mRNAs controls the differentiation of TH17 and TH cells and potentially apoptotic events and Treg differentiation in the thymus.

First, I identified that multiple Roquin proteins act on the regulation of their mRNA targets at least in an additive but potentially cooperative or synergistic manner. This was exemplified for

the Roquin exclusive target genes *Ox40* (Figure 13) and *Nfkbid* (Figure 20). Here, Roquin enables binding of high-affinity stem loop structures to confer strong post-transcriptional gene regulation by inducing mRNA decay or mRNA decay and translational inhibition (Figure 21). I therefore propose, that the specific mode of regulation in this system is encoded within its very different *cis*-elements.

Second, the major molecular gene regulation is cooperative, which occurs at different degrees – either by Roquin on multiple stem loop structures as shown for the prototypical target *Nfkbid* or by the cooperation with the endonuclease Regnase-1 and may include other, so-far unknown, factors. The cooperativity with Regnase-1 results in a selective repression of certain target genes presumably harboring mainly cooperative or redundant elements. However, Roquin exclusive targets such as *Ox40* also exist. This concept was proven by reconstitution experiments that enabled a separation of the molecular functions of Roquin and Regnase-1 (Figure 51). And finally, evaluating the direct interaction of Roquin and Regnase-1, provided the molecular mechanism underlying cooperativity (Figure 53). The involvement of additional post-transcriptional effectors associated with Regnase-1, such as UPF1, may not contradict cooperativity, but rather contribute and increase the regulatory potential.

The cooperativity of Roquin and Regnase-1 is further supported by comparing conditional T cell-specific knockout mice of Roquin and Regnase-1 and mixed bone marrow chimeric mice, where we identified that cellular phenotypes such as thymic regulatory T cell development (Figure 32) and T cell activation (Figure 37) as well as  $T_H17$  differentiation (Figure 39) are enhanced in  $TKO^T$  mice. These phenotypes most likely arise from an aberrant cooperative gene regulation of previously described targets (*Icos*, *Ctla-4*,  $I\kappa B_{NS}$ ,  $I\kappa B\zeta$ , *cRel*) and newly identified Roquin and Regnase-1 targets (*Bcl-X<sub>L</sub>*, *cKit*, *CD30*) (Figure 26). Whether or not Roquin- and Regnase-1-deficiency influences selection processes in the thymus by direct target regulation or indirect effects, and how this affects the development of autoimmunity needs to be addressed in the future.

Additionally, the strong and additive peripheral autoinflammatory and autoimmune phenotype of mice devoid of Roquin and Regnase-1 in T cells in comparison to only Roquin- or Regnase-1-deficiency, support a cooperative regulation of these cellular processes. The autoimmunity is characterized by an increased GC reaction accompanied by a defective humoral immune response which results in the production of autoantibodies (Figure 35). However, mice deficient for Regnase-1 expressed the highest levels of autoantibodies. The degree of perturbation of gene expression in T cells deficient for Roquin and Regnase-1 and Roquin-deficient T cells was much stronger as the gene expression of Regnase-1-deficient T cells. Thus, the strong alterations in gene expression in mice deficient for Roquin and Regnase-1 ( $TKO^T$ ) and Roquin ( $DKO^T$ ) in T cells might quantitatively exceed the gene expression changes



that effectively induce the production of autoantibodies, a limitation which is not reached in KO<sup>T</sup> mice, yet.

Collectively, the data generated in this thesis enable a novel understanding of Roquin and Regnase-1, which participate in a complex, cooperative network of post-transcriptional gene regulation during activation and differentiation of T cells. The mouse models investigated in this study clearly show that an appropriate and dynamic expression of certain genes such as co-stimulatory receptors or transcription factors during these fragile immune processes are mandatory to prevent the development of autoinflammatory and autoimmune diseases. Understanding the molecular function of Roquin and Regnase-1 and how they are connected in a post-transcriptional network is critical for the establishment of targeting strategies of the system in future therapies of autoimmune diseases.



## Literature

Akiba, H., Takeda, K., Kojima, Y., Usui, Y., Harada, N., Yamazaki, T., . . . Okumura, K. (2005). The role of ICOS in the CXCR5+ follicular B helper T cell maintenance in vivo. *J Immunol* 175, 2340-2348.

Amsen, D., Spilianakis, C.G., and Flavell, R.A. (2009). How are T(H)1 and T(H)2 effector cells made? *Curr Opin Immunol* 21, 153-160.

Amsen, D., van Gisbergen, K., Hombrink, P., and van Lier, R.A.W. (2018). Tissue-resident memory T cells at the center of immunity to solid tumors. *Nat Immunol* 19, 538-546.

Anantharaman, V., and Aravind, L. (2006). The NYN domains: novel predicted RNases with a PIN domain-like fold. *RNA Biol* 3, 18-27.

Annemann, M., Wang, Z., Plaza-Sirvent, C., Glauben, R., Schuster, M., Ewald Sander, F., . . . Schmitz, I. (2015). IkappaBNS regulates murine Th17 differentiation during gut inflammation and infection. *J Immunol* 194, 2888-2898.

Athanasopoulos, V., Barker, A., Yu, D., Tan, A.H., Srivastava, M., Contreras, N., . . . Vinuesa, C.G. (2010). The ROQUIN family of proteins localizes to stress granules via the ROQ domain and binds target mRNAs. *FEBS J* 277, 2109-2127.

Baccala, R., Hoebe, K., Kono, D.H., Beutler, B., and Theofilopoulos, A.N. (2007). TLR-dependent and TLR-independent pathways of type I interferon induction in systemic autoimmunity. *Nat Med* 13, 543-551.

Bacchetta, R., Barzaghi, F., and Roncarolo, M.G. (2018). From IPEX syndrome to FOXP3 mutation: a lesson on immune dysregulation. *Ann N Y Acad Sci* 1417, 5-22.

Barber, D.L., Wherry, E.J., and Ahmed, R. (2003). Cutting edge: rapid in vivo killing by memory CD8 T cells. *J Immunol* 171, 27-31.

Baumjohann, D. (2018). Diverse functions of miR-17-92 cluster microRNAs in T helper cells. *Cancer Lett* 423, 147-152.

Behrens, G., Winzen, R., Rehage, N., Dorrie, A., Barsch, M., Hoffmann, A., . . . Holtmann, H. (2018). A translational silencing function of MCPIP1/Regnase-1 specified by the target site context. *Nucleic Acids Res* 46, 4256-4270.

Bertossi, A., Aichinger, M., Sansonetti, P., Lech, M., Neff, F., Pal, M., . . . Schmidt-Suppran, M. (2011). Loss of Roquin induces early death and immune deregulation but not autoimmunity. *J Exp Med* 208, 1749-1756.

Bettelli, E., Carrier, Y., Gao, W., Korn, T., Strom, T.B., Oukka, M., . . . Kuchroo, V.K. (2006). Reciprocal developmental pathways for the generation of pathogenic effector TH17 and regulatory T cells. *Nature* 441, 235-238.

Beyan, H., Riese, H., Hawa, M.I., Beretta, G., Davidson, H.W., Hutton, J.C., . . . Leslie, R.D. (2012). Glycotoxin and autoantibodies are additive environmentally determined predictors of type 1 diabetes: a twin and population study. *Diabetes* 61, 1192-1198.

Boomer, J.S., and Green, J.M. (2010). An enigmatic tail of CD28 signaling. *Cold Spring Harb Perspect Biol* 2, a002436.

- Boratyn, E., Nowak, I., Durbas, M., Horwacik, I., Sawicka, A., and Rokita, H. (2017). MCPIP1 Exogenous Overexpression Inhibits Pathways Regulating MYCN Oncoprotein Stability in Neuroblastoma. *J Cell Biochem* 118, 1741-1755.
- Borbely, G., Haldosen, L.A., Dahlman-Wright, K., and Zhao, C. (2015). Induction of USP17 by combining BET and HDAC inhibitors in breast cancer cells. *Oncotarget* 6, 33623-33635.
- Bouillet, P., Metcalf, D., Huang, D.C., Tarlinton, D.M., Kay, T.W., Kontgen, F., . . . Strasser, A. (1999). Proapoptotic Bcl-2 relative Bim required for certain apoptotic responses, leukocyte homeostasis, and to preclude autoimmunity. *Science* 286, 1735-1738.
- Bouneaud, C., Kourilsky, P., and Bousso, P. (2000). Impact of negative selection on the T cell repertoire reactive to a self-peptide: a large fraction of T cell clones escapes clonal deletion. *Immunity* 13, 829-840.
- Bradford, M.M. (1976). A rapid and sensitive method for the quantitation of microgram quantities of protein utilizing the principle of protein-dye binding. *Analytical biochemistry* 72, 248-254.
- Braun, J., Fischer, S., Xu, Z.Z., Sun, H., Ghoneim, D.H., Gimbel, A.T., . . . Weigand, J.E. (2018). Identification of new high affinity targets for Roquin based on structural conservation. *Nucleic Acids Res* 46, 12109-12125.
- Breed, E.R., Watanabe, M., and Hogquist, K.A. (2019). Measuring Thymic Clonal Deletion at the Population Level. *J Immunol* 202, 3226-3233.
- Bretscher, P., and Cohn, M. (1970). A theory of self-nonself discrimination. *Science* 169, 1042-1049.
- Brunkow, M.E., Jeffery, E.W., Hjerrild, K.A., Paeper, B., Clark, L.B., Yasayko, S.A., . . . Ramsdell, F. (2001). Disruption of a new forkhead/winged-helix protein, scurf, results in the fatal lymphoproliferative disorder of the scurfy mouse. *Nat Genet* 27, 68-73.
- Brustle, A., Heink, S., Huber, M., Rosenplanter, C., Stadelmann, C., Yu, P., . . . Lohoff, M. (2007). The development of inflammatory T(H)-17 cells requires interferon-regulatory factor 4. *Nat Immunol* 8, 958-966.
- Burchill, M.A., Yang, J., Vogtenhuber, C., Blazar, B.R., and Farrar, M.A. (2007). IL-2 receptor beta-dependent STAT5 activation is required for the development of Foxp3+ regulatory T cells. *J Immunol* 178, 280-290.
- Burnet, F.M. (1962). The immunological significance of the thymus: an extension of the clonal selection theory of immunity. *Australas Ann Med* 11, 79-91.
- Camacho, C., Coulouris, G., Avagyan, V., Ma, N., Papadopoulos, J., Bealer, K., and Madden, T.L. (2009). BLAST+: architecture and applications. *BMC Bioinformatics* 10, 421.
- Carballo, E., Lai, W.S., and Blackshear, P.J. (2000). Evidence that tristetraprolin is a physiological regulator of granulocyte-macrophage colony-stimulating factor messenger RNA deadenylation and stability. *Blood* 95, 1891-1899.
- Chambers, C.A., Sullivan, T.J., and Allison, J.P. (1997). Lymphoproliferation in CTLA-4-deficient mice is mediated by costimulation-dependent activation of CD4+ T cells. *Immunity* 7, 885-895.
- Chattopadhyay, K., Lazar-Molnar, E., Yan, Q., Rubinstein, R., Zhan, C., Vigdorovich, V., . . . Almo, S.C. (2009). Sequence, structure, function, immunity: structural genomics of costimulation. *Immunol Rev* 229, 356-386.
- Chen, G., Hardy, K., Pagler, E., Ma, L., Lee, S., Gerondakis, S., . . . Shannon, M.F. (2011). The NF-kappaB transcription factor c-Rel is required for Th17 effector cell development in experimental autoimmune encephalomyelitis. *J Immunol* 187, 4483-4491.

- Chen, L., and Flies, D.B. (2013). Molecular mechanisms of T cell co-stimulation and co-inhibition. *Nat Rev Immunol* 13, 227-242.
- Chinen, T., Kannan, A.K., Levine, A.G., Fan, X., Klein, U., Zheng, Y., . . . Rudensky, A.Y. (2016). An essential role for the IL-2 receptor in Treg cell function. *Nat Immunol* 17, 1322-1333.
- Codutti, L., Leppek, K., Zalesak, J., Windeisen, V., Masiewicz, P., Stoecklin, G., and Carlomagno, T. (2015). A Distinct, Sequence-Induced Conformation Is Required for Recognition of the Constitutive Decay Element RNA by Roquin. *Structure* 23, 1437-1447.
- Collart, M.A. (2016). The Ccr4-Not complex is a key regulator of eukaryotic gene expression. *Wiley Interdiscip Rev RNA* 7, 438-454.
- Cowan, J.E., McCarthy, N.I., and Anderson, G. (2016). CCR7 Controls Thymus Recirculation, but Not Production and Emigration, of Foxp3(+) T Cells. *Cell Rep* 14, 1041-1048.
- Croft, M. (2003). Co-stimulatory members of the TNFR family: keys to effective T-cell immunity? *Nat Rev Immunol* 3, 609-620.
- Croft, M. (2009). The role of TNF superfamily members in T-cell function and diseases. *Nat Rev Immunol* 9, 271-285.
- Croft, M., Duan, W., Choi, H., Eun, S.Y., Madireddi, S., and Mehta, A. (2012). TNF superfamily in inflammatory disease: translating basic insights. *Trends Immunol* 33, 144-152.
- Crotty, S. (2011). Follicular helper CD4 T cells (TFH). *Annu Rev Immunol* 29, 621-663.
- Cui, X., Mino, T., Yoshinaga, M., Nakatsuka, Y., Hia, F., Yamasoba, D., . . . Takeuchi, O. (2017). Regnase-1 and Roquin Nonredundantly Regulate Th1 Differentiation Causing Cardiac Inflammation and Fibrosis. *J Immunol* 199, 4066-4077.
- Daniels, M.A., Teixeira, E., Gill, J., Hausmann, B., Roubaty, D., Holmberg, K., . . . Palmer, E. (2006). Thymic selection threshold defined by compartmentalization of Ras/MAPK signalling. *Nature* 444, 724-729.
- Decker, C.J., and Parker, R. (2012). P-bodies and stress granules: possible roles in the control of translation and mRNA degradation. *Cold Spring Harb Perspect Biol* 4, a012286.
- Deobagkar-Lele, M., Chacko, S.K., Victor, E.S., Kadthur, J.C., and Nandi, D. (2013). Interferon-gamma- and glucocorticoid-mediated pathways synergize to enhance death of CD4(+) CD8(+) thymocytes during *Salmonella enterica* serovar Typhimurium infection. *Immunology* 138, 307-321.
- Doma, M.K., and Parker, R. (2006). Endonucleolytic cleavage of eukaryotic mRNAs with stalls in translation elongation. *Nature* 440, 561-564.
- Dong, C., Juedes, A.E., Temann, U.A., Shrestha, S., Allison, J.P., Ruddle, N.H., and Flavell, R.A. (2001). ICOS co-stimulatory receptor is essential for T-cell activation and function. *Nature* 409, 97-101.
- Drees, C., Vahl, J.C., Bortoluzzi, S., Heger, K.D., Fischer, J.C., Wunderlich, F.T., . . . Schmidt-Supprian, M. (2017). Roquin Paralogs Differentially Regulate Functional NKT Cell Subsets. *J Immunol* 198, 2747-2759.
- Ekhterae, D., Platoshyn, O., Krick, S., Yu, Y., McDaniel, S.S., and Yuan, J.X. (2001). Bcl-2 decreases voltage-gated K<sup>+</sup> channel activity and enhances survival in vascular smooth muscle cells. *Am J Physiol Cell Physiol* 281, C157-165.
- Essig, K., Hu, D., Guimaraes, J.C., Alterauge, D., Edelmann, S., Raj, T., . . . Heissmeyer, V. (2017). Roquin Suppresses the PI3K-mTOR Signaling Pathway to Inhibit T Helper Cell Differentiation and Conversion of Treg to Tfr Cells. *Immunity* 47, 1067-1082 e1012.

- Essig, K., Kronbeck, N., Guimaraes, J.C., Lohs, C., Schlundt, A., Hoffmann, A., . . . Heissmeyer, V. (2018). Roquin targets mRNAs in a 3'-UTR-specific manner by different modes of regulation. *Nat Commun* 9, 3810.
- Fathman, C.G., and Lineberry, N.B. (2007). Molecular mechanisms of CD4+ T-cell anergy. *Nat Rev Immunol* 7, 599-609.
- Ferguson, S.E., Han, S., Kelsoe, G., and Thompson, C.B. (1996). CD28 is required for germinal center formation. *J Immunol* 156, 4576-4581.
- Finney, H.M., Lawson, A.D., Bebbington, C.R., and Weir, A.N. (1998). Chimeric receptors providing both primary and costimulatory signaling in T cells from a single gene product. *J Immunol* 161, 2791-2797.
- Fiorini, E., Schmitz, I., Marissen, W.E., Osborn, S.L., Touma, M., Sasada, T., . . . Clayton, L.K. (2002). Peptide-induced negative selection of thymocytes activates transcription of an NF-kappa B inhibitor. *Mol Cell* 9, 637-648.
- Fonseca, V.R., Romao, V.C., Agua-Doce, A., Santos, M., Lopez-Presa, D., Ferreira, A.C., . . . Graca, L. (2018). The Ratio of Blood T Follicular Regulatory Cells to T Follicular Helper Cells Marks Ectopic Lymphoid Structure Formation While Activated Follicular Helper T Cells Indicate Disease Activity in Primary Sjogren's Syndrome. *Arthritis Rheumatol* 70, 774-784.
- Forrester, J.V., Xu, H., Lambe, T., and Cornall, R. (2008). Immune privilege or privileged immunity? *Mucosal Immunol* 1, 372-381.
- Frischmeyer, P.A., van Hoof, A., O'Donnell, K., Guerrerio, A.L., Parker, R., and Dietz, H.C. (2002). An mRNA surveillance mechanism that eliminates transcripts lacking termination codons. *Science* 295, 2258-2261.
- Frischmeyer-Guerrerio, P.A., Montgomery, R.A., Warren, D.S., Cooke, S.K., Lutz, J., Sonnenday, C.J., . . . Dietz, H.C. (2011). Perturbation of thymocyte development in nonsense-mediated decay (NMD)-deficient mice. *Proc Natl Acad Sci U S A* 108, 10638-10643.
- Frumento, G., Zuo, J., Verma, K., Croft, W., Ramagiri, P., Chen, F.E., and Moss, P. (2019). CD117 (c-Kit) Is Expressed During CD8(+) T Cell Priming and Stratifies Sensitivity to Apoptosis According to Strength of TCR Engagement. *Front Immunol* 10, 468.
- Fu, G., Vallee, S., Rybakina, V., McGuire, M.V., Ampudia, J., Brockmeyer, C., . . . Gascoigne, N.R. (2009). Themis controls thymocyte selection through regulation of T cell antigen receptor-mediated signaling. *Nat Immunol* 10, 848-856.
- Fu, W., Liu, X., Lin, X., Feng, H., Sun, L., Li, S., . . . Dong, C. (2018). Deficiency in T follicular regulatory cells promotes autoimmunity. *J Exp Med* 215, 815-825.
- Garneau, N.L., Wilusz, J., and Wilusz, C.J. (2007). The highways and byways of mRNA decay. *Nat Rev Mol Cell Biol* 8, 113-126.
- Gaspal, F., Withers, D., Saini, M., Bekiaris, V., McConnell, F.M., White, A., . . . Lane, P.J. (2011). Abrogation of CD30 and OX40 signals prevents autoimmune disease in FoxP3-deficient mice. *J Exp Med* 208, 1579-1584.
- Gehring, N.H., Hentze, M.W., and Kulozik, A.E. (2008). Tethering assays to investigate nonsense-mediated mRNA decay activating proteins. *Methods Enzymol* 448, 467-482.
- Gerondakis, S., Fulford, T.S., Messina, N.L., and Grumont, R.J. (2014). NF-kappaB control of T cell development. *Nat Immunol* 15, 15-25.
- Gewies, A., Gorka, O., Bergmann, H., Pechloff, K., Petermann, F., Jeltsch, K.M., . . . Ruland, J. (2014). Uncoupling Malt1 threshold function from paracaspase activity results in destructive autoimmune inflammation. *Cell Rep* 9, 1292-1305.

- Ghoreschi, K., Laurence, A., Yang, X.P., Tato, C.M., McGeachy, M.J., Konkel, J.E., . . . O'Shea, J.J. (2010). Generation of pathogenic T(H)17 cells in the absence of TGF-beta signalling. *Nature* 467, 967-971.
- Glasmacher, E., Hoefig, K.P., Vogel, K.U., Rath, N., Du, L., Wolf, C., . . . Heissmeyer, V. (2010). Roquin binds inducible costimulator mRNA and effectors of mRNA decay to induce microRNA-independent post-transcriptional repression. *Nat Immunol* 11, 725-733.
- Godfrey, V.L., Wilkinson, J.E., and Russell, L.B. (1991). X-linked lymphoreticular disease in the scurfy (sf) mutant mouse. *Am J Pathol* 138, 1379-1387.
- Gonzalo, J.A., Delaney, T., Corcoran, J., Goodearl, A., Gutierrez-Ramos, J.C., and Coyle, A.J. (2001). Cutting edge: the related molecules CD28 and inducible costimulator deliver both unique and complementary signals required for optimal T cell activation. *J Immunol* 166, 1-5.
- Gramaglia, I., Jember, A., Pippig, S.D., Weinberg, A.D., Killeen, N., and Croft, M. (2000). The OX40 costimulatory receptor determines the development of CD4 memory by regulating primary clonal expansion. *J Immunol* 165, 3043-3050.
- Grawunder, U., Zimmer, D., Fugmann, S., Schwarz, K., and Lieber, M.R. (1998). DNA ligase IV is essential for V(D)J recombination and DNA double-strand break repair in human precursor lymphocytes. *Mol Cell* 2, 477-484.
- Guo, L., and Shorter, J. (2015). It's Raining Liquids: RNA Tunes Viscoelasticity and Dynamics of Membraneless Organelles. *Mol Cell* 60, 189-192.
- Habacher, C., Guo, Y., Venz, R., Kumari, P., Neagu, A., Gaidatzis, D., . . . Ciosk, R. (2016). Ribonuclease-Mediated Control of Body Fat. *Dev Cell* 39, 359-369.
- Halenius, A., Gerke, C., and Hengel, H. (2015). Classical and non-classical MHC I molecule manipulation by human cytomegalovirus: so many targets-but how many arrows in the quiver? *Cell Mol Immunol* 12, 139-153.
- Hanieh, H., Masuda, K., Metwally, H., Chalise, J.P., Mohamed, M., Nyati, K.K., . . . Kishimoto, T. (2018). Arid5a stabilizes OX40 mRNA in murine CD4(+) T cells by recognizing a stem-loop structure in its 3'UTR. *Eur J Immunol* 48, 593-604.
- Hayden, M.S., and Ghosh, S. (2012). NF-kappaB, the first quarter-century: remarkable progress and outstanding questions. *Genes Dev* 26, 203-234.
- Heissmeyer, V., and Vogel, K.U. (2013). Molecular control of Tfh-cell differentiation by Roquin family proteins. *Immunol Rev* 253, 273-289.
- Hickman, H.D., Takeda, K., Skon, C.N., Murray, F.R., Hensley, S.E., Loomis, J., . . . Yewdell, J.W. (2008). Direct priming of antiviral CD8+ T cells in the peripheral interfollicular region of lymph nodes. *Nat Immunol* 9, 155-165.
- Hochedlinger, K., Yamada, Y., Beard, C., and Jaenisch, R. (2005). Ectopic expression of Oct-4 blocks progenitor-cell differentiation and causes dysplasia in epithelial tissues. *Cell* 121, 465-477.
- Hoefig, K.P., and Heissmeyer, V. (2018). Posttranscriptional regulation of T helper cell fate decisions. *J Cell Biol* 217, 2615-2631.
- Hofstetter, H.H., Ibrahim, S.M., Koczan, D., Kruse, N., Weishaupt, A., Toyka, K.V., and Gold, R. (2005). Therapeutic efficacy of IL-17 neutralization in murine experimental autoimmune encephalomyelitis. *Cell Immunol* 237, 123-130.
- Houalla, R., Devaux, F., Fatica, A., Kufel, J., Barrass, D., Torchet, C., and Tollervy, D. (2006). Microarray detection of novel nuclear RNA substrates for the exosome. *Yeast* 23, 439-454.

- Houseley, J., LaCava, J., and Tollervey, D. (2006). RNA-quality control by the exosome. *Nat Rev Mol Cell Biol* 7, 529-539.
- Hu, Y.L., Metz, D.P., Chung, J., Siu, G., and Zhang, M. (2009). B7RP-1 blockade ameliorates autoimmunity through regulation of follicular helper T cells. *J Immunol* 182, 1421-1428.
- Huang, S., Qi, D., Liang, J., Miao, R., Minagawa, K., Quinn, T., . . . Fu, M. (2012). The putative tumor suppressor Zc3h12d modulates toll-like receptor signaling in macrophages. *Cell Signal* 24, 569-576.
- Ingolia, N.T., Ghaemmaghami, S., Newman, J.R., and Weissman, J.S. (2009). Genome-wide analysis in vivo of translation with nucleotide resolution using ribosome profiling. *Science* 324, 218-223.
- Irving, B.A., and Weiss, A. (1991). The cytoplasmic domain of the T cell receptor zeta chain is sufficient to couple to receptor-associated signal transduction pathways. *Cell* 64, 891-901.
- Ishida, Y., Agata, Y., Shibahara, K., and Honjo, T. (1992). Induced expression of PD-1, a novel member of the immunoglobulin gene superfamily, upon programmed cell death. *EMBO J* 11, 3887-3895.
- Iwasaki, H., Takeuchi, O., Teraguchi, S., Matsushita, K., Uehata, T., Kuniyoshi, K., . . . Akira, S. (2011). The IkappaB kinase complex regulates the stability of cytokine-encoding mRNA induced by TLR-IL-1R by controlling degradation of regnase-1. *Nat Immunol* 12, 1167-1175.
- Janeway, C.A., Jr., and Medzhitov, R. (2002). Innate immune recognition. *Annu Rev Immunol* 20, 197-216.
- Janowski, R., Heinz, G.A., Schlundt, A., Wommelsdorf, N., Brenner, S., Gruber, A.R., . . . Sattler, M. (2016). Roquin recognizes a non-canonical hexaloop structure in the 3'-UTR of Ox40. *Nat Commun* 7, 11032.
- Jeltsch, K.M., Hu, D., Brenner, S., Zoller, J., Heinz, G.A., Nagel, D., . . . Heissmeyer, V. (2014). Cleavage of roquin and regnase-1 by the paracaspase MALT1 releases their cooperatively repressed targets to promote T(H)17 differentiation. *Nat Immunol* 15, 1079-1089.
- Jia, X., Wang, B., Zhai, T., Yao, Q., Li, Q., and Zhang, J.A. (2018). T cell receptor revision and immune repertoire changes in autoimmune diseases. *Clin Immunol*.
- John, B., Harris, T.H., Tait, E.D., Wilson, E.H., Gregg, B., Ng, L.G., . . . Hunter, C.A. (2009). Dynamic Imaging of CD8(+) T cells and dendritic cells during infection with *Toxoplasma gondii*. *PLoS Pathog* 5, e1000505.
- Jonas, S., and Izaurralde, E. (2015). Towards a molecular understanding of microRNA-mediated gene silencing. *Nat Rev Genet* 16, 421-433.
- Jordan, M.S., Boesteanu, A., Reed, A.J., Petrone, A.L., Hohenbeck, A.E., Lerman, M.A., . . . Caton, A.J. (2001). Thymic selection of CD4+CD25+ regulatory T cells induced by an agonist self-peptide. *Nat Immunol* 2, 301-306.
- Kalekar, L.A., Schmiel, S.E., Nandiwada, S.L., Lam, W.Y., Barsness, L.O., Zhang, N., . . . Mueller, D.L. (2016). CD4(+) T cell anergy prevents autoimmunity and generates regulatory T cell precursors. *Nat Immunol* 17, 304-314.
- Kanarek, N., and Ben-Neriah, Y. (2012). Regulation of NF-kappaB by ubiquitination and degradation of the IkappaBs. *Immunol Rev* 246, 77-94.
- Kanno, Y., Vahedi, G., Hirahara, K., Singleton, K., and O'Shea, J.J. (2012). Transcriptional and epigenetic control of T helper cell specification: molecular mechanisms underlying commitment and plasticity. *Annu Rev Immunol* 30, 707-731.



- Kedersha, N., Stoecklin, G., Ayodele, M., Yacono, P., Lykke-Andersen, J., Fritzler, M.J., . . . Anderson, P. (2005). Stress granules and processing bodies are dynamically linked sites of mRNP remodeling. *J Cell Biol* 169, 871-884.
- Kent, W.J. (2002). BLAT--the BLAST-like alignment tool. *Genome Res* 12, 656-664.
- Kim, Y.U., Lim, H., Jung, H.E., Wetsel, R.A., and Chung, Y. (2015). Regulation of autoimmune germinal center reactions in lupus-prone BXD2 mice by follicular helper T cells. *PLoS One* 10, e0120294.
- Kishimoto, T. (2005). Interleukin-6: from basic science to medicine--40 years in immunology. *Annu Rev Immunol* 23, 1-21.
- Kitamura, H., Kanehira, K., Okita, K., Morimatsu, M., and Saito, M. (2000). MAIL, a novel nuclear I kappa B protein that potentiates LPS-induced IL-6 production. *FEBS Lett* 485, 53-56.
- Klein, L., Kyewski, B., Allen, P.M., and Hogquist, K.A. (2014). Positive and negative selection of the T cell repertoire: what thymocytes see (and don't see). *Nat Rev Immunol* 14, 377-391.
- Knochelmann, H.M., Dwyer, C.J., Bailey, S.R., Amaya, S.M., Elston, D.M., Mazza-McCrann, J.M., and Paulos, C.M. (2018). When worlds collide: Th17 and Treg cells in cancer and autoimmunity. *Cell Mol Immunol* 15, 458-469.
- Kobayashi, S., Hara, A., Isagawa, T., Manabe, I., Takeda, K., and Maruyama, T. (2014). The nuclear I kappa B family protein I kappa BNS influences the susceptibility to experimental autoimmune encephalomyelitis in a murine model. *PLoS One* 9, e110838.
- Kolluri, S.K., Zhu, X., Zhou, X., Lin, B., Chen, Y., Sun, K., . . . Zhang, X.K. (2008). A short Nur77-derived peptide converts Bcl-2 from a protector to a killer. *Cancer Cell* 14, 285-298.
- Komiyama, Y., Nakae, S., Matsuki, T., Nambu, A., Ishigame, H., Kakuta, S., . . . Iwakura, Y. (2006). IL-17 plays an important role in the development of experimental autoimmune encephalomyelitis. *J Immunol* 177, 566-573.
- Kouro, T., and Takatsu, K. (2009). IL-5- and eosinophil-mediated inflammation: from discovery to therapy. *Int Immunol* 21, 1303-1309.
- Kroenke, M.A., Eto, D., Locci, M., Cho, M., Davidson, T., Haddad, E.K., and Crotty, S. (2012). Bcl6 and Maf cooperate to instruct human follicular helper CD4 T cell differentiation. *J Immunol* 188, 3734-3744.
- Kshirsagar, M., and Parker, R. (2004). Identification of Edc3p as an enhancer of mRNA decapping in *Saccharomyces cerevisiae*. *Genetics* 166, 729-739.
- Lai, W.S., Carballo, E., Strum, J.R., Kennington, E.A., Phillips, R.S., and Blackshear, P.J. (1999). Evidence that tristetraprolin binds to AU-rich elements and promotes the deadenylation and destabilization of tumor necrosis factor alpha mRNA. *Mol Cell Biol* 19, 4311-4323.
- Leach, D.R., Krummel, M.F., and Allison, J.P. (1996). Enhancement of antitumor immunity by CTLA-4 blockade. *Science* 271, 1734-1736.
- Lee, F.C.Y., and Ule, J. (2018). Advances in CLIP Technologies for Studies of Protein-RNA Interactions. *Mol Cell* 69, 354-369.
- Lee, P.P., Fitzpatrick, D.R., Beard, C., Jessup, H.K., Lehar, S., Makar, K.W., . . . Wilson, C.B. (2001). A critical role for Dnmt1 and DNA methylation in T cell development, function, and survival. *Immunity* 15, 763-774.
- Lee, S.K., Silva, D.G., Martin, J.L., Pratama, A., Hu, X., Chang, P.P., . . . Vinuesa, C.G. (2012). Interferon-gamma excess leads to pathogenic accumulation of follicular helper T cells and germinal centers. *Immunity* 37, 880-892.

- Leppek, K., Schott, J., Reitter, S., Poetz, F., Hammond, M.C., and Stoecklin, G. (2013). Roquin promotes constitutive mRNA decay via a conserved class of stem-loop recognition motifs. *Cell* 153, 869-881.
- Li, W., Gao, B., Lee, S.M., Bennett, K., and Fang, D. (2007). RLE-1, an E3 ubiquitin ligase, regulates *C. elegans* aging by catalyzing DAF-16 polyubiquitination. *Dev Cell* 12, 235-246.
- Li, Y., Huang, X., Huang, S., He, H., Lei, T., Saaoud, F., . . . Fu, M. (2017). Central role of myeloid MCP1 in protecting against LPS-induced inflammation and lung injury. *Signal Transduct Target Ther* 2, 17066.
- Liang, J., Saad, Y., Lei, T., Wang, J., Qi, D., Yang, Q., . . . Fu, M. (2010). MCP-induced protein 1 deubiquitinates TRAF proteins and negatively regulates JNK and NF-kappaB signaling. *J Exp Med* 207, 2959-2973.
- Liang, J., Song, W., Tromp, G., Kolattukudy, P.E., and Fu, M. (2008). Genome-wide survey and expression profiling of CCCH-zinc finger family reveals a functional module in macrophage activation. *PLoS One* 3, e2880.
- Lin, R.J., Chien, H.L., Lin, S.Y., Chang, B.L., Yu, H.P., Tang, W.C., and Lin, Y.L. (2013). MCP1 ribonuclease exhibits broad-spectrum antiviral effects through viral RNA binding and degradation. *Nucleic Acids Res* 41, 3314-3326.
- Lin, R.J., Chu, J.S., Chien, H.L., Tseng, C.H., Ko, P.C., Mei, Y.Y., . . . Lin, S.Y. (2014). MCP1 suppresses hepatitis C virus replication and negatively regulates virus-induced proinflammatory cytokine responses. *J Immunol* 193, 4159-4168.
- Ling, V., Wu, P.W., Finnerty, H.F., Agostino, M.J., Graham, J.R., Chen, S., . . . Collins, M. (2001). Assembly and annotation of human chromosome 2q33 sequence containing the CD28, CTLA4, and ICOS gene cluster: analysis by computational, comparative, and microarray approaches. *Genomics* 78, 155-168.
- Linterman, M.A., Pierson, W., Lee, S.K., Kallies, A., Kawamoto, S., Rayner, T.F., . . . Vinuesa, C.G. (2011). Foxp3<sup>+</sup> follicular regulatory T cells control the germinal center response. *Nat Med* 17, 975-982.
- Linterman, M.A., Rigby, R.J., Wong, R., Silva, D., Withers, D., Anderson, G., . . . Vinuesa, C.G. (2009). Roquin differentiates the specialized functions of duplicated T cell costimulatory receptor genes CD28 and ICOS. *Immunity* 30, 228-241.
- Lio, C.W., and Hsieh, C.S. (2008). A two-step process for thymic regulatory T cell development. *Immunity* 28, 100-111.
- Lipert, B., Wilamowski, M., Gorecki, A., and Jura, J. (2017). MCP1, alias Regnase-1 binds and cleaves mRNA of C/EBPbeta. *PLoS One* 12, e0174381.
- Liu, H., Rodgers, N.D., Jiao, X., and Kiledjian, M. (2002). The scavenger mRNA decapping enzyme DcpS is a member of the HIT family of pyrophosphatases. *EMBO J* 21, 4699-4708.
- Liu, L., Zhou, Z., Huang, S., Guo, Y., Fan, Y., Zhang, J., . . . Chen, Y.E. (2013a). Zc3h12c inhibits vascular inflammation by repressing NF-kappaB activation and pro-inflammatory gene expression in endothelial cells. *Biochem J* 451, 55-60.
- Liu, S., Qiu, C., Miao, R., Zhou, J., Lee, A., Liu, B., . . . Wang, T. (2013b). MCP1 restricts HIV infection and is rapidly degraded in activated CD4<sup>+</sup> T cells. *Proc Natl Acad Sci U S A* 110, 19083-19088.
- Liu, Z., Gerner, M.Y., Van Panhuys, N., Levine, A.G., Rudensky, A.Y., and Germain, R.N. (2015). Immune homeostasis enforced by co-localized effector and regulatory T cells. *Nature* 528, 225-230.
- Lohr, J., Knoechel, B., Nagabhushanam, V., and Abbas, A.K. (2005). T-cell tolerance and autoimmunity to systemic and tissue-restricted self-antigens. *Immunol Rev* 204, 116-127.

- Long, M., Park, S.G., Strickland, I., Hayden, M.S., and Ghosh, S. (2009). Nuclear factor-kappaB modulates regulatory T cell development by directly regulating expression of Foxp3 transcription factor. *Immunity* 31, 921-931.
- Lu, W., Ning, H., Gu, L., Peng, H., Wang, Q., Hou, R., . . . Liu, J. (2016). MCPIP1 Selectively Destabilizes Transcripts Associated with an Antiapoptotic Gene Expression Program in Breast Cancer Cells That Can Elicit Complete Tumor Regression. *Cancer Res* 76, 1429-1440.
- Lykke-Andersen, J., and Wagner, E. (2005). Recruitment and activation of mRNA decay enzymes by two ARE-mediated decay activation domains in the proteins TTP and BRF-1. *Genes Dev* 19, 351-361.
- Lykke-Andersen, S., and Jensen, T.H. (2015). Nonsense-mediated mRNA decay: an intricate machinery that shapes transcriptomes. *Nat Rev Mol Cell Biol* 16, 665-677.
- Maruyama, T., Araki, T., Kawarazaki, Y., Naguro, I., Heynen, S., Aza-Blanc, P., . . . Ichijo, H. (2014). Roquin-2 promotes ubiquitin-mediated degradation of ASK1 to regulate stress responses. *Sci Signal* 7, ra8.
- Masuda, K., Ripley, B., Nishimura, R., Mino, T., Takeuchi, O., Shioi, G., . . . Kishimoto, T. (2013). Arid5a controls IL-6 mRNA stability, which contributes to elevation of IL-6 level in vivo. *Proc Natl Acad Sci U S A* 110, 9409-9414.
- Matsushita, K., Takeuchi, O., Standley, D.M., Kumagai, Y., Kawagoe, T., Miyake, T., . . . Akira, S. (2009). Zc3h12a is an RNase essential for controlling immune responses by regulating mRNA decay. *Nature* 458, 1185-1190.
- McAdam, A.J., Greenwald, R.J., Levin, M.A., Chernova, T., Malenkovich, N., Ling, V., . . . Sharpe, A.H. (2001). ICOS is critical for CD40-mediated antibody class switching. *Nature* 409, 102-105.
- McCaughy, T.M., Baldwin, T.A., Wilken, M.S., and Hogquist, K.A. (2008). Clonal deletion of thymocytes can occur in the cortex with no involvement of the medulla. *J Exp Med* 205, 2575-2584.
- McGarvey, K.M., Goldfarb, T., Cox, E., Farrell, C.M., Gupta, T., Joardar, V.S., . . . Pruitt, K.D. (2015). Mouse genome annotation by the RefSeq project. *Mamm Genome* 26, 379-390.
- Metcalf, D. (1960). The effect of thymectomy on the lymphoid tissues of the mouse. *Br J Haematol* 6, 324-333.
- Miao, R., Huang, S., Zhou, Z., Quinn, T., Van Treeck, B., Nayyar, T., . . . Fu, M. (2013). Targeted disruption of MCPIP1/Zc3h12a results in fatal inflammatory disease. *Immunol Cell Biol* 91, 368-376.
- Minagawa, K., Wakahashi, K., Kawano, H., Nishikawa, S., Fukui, C., Kawano, Y., . . . Matsui, T. (2014). Posttranscriptional modulation of cytokine production in T cells for the regulation of excessive inflammation by TFL. *J Immunol* 192, 1512-1524.
- Mino, T., Iwai, N., Endo, M., Inoue, K., Akaki, K., Hia, F., . . . Takeuchi, O. (2019). Translation-dependent unwinding of stem-loops by UPF1 licenses Regnase-1 to degrade inflammatory mRNAs. *Nucleic Acids Res.*
- Mino, T., Murakawa, Y., Fukao, A., Vandenbon, A., Wessels, H.H., Ori, D., . . . Takeuchi, O. (2015). Regnase-1 and Roquin Regulate a Common Element in Inflammatory mRNAs by Spatiotemporally Distinct Mechanisms. *Cell* 161, 1058-1073.
- Mino, T., and Takeuchi, O. (2015). Regnase-1 and Roquin regulate inflammatory mRNAs. *Oncotarget* 6, 17869-17870.
- Mosmann, T.R., Cherwinski, H., Bond, M.W., Giedlin, M.A., and Coffman, R.L. (1986). Two types of murine helper T cell clone. I. Definition according to profiles of lymphokine activities and secreted proteins. *J Immunol* 136, 2348-2357.

- Mugridge, J.S., Collier, J., and Gross, J.D. (2018). Structural and molecular mechanisms for the control of eukaryotic 5'-3' mRNA decay. *Nat Struct Mol Biol* 25, 1077-1085.
- Murakawa, Y., Hinz, M., Mothes, J., Schuetz, A., Uhl, M., Wyler, E., . . . Landthaler, M. (2015). RC3H1 post-transcriptionally regulates A20 mRNA and modulates the activity of the IKK/NF-kappaB pathway. *Nat Commun* 6, 7367.
- Murata, K., Nose, M., Ndhlovu, L.C., Sato, T., Sugamura, K., and Ishii, N. (2002). Constitutive OX40/OX40 ligand interaction induces autoimmune-like diseases. *J Immunol* 169, 4628-4636.
- Murphy, K., and Weaver, C. (2017). *Janeway's Immunobiology*, 9 edn (New York: Garland Science/Taylor & Francis Group).
- Muthana, M., Hawtree, S., Wilshaw, A., Linehan, E., Roberts, H., Khetan, S., . . . Wilson, A.G. (2015). C5orf30 is a negative regulator of tissue damage in rheumatoid arthritis. *Proc Natl Acad Sci U S A* 112, 11618-11623.
- Nakatsuka, Y., Vandenbon, A., Mino, T., Yoshinaga, M., Uehata, T., Cui, X., . . . Takeuchi, O. (2018). Pulmonary Regnase-1 orchestrates the interplay of epithelium and adaptive immune systems to protect against pneumonia. *Mucosal Immunol* 11, 1203-1218.
- Neill, D.R., and Flynn, R.J. (2018). Origins and evolution of innate lymphoid cells: Wardens of barrier immunity. *Parasite Immunol* 40.
- Nguyen, T.T., and Baumgarth, N. (2016). Natural IgM and the Development of B Cell-Mediated Autoimmune Diseases. *Crit Rev Immunol* 36, 163-177.
- Nikolich-Zugich, J., Slifka, M.K., and Messaoudi, I. (2004). The many important facets of T-cell repertoire diversity. *Nat Rev Immunol* 4, 123-132.
- Niu, J., Shi, Y., Xue, J., Miao, R., Huang, S., Wang, T., . . . Wu, Z.H. (2013). USP10 inhibits genotoxic NF-kappaB activation by MCP1P1-facilitated deubiquitination of NEMO. *EMBO J* 32, 3206-3219.
- Notredame, C., Higgins, D.G., and Heringa, J. (2000). T-Coffee: A novel method for fast and accurate multiple sequence alignment. *J Mol Biol* 302, 205-217.
- Nunes-Alves, C., Nobrega, C., Behar, S.M., and Correia-Neves, M. (2013). Tolerance has its limits: how the thymus copes with infection. *Trends Immunol* 34, 502-510.
- O'Shea, J.J., Lahesmaa, R., Vahedi, G., Laurence, A., and Kanno, Y. (2011). Genomic views of STAT function in CD4+ T helper cell differentiation. *Nat Rev Immunol* 11, 239-250.
- Odegard, J.M., Marks, B.R., DiPlacido, L.D., Poholek, A.C., Kono, D.H., Dong, C., . . . Craft, J. (2008). ICOS-dependent extrafollicular helper T cells elicit IgG production via IL-21 in systemic autoimmunity. *J Exp Med* 205, 2873-2886.
- Okamoto, K., Iwai, Y., Oh-Hora, M., Yamamoto, M., Morio, T., Aoki, K., . . . Takayanagi, H. (2010). IkappaBzeta regulates T(H)17 development by cooperating with ROR nuclear receptors. *Nature* 464, 1381-1385.
- Ouyang, W., Kolls, J.K., and Zheng, Y. (2008). The biological functions of T helper 17 cell effector cytokines in inflammation. *Immunity* 28, 454-467.
- Ouyang, W., Lohning, M., Gao, Z., Assenmacher, M., Ranganath, S., Radbruch, A., and Murphy, K.M. (2000). Stat6-independent GATA-3 autoactivation directs IL-4-independent Th2 development and commitment. *Immunity* 12, 27-37.
- Parker, R., and Sheth, U. (2007). P bodies and the control of mRNA translation and degradation. *Mol Cell* 25, 635-646.

- Parry, R.V., Chemnitz, J.M., Frauwirth, K.A., Lanfranco, A.R., Braunstein, I., Kobayashi, S.V., . . . Riley, J.L. (2005). CTLA-4 and PD-1 receptors inhibit T-cell activation by distinct mechanisms. *Mol Cell Biol* 25, 9543-9553.
- Paschou, S.A., Papadopoulou-Marketou, N., Chrousos, G.P., and Kanaka-Gantenbein, C. (2018). On type 1 diabetes mellitus pathogenesis. *Endocr Connect* 7, R38-R46.
- Paterson, A.M., and Sharpe, A.H. (2010). Taming tissue-specific T cells: CTLA-4 reins in self-reactive T cells. *Nat Immunol* 11, 109-111.
- Piecyk, M., Wax, S., Beck, A.R., Kedersha, N., Gupta, M., Maritim, B., . . . Anderson, P. (2000). TIA-1 is a translational silencer that selectively regulates the expression of TNF-alpha. *EMBO J* 19, 4154-4163.
- Pratama, A., Ramiscal, R.R., Silva, D.G., Das, S.K., Athanasopoulos, V., Fitch, J., . . . Vinuesa, C.G. (2013). Roquin-2 shares functions with its paralog Roquin-1 in the repression of mRNAs controlling T follicular helper cells and systemic inflammation. *Immunity* 38, 669-680.
- Qureshi, O.S., Zheng, Y., Nakamura, K., Attridge, K., Manzotti, C., Schmidt, E.M., . . . Sansom, D.M. (2011). Trans-endocytosis of CD80 and CD86: a molecular basis for the cell-extrinsic function of CTLA-4. *Science* 332, 600-603.
- Ramiscal, R.R., Parish, I.A., Lee-Young, R.S., Babon, J.J., Blagih, J., Pratama, A., . . . Athanasopoulos, V. (2015). Attenuation of AMPK signaling by ROQUIN promotes T follicular helper cell formation. *Elife* 4.
- Rehage, N., Davydova, E., Conrad, C., Behrens, G., Maiser, A., Stehklein, J.E., . . . Heissmeyer, V. (2018). Binding of NUFIP2 to Roquin promotes recognition and regulation of ICOS mRNA. *Nat Commun* 9, 299.
- Reijns, M.A., Alexander, R.D., Spiller, M.P., and Beggs, J.D. (2008). A role for Q/N-rich aggregation-prone regions in P-body localization. *J Cell Sci* 121, 2463-2472.
- Rissland, O.S. (2017). The organization and regulation of mRNA-protein complexes. *Wiley Interdiscip Rev RNA* 8.
- Rogers, P.R., Song, J., Gramaglia, I., Killeen, N., and Croft, M. (2001). OX40 promotes Bcl-xL and Bcl-2 expression and is essential for long-term survival of CD4 T cells. *Immunity* 15, 445-455.
- Roux, K.J., Kim, D.I., Burke, B., and May, D.G. (2018). BioID: A Screen for Protein-Protein Interactions. *Curr Protoc Protein Sci* 91, 19 23 11-19 23 15.
- Ruan, Q., Kameswaran, V., Tone, Y., Li, L., Liou, H.C., Greene, M.I., . . . Chen, Y.H. (2009). Development of Foxp3(+) regulatory t cells is driven by the c-Rel enhanceosome. *Immunity* 31, 932-940.
- Rudd, C.E., Taylor, A., and Schneider, H. (2009). CD28 and CTLA-4 coreceptor expression and signal transduction. *Immunol Rev* 229, 12-26.
- Sakaguchi, S., Sakaguchi, N., Asano, M., Itoh, M., and Toda, M. (1995). Immunologic self-tolerance maintained by activated T cells expressing IL-2 receptor alpha-chains (CD25). Breakdown of a single mechanism of self-tolerance causes various autoimmune diseases. *J Immunol* 155, 1151-1164.
- Sakaguchi, S., Yamaguchi, T., Nomura, T., and Ono, M. (2008). Regulatory T cells and immune tolerance. *Cell* 133, 775-787.
- Sakurai, S., Ohto, U., and Shimizu, T. (2015). Structure of human Roquin-2 and its complex with constitutive-decay element RNA. *Acta Crystallogr F Struct Biol Commun* 71, 1048-1054.

- Sallusto, F. (2016). Heterogeneity of Human CD4(+) T Cells Against Microbes. *Annu Rev Immunol* 34, 317-334.
- Salomon, B., Lenschow, D.J., Rhee, L., Ashourian, N., Singh, B., Sharpe, A., and Bluestone, J.A. (2000). B7/CD28 costimulation is essential for the homeostasis of the CD4+CD25+ immunoregulatory T cells that control autoimmune diabetes. *Immunity* 12, 431-440.
- Sawada, S., Scarborough, J.D., Killeen, N., and Littman, D.R. (1994). A lineage-specific transcriptional silencer regulates CD4 gene expression during T lymphocyte development. *Cell* 77, 917-929.
- Schlundt, A., Heinz, G.A., Janowski, R., Geerlof, A., Stehle, R., Heissmeyer, V., . . . Sattler, M. (2014). Structural basis for RNA recognition in roquin-mediated post-transcriptional gene regulation. *Nat Struct Mol Biol* 21, 671-678.
- Schlundt, A., Niessing, D., Heissmeyer, V., and Sattler, M. (2016). RNA recognition by Roquin in posttranscriptional gene regulation. *Wiley Interdiscip Rev RNA* 7, 455-469.
- Schuetz, A., Murakawa, Y., Rosenbaum, E., Landthaler, M., and Heinemann, U. (2014). Roquin binding to target mRNAs involves a winged helix-turn-helix motif. *Nat Commun* 5, 5701.
- Schuster, M., Glauben, R., Plaza-Sirvent, C., Schreiber, L., Annemann, M., Floess, S., . . . Schmitz, I. (2012). IkappaB(NS) protein mediates regulatory T cell development via induction of the Foxp3 transcription factor. *Immunity* 37, 998-1008.
- Schuster, M., Plaza-Sirvent, C., Matthies, A.M., Heise, U., Jeron, A., Bruder, D., . . . Schmitz, I. (2017). c-REL and IkappaBNS Govern Common and Independent Steps of Regulatory T Cell Development from Novel CD122-Expressing Pre-Precursors. *J Immunol* 199, 920-930.
- Sen, R., and Baltimore, D. (1986). Multiple nuclear factors interact with the immunoglobulin enhancer sequences. *Cell* 46, 705-716.
- Seto, E., and Yoshida, M. (2014). Erasers of histone acetylation: the histone deacetylase enzymes. *Cold Spring Harb Perspect Biol* 6, a018713.
- Shahinian, A., Pfeffer, K., Lee, K.P., Kundig, T.M., Kishihara, K., Wakeham, A., . . . Mak, T.W. (1993). Differential T cell costimulatory requirements in CD28-deficient mice. *Science* 261, 609-612.
- Sheppard, K.A., Fitz, L.J., Lee, J.M., Benander, C., George, J.A., Wooters, J., . . . Chaudhary, D. (2004). PD-1 inhibits T-cell receptor induced phosphorylation of the ZAP70/CD3zeta signalosome and downstream signaling to PKCtheta. *FEBS Lett* 574, 37-41.
- Shevach, E.M. (2000). Regulatory T cells in autoimmunity\*. *Annu Rev Immunol* 18, 423-449.
- Siess, D.C., Vedder, C.T., Merkens, L.S., Tanaka, T., Freed, A.C., McCoy, S.L., . . . Hefeneider, S.H. (2000). A human gene coding for a membrane-associated nucleic acid-binding protein. *J Biol Chem* 275, 33655-33662.
- Simpson, T.R., Quezada, S.A., and Allison, J.P. (2010). Regulation of CD4 T cell activation and effector function by inducible costimulator (ICOS). *Curr Opin Immunol* 22, 326-332.
- Sledzinska, A., Hemmers, S., Mair, F., Gorka, O., Ruland, J., Fairbairn, L., . . . Buch, T. (2013). TGF-beta signalling is required for CD4(+) T cell homeostasis but dispensable for regulatory T cell function. *PLoS Biol* 11, e1001674.
- Smith, C., Heyne, S., Richter, A.S., Will, S., and Backofen, R. (2010). Freiburg RNA Tools: a web server integrating INTARNA, EXPARNA and LOCARNA. *Nucleic Acids Res* 38, W373-377.
- Srivastava, M., Duan, G., Kershaw, N.J., Athanasopoulos, V., Yeo, J.H., Ose, T., . . . Vinuesa, C.G. (2015). Roquin binds microRNA-146a and Argonaute2 to regulate microRNA homeostasis. *Nat Commun* 6, 6253.

- Stoecklin, G., Lu, M., Rattenbacher, B., and Moroni, C. (2003). A constitutive decay element promotes tumor necrosis factor alpha mRNA degradation via an AU-rich element-independent pathway. *Mol Cell Biol* 23, 3506-3515.
- Stritesky, G.L., Xing, Y., Erickson, J.R., Kalekar, L.A., Wang, X., Mueller, D.L., . . . Hogquist, K.A. (2013). Murine thymic selection quantified using a unique method to capture deleted T cells. *Proc Natl Acad Sci U S A* 110, 4679-4684.
- Suzuki, H.I., Arase, M., Matsuyama, H., Choi, Y.L., Ueno, T., Mano, H., . . . Miyazono, K. (2011). MCP1P1 ribonuclease antagonizes dicer and terminates microRNA biogenesis through precursor microRNA degradation. *Mol Cell* 44, 424-436.
- Tafari, A., Shahinian, A., Bladt, F., Yoshinaga, S.K., Jordana, M., Wakeham, A., . . . Mak, T.W. (2001). ICOS is essential for effective T-helper-cell responses. *Nature* 409, 105-109.
- Tai, X., Van Laethem, F., Pobezinsky, L., Ginter, T., Sharrow, S.O., Adams, A., . . . Singer, A. (2012). Basis of CTLA-4 function in regulatory and conventional CD4(+) T cells. *Blood* 119, 5155-5163.
- Tan, D., Zhou, M., Kiledjian, M., and Tong, L. (2014). The ROQ domain of Roquin recognizes mRNA constitutive-decay element and double-stranded RNA. *Nat Struct Mol Biol* 21, 679-685.
- Tavernier, S., Athanasopoulos, V., Verloo, P., Behrens, G., Staal, J., Bogaert, D.J., . . . Haerynck, F. (2019). A human immune dysregulation syndrome characterized by severe hyperinflammation with a homozygous nonsense Roquin-1 mutation. *Nat Commun* 10, 4779.
- Tharun, S., and Parker, R. (2001). Targeting an mRNA for decapping: displacement of translation factors and association of the Lsm1p-7p complex on deadenylated yeast mRNAs. *Mol Cell* 8, 1075-1083.
- Thompson, J., and Winoto, A. (2008). During negative selection, Nur77 family proteins translocate to mitochondria where they associate with Bcl-2 and expose its proapoptotic BH3 domain. *J Exp Med* 205, 1029-1036.
- Tischner, D., Woess, C., Ottina, E., and Villunger, A. (2010). Bcl-2-regulated cell death signalling in the prevention of autoimmunity. *Cell Death Dis* 1, e48.
- Toomer, K.H., Lui, J.B., Altman, N.H., Ban, Y., Chen, X., and Malek, T.R. (2019). Essential and non-overlapping IL-2Ralpha-dependent processes for thymic development and peripheral homeostasis of regulatory T cells. *Nat Commun* 10, 1037.
- Touma, M., Keskin, D.B., Shiroki, F., Saito, I., Koyasu, S., Reinherz, E.L., and Clayton, L.K. (2011). Impaired B cell development and function in the absence of IkappaBNS. *J Immunol* 187, 3942-3952.
- Tsokos, G.C., Lo, M.S., Costa Reis, P., and Sullivan, K.E. (2016). New insights into the immunopathogenesis of systemic lupus erythematosus. *Nat Rev Rheumatol* 12, 716-730.
- Uehata, T., Iwasaki, H., Vandenbon, A., Matsushita, K., Hernandez-Cuellar, E., Kuniyoshi, K., . . . Akira, S. (2013). Malt1-induced cleavage of regnase-1 in CD4(+) helper T cells regulates immune activation. *Cell* 153, 1036-1049.
- Ueno, H., and Blanco, P. (2015). OX40/OX40L axis: not a friend in autoimmunity. *Oncotarget* 6, 21779-21780.
- van Hoof, A., Frischmeyer, P.A., Dietz, H.C., and Parker, R. (2002). Exosome-mediated recognition and degradation of mRNAs lacking a termination codon. *Science* 295, 2262-2264.
- Vinuesa, C.G., Cook, M.C., Angelucci, C., Athanasopoulos, V., Rui, L., Hill, K.M., . . . Goodnow, C.C. (2005). A RING-type ubiquitin ligase family member required to repress follicular helper T cells and autoimmunity. *Nature* 435, 452-458.

- Vogel, K.U., Edelmann, S.L., Jeltsch, K.M., Bertossi, A., Heger, K., Heinz, G.A., . . . Heissmeyer, V. (2013). Roquin paralogs 1 and 2 redundantly repress the Icos and Ox40 costimulator mRNAs and control follicular helper T cell differentiation. *Immunity* 38, 655-668.
- von Gamm, M., Schaub, A., Jones, A.N., Wolf, C., Behrens, G., Lichti, J., . . . Glasmacher, E. (2019). Immune homeostasis and regulation of the interferon pathway require myeloid-derived Regnase-3. *J Exp Med*.
- Voo, K.S., Wang, Y.H., Santori, F.R., Boggiano, C., Wang, Y.H., Arima, K., . . . Liu, Y.J. (2009). Identification of IL-17-producing FOXP3<sup>+</sup> regulatory T cells in humans. *Proc Natl Acad Sci U S A* 106, 4793-4798.
- Walker, L.S., Gulbranson-Judge, A., Flynn, S., Brocker, T., Raykundalia, C., Goodall, M., . . . Lane, P. (1999). Compromised OX40 function in CD28-deficient mice is linked with failure to develop CXC chemokine receptor 5-positive CD4 cells and germinal centers. *J Exp Med* 190, 1115-1122.
- Wang, D., Zheng, M., Lei, L., Ji, J., Yao, Y., Qiu, Y., . . . Lu, L. (2012). Tespa1 is involved in late thymocyte development through the regulation of TCR-mediated signaling. *Nat Immunol* 13, 560-568.
- Waskow, C., Paul, S., Haller, C., Gassmann, M., and Rodewald, H.R. (2002). Viable c-Kit(W/W) mutants reveal pivotal role for c-kit in the maintenance of lymphopoiesis. *Immunity* 17, 277-288.
- Wawro, M., Kochan, J., Krzanik, S., Jura, J., and Kasza, A. (2017). Intact NYN/PIN-Like Domain is Crucial for the Degradation of Inflammation-Related Transcripts by ZC3H12D. *J Cell Biochem* 118, 487-498.
- Webb, L.M.C., and Linterman, M.A. (2017). Signals that drive T follicular helper cell formation. *Immunology* 152, 185-194.
- Weinberg, A.D. (2010). The role of OX40 (CD134) in T-cell memory generation. *Adv Exp Med Biol* 684, 57-68.
- Will, S., Reiche, K., Hofacker, I.L., Stadler, P.F., and Backofen, R. (2007). Inferring noncoding RNA families and classes by means of genome-scale structure-based clustering. *PLoS Comput Biol* 3, e65.
- Wing, J.B., Kitagawa, Y., Locci, M., Hume, H., Tay, C., Morita, T., . . . Sakaguchi, S. (2017). A distinct subpopulation of CD25(-) T-follicular regulatory cells localizes in the germinal centers. *Proc Natl Acad Sci U S A* 114, E6400-e6409.
- Wolf, J., and Passmore, L.A. (2014). mRNA deadenylation by Pan2-Pan3. *Biochem Soc Trans* 42, 184-187.
- Wulczyn, F.G., Naumann, M., and Scheidereit, C. (1992). Candidate proto-oncogene bcl-3 encodes a subunit-specific inhibitor of transcription factor NF-kappa B. *Nature* 358, 597-599.
- Xu, J., Peng, W., Sun, Y., Wang, X., Xu, Y., Li, X., . . . Rao, Z. (2012). Structural study of MCP1P1 N-terminal conserved domain reveals a PIN-like RNase. *Nucleic Acids Res* 40, 6957-6965.
- Yamaguchi, T., Cubizolles, F., Zhang, Y., Reichert, N., Kohler, H., Seiser, C., and Matthias, P. (2010). Histone deacetylases 1 and 2 act in concert to promote the G1-to-S progression. *Genes Dev* 24, 455-469.
- Yamaguchi, T., Kishi, A., Osaki, M., Morikawa, H., Prieto-Martin, P., Wing, K., . . . Sakaguchi, S. (2013). Construction of self-recognizing regulatory T cells from conventional T cells by controlling CTLA-4 and IL-2 expression. *Proc Natl Acad Sci U S A* 110, E2116-2125.
- Yamane, H., and Paul, W.E. (2013). Early signaling events that underlie fate decisions of naive CD4(+) T cells toward distinct T-helper cell subsets. *Immunol Rev* 252, 12-23.

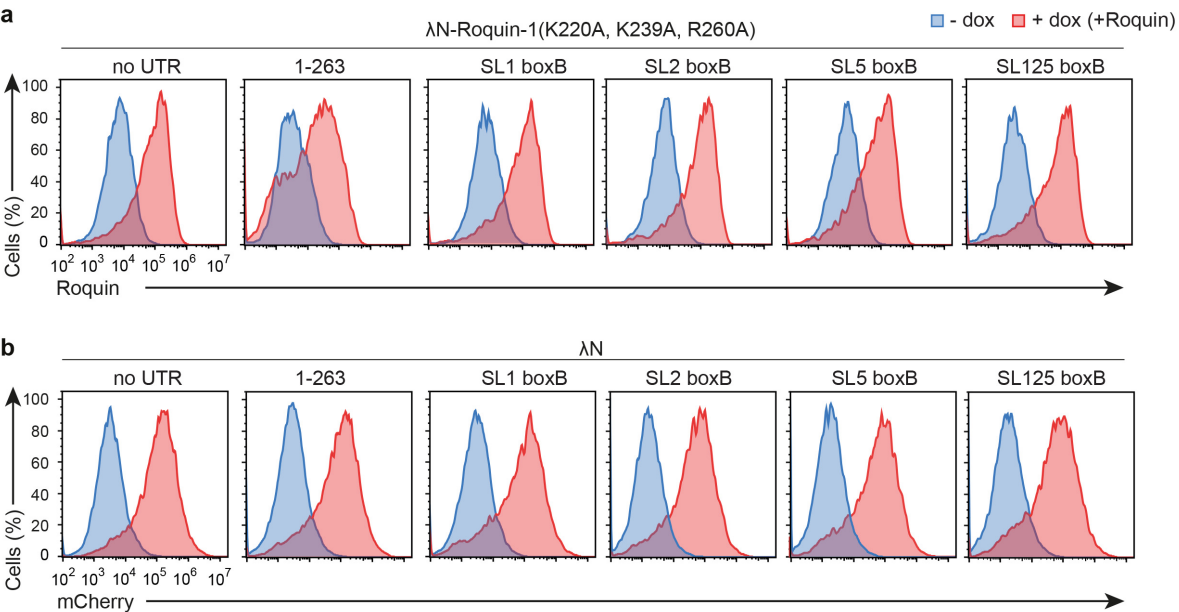


- Yamauchi, S., Ito, H., and Miyajima, A. (2010). IkappaBeta, a nuclear IkappaB protein, positively regulates the NF-kappaB-mediated expression of proinflammatory cytokines. *Proc Natl Acad Sci U S A* 107, 11924-11929.
- Yang, W.M., Inouye, C., Zeng, Y., Bearss, D., and Seto, E. (1996). Transcriptional repression by YY1 is mediated by interaction with a mammalian homolog of the yeast global regulator RPD3. *Proc Natl Acad Sci U S A* 93, 12845-12850.
- Yao, S., Zhu, Y., Zhu, G., Augustine, M., Zheng, L., Goode, D.J., . . . Chen, L. (2011). B7-h2 is a costimulatory ligand for CD28 in human. *Immunity* 34, 729-740.
- Yokogawa, M., Tsushima, T., Noda, N.N., Kumeta, H., Enokizono, Y., Yamashita, K., . . . Inagaki, F. (2016). Structural basis for the regulation of enzymatic activity of Regnase-1 by domain-domain interactions. *Sci Rep* 6, 22324.
- Yokosuka, T., Takamatsu, M., Kobayashi-Imanishi, W., Hashimoto-Tane, A., Azuma, M., and Saito, T. (2012). Programmed cell death 1 forms negative costimulatory microclusters that directly inhibit T cell receptor signaling by recruiting phosphatase SHP2. *J Exp Med* 209, 1201-1217.
- Yoshinaga, M., Nakatsuka, Y., Vandenbon, A., Ori, D., Uehata, T., Tsujimura, T., . . . Takeuchi, O. (2017). Regnase-1 Maintains Iron Homeostasis via the Degradation of Transferrin Receptor 1 and Prolyl-Hydroxylase-Domain-Containing Protein 3 mRNAs. *Cell Rep* 19, 1614-1630.
- Youle, R.J., and Strasser, A. (2008). The BCL-2 protein family: opposing activities that mediate cell death. *Nat Rev Mol Cell Biol* 9, 47-59.
- Yu, D., Tan, A.H., Hu, X., Athanasopoulos, V., Simpson, N., Silva, D.G., . . . Vinuesa, C.G. (2007). Roquin represses autoimmunity by limiting inducible T-cell co-stimulator messenger RNA. *Nature* 450, 299-303.
- Zhan, Y., Zhang, Y., Gray, D., Carrington, E.M., Bouillet, P., Ko, H.J., . . . Lew, A.M. (2011). Defects in the Bcl-2-regulated apoptotic pathway lead to preferential increase of CD25 low Foxp3+ anergic CD4+ T cells. *J Immunol* 187, 1566-1577.
- Zhang, H., Wang, W.C., Chen, J.K., Zhou, L., Wang, M., Wang, Z.D., . . . Jiang, T. (2015). ZC3H12D attenuated inflammation responses by reducing mRNA stability of proinflammatory genes. *Mol Immunol* 67, 206-212.
- Zheng, W., and Flavell, R.A. (1997). The transcription factor GATA-3 is necessary and sufficient for Th2 cytokine gene expression in CD4 T cells. *Cell* 89, 587-596.
- Zheng, Y., Josefowicz, S., Chaudhry, A., Peng, X.P., Forbush, K., and Rudensky, A.Y. (2010). Role of conserved non-coding DNA elements in the Foxp3 gene in regulatory T-cell fate. *Nature* 463, 808-812.
- Zhou, L., Azfer, A., Niu, J., Graham, S., Choudhury, M., Adamski, F.M., . . . Kolattukudy, P.E. (2006). Monocyte chemoattractant protein-1 induces a novel transcription factor that causes cardiac myocyte apoptosis and ventricular dysfunction. *Circ Res* 98, 1177-1185.
- Zhu, Y., Yao, S., and Chen, L. (2011). Cell surface signaling molecules in the control of immune responses: a tide model. *Immunity* 34, 466-478.
- Zinder, J.C., and Lima, C.D. (2017). Targeting RNA for processing or destruction by the eukaryotic RNA exosome and its cofactors. *Genes Dev* 31, 88-100.

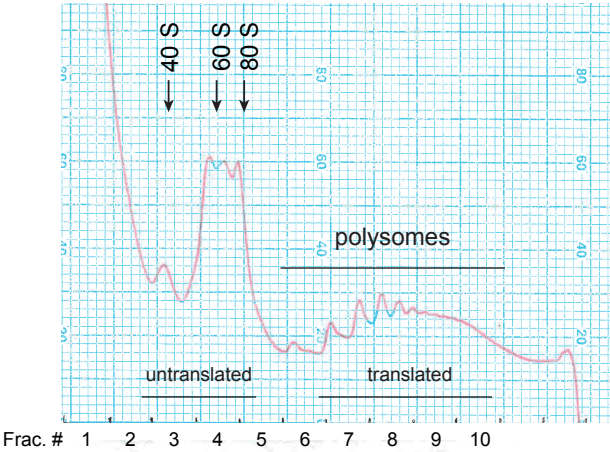


# Appendices

**Appendix 1 |** Flow cytometry analysis of Roquin and mCherry expression in *Rc3h1*<sup>-/-</sup>, rtTA3 MEF cells upon doxycycline-induced expression of λN-Roquin-1(K220A, K239A, R260A) and λN-p2A-mCherry.

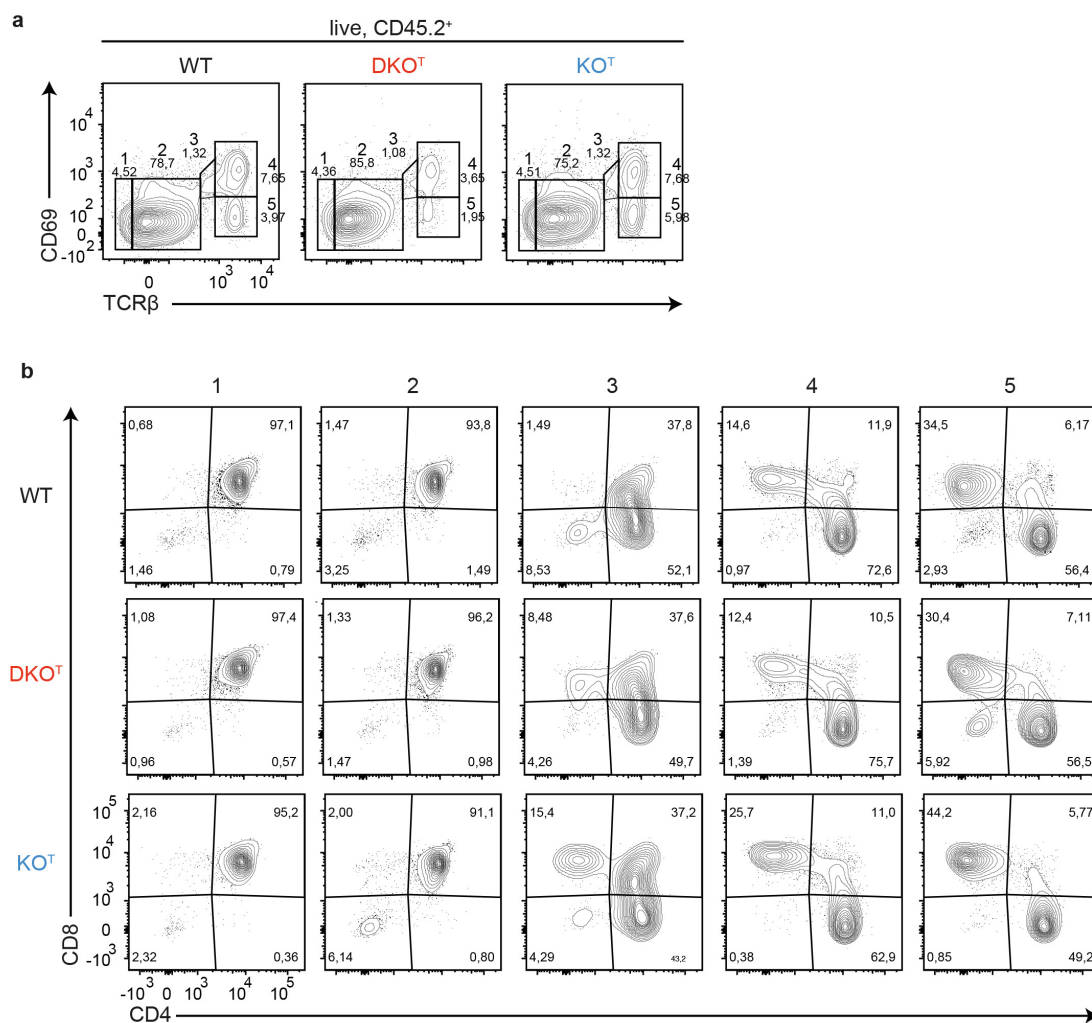


**Appendix 2 |** Absorbance profiles at 260 nm obtained during fractionations of sucrose gradients in Figure 21.



### Appendix 3 | Analyzing positive selection and maturation of CD4 and CD8 T cells in WT, KO<sup>T</sup> and DKO<sup>T</sup> mice.

a) Positive selection was determined in thymi of live, CD45.2<sup>+</sup> cells from WT, DKO<sup>T</sup> and KO<sup>T</sup> mice by CD69 and TCR $\beta$  expression pattern in populations 1-5. b) CD4 and CD8 expression in the 5 populations defined by TCR $\beta$  and CD69 expression in a) of WT, DKO<sup>T</sup> and KO<sup>T</sup> thymocytes.



## Appendix 4 | Gene list of cooperative targets in cluster 2 and 4.

Gene	cluster	0h				TKO/ KO	TKO/ DKO
		WT	KO	DKO	TKO		
Gm15987	4	0.0	3.4	1.3	5.5	1.6	4.3
Cebpd	4	0.0	1.2	0.7	5.5	4.4	7.5
Kit	4	0.0	2.0	1.9	5.0	2.5	2.6
Tnfrsf8	4	0.0	0.6	2.1	4.8	7.4	2.2
Tlr9	4	0.0	1.3	2.4	4.6	3.6	1.9
Gm14718	4	0.0	1.7	2.0	4.5	2.6	2.2
Zcchc18	4	0.0	2.6	2.7	4.4	1.7	1.6
Fam43a	4	0.0	0.8	1.2	4.4	5.5	3.7
Ebi3	4	0.0	1.0	3.3	4.1	4.3	1.3
Tox2	4	0.0	0.4	1.6	4.1	10.9	2.6
Ppic	4	0.0	1.8	1.4	4.0	2.3	2.9
Prickle1	4	0.0	2.2	1.1	3.9	1.8	3.6
Fcrl1	4	0.0	1.0	0.7	3.7	3.7	5.2
Icos	4	0.0	1.9	2.4	3.6	1.9	1.5
Mpz11	4	0.0	1.1	0.9	3.5	3.2	3.7
Cpd	4	0.0	1.0	1.8	3.4	3.3	1.9
Lmna	4	0.0	0.4	1.6	3.3	9.5	2.1
P24-312B12	4	0.0	2.2	2.0	3.2	1.5	1.7
Zc3h12c	4	0.0	0.4	0.9	3.2	8.8	3.5
Fam84a	4	0.0	0.7	1.2	3.2	4.4	2.6
Upp1	4	0.0	0.6	0.5	3.2	5.5	6.7
Gatm	4	0.0	0.6	1.4	3.1	5.0	2.3
Rhov	4	0.0	0.4	0.8	2.9	7.3	3.5
Tex15	4	0.0	1.0	1.0	2.8	2.9	2.8
Smox	4	0.0	1.1	1.3	2.7	2.4	2.2
Nfkbia	4	0.0	0.8	0.9	2.7	3.4	3.1
Rims3	2	0.0	1.2	1.1	2.7	2.2	2.4
Alcam	4	0.0	1.3	1.3	2.7	2.1	2.1
Marcks	4	0.0	0.5	0.9	2.7	5.8	3.1
Rilpl2	4	0.0	1.6	1.4	2.7	1.6	1.9
Pou2f2	4	0.0	2.0	1.8	2.7	1.3	1.5
Ankrd55	4	0.0	1.2	1.2	2.6	2.2	2.1
Tubb6	4	0.0	0.5	1.2	2.6	5.0	2.3
Nme4	2	0.0	0.4	0.8	2.6	6.7	3.1
Adap1	2	0.0	1.1	1.7	2.6	2.4	1.5
Clip3	2	0.0	1.1	1.5	2.6	2.3	1.8
Asns	4	0.0	0.8	1.0	2.6	3.1	2.6
Gstt1	4	0.0	0.8	1.7	2.6	3.2	1.5
Ctla4	2	0.0	0.7	1.6	2.6	3.8	1.7
Slamf6	4	0.0	1.0	1.9	2.6	2.5	1.3
Tmem121	2	0.0	0.6	1.2	2.5	4.1	2.1
Batf	4	0.0	1.2	1.4	2.5	2.1	1.8
Pnpla3	2	0.0	0.4	1.6	2.5	5.6	1.5
Batf3	4	0.0	0.6	0.5	2.5	4.2	4.5
Sox12	4	0.0	0.6	0.9	2.5	4.4	2.6
Ctsl	4	0.0	0.7	0.9	2.4	3.4	2.8
Furin	4	0.0	1.1	1.3	2.4	2.2	1.8
Zfp827	4	0.0	1.2	1.7	2.4	2.1	1.4
Asb2	2	0.0	0.8	1.4	2.4	2.9	1.7
Zbtb18	2	0.0	1.6	1.2	2.4	1.5	2.0
Sptb	4	0.0	0.4	0.5	2.4	6.9	4.7
Eno2	4	0.0	0.5	1.0	2.4	4.9	2.4
Foxj1	4	0.0	0.5	0.5	2.3	5.1	4.6
Dnnd2	2	0.0	0.5	1.0	2.3	4.5	2.4
Otud5	2	0.0	0.9	1.6	2.3	2.6	1.4
Ceacam16	2	0.0	0.5	0.9	2.3	4.2	2.6
Gpr125	2	0.0	0.6	1.3	2.3	3.6	1.7
Ctsf	2	0.0	0.9	1.4	2.3	2.6	1.7
Slc15a3	4	0.0	0.5	0.7	2.2	4.2	3.4
Pfn2	2	0.0	0.7	1.0	2.2	3.1	2.1
Cd40lq	4	0.0	1.4	1.7	2.2	1.6	1.3
Spock2	2	0.0	0.7	1.0	2.2	3.1	2.2
P24-113D2	4	0.0	1.0	1.1	2.1	2.2	2.0
Fah	2	0.0	1.1	1.0	2.1	1.9	2.1
Zc3h12d	2	0.0	1.0	1.5	2.1	2.2	1.4
Pik3c2b	2	0.0	0.8	1.5	2.1	2.7	1.4
Slc35f5	2	0.0	0.4	1.1	2.1	5.4	1.8
Gpr179	2	0.0	0.5	1.6	2.0	4.4	1.3
Trim71	4	0.0	1.2	0.5	2.0	1.7	4.0
Slc2a6	4	0.0	0.7	0.8	2.0	2.8	2.5
Hif3a	2	0.0	0.4	1.1	2.0	5.4	1.9
Mqmn1	2	0.0	0.7	0.8	2.0	2.7	2.5
Rab31	2	0.0	0.4	0.4	2.0	5.3	5.2
Zak	2	0.0	0.6	0.8	2.0	3.2	2.5
Ankrd34b	4	0.0	0.6	0.6	2.0	3.6	3.4
Irak3	2	0.0	0.9	0.7	2.0	2.1	2.7
Fam213a	2	0.0	0.5	1.4	2.0	3.8	1.4
Mlr1	2	0.0	0.9	0.6	1.9	2.2	3.1
Gm7645	2	0.0	0.5	0.9	1.9	3.7	2.3
Abhd17c	4	0.0	1.1	1.0	1.9	1.7	1.8
Perp	4	0.0	0.5	0.6	1.9	3.5	3.0
Usp6nl	2	0.0	1.0	1.0	1.9	1.9	1.9
Tead1	4	0.0	1.2	0.5	1.9	1.6	3.9
Armcx2	2	0.0	0.7	1.0	1.9	2.6	1.9
Ltbp3	2	0.0	0.4	0.9	1.9	4.3	2.2
Ell2	4	0.0	1.0	1.2	1.9	1.8	1.6
Lama5	2	0.0	1.2	1.0	1.9	1.6	1.9
Gm15051	2	0.0	0.4	0.7	1.9	4.2	2.7
Tnp2	2	0.0	0.4	0.8	1.9	4.7	2.2
Gm13012	2	0.0	0.5	0.9	1.8	3.4	2.0
Tmsb15b1	2	0.0	0.9	1.0	1.8	2.0	1.8
Ikzf4	2	0.0	1.1	0.9	1.8	1.6	2.0

Gm20645	4	0.0	0.5	1.0	1.8	4.1	1.8
Gab2	2	0.0	1.0	0.7	1.8	1.8	2.5
Gm12699	4	0.0	0.5	0.8	1.8	4.0	2.4
Plscr1	4	0.0	0.4	1.3	1.8	5.0	1.5
Hrsp12	2	0.0	0.4	1.4	1.8	5.0	1.3
Ifnlr1	2	0.0	0.6	0.6	1.8	2.9	3.1
Slc37a2	4	0.0	0.5	0.9	1.8	3.5	2.1
Ccdc50	4	0.0	0.6	0.9	1.8	3.0	2.0
Fam46a	2	0.0	1.2	1.2	1.8	1.5	1.4
Itqb5	2	0.0	1.0	0.5	1.8	1.8	3.4
Tnfrsf25	2	0.0	0.7	1.2	1.8	2.5	1.4
Espn	2	0.0	0.6	0.8	1.8	2.7	2.3
H2-Eb1	2	0.0	0.6	0.6	1.7	2.8	3.1
Hk2	4	0.0	0.6	0.8	1.7	2.8	2.1
Ypel2	2	0.0	0.5	0.6	1.7	3.6	2.7
Rbpsuh-rs3	4	0.0	0.5	0.8	1.7	3.3	2.2
Abca1	4	0.0	0.6	0.9	1.7	2.8	1.9
Nfkbiz	4	0.0	1.1	0.9	1.7	1.5	2.0
Ccdc17	2	0.0	0.8	0.9	1.7	2.2	1.9
Nlmg2	4	0.0	1.2	1.2	1.7	1.4	1.4
Ggn	2	0.0	0.6	1.0	1.7	3.1	1.7
Mvb	2	0.0	0.5	1.3	1.7	3.3	1.3
Hip1r	2	0.0	0.9	0.9	1.7	1.8	1.8
Tnfrsf8	4	0.0	0.9	0.8	1.7	2.0	2.0
Jdp2	2	0.0	0.7	1.3	1.7	2.5	1.3
Pde8a	2	0.0	0.8	0.8	1.6	2.1	1.9
Agpat4	4	0.0	0.7	0.8	1.6	2.2	2.0
Ksr1	4	0.0	0.5	1.1	1.6	3.3	1.4
Arhgef5	2	0.0	0.4	1.1	1.6	4.2	1.5
Cd72	2	0.0	0.4	0.6	1.6	4.1	2.8
Tcf7	2	0.0	0.8	0.9	1.6	2.1	1.8
Slc25a53	2	0.0	1.0	1.0	1.6	1.6	1.5
Stx11	4	0.0	0.6	1.1	1.6	2.6	1.5
Ston2	2	0.0	0.5	0.8	1.6	3.3	2.0
Hddc3	2	0.0	0.6	1.1	1.6	2.6	1.5
Rbpj	4	0.0	0.4	0.8	1.6	3.7	2.0
Bcl6	4	0.0	0.7	1.0	1.6	2.4	1.6
Tspan5	4	0.0	0.6	0.5	1.6	2.5	2.9
Fndc3a	2	0.0	0.8	0.7	1.6	2.0	2.2
Tcn2	2	0.0	0.8	1.0	1.6	1.9	1.5
Ldhd	2	0.0	0.4	1.0	1.6	3.8	1.6
Dynlt3	2	0.0	0.5	1.0	1.6	3.0	1.6
Gm12764	2	0.0	1.0	0.9	1.6	1.6	1.7
20401G13	2	0.0	0.5	0.9	1.6	3.4	1.7
Abhd4	2	0.0	0.6	0.9	1.6	2.6	1.7
Pla2g12a	4	0.0	0.5	0.7	1.6	2.9	2.1
Cd200	4	0.0	0.9	1.0	1.5	1.7	1.5
Mcam	2	0.0	0.5	0.6	1.5	2.9	2.5
Gm14680	2	0.0	0.5	0.6	1.5	3.3	2.7
Cxx1c	2	0.0	0.7	0.6	1.5	2.0	2.6
Slc39a13	2	0.0	0.5	0.7	1.5	3.3	2.0
Gm15473	2	0.0	0.6	1.0	1.5	2.4	1.4
Tmsb15l	2	0.0	0.9	0.9	1.5	1.7	1.6
Rundc3a	2	0.0	0.6	0.9	1.5	2.6	1.7
Mrpl45	2	0.0	0.4	1.1	1.5	3.4	1.3
Trerf1	2	0.0	0.5	1.0	1.5	3.0	1.4
Rragd	2	0.0	0.8	0.9	1.5	1.8	1.6
30402F18f	4	0.0	1.1	0.9	1.4	1.3	1.6
Chic1	2	0.0	0.6	0.9	1.4	2.3	1.6
Cpt1c	2	0.0	0.5	0.6	1.4	2.9	2.6
Adam8	2	0.0	0.6	0.5	1.4	2.2	3.1
Fam46c	2	0.0	0.7	0.5	1.4	2.0	3.0
Zfp518b	2	0.0	0.5	0.9	1.4	2.8	1.6
Zc2hc1a	2	0.0	0.4	0.9	1.4	3.7	1.5
Lpxn	2	0.0	0.7	1.0	1.4	2.0	1.4
Plcb4	2	0.0	0.4	0.8	1.4	3.9	1.7
Hmgn3	2	0.0	0.6	0.9	1.4	2.3	1.6
Ndst1	2	0.0	0.6	0.8	1.4	2.4	1.8
Rapgef5	2	0.0	0.5	0.5	1.4	2.6	2.7
Plk2	4	0.0	0.8	0.6	1.4	1.6	2.2
Cldn12	2	0.0	0.5	0.9	1.4	2.8	1.5
Pecam1	2	0.0	0.8	0.6	1.4	1.8	2.1
Ccr4	2	0.0	0.9	1.0	1.4	1.6	1.3
Prrg4	4	0.0	0.6	0.9	1.3	2.3	1.5
Gstt2	2	0.0	0.4	0.9	1.3	3.6	1.5
Tmem198b	2	0.0	0.5	0.8	1.3	2.6	1.6
Gpr18	2	0.0	1.1	0.9	1.3	1.3	1.4
Armxc4	2	0.0	0.5	0.6	1.3	2.9	2.2
Ahr	4	0.0	0.8	0.9	1.3	1.6	1.5
Sdcbp2	2	0.0	0.6	1.0	1.3	2.3	1.3
Akr7a5	2	0.0	0.4	0.5	1.3	3.1	2.7
Ggt7	2	0.0	0.7	0.9	1.3	1.8	1.5
Zfp516	2	0.0	0.5	1.0	1.3	2.9	1.3
Cyp4v3	2	0.0	0.6	0.9	1.3	2.2	1.4
Tab2	2	0.0	0.9	1.0	1.3	1.4	1.3
Gucy1b3	2	0.0	0.8	1.0	1.3	1.7	1.3
Fam210b	2	0.0	0.4	1.0	1.2	3.3	1.3
Per2	4	0.0	0.4	0.4	1.2	2.9	2.8
Gls2	2	0.0	0.4	0.7	1.2	3.5	1.9
Pgic1	2	0.0	0.5	0.9	1.2	2.4	1.4
Itfg3	2	0.0	0.4	0.7	1.2	2.8	1.8

Xk	2	0,0	0,4	0,6	1,2	2,9	2,2
Pkxna1	4	0,0	0,5	0,7	1,2	2,5	1,7
Rybp	2	0,0	0,6	0,6	1,2	2,1	2,0
Ube2q2	4	0,0	0,5	0,5	1,2	2,2	2,3
Slc39a4	2	0,0	0,4	0,6	1,2	3,1	2,1
10001H17f	2	0,0	0,5	0,7	1,2	2,2	1,7
Bcl2l2	2	0,0	0,5	0,9	1,2	2,2	1,3
Tmtc4	2	0,0	0,5	0,4	1,2	2,5	2,8
Gm20689	4	0,0	0,6	0,8	1,2	2,1	1,5
Gaa	2	0,0	0,4	0,6	1,2	2,7	1,9
Phyh	2	0,0	0,5	0,9	1,2	2,2	1,3
Lta	2	0,0	0,4	0,8	1,1	2,8	1,4
Tmbim1	4	0,0	0,4	0,6	1,1	3,1	2,0
Nabp1	2	0,0	0,6	0,8	1,1	1,9	1,3
Malt1	4	0,0	0,4	0,6	1,1	2,9	1,7
Cdc14b	2	0,0	0,4	0,5	1,1	2,8	2,2
Ube2f	2	0,0	0,7	0,8	1,1	1,5	1,3
Mink1	2	0,0	0,5	0,6	1,1	2,3	1,9
Map9	2	0,0	0,5	0,7	1,1	2,1	1,6
Hspa13	2	0,0	0,4	0,6	1,1	2,8	1,9
Slc4a7	4	0,0	0,6	0,5	1,1	1,9	1,9
Rrad	4	0,0	0,4	0,7	1,1	2,3	1,4
Acp6	2	0,0	0,6	0,8	1,1	1,8	1,3
Tspsyl2	2	0,0	0,5	0,5	1,0	2,1	2,0
Atcay	2	0,0	0,4	0,7	1,0	2,4	1,6
Aldh7a1	2	0,0	0,6	0,7	1,0	1,7	1,5
Ocr1	2	0,0	0,4	0,6	1,0	2,5	1,6
Tcf4	2	0,0	0,6	0,5	1,0	1,7	2,0
Stat3	2	0,0	0,5	0,6	1,0	1,9	1,6
Fyttd1	2	0,0	0,5	0,5	1,0	2,2	2,0
Cited2	2	0,0	0,6	0,5	1,0	1,6	2,0
Ppt1	2	0,0	0,4	0,5	1,0	2,5	1,9
Cldn25	2	0,0	0,6	0,6	1,0	1,7	1,6
Cdkn1a	2	0,0	0,6	0,5	1,0	1,7	2,1
Hif1a	2	0,0	0,7	0,6	1,0	1,4	1,6
Gm5884	2	0,0	0,7	0,6	1,0	1,5	1,7
Pqbp1	2	0,0	0,4	0,6	1,0	2,4	1,6
Tspan3	2	0,0	0,5	0,6	0,9	1,8	1,5
Tes	2	0,0	0,5	0,7	0,9	1,8	1,4
Gnpat1	2	0,0	0,4	0,5	0,9	2,2	2,0
Ddt	2	0,0	0,5	0,5	0,9	2,0	2,1
St3gal2	2	0,0	0,5	0,7	0,9	1,9	1,3
Plekha8	2	0,0	0,4	0,5	0,9	2,4	1,7
Em1	2	0,0	0,6	0,5	0,9	1,5	1,8
Em15	2	0,0	0,5	0,5	0,9	1,9	1,9
Tmem237	2	0,0	0,5	0,6	0,9	1,8	1,5
Gm	2	0,0	0,4	0,7	0,9	1,9	1,3
Slc25a36	2	0,0	0,5	0,6	0,9	1,7	1,4
Adam9	2	0,0	0,5	0,5	0,9	1,8	1,8
Usp33	2	0,0	0,4	0,6	0,8	1,9	1,4
Fam71b	2	0,0	0,4	0,5	0,8	1,9	1,6
Arhgef12	2	0,0	0,4	0,5	0,8	2,0	1,5
Sdf4	2	0,0	0,4	0,6	0,8	2,3	1,3
Tnfrsf14	2	0,0	0,4	0,6	0,8	2,2	1,5
Ccdc66	2	0,0	0,4	0,6	0,8	2,2	1,3
Tet2	4	0,0	0,5	0,5	0,8	1,7	1,6
Bmi1	2	0,0	0,4	0,5	0,8	2,3	1,7
Arrdc3	2	0,0	0,4	0,5	0,8	2,0	1,6
Ttc39c	2	0,0	0,4	0,5	0,8	1,9	1,5
Sqstm1	2	0,0	0,5	0,5	0,8	1,7	1,5
Tbrg1	2	0,0	0,4	0,6	0,8	1,9	1,3
Rab8b	4	0,0	0,4	0,4	0,8	2,1	1,7
Tmbim4	2	0,0	0,5	0,5	0,8	1,6	1,6
Plekha2	2	0,0	0,4	0,5	0,7	1,9	1,3
Il12rb1	2	0,0	0,5	0,4	0,7	1,5	1,8
Arhgap26	2	0,0	0,4	0,4	0,7	1,7	1,8
Wsb2	4	0,0	0,5	0,4	0,7	1,3	1,7
Tmem30a	2	0,0	0,4	0,4	0,7	1,7	1,9

## Appendix 5 | Gene list of Regnase-1 exclusive targets in cluster 2 and 4.

Gene	cluster	oh				TKO/ KO	TKO/ DKO
		WT	KO	DKO	TKO		
Ecm1	2	0,0	1,4	0,3	1,4	1,0	4,2
Arhgap5	2	0,0	1,1	0,2	0,9	0,8	5,1
Gbp2	2	0,0	1,1	0,2	0,6	0,5	2,9
Pld3	2	0,0	0,5	0,3	0,6	1,2	2,1
32428N05f	2	0,0	0,6	0,3	0,5	0,9	2,0
Ptpn6	2	0,0	0,5	0,3	0,5	1,2	2,0
Hrh2	2	0,0	0,8	0,2	0,5	0,6	2,5
Zhx2	4	0,0	0,5	0,0	0,5	1,1	11,3
Helz2	2	0,0	0,5	0,2	0,5	0,9	2,1

**Appendix 6 | Gene list of Roquin exclusive targets in cluster 2 and 4.**

Gene	cluster	0h				TKO/ KO	TKO/ DKO
		WT	KO	DKO	TKO		
Tnfrsf4	4	0,0	0,3	1,7	2,1	6,8	1,2
Unc5b	2	0,0	-0,2	2,0	1,9	-9,1	0,9
Slc30a2	2	0,0	-0,1	1,5	1,8	-12,4	1,2
Ndst2	2	0,0	0,3	1,2	1,5	5,3	1,2
Fchs2	2	0,0	0,2	1,2	1,5	6,3	1,2
Irf5	2	0,0	0,3	1,1	1,3	4,9	1,2
Atp13a2	2	0,0	0,2	1,1	1,3	8,4	1,2
10015A10F	2	0,0	0,0	1,1	1,3	0,0	1,2
Cep85l	2	0,0	0,3	1,0	1,2	3,7	1,2
Zc4h2	2	0,0	0,1	1,0	1,2	11,4	1,2
Ptpn21	2	0,0	0,2	1,1	1,2	6,1	1,1
Zfp446	2	0,0	0,2	1,2	1,1	6,1	0,9
Wdr60	2	0,0	0,2	0,9	1,1	6,6	1,2
Mea1	2	0,0	0,3	1,0	1,1	3,3	1,1
Serpinc6b	4	0,0	-0,2	1,3	1,1	-5,1	0,8
Zfp219	2	0,0	0,3	0,9	1,1	3,6	1,2
Fuca2	2	0,0	0,1	0,9	1,1	11,9	1,2
Bcr	2	0,0	0,3	1,1	1,0	3,7	0,9
Gm11998	2	0,0	0,3	1,0	1,0	3,9	1,0
Junb	4	0,0	0,3	0,8	1,0	2,9	1,2
Gfi1	4	0,0	0,1	1,5	0,9	17,5	0,6
Tnfrsf11	4	0,0	0,3	1,1	0,9	2,9	0,8
Med23	2	0,0	0,0	0,8	0,9	459,5	1,1
Wdr59	4	0,0	0,3	0,8	0,9	2,9	1,2
Kif3b	2	0,0	0,3	0,7	0,8	2,4	1,2
Cd84	4	0,0	0,3	0,8	0,8	2,8	1,0
10111101F	2	0,0	0,2	0,7	0,8	3,8	1,1
Fam129a	4	0,0	0,0	0,7	0,8	0,0	1,1
Sh3bgrl	2	0,0	0,3	0,6	0,8	2,6	1,2
Stx6	4	0,0	0,2	0,7	0,7	3,6	1,1
Tada1	2	0,0	0,0	0,7	0,7	0,0	1,0
Rnpep	2	0,0	0,2	0,6	0,7	4,0	1,2
Spg20	2	0,0	0,1	0,6	0,7	8,1	1,2
Eif2ak4	2	0,0	0,0	0,6	0,7	14,3	1,1
Wdfy2	2	0,0	0,2	0,7	0,7	3,1	0,9
Lime1	2	0,0	0,3	0,5	0,7	2,0	1,2
Ddx17	2	0,0	0,3	0,6	0,7	2,3	1,2
Wdr11	2	0,0	0,3	0,6	0,7	2,3	1,2
Ptgr2	2	0,0	0,1	0,7	0,7	5,7	1,0
Lpin2	2	0,0	0,0	0,8	0,7	0,0	0,8
Ezh2	2	0,0	0,1	0,6	0,6	5,6	1,1
Ccdc104	2	0,0	0,2	0,7	0,6	3,0	1,0
Braf	2	0,0	0,3	0,5	0,6	2,5	1,2
Chd9	2	0,0	0,2	0,5	0,6	2,8	1,2
Etaa1	2	0,0	0,0	0,6	0,6	0,0	1,1
Rnf2	2	0,0	0,3	0,5	0,6	1,8	1,2
Gpr174	4	0,0	0,3	0,9	0,6	2,1	0,7
Nfkb1	4	0,0	0,3	0,5	0,6	2,1	1,1
Clk1	2	0,0	0,3	0,6	0,6	2,1	1,1
Trabd	2	0,0	0,0	0,6	0,6	46,2	1,0
Mif4gd	2	0,0	0,2	0,5	0,6	3,0	1,2
Jmjd1c	2	0,0	0,2	0,6	0,6	3,6	0,9
Tfrc	2	0,0	0,2	0,6	0,6	2,7	1,1
Cd44	4	0,0	0,1	0,6	0,6	4,3	0,9
Ttpal	2	0,0	0,3	0,6	0,6	2,3	1,0
Paip2	2	0,0	0,3	0,5	0,6	1,7	1,2
Ncoa1	2	0,0	0,2	0,5	0,6	2,5	1,2
Zfp275	2	0,0	0,1	0,5	0,6	10,0	1,1
Reep3	4	0,0	0,3	0,7	0,6	2,2	0,8
Itgal	2	0,0	0,1	0,6	0,6	7,1	0,9
Map3k14	2	0,0	0,2	0,5	0,5	2,4	1,2
Slc43a3	2	0,0	0,1	0,5	0,5	3,7	1,1
Cog2	2	0,0	0,1	0,5	0,5	5,9	1,0
Elk3	2	0,0	0,1	0,5	0,5	7,3	1,1
Zc3h12a	4	0,0	0,3	1,7	0,5	1,6	0,3
Casp3	2	0,0	0,3	0,5	0,5	1,7	1,1
Secisbp2l	2	0,0	0,3	0,4	0,5	1,9	1,2
Zfp369	2	0,0	0,0	0,5	0,5	12,0	1,1
Tnrc6a	2	0,0	0,2	0,4	0,5	2,8	1,2
Cep170b	2	0,0	0,2	0,5	0,5	3,4	1,1
Dcaf12	2	0,0	0,2	0,4	0,5	3,0	1,1
Plxnc1	2	0,0	0,0	0,7	0,5	0,0	0,7
Brwd1	2	0,0	0,2	0,4	0,5	2,9	1,2
Paxbp1	2	0,0	0,3	0,4	0,5	1,9	1,2
Lmbrd1	2	0,0	0,3	0,4	0,5	1,7	1,2
Kdsr	2	0,0	0,2	0,4	0,5	2,5	1,2
Gramd1b	4	0,0	0,2	0,5	0,5	3,2	0,9
Heg1	2	0,0	0,0	0,6	0,5	0,0	0,8
Ak3	2	0,0	0,1	0,5	0,5	4,3	1,0
Rc3h2	2	0,0	0,2	0,4	0,5	2,0	1,2
Med13	2	0,0	0,1	0,5	0,4	3,7	1,0



Atp2c1	2	0,0	0,3	0,4	0,4	1,6	1,1
Prkcb	2	0,0	-0,1	0,6	0,4	-6,3	0,7
Rbm5	2	0,0	0,2	0,4	0,4	1,8	1,1
Inpp5b	2	0,0	0,3	0,4	0,4	1,7	1,1
Csnk1a1	2	0,0	0,1	0,4	0,4	3,7	1,1
Gpbp111	2	0,0	0,1	0,5	0,4	7,4	0,9

## Appendix 7 | Gene list of redundant targets in cluster 2 and 4.

Gene	cluster	0h				TKO/ KO	TKO/ DKO
		WT	KO	DKO	TKO		
Picg2	2	0,00	0,28	0,31	2,19	7,80	7,16
Epha2	4	0,00	0,17	0,13	2,15	12,52	17,09
Tmem176a	2	0,00	0,20	0,32	2,11	10,39	6,57
Lrp4	2	0,00	0,02	0,21	1,97	98,50	9,62
30451A03f	2	0,00	0,07	0,32	1,73	26,17	5,36
Arxes2	2	0,00	0,18	0,27	1,70	9,59	6,31
Coprs	2	0,00	0,15	0,33	1,55	10,64	4,66
Zfp703	4	0,00	0,12	0,29	1,46	12,00	5,10
BC018242	2	0,00	0,04	0,22	1,45	41,34	6,70
Mesdc1	2	0,00	0,34	0,29	1,44	4,28	5,02
30003M21f	2	0,00	0,06	0,16	1,41	24,33	8,93
Bcat1	4	0,00	0,07	0,12	1,41	19,32	11,85
Cd320	4	0,00	0,33	0,20	1,41	4,33	6,90
Gsto1	4	0,00	0,21	0,28	1,22	5,87	4,36
Itsn1	2	0,00	0,34	0,27	1,17	3,45	4,35
Slc25a33	4	0,00	0,18	0,11	1,17	6,55	10,66
Gm9824	2	0,00	0,26	0,02	1,07	4,05	46,52
Tgif1	4	0,00	0,23	0,32	1,07	4,67	3,31
Prdm5	2	0,00	0,19	0,30	1,06	5,54	3,50
Purg	2	0,00	0,19	0,23	1,04	5,42	4,53
Ndr3	2	0,0	0,3	0,3	1,0	2,8	2,8
Pdia6	2	0,00	0,20	0,14	0,96	4,80	6,92
Pebp1	2	0,00	0,26	0,29	0,95	3,70	3,25
March8	2	0,00	0,16	0,19	0,95	6,03	4,90
Lpcat3	2	0,00	0,22	0,15	0,93	4,28	6,23
Gm6166	2	0,00	0,20	0,11	0,92	4,60	8,72
Ralb	2	0,0	0,3	0,3	0,9	2,8	2,8
Nek6	4	0,00	0,20	0,11	0,91	4,66	8,08
Usp22	2	0,00	0,32	0,27	0,88	2,74	3,34
Mesdc2	2	0,00	0,24	0,34	0,87	3,61	2,57
Plbd2	2	0,00	0,05	0,19	0,86	19,11	4,48
Uhrf1bp1	2	0,00	0,18	0,29	0,86	4,73	2,97
Stat5a	4	0,00	0,18	0,30	0,85	4,74	2,85
Cd69	4	0,00	0,29	0,29	0,83	2,90	2,89
Ubf1	2	0,00	0,31	0,27	0,83	2,73	3,13
Bhlhb9	2	0,00	0,21	0,27	0,80	3,86	2,94
Gm20458	2	0,00	0,28	0,28	0,80	2,92	2,86
Slc41a1	4	0,00	0,19	0,22	0,80	4,19	3,67
Coq9	2	0,00	0,34	0,28	0,80	2,34	2,82
Ssr2	2	0,00	0,25	0,07	0,79	3,16	11,17
Nip7	4	0,00	0,20	0,24	0,79	3,88	3,34
Sbno2	2	0,00	0,20	0,24	0,78	3,93	3,30
Creg1	2	0,00	0,14	0,13	0,77	5,69	5,91
Rictor	2	0,00	0,29	0,27	0,76	2,58	2,86
Naa30	2	0,00	0,23	0,09	0,75	3,22	8,04
Hspa5	4	0,00	0,15	0,05	0,73	4,82	13,57
Ptplad1	2	0,00	0,32	0,21	0,73	2,29	3,54
Iqcb1	2	0,00	0,15	0,30	0,73	5,03	2,42
Gm5560	2	0,00	0,29	0,07	0,73	2,49	10,11
Ube2e3	2	0,00	0,10	0,10	0,72	6,93	7,28
30354K17f	2	0,00	0,25	0,27	0,72	2,87	2,69
Prkcsh	2	0,00	0,23	0,29	0,71	3,11	2,48

## Publications

### Publications related to this thesis

Katharina Essig\*, **Nina Kronbeck**\*, Joao C. Guimaraes\*, Claudia Lohs\*, Andreas Schlundt, Anne Hoffmann, Gesine Behrens, Sven Brenner, Joanna Kowalska, Cristina Lopez-Rodriguez, Jacek Jemielity, Helmut Holtmann, Kristin Reiche, Jörg Hackermüller, Michael Sattler, Mihaela Zavolan & Vigo Heissmeyer. **Roquin targets mRNAs in a 3'-UTR-specific manner by different modes of regulation.** *Nature Communications*. 2018; 9: 3810

\* authors contributed equally

Robert Janowski\*, Gitta A. Heinz\*, Andreas Schlundt\*, **Nina Wommelsdorf**, Sven Brenner, Andreas R. Gruber, Michael Blank, Thorsten Buch, Raymund Buhmann, Mihaela Zavolan, Dierk Niessing, Vigo Heissmeyer & Michael Sattler. **Roquin recognizes a non-canonical hexaloop structure in the 3'-UTR of *Ox40*.** *Nature Communications*. 2016; 7: 11032

\* authors contributed equally

### Additional publications

Sebastian Pünzeler\*, Stephanie Link\*, Gabriele Wagner, Eva C. Keilhauer, **Nina Kronbeck**, Ramona M.M. Spitzer, Susanne Leidescher, Yolanda Markaki, Edith Mentele, Catherine Regnard, Katrin Schneider, Daisuke Takahashi, Masayuki Kusakabe, Chiara Vardabasso, Lisa M. Zink, Tobias Straub, Emily Bernstein, Masahiko Harata, Heinrich Leonhardt, Matthias Mann, Ralph A.W. Rupp, Sandra B. Hake. **Multivalent binding of PWWP2A to H2A.Z regulates mitosis and neural crest differentiation.** *The EMBO Journal*. 2017; 36: 2263-2279

\* authors contributed equally

## Presentations

### Oral presentations based on this thesis

SFB 1054 Annual Meeting 2018, Bad Kohlgrub, Germany

“Roquin and Regnase-1 cooperatively regulate target mRNAs to determine cell fate decisions of T cells”

RIKEN IMS Summer School 2017, Yokohama, Japan

“Post-transcriptional control of T cell activation and differentiation”

### Poster presentations based on this thesis

II Joint Meeting of the German Society for Immunology (DGfI) and the Italian Society of Immunology, Clinical Immunology and Allergology (SIIICA) 2019, München, Germany

“Roquin and Regnase-1 cooperatively determine cell fate decisions in T cells”

Midwinter Conference 2019, Seefeld, Austria

“Investigating the post-transcriptional cooperation of Roquin and Regnase-1 in T cell differentiation”

European Congress of Immunology 2018, Amsterdam, Netherlands

“Investigating the post-transcriptional cooperation of Roquin and Regnase-1 in T cell differentiation”

SFB 1054 Annual Meeting 2017, Bad Kohlgrub, Germany

“Investigating the post-transcriptional cooperation of Roquin and Regnase-1 in T cell differentiation”

RIKEN IMS Summer School 2017, Yokohama, Japan

“Post-transcriptional control of T cell activation and differentiation”

Midwinter Conference 2017, Seefeld, Austria

“Post-transcriptional control of T cell activation and differentiation”

SFB 1054 Begutachtung 2016, München, Germany

“Post-transcriptional control of T cell activation and differentiation”

SFB 1054 Symposium “Cell-fate decisions in the immune system” 2016, München, Germany

“Roquin induces mRNA decay and translational repression”

SFB 1054 Annual Meeting 2015, Grainau, Germany

“Roquin induces mRNA decay and translational repression”

## Acknowledgement

I would like to take the opportunity to express my deepest gratefulness to all people who have supported me throughout the last 5 years. Without these people this thesis would not have been possible.

First, I would like to thank my supervisor Prof. Dr. Vigo Heissmeyer for giving me the opportunity to work on this fantastic and exciting project, for being a great mentor and for all the fruitful discussions that highly improved my progress in the projects.

I cordially thank Prof. Dr. Dierk Niessing and Dr. Dirk Baumjohann as members of my thesis advisory comitée for their suggestions and experimental input.

I want to express my gratitude to my collaborators that strongly contributed to this research work:

Dr. Gergely Csaba and Prof. Dr. Ralf Zimmer from the Institute for Informatics at the LMU München for their great support in this project by contributing the bioinformatical analysis of the mRNA-sequencing data (section 4.3.3).

Dr. Jörg Hackermüller, Dr. Kristin Reiche and Anne Hoffmann, for performing secondary structure predictions and mlocARNA (Figure 15), which was very helpful to design the mutations for analyses of the Nfkbid 3'-UTR reporter.

Anneke Dörrie from the group of Prof. Dr. Helmut Holtmann at the Medizinische Hochschule Hannover for performing the polysome profiles in Figure 21.

I want to thank all present and former members of the Heissmeyer lab, both at the Biomedical Center and the Helmholtz Zentrum for the wonderful working atmosphere. Additionally, I would like to acknowledge people that have provided me with figures, technical support and advice in this thesis.

In particular, I would like to thank Dr. Gesine Behrens deeply for the great collaboration in the Roquin-Regnase project. I highly appreciate your endless help and the wonderful, collegial working atmosphere. Dr. Gesine Behrens contributed the reconstitution assays in Figure 51 and Figure 52.

Christine Conrad, for proofreading of my thesis and for being the best bench-neighbor.

Dr. Taku Kureha, for helping me with the mixed bone marrow chimeras and the input regarding thymus T cell immunology.

Elaine Wong, for performing all ELISAs in Figure 35 and Dr. Katharina Essig, for the immunoblot in Figure 14 a.

Claudia Lohs and Dr. Katharina Essig, for the great collaboration in the Nfkbid project that resulted in a high-quality publication.

Juliane Klein, Claudia Lohs, Elaine Wong, Desirée Argiriou and Silviya Wolkerstorfer, for mouse line organization, your huge effort in lab maintenance and for your technical support whenever I needed it.

Additionally, I would like to thank Dr. Lisa Richter from the Flow Cytometry Core Facility at the BMC, the staff of the mouse facility at the BMC and the animal caretakers of the Helmholtz Zentrum, especially Franziska Liebl and Michael Hagemann.

My deepest gratefulness goes out to my family. Even though we have struggled hard times in the last years, you always believed in me and endlessly supported me.

Finally, I want to thank Alex. Thank you for catching me up during hard times and for your never-ending support and advice in every imaginable way.